THE MODULATORY ROLE OF TAAR1 IN NEUROTOXICITY OF SUBSTITUTED AMPHETAMINES

By

Nicholas B. Miner

A DISSERTATION

Presented to the Department of Behavioral Neuroscience

and the Oregon Health & Science University

School of Medicine

In partial fulfillment of the requirements for the degree of

Doctor of Philosophy

February 2019

School of Medicine

Oregon Health & Science University

CERTIFICATE OF APPROVAL

This is to certify that the Ph.D. dissertation of

Nicholas B. Miner

has been approved

Mentor – Aaron Janowsky, Ph.D.

Committee Chair – Tamara Richards, Ph.D.

Committee Member – Charles Meshul, Ph.D.

Committee Member – Jennifer Loftis, Ph.D.

Committee Member – Matthew Lattal, Ph.D.

TABLE OF CONTENTS

List of figures and tables

List of abbreviations

2,3-DHBA: 2,3-dihydrobenzoic acid

5HIAA: 5-hydroxyindoleacetic acid

5HT: serotonin

5HT2AR: serotonin 2A-type receptor

Akt: protein kinase B

AMPH: amphetamine

ANOVA: analysis of variance

ATP: adenosine triphosphate

AUC: area under the curve

ß-Arr2: ß-arrestin2

ß-PEA: ß-phenethylamine

B6: C57BL/6J

BCA: bicinchoninic acid

B_{max}: maximum number of binding sites

°C: degrees Celsius

cAMP: cyclic adenosine monophosphate

CD11B: integrin alpha M

CNS: central nervous system

CPA: conditioned place aversion

CPP: conditioned place preference

CR3/43: human complement receptor 3

CTA: conditioned taste aversion

D1R: dopamine D1-type receptor

D2R: dopamine D2-type receptor

D2: DBA/2J

DA: dopamine

DAT: dopamine transporter

DHTB: dihydrotetrabenazine

DOPAC: 3,4-dihydroxyphenylacetic acid

EAAT: excitatory amino acid transporter

EC_{50}: concentration of drug eliciting half the maximal response

ELISA: enzyme-linked immunosorbent assay

EPPTB: *N*-(3-Ethoxyphenyl)-4-(1-pyrrolidinyl)-3-(trifluoromethyl) benzamide

ES: embryonic stem

F2: second filial generation

FR: fixed ratio

FSCV: fast-scan cyclic voltammetry

g: relative centrifugal force

g: gram

GFAP: glial fibrillary acidic protein

G_i: inhibitory G protein

GLU: glutamate

GluN1: N-methyl-D-aspartate receptor subunit 1

G_s: stimulatory G protein

GSK3: glycogen synthase kinase-3

GPCR: G-protein coupled receptor

h: hour

H_2O_2: hydrogen peroxide

HET: heterozygous

hGLUT5: human glucose transporter 5

HPLC-ECD: high performance liquid chromatography with electrochemical detection

HVA: homovanillic acid

IC_{50}: concentration of drug eliciting half the maximal inhibitory response

ICV: intracerebroventricular

IL-15: interleukin 15

ILB4: isolectin B4

inj: injection

ip: intraperitoneal

IVSA: intra-venous self-administration

fmol: femtomole

JAK2-STAT3: janus kinase 2 – signal transducer activator of transcription 3

kb: kilobase

K_D: affinity - ligand concentration that binds to half the binding sites

kDa: kilodalton

kg: kilogram

KO: knockout

KOMP: knockout mouse project

l: liter

LMA: locomotor activity

LPR: low perfusion rate

MDMA: 3,4-methylenedioxymethamphetamine

MA: methamphetamine

Mac-1: macrophage-1 antigen

MADR: methamphetamine drinking

MAHDR: methamphetamine high drinking line

MALDR: methamphetamine low drinking line

MAO: monoamine oxidase

MDPV: 3,4-methylenedioxypyrovalerone

µg: microgram

µl: microliter

µM: micro molar

mg: milligram

mGlu: metabotropic glutamate

min: minute

ml: milliter

mM: millimolar

mPFC: medial prefrontal cortex

MRI: magnetic resonance imaging

mRNA: messenger ribonucleic acid

NAc: nucleus accumbens

NE: norepinephrine

NET: norepinephrine transporter

NFLIS: National Forensic Laboratory Information System

nm: nanometer

nM: nanomolar

NMDA: N-methyl-D-aspartate

OE: over-expressed

PBR: peripheral benzodiazepine receptor

PET: positron emission tomography

PFC: prefrontal cortex

pg: picogram

pH: logarithmic scale of acidity

PK11195: 1-(2-chlorophenyl)-N-methyl-(1-methypropyl)-3-isoquinoline carboxamide

PKA: protein kinase a

PKC: protein kinase c

pmol: picomole

PPI: pre-pulse inhibition

QTL: quantitative trait locus

ROS: reactive oxygen species

s: second

SDS: sodium dodecyl sulfate

SEM: standard error of the mean

SERT: serotonin transporter

SN: substantia nigra

SNP: single nucleotide polymorphism

TAAR1: trace amine-associated receptor 1

Taar1: trace amine-associated receptor 1 encoding gene

TH: tyrosine hydroxylase

TSPO: 18 kDa translocator protein

VMAT2: vesicular monoamine transporter 2

VTA: ventral tegmental area

WT: wild-type

Acknowledgements

First and foremost, I would like to thank my mentor Dr. Aaron Janowsky. From my first rotation here at OHSU in his lab to my final experiment, he has provided support, direction, and knowledge. He has continuously emphasized the importance of curiosity within the pursuit of science, encouraging exploration of presented challenges and obstacles. His mentorship provided the structure to develop my own ability to design and execute experiments, the guidance to analyze and synthesize data, and the freedom to move beyond and integrate my results into a larger picture and new avenues of research. Finally, while his steadfast claim that science should be enjoyable often appears dubious, the adage has ultimately served me well and is a good reminder. I have also been very fortunate to work with Dr. Tamara Phillips-Richardson, chair of my dissertation advisory committee. Dr. Phillips-Richardson has helped me hone my analytic and writing skills. Her high standards have made me a better scientist.

I would like to thank the other members of my dissertation advisory committee, Drs. Charlie Meshul and Jennifer Loftis, for their insight and guidance throughout this project, as well as the input from my ad hoc committee member, Dr. Matt Lattal. I would also like to thank Dr. Kim Neve for my time spent in rotation, as well as our discussions and the input I have received over the years since. I would like to especially thank Dr. Suzanne Mitchell, who provided me my first research opportunity and experience at OHSU as a research assistant in her lab.

Members of the Janowsky lab have also been essential to my development as a research scientist. In particular, Dr. Eshleman has been an invaluable source of practical and theoretical knowledge. Dr. Xiao Shi, my office mate, has also been extremely helpful in thoughtful discussions of my experiments and projects. I want to thank all the members of the lab I worked with, especially Kat Wolfrum, John Reed, Tracy Swanson, and Bob Johnson, for their patience and willingness to answer any and all questions, even at inopportune times. Additionally, I am very grateful for the assistance and support of the Phillips lab, particularly Cheryl Reed-Williams, as well as Jason Erk and Harue Baba. Kris Thomason and Jeanne Sutter of BEHN

and Bill Schutzer of the MARC all deserve special commendations for their amazing work in keeping things running, knowledge of the intricacies of this institution, and willingness to assist me in any way they could.

I have had the pleasure of being in the very fine company of many BEHN graduate students, past and present, particularly my cohort: Christie Pizzimenti, Daicia Allen, Vanessa Wakeling, Brett Dufour, and Brian Mills, as well as Rebecca Hood, Amy Williams, Bene Ramirez, and Drs. Morgan Wirthlin, Lauren Kruse, Monique Smith, Melanie Pina, Travis Moschak, and John Harkness.

I could not have completed this process without the support of my friends and family. Bryndl Mar, Carrie Kent, Ashley Ward, and Miriam Burke have been pillars of support throughout, bolstering me when I have fallen, buoying me when I tread water, and championing me when I succeed. Thank you to J.M., M.R., and G.F. for the support you provided at the times you did. I would also like to thank Dr. Mowgli Holmes and Dallas Swindle for the provision of scientific context outside of OHSU. Finally, thank you to my mom, dad, and step-mom for their continued love and support through this whole journey.

Abstract

Methamphetamine (MA) use is a global epidemic, causing mental, physical, and societal damage. Although dopamine (DA) dysregulation is the hallmark of MA-induced neurotoxicity, many underlying mechanisms remain unknown. The trace amine-associated receptor 1 (TAAR1) is activated by numerous agonists, including MA and 3,4-methylenedioxymethamphetamine (MDMA). Activation of TAAR1 inhibits DA neuronal firing and decreases rewarding effects of amphetamines, suggesting TAAR1 mitigates their harmful effects. This dissertation investigated the regulatory role of TAAR1 on transitory and sustained neurotoxic effects of amphetamines in a mouse model. Neurotoxicity was assessed through quantification of striatal biomarkers indicative of DA terminal degeneration and astrocyte activation. Thermal response to amphetamines was also recorded as hyperthermia exacerbates neurotoxicity and hypothermia can provide neuroprotection.

In Chapter 2, I examined the neurotoxic effects of combining MDMA with substituted methcathinones, methylone and 3,4-methylenedioxypyrovalerone (MDPV). The combination of MDMA with either methcathinone abolished transitory MDMA-induced astrocyte activation. However, there were no sustained effects and MDMA did not decrease DA markers. As it is questionable whether neurotoxicity was induced, the modulatory ability of these methcathinones remains unclear. MDMA and methylone, transporter substrates, induced acute hypothermia, whereas MDPV, a transporter inhibitor, did not differ from control animals.

In Chapter 3, I investigated the effect of TAAR1 on MDMA-induced neurotoxicity in mice bidirectionally selectively bred for high (MAHDR) or low (MALDR) MA consumption. MAHDR mice possess a non-functional TAAR1, while MALDR mice possess a functional TAAR1. Although there were no differences in biomarkers between lines, the results were inconclusive as DA levels were again unaltered by MDMA. Interestingly, MDMA-induced hypothermia was absent in MAHDR and transgenic *Taar1*-knockout (KO) mice, indicating TAAR1 modulates

thermal response to MDMA. Thermal response to methylone, which lacks affinity for TAAR1, did not differ between lines.

In Chapter 4, I demonstrated activation of TAAR1 diminishes MA-induced neurotoxicity. MA decreased DA levels in *Taar1*-KO compared to wild-type (WT) mice 7 days later and astrocyte activation was further increased in *Taar1*-KO mice 2 and 7 days later. Only the lower MA doses elicited genotype differences indicating TAAR1 modulatory effects may be superseded at higher doses. Serotonin and norepinephrine levels were unaltered, indicating effects were DA specific. MA, like MDMA, elicited hypothermia in *Taar1*-WT mice only.

In Chapter 5, I examined interactions between TAAR1 and monoamine transporters as potential mechanisms mediating MA-induced neurotoxicity. Using the same neurotoxic MA dose as in Chapter 4, vesicular monoamine transporter 2 (VMAT2) function, i.e. DA uptake, was impaired 24 hours in whole synaptosomes and cytosolic vesicles from *Taar1*-KO compared to –WT mice, but not in membrane-associated vesicles. *In vitro* treatment with MA revealed activation of TAAR1 does not alter DA transporter (DAT) function: DA uptake or release. Using the *Taar1* and MADR models, there were no differences between genotypes or selected lines for VMAT2 or DAT expression. While TAAR1 mediates intracellular VMAT2 function, there is little evidence of TAAR1 interaction with DAT or modulation of either transporter expression.

Together, these experiments demonstrate TAAR1 regulates MA-induced neurotoxicity and thermal response. The results of this research may inform future studies on the mechanisms of neurotoxicity and development of pharmacotherapeutic treatments for MA use disorder.

Chapter 1: Introduction

1. Methamphetamine and MDMA

The use of amphetamine family of drugs continues unabated. Methamphetamine (MA) use is referred to as a “global epidemic” and is the second most commonly used illicit drug worldwide, exceeded only by cannabis (UNODC, 2017). The same report found annual amphetamine seizures doubled in quantity between 2010 and 2015 to over 190 tons, with MA accounting for 70%. In 2016, over 1.6 million Americans reported using MA within the past year and 700,000 within the past month (NSDUH, 2017). The increased use and fatal consequences of this drug are reflected in MA overdose deaths in the U.S, which more than doubled from 2010 to 2014, reaching over 3,700 fatalities (Warner et al., 2016)

MA is ingested for its ability to increase feelings of euphoria, productivity, alertness, energy, and hyper-sexuality, and is accompanied by dose-dependent physiological alterations of increased blood pressure, heart rate, breathing rate and body temperature (Homer et al., 2008; Cruickshank and Dyer, 2009). These effects are due to rapid spikes in catecholamine levels and increases in DA levels are primarily responsible for the rewarding and addictive effects (Nutt et al., 2015; Volkow and Morales, 2015). Following MA binge use and DA depletion, withdrawal causes feelings of depression, anhedonia, aggression, anxiety and MA-craving (McGregor et al., 2005; Volkow et al., 2016). Repeated excessive use leads to neurotoxicity and damage throughout the central nervous system (CNS). The impact of neurotoxic effects of MA are manifold: impairing information processing, learning and memory, and increasing impulsivity (Jentsch et al., 2014; Bernheim et al., 2016; Zhong et al., 2016; Potvin et al., 2018), as well as increasing likelihood of mental illnesses, such as anxiety, depression, and psychosis (Lecomte et al., 2013; Glasner-Edwards and Mooney, 2014). Post-mortem analyses and imaging studies of MA users reveal the neurotoxic effects on the dopaminergic system: striatal DA depletion and down regulation of the DA transporter (DAT), DA synthesis, and DA D2-type receptors (D2R)

(Wilson et al., 1996; Volkow et al., 2001; McCann et al., 2008). Beyond its cognitive effects, chronic MA use is detrimental to physical health, increasing cardiovascular and cerebrovascular pathologies (Darke et al., 2008; Mooney et al., 2009). As a class of drugs, amphetamines are second only to opioids in terms of drug-related health disorders (mental and physical), with MA being the greatest contributor within the amphetamine family (UNODC, 2017). Following large doses, MA can cause extreme hyperthermia, seizures, cardiac arrest, cerebral hemorrhage, and rhabdomyolysis (breakdown of damaged skeletal muscle), with fatal consequences (Cadet et al., 2007; Paratz et al., 2016; Darke et al., 2017).

3,4-methylenedioxymethamphetamine (MDMA), commonly referred to as ecstasy, has been dubbed an empathogen or entactogen for its ability to produce feelings of increased well-being, empathy, self-esteem, and emotional openness, alongside similar physiological properties of amphetamines, including increases in body temperature, heart rate, and blood pressure (Kirkpatrick and de Wit, 2015; Vizeli and Liechti, 2017). As an amphetamine, MDMA causes a rapid increase in catecholamine levels, but it preferentially increases serotonin (5HT) levels, responsible for many of the desired subjective effects (Hasler et al., 2009). Following this acute increase, 5HT levels become depleted, reaching a nadir 2-3 days later, often resulting in feelings of depression and anxiety (Hoshi et al., 2006). Positron emission tomography (PET) and single photon emission computed tomography imaging studies of MDMA users reveal 5HT transporter (SERT) levels are diminished and 5HT 2A-type receptor (5HT2AR) binding is increased (associated with decreases in 5HT levels), while DAT levels were unaltered (Reneman et al., 2001; Urban et al., 2012). MDMA also has a greater effect than MA on the neuroendrocrine system due to serotonergic modulation of the hypothalamic-pituitary-adrenal axis leading to increases in oxytocin, cortisol, and arginine vasopressin levels (de la Torre et al., 2000; Wolff et al., 2006). The consumption of large amounts of MDMA can have severe adverse effects similar to MA. The risk of extreme hyperthermia (body temperature > 40 °C) is exacerbated by the environment in which MDMA is commonly ingested: discos, raves, and

music festivals, where ambient temperature is elevated and participants engage in dancing for extended periods of time in a crowded setting (Capela et al., 2009). Profuse sweating, reduced dissipation of heat, and vasoconstriction contribute to increases in body temperature. This degree of hyperthermia often precedes rhabdomyolysis, intravascular coagulation, and renal failure, events that can be fatal (Liechti, 2014). Increased arginine vasopressin secretion in combination with excessive water drinking can also lead to hyponatremia (Fallon et al., 2002).

This dissertation will focus primarily on the neurotoxic effects of the substituted amphetamines MA and MDMA, as modulated by TAAR1, and secondarily address the substituted methcathinones methylone and MDPV. All four substances share an amphetamine-based chemical compound structure. MA is differentiated from amphetamine (AMPH) by an additional methyl group at the α-carbon; and MDMA from MA with the addition of a methylenedioxy bridge (Fig. 1). The substituted methcathinones possess an amphetamine chemical backbone, but is differentiated and identified by a ketone moiety attached to the ß-carbon position. Methylone is the methcathinone analog to MDMA, the only difference being the ketone addition. While MDPV possesses a methylenedioxy bridge, similar to MDMA and methylone, additional moieties alter its structure and properties.

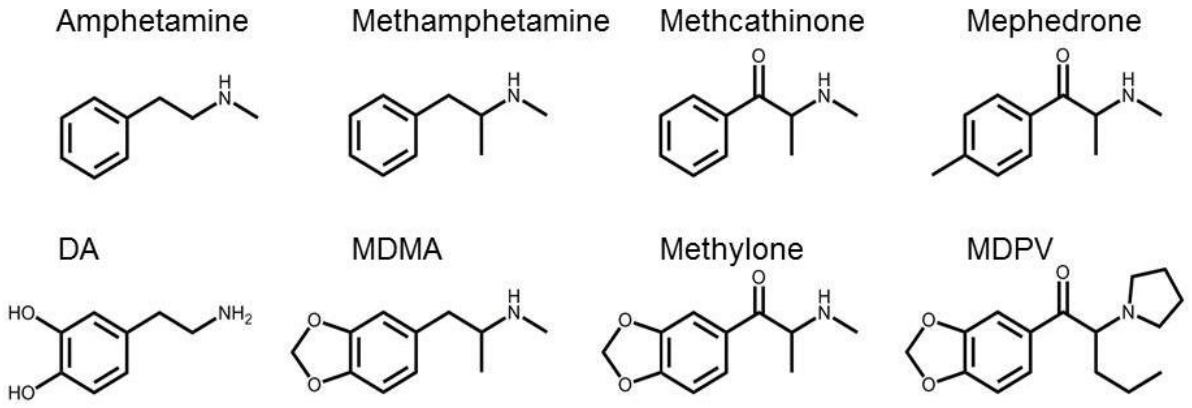

Figure 1. Molecular structures for amphetamine related compounds. Amphetamine and DA, methamphetamine and substituted derivative MDMA; methcathinone and substituted derivatives methylone, mephedrone, and MDPV.

Monoamines

The effects of MA and MDMA on the CNS are primarily mediated by their ability to increase intra- and extracellular levels of monoamines (DA, 5HT, and NE). The drugs are taken into axon terminals where they elevate cytosolic levels of monoamines by increasing secretory vesicle release *via* the vesicular monoamine transporter 2 (VMAT2) and increase extracellular levels through reverse transport at the plasmalemmal transporters (Fig. 2) (Sulzer et al., 2005). As transporter substrates, both drugs inhibit monoamine uptake and induce release (Rothman and Baumann, 2003). MA has greater affinity for DAT than MDMA and therefore more potent at inhibiting DA uptake and inducing DA release, while the inverse is true at SERT (Eshleman et al., 2013). Although less relevant to neurotoxicity, both drugs are more potent at releasing NE than DA or 5HT, a contributing factor to the stimulating effects of amphetamines (Rothman et al., 2001). MA and MDMA share similar affinity and potency at VMAT2 (Partilla et al., 2006).

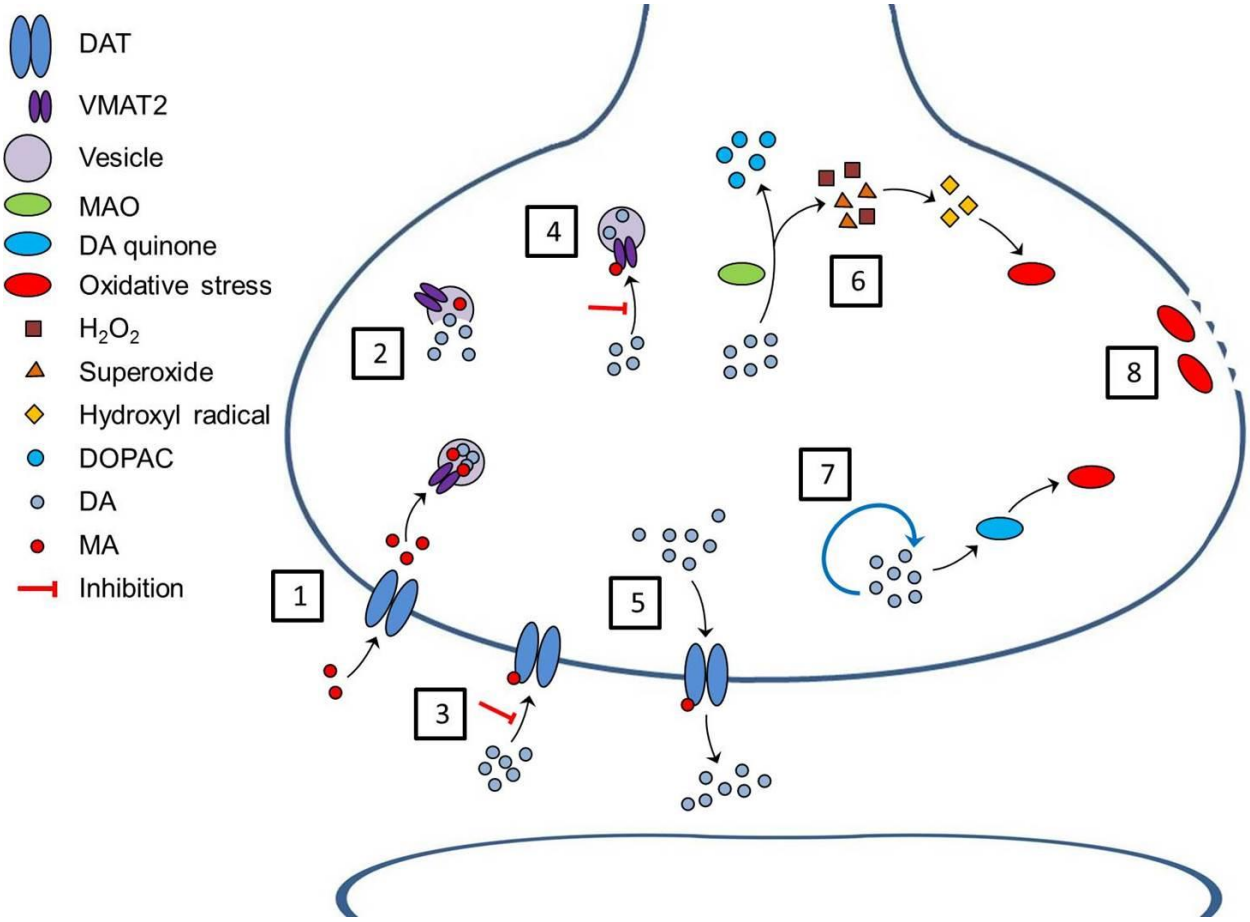

Figure 2. Schematic of the actions of amphetamines at the DA terminal. Amphetamines (i.e. MA) cross the plasmalemmal membrane *via* DAT and are taken into vesicles by VMAT2 (1). MA causes vesicles to rupture and disperse sequestered DA, increasing cytosolic DA levels (2). MA inhibits DA uptake by DAT, reducing clearance from the synapse (3). MA also inhibits DA uptake by VMAT2, reducing the packaging of DA into vesicles (4). MA reverses transport at DAT, increasing extracellular DA levels (5). DA is metabolized by MAO to produce DOPAC, but due to elevated cytosolic DA levels, an abundance of H_2O_2 and superoxides are produced, which react to form hydroxyl radicals, leading to oxidative stress (6). DA is auto-oxidized to form DA quinones which increase oxidative stress (7). Oxidative stress causes lipid peroxidation and break down of the plasma membrane (8).

MA causes both DA and 5HT terminal degeneration, while MDMA is selective for 5HT terminals (Battaglia et al., 1987; Seiden et al., 1988). However, in terms of monoaminergic causality, these effects are primarily attributed to increased levels of DA with a lesser role of 5HT (Stone et al., 1988; Cubells et al., 1994; Thomas et al., 2010). Although the increase in NE elicits behavioral effects, it is not believed to contribute to neurotoxicity and there is no evidence of NE terminal degeneration following administration (Wagner et al., 1980; Battaglia et al., 1987). As such, below is a general discussion of the mechanisms by which amphetamines (AMPH, MA, and MDMA) increase intra- and extracellular DA levels. Distinctions between MA- and MDMA-specific effects on monoamines and downstream effects will follow.

Amphetamine-induced vesicular release is primarily attributed to the weak base properties of amphetamines, explained by the eponymous weak base hypothesis (Sulzer and Rayport, 1990). As lipophilic weak bases, DAT-transported amphetamines diffuse from the cytoplasm into the acidic environment of vesicles. The internalized amphetamines compete for protons with sequestered monoamines, creating an electro-chemical concentration gradient, and causing the stored and uncharged neurotransmitters to diffuse out of the vesicles. The alkalinization of vesicles also disrupts vesicular sequestration of monoamines, increasing intracellular DA levels. As VMAT2 substrates, amphetamines impair VMAT2 function, inhibiting vesicular DA uptake and inducing release, further increasing intracellular levels of DA (Teng et al., 1998; Brown et al., 2000). Amphetamines also redistribute VMAT2, supported by differential expression of VMAT2 in subcellular fractions following administration, contributing to impaired function (Hogan et al., 2000; Hansen et al., 2002; Riddle et al., 2002). This cumulative elevation of cytosolic DA levels alters the concentration gradient, contributing to reverse transport at DAT and increased levels of extracellular DA (Sulzer et al., 1995).

Amphetamines induce DA release into the extracellular space through a variety of mechanisms: 1) exchange diffusion, during which extracellular amphetamines at low concentrations are exchanged for intracellular DA, 2) reverse transport of intracellular DA at

higher concentrations, and 3) channel-like transference of DA (Fischer and Cho, 1979; Liang and Rutledge, 1982; Kahlig et al., 2005). Amphetamines also activate the protein kinase C (PKC) signaling cascade, which increases DA release, an effect blocked by PKC inhibitors (Giambalvo, 2004; Johnson et al., 2005; Fleckenstein et al., 2007). MA-induced PKC activation also phosphorylates DAT leading to down-regulation, although DAT internalization occurs independently of PKC activation (Khoshbouei et al., 2004; Cervinski et al., 2005; Boudanova et al., 2008). Additionally, amphetamines inhibit monoamine oxidase (MAO) and DA metabolism, elevating DA (Sulzer et al., 2005).

As mentioned, MDMA has a higher affinity for SERT than MA and is more potent at releasing 5HT (Eshleman et al., 2013). MDMA increases extracellular 5HT levels in the striatum, prefrontal cortex (PFC), and hippocampus through many of the same mechanisms: disruption of VMAT2 sequestration, SERT reverse transport, 5HT uptake inhibition and release, and inhibition of MAO (Leonardi and Azmitia, 1994; Cozzi et al., 1999; Gudelsky and Yamamoto, 2008). Additionally, MDMA causes an acute and long-term decrease in tryptophan hydroxylase activity, the precursor to 5HT, resulting in depletion of 5HT stores in the same brain regions (Schmidt and Taylor, 1988).

2. Neurotoxicity

Neurotoxicity is most broadly defined as neuronal damage due to a neurotoxin or injury. This broad definition encompasses an array of causes ranging from environmental exposure to pesticides to neurodegenerative diseases, such as Alzheimer's and Parkinson's disease, to traumatic brain injury (Majd et al., 2015; Dambinova et al., 2016; NINDS, 2018). Of course the focus here is amphetamines, acting as neurotoxins. The spectrum of damage encompasses partial and complete loss of neurons, alterations in neuron structure and morphology, and impairment of neuronal function and behavior (Moszczynska and Callan, 2017). This damage can be either permanent or reversible. While factors contributing to neurotoxicity may be quantified in the presence of the neurotoxin, markers of neurotoxicity are typically measured in

the absence of the drug in order to ensure the results reflect neural damage as opposed to direct effects of the drug while it is present in the system.

Although MA affects DA levels in all DA projections, the neurotoxic effects are most severe in the striatum (O'Callaghan and Miller, 1994; Yamamoto et al., 2010; McConnell et al., 2015). The mesolimbic pathway is spared and terminal degeneration is not observed in the nucleus accumbens (NAc) (Granado et al., 2010; Kuhn et al., 2011). Although there is some evidence of cell death and degeneration of cell bodies in the substantia nigra (SN) (Sonsalla et al., 1996; Ares-Santos et al., 2014), damage is predominantly restricted to striatal DA axon terminals (Harvey et al., 2000; Anderson and Itzhak, 2006). DA terminal degeneration also occurs in the cortex, but to a lesser degree (Fantegrossi et al., 2008; McConnell et al., 2015). While MA impacts the serotonergic system, causing degeneration of 5HT terminals in the striatum, PFC, hippocampus and amygdala, it does so with less severity than in DA terminals (Yamamoto et al., 2010).

In humans, non-human primates, and rats, MDMA selectively affects 5HT terminals in similar areas to MA, sparing DA axon terminals (Ricaurte et al., 1988; Green et al., 2003; Sanchez et al., 2003). An exception is the mouse model for MDMA. For reasons that remain unknown, MDMA has neurotoxic specificity for DA terminals in mice and 5HT terminals are largely unaffected (O'Callaghan and Miller, 2002; Mueller et al., 2013). As such, many MDMA studies in mice have focused on DA activity and terminal degeneration based on the theory that MDMA neurotoxicity is due to increased levels of DA taken into 5HT terminals (Sprague et al., 1998; Colado et al., 2001; Puerta et al., 2009). It has also been argued that mice provide a better animal model than rats to study the neurotoxicity of amphetamines in general. Although rats display monoamine and related marker deficits in reaction to amphetamines, these changes are not consistently accompanied by neuronal damage, as opposed to mice (Guilarte et al., 2003; Baumann et al., 2007; O'Callaghan et al., 2008). Since all experiments in this dissertation

were performed using a mouse model of neurotoxicity, the literature cited refers to research conducted in a mouse model, unless otherwise noted.

Neurotoxicity models and markers

Amphetamine neurotoxicity is commonly induced using a binge-like regimen of multiple injections over a single day. Most paradigms consist of 3 or 4 injections, spaced 3 or 2 h apart (O'Callaghan and Miller, 1994; Granado et al., 2011). This allows for the assessment of a high dose of accumulated drug that could be lethal when administered in a single bolus or metabolized with longer intervals between doses. Alternatively, some researchers utilize a higher, but sub-lethal, single dose model or chronic models using consistent or escalating doses (Kobeissy et al., 2012). Again, as all neurotoxicity experiments in this dissertation were conducted using a single-day binge-like regimen, all cited research was performed using a similar paradigm, unless otherwise noted.

MA- and MDMA-induced neurotoxicity in a mouse model is characterized by decreases in striatal DA biomarkers, indicative of DA terminal degeneration. Typical markers include: DA and its metabolites 3,4-dihydroxyphenylacetic acid (DOPAC) and homovanillic acid (HVA), tyrosine hydroxylase (TH), the rate limiting enzyme for DA synthesis, and DAT (Krasnova and Cadet, 2009; Moratalla et al., 2017). These markers correspond with studies in post-mortem human studies where DA, TH, and DAT levels were decreased in striatal tissue of chronic MA users compared to controls (Wilson et al., 1996). Habitual and abstinent MA users also display decreases in DAT expression, measured *via* PET imaging (Volkow et al., 2001; McCann et al., 2008). In animals, these biomarkers are frequently measured 2-3 days post-treatment to capture maximal effects (Fantegrossi et al., 2008; Guillot et al., 2008; Anneken et al., 2015). However, decreases at this time may only represent transient neurotoxicity. Quantification of these markers at a later time point, such as 7, 14, or 21 days post-treatment reflects sustained neurotoxicity (O'Callaghan and Miller, 1994; McConnell et al., 2015). A MA dose as low as 2.5 mg/kg (4 inj, 2 h apart) diminishes DA and DAT levels 2 days following administration (Angoa-

Perez et al., 2013b), while low doses of MDMA (5 mg/kg, 4 inj, 2 h apart) diminishes DA, DOPAC, HVA, and TH levels 7 days later (Fornai et al., 2004). These markers are commonly used to quantify neurotoxicity as their reduction reflects a loss of structural integrity in DA neuron terminals. For a selected review of MA and MDMA-induced neurotoxicity, see Table 1. Fluoro-Jade and silver staining, as well as electron microscopy, directly examine DA fiber degeneration, although these methodologies are not as frequently used (Bowyer et al., 2008; Ares-Santos et al., 2014). Alternative measures of neurotoxicity include the quantification of reactive oxygen species (ROS), DA quinones, and oxidative stress (Larsen et al., 2002; Sanchez et al., 2003; Guillot et al., 2008). Serotonergic markers, such 5HT, its metabolite 5-hydroxyindoleacetic acid (5HIAA), and SERT levels are also used, though not as commonly in mouse models (Green et al., 2003; Krasnova and Cadet, 2009).

Table 1. Summary of studies: MA and MDMA-induced neurotoxicity in a mouse model

Drug	Dose (mg/kg)	Time points (days)	Measures	Notes	Reference
MA	1,2,5,10	2	↓DA	↓DA: only by 5 and 10 mg/kg	Thomas *et al*., 2004
	2	1,3,7,14	- DA,TH,DAT; ↑GFAP		McConnell *et al*., 2015
	4	1,3,7,14	↓DA,TH,DAT; ↑GFAP	↓TH: 1 day only; ↓DAT: 1,3 days only	
	6,8	1,3,7,14	↓DA,TH,DAT; ↑GFAP	DAT: unchanged at 14 days	
	2.5,5,10	2	↓DA,TH,DAT; ↑GFAP	TH: unchanged by 2.5 mg/kg	Anneken *et al*., 2015
	4[a]	1,7	↓DA,TH,DAT; ↑GFAP		Granado *et al*., 2011
	5[a]	7	↓DA,TH		Fornai *et al*., 2005
	5	3,7,14	↓DA,DAT; ↑PK11195	↓DAT: only measured at 14 days	Ladenheim *et al*., 2000
	5	3	- DA,PK11195		Fantegrossi *et al*., 2008
	10	3	↓DA; ↑PK11195		
	10	1,6	↓DA,TH		Hogan *et al*., 2000
	10	7	↓TH,DAT; ↑GFAP		Deng *et al*., 1999
	10	1,2,3,4,5,7,14,21	↓DA,TH; ↑GFAP	GFAP: unchanged at 21 days	O'Callaghan and Miller, 1994
	15[a]	2	↓DA,DAT; -TH; ↑GFAP		Guillot *et al*., 2008
	15	7	↓DA,TH		Bowyer *et al*., 2001

Drug	Dose (mg/kg)	Time points (days)	Measures	Notes	Reference
MDMA	5	7	↓DA,TH,DAT		Fornai *et al*., 2004
	5	3	- DA,GFAP		Johnson *et al*., 2002
	10	3	↓DA; ↑GFAP		
	15	3	↓DA,TH; ↑GFAP		Johnson *et al*., 2004
	15[a]	7	↓DA		Sanchez *et al*., 2003
	20	1,2,3,4,5,7,14,21	↓DA,TH; ↑GFAP	GFAP: unchanged at 21 days	O'Callaghan and Miller, 1994
	20	2	↓DA,TH,DAT; ↑GFAP		Anneken *et al*., 2015
	20[a]	7	↓TH,DAT; ↑GFAP		Granado *et al*., 2008
	30	1,3,7,30	↓TH,DAT; ↑GFAP	GFAP: unchanged at 30 days	
	10,20	3	- DA,PK11195		Fantegrossi *et al*., 2008
	30	3	↓DA; -PK11195		

All experiments were conducted using a dose regimen of 4 inj, 2 h apart, administered in a normothermic environment (20-23 °C), and quantified in striatal tissue, unless noted. Arrows indicate significant differences between drug treated animals and saline-treated controls. ↓: decreased; ↑: increased; -: no difference. [a] dose regimen: 3 inj, 3 h apart.

Neuroinflammation

Neuroinflammation, literally the inflammation of neuronal tissue, is caused by activation of glial cells and characterized by the synthesis and release of proinflammatory cytokines and chemokines in the CNS. Separated into the categories of astrocytes and microglia, both types of glial cells are activated in response to neuronal injury caused by amphetamines (Loftis and Janowsky, 2014). While this response initially mitigates neuronal damage through the release of anti-inflammatory mediators, sustained elevated activation increases neuroinflammation and neuronal damage through the production and release of proinflammatory cytokines and chemokines, including interferons, interleukins, macrophages, and chemoattractant proteins (Whitney et al., 2009). Activation of astrocytes is characterized by expression of glial fibrillary acidic protein (GFAP) (O'Callaghan and Sriram, 2005). Astrocytes metabolize DA to form ROS and cause lipid peroxidation, an effect exacerbated when astrocytes are activated by MA (Lau et al., 2000; Vaarmann et al., 2010; O'Callaghan et al., 2014). Astrocytes are also responsible for glutamate (GLU) clearance and prolonged activation disrupts excitatory amino acid transporter 2 (EAAT2) function, leading to increased levels of extracellular GLU and excitotoxicity (Anderson and Swanson, 2000). Primarily responsible for immune response in the CNS, microglia release a wider array of cytokines and chemokines than astrocytes when activated. As such, there are a range of markers used to quantify microglia activation, such as isolectin B4 ($ILB4_)$, integrin alpha M (CD11b), macrophage-1 antigen (Mac-1), and interleukin 15 (IL-15) (Hanisch, 2002). When activated, microglia produce superoxides, hydrogen peroxide (H_2O_2), nitric oxide, and tumor necrosis factor-α (Block et al., 2007). Production of these

cytotoxic factors leads to increased oxidative stress and a potential feedback loop between neurons and glia increasing both neuronal damage and neuroinflammation (Beardsley and Hauser, 2014).

Similar to other markers of neurotoxicity, amphetamine-induced gliosis is observed in multiple regions of the brain, including the cortex, cerebellum, and hippocampus, but is most pronounced in the striatum and absent in the NAc (O'Callaghan and Miller, 1994; Escubedo et al., 1998; Granado et al., 2008). Among amphetamines, astrocyte and microglia activation are selective for those that are neurotoxic. When compared with AMPH, MA, and MDMA, the amphetamine fenfluramine does not induce neurotoxicity and does not activate astrocytes or microglia (O'Callaghan and Miller, 1994; Thomas et al., 2004a). Astrocyte and microglia are also more sensitive to the effects of amphetamines and their activation precedes DA terminal degeneration (LaVoie et al., 2004; O'Callaghan et al., 2008). A sliding dose experiment reported MA (2 mg/kg, 4 inj, 2 h apart) increases striatal astrocyte and microglia activation, while DA, TH, and DAT levels are unaltered until the dose is increased to 4 mg/kg (McConnell et al., 2015). However, temporal activation differs between the two types of glial cells. Astrocyte activation peaks 2-3 days following MA and MDMA administration and can remain elevated up to 14 days later, whereas microglia activation rapidly increases, peaking 24-48 h later, but returns to baseline by 3 days later (Thomas et al., 2004b; Granado et al., 2008; McConnell et al., 2015).

An additional marker of gliosis, indicative of both astrocyte and microglia activation, is increased expression of the 18 kDa translocator protein (TSPO), previously known as the peripheral benzodiazepine receptor (PBR) (Papadopoulos et al., 2006). TSPO is absent in neurons, but expressed on glial cells and co-localizes with both astrocytes and microglia (Kuhlmann and Guilarte, 1999). TSPO expression can be quantified using a radioligand binding assay and the selective ligand PK11195 (1-(2-chlorophenyl)-N-methyl-(1-methypropyl)-3-isoquinoline carboxamide) (Benavides et al., 2001). The majority of amphetamine-induced gliosis studies using [^{3}H]PK11195 binding have been conducted using MA. Three days following

administration, MA (5 and 10 mg/kg, 4 inj, 2 h apart) increases [^{3}H]PK11195 binding in the striatum, but not cortex (Ladenheim et al., 2000; Fantegrossi et al., 2008). A time course experiment, conducted in rats treated with MA (10 mg/kg, 4 inj, 2 h apart) revealed TSPO expression is elevated 2 days following administration, peaks at 3 days, and returns to baseline by 7 days (Escubedo et al., 1998). In mice treated with MDMA (25 mg/kg, 3 inj, 3 h apart), striatal [^{3}H]PK11195 binding increases at an early time point of 16 h (Chipana et al., 2006).

Clinical research, using PET imaging and radiolabeled PK11195, reveal microglia activation in the striatum is increased in abstinent MA users (Sekine et al., 2008). Furthermore, microglia activation is inversely correlated with duration of abstinence from MA. The pro-inflammatory cytokine IL-6 is also elevated in current MA users, associating with decreased corticostriatal functional connectivity (Kohno et al., 2018). However, an immunohistochemical analysis of post-mortem tissue from MA users did not find increases in markers of reactive astrocytes (GFAP and S100 calcium-binding protein B) or microglia (CR3/43, the human complement receptor 3), although there was an in increase in a marker of resting microglia (human glucose transporter 5, hGLUT5) (Kitamura et al., 2010). Another study using post-mortem tissue of MA users, quantified protein levels of various markers of astrocytes (GFAP, vimentin, and heat shock protein-27, HSP-27) and microglia (hGLUT5 and CR3/4) (Tong et al., 2014). Protein concentrations of intact proteins were not elevated in MA users, though fragmented vimentin and HSP-27 proteins were increased, suggesting astrocyte damage.

Although these studies do not provide a clear demonstration of increased gliosis in MA users, one possible explanation is drug tolerance as all subjects were chronic MA users. Animal research typically employs a single day neurotoxic regimen to naïve mice. Although fewer studies have been conducted using repeated or chronic exposure to MA, there is evidence that tolerance builds and neuroinflammation is reduced. An experiment in rats reported astrocyte activation (GFAP) is not elevated by a neurotoxic regimen of MA (7.5 mg/kg, 4 inj, 2 apart) when administered following 7 days of MA self-administration (McFadden et al., 2012). Pre-treatment

of mice with low levels of MA (2 mg/kg) for 7 days prior to a neurotoxic regimen of MA (5 mg/kg, 4 inj, 2 h apart) also mitigates microglia activation (ILB4). In both studies, the glial markers were elevated in animals who did not receive MA pretreatment prior to the neurotoxic regimen. Further clinical research of gliosis is needed.

It is important to keep in mind that while markers of astrocyte and microglia activation are biomarkers of amphetamine-induced neurotoxicity that are initiated by neuronal injury and often correspond with DA terminal degeneration; gliosis reflects neuroinflammation and does not measure DA terminal degeneration (Pu and Vorhees, 1993; O'Callaghan and Sriram, 2005).

Dopamine transporter

As described above, the origin of MA-induced neurotoxicity is primarily attributed to the effects of MA on the monoaminergic transporters: DAT and VMAT2. Dysregulation of the transporters leads to increased cytosolic levels of DA and terminal degeneration (Fleckenstein et al., 2007). The ability of MA to alter DAT function acutely is well documented. Radioligand assays of [^{3}H]DA uptake and release are often performed using *in vitro* treated cells or tissue homogenate to report the affinity of MA and other psychostimulants for DAT and their potency at inhibiting uptake and inducing release (Rothman and Baumann, 2003; Eshleman et al., 2013). Shifts in these values following pharmacological treatments or in genetically altered mice can reveal the involvement of different receptors and proteins in the underlying mechanisms of these drugs. DA release is also measured *in vivo* using microdialysis collection of cerebrospinal fluid (Weinshenker et al., 2008; Baumann et al., 2012; Lominac et al., 2014).

While impaired DAT function increases cytosolic levels of DA contributing to neurotoxicity, the expression of DAT is more complicated. In a DAT-KO mouse model, acute [^{3}H]DA release is diminished and markers of striatal neurotoxicity (DA and ROS) are diminished in DAT-KO compared to DAT-WT mice (Fumagalli et al., 1998). Although this indicates that decreased DAT levels prior to MA administration is protective, DAT levels are a common biomarker of neurotoxicity following administration. One hour following MA administration, DAT is sometimes

unchanged and other times diminished (Saunders et al., 2000; German et al., 2012; Fricks-Gleason et al., 2016). However, DAT levels are robustly diminished 24 h after MA treatment. A time course experiment using immunoreactivity revealed DAT protein is significantly decreased 24 h following various doses of MA (4, 6, or 8 mg/kg, 4 inj, 2 h apart) reaching its lowest point 3 days later, and still is diminished 7 days following administration (McConnell et al., 2015). Another time course experiment using autoradiography and a single bolus of MA (30 mg/kg) revealed DAT is not decreased 16 h following administration, but is diminished 24 h later with lowest expression 2 days after the last injection (Zhu et al., 2005). A study using both techniques, reported DAT protein levels and expression are decreased 24 h following a single injection of MA (40 mg/kg) (Bourque et al., 2012). These results demonstrate the decrease in DAT, 24 h following MA, is not solely due to down-regulation of the transporter. Diminished levels of DAT, 7 days or later following MA administration, are reflective of persistent terminal degeneration (Deng et al., 1999; Fumagalli et al., 1999; McConnell et al., 2015).

Vesicular monoamine transporter 2

VMAT2 is the second key modulator of MA-induced neurotoxicity. Decreased basal VMAT2 expression increases neurotoxicity. The neurotoxic effects of MA (15 mg/kg, 4 inj, 2 h apart) are exacerbated in a mutant strain of mice expressing low amounts of VMAT2 in comparison to their wild-type counterparts, demonstrated by lower DA and TH levels alongside higher astrocyte and microglia activation, (Guillot et al., 2008). A similar effect occurs in a different VMAT2 model, using knockout mice heterozygous VMAT2 (HET), where MA (15 mg/kg, 4 inj, 2 h apart) decreases DA and DAT levels 2 days following administration in VMAT2-HET compared to VMAT2-WT mice (Fumagalli et al., 1999). While diminished levels of basal VMAT2 increase MA-induced neurotoxicity, increased baseline VMAT2 levels provide neuroprotection. In transgenic mice over-expressing VMAT2, striatal TH and DAT levels are unaltered by MA (10 mg/kg, 4 inj, 2 h apart) two days following administration, while TH and DAT levels are diminished in VMAT2-WT mice (Lohr et al., 2015).

VMAT2 expression is often measured in separate subcellular compartments obtained by fractionation (Staal et al., 2000). Centrifugation is commonly used to separate striatal homogenate into crude synaptosomal, membrane-associated (mainly mitochondria, myelin, nerve-ending, and other plasmalemmal-associated membranes), and enriched vesicular fractions (De Robertis et al., 1962; Scherman, 1986). This process allows for examination of VMAT2 localized to cytosolic vesicles, separate from those found on membrane-associated vesicles at the plasmalemmal surface. Verification of the vesicular fraction purity has been confirmed by EM analysis; the predominant membrane structure in the vesicular preparation matches the synaptic vesicle profile: spherical or ellipsoid, ~50 nm in diameter, with less than 1% of the fraction containing contaminating membranes (Teng et al., 1997; Staal et al., 2000). Quantification of VMAT2 is performed using a radioligand binding assay with the VMAT2 selective antagonist dihydrotetrabenazine (DHTB) or immunohistochemistry to quantify whole protein levels (Teng et al., 1998; Eyerman and Yamamoto, 2005). Following MA administration (10 mg/kg, 4 inj, 2 h apart), [^{3}H]DHTB binding is decreased in the enriched vesicular fraction 1 and 24 h later (Hogan et al., 2000; Ugarte et al., 2003). In a study with rats, MA (10 mg/kg, 4 inj, 2 h apart) decreases [^{3}H]DHTB binding in the vesicular fraction at 1 h post-treatment and to the same degree 24 h later (Brown et al., 2000). Similar results were found utilizing the same dose and immunohistochemistry analysis: MA diminishes VMAT2 protein 1 h, 24 h, and 7 days following administration (Eyerman and Yamamoto, 2005, 2007). However, this decrease is limited to VMAT2 in the enriched vesicular fraction and there is no difference in VMAT2 expression in the synaptosomal or membrane-associated fractions either 1 or 24 h later (Sandoval et al., 2003; Ugarte et al., 2003). VMAT2 expression is decreased in all fractions 6 days later, attributed to DA terminal degeneration. The disparity in VMAT2 expression between the synaptosomal and vesicular fraction has led to the hypothesis that MA rapidly redistributes cytosolic vesicles, which, along with inhibition of vesicular DA sequestration, leads to increased

cytosolic levels of DA and increased neurotoxicity (Riddle et al., 2002; Fleckenstein et al., 2007).

VMAT2-mediated [^{3}H]DA uptake in the vesicular fraction is also inhibited 1 and 24 h following MA administration, further contributing to increased intracellular DA levels (Brown et al., 2000; Hogan et al., 2000; Sandoval et al., 2003). Although research on VMAT2 function is primarily conducted in this fraction consisting of cytosolic vesicles, Fleckenstein and coworkers have examined VMAT2-mediated DA uptake in membrane-associated vesicles. This is performed in the membrane-associated fraction, consisting of synaptosomal membranes and fragments following osmotic lysis. The group first reported VMAT2 localized to membrane-bound vesicles are able to transport greater than five times the amount of DA compared to VMAT2 found in the vesicular fraction, speculating plasmalemmal membrane-bound vesicles may serve to sequester a larger quantity of intracellular DA than cytoplasmic vesicles (Volz et al., 2007a). A follow-up study found MA inhibits VMAT2-mediated [^{3}H]DA uptake 1, 24, and 72 h following administration in the membrane-associated fraction, similar to the vesicular fraction (Chu et al., 2010). These changes in VMAT2 expression and function, extending beyond the acute effects of MA, indicate a persistent role of VMAT2 in MA-induced neurotoxicity.

Oxidative stress

MA-induced neurotoxicity may begin with increased DA levels, but it is the downstream effects of this elevation that cause the degeneration of DA terminals. Increased cytosolic, not extracellular, levels of DA are primarily responsible for degeneration (Fumagalli et al., 1999; LaVoie and Hastings, 1999). When cytosolic DA rises, the excess is either metabolized by MAO-B, generating H_2O_2 and superoxides, or auto-oxidized to form reactive DA quinones and superoxides (Cubells et al., 1994; Cadet and Brannock, 1998). DA quinones reflect cytosolic-specific oxidative stress and can be quantified by measuring cysteinyl-conjugated DA and DOPAC or quinoproteins (LaVoie and Hastings, 1999; Miyazaki et al., 2006). In turn, these reactions lead to the formation of hydroxyl radicals (Kita et al., 2009). Hydroxyl formation can be

measured through salicylate trapping, followed by quantification of 2,3-dihydrobenzoic acid (2,3-DHBA) (Giovanni et al., 1995). This is commonly performed using *in vivo* microdialysis immediately following MA administration (Yamamoto and Zhu, 1998), but has also been studied at later time points, such as 7 days following AMPH administration (Wan et al., 2000). An indicator of oxidative stress, MA also increases protein carbonyl formation 2 days later, (Guillot et al., 2008). Compounding these effects, MA decreases anti-oxidant enzymes (Jayanthi et al., 1998). MA also produces excitotoxicity and reactive nitrogen species (Yamamoto and Raudensky, 2008). MA acutely increases GLU levels in the striatum and hippocampus of rats, while MDMA only elicits a delayed response in the hippocampus (Nash and Yamamoto, 1992; Rocher and Gardier, 2001). The mechanism by which MA increases GLU levels is believed to be DA-mediated by activation of the DA D1-type receptor (D1R), not the GLU transporter (Kokoshka et al., 1998; Mark et al., 2004). Activation of the N-methyl-D-aspartate receptor (NMDAR) leads to the formation of nitric oxide, which reacts with superoxide to form the oxidant peroxynitrite. It is the MA-induced formation of the cytotoxic hydroxyl radicals and peroxynitrite in the striatum that leads to increased oxidative stress. This is followed by lipid peroxidation, protein damage, and fragmentation of the plasmalemmal membrane, all leading to DA terminal degeneration (McDonnell-Dowling and Kelly, 2017).

MDMA also increases free radicals and oxidative stress. MDMA induces free radical formation in the hippocampus and striatum of rats and mice, indicated by increased 2,3-DHBA (Colado and Green, 1994; Colado et al., 2001; Camarero et al., 2002). Conversely, the administration of anti-oxidants and spin trap agents diminish MDMA-neurotoxicity (Cadet et al., 1995; Colado and Green, 1995; Sanchez et al., 2003). Contributing to these cytotoxic products is the breakdown of monoamines by MAO-B to form H_2O_2, an effect blocked by the MAO inhibitor selegiline (Alves et al., 2007). The MDMA-induced increase in extracellular DA levels is implicated in 5HT terminal degeneration caused by oxidative stress. DA release is enhanced by 5HT activation of post-synaptic 5HT2AR, amplifying extracellular DA levels (Gudelsky and

Yamamoto, 2008). DA is taken into 5HT terminals by SERT, where it is auto-oxidized and metabolized to form DA quinones and free radicals (Sprague et al., 1998; Capela et al., 2009). Although MDMA metabolites cause oxidative stress leading to terminal degeneration, MDMA itself does not. MDMA is metabolized to form harmful ortho-quinones and glutathione in the periphery, which cross the blood brain barrier and are taken into 5HT terminals by SERT (Capela et al., 2009; Barbosa et al., 2014). Perfused directly into the hippocampus of rats, MDMA acutely increases 5HT release, but does not cause long-term 5HT depletion, unlike systemic administration (Esteban et al., 2001). Perfused into the striatum of mice, MDMA caused neither an acute increase in DA nor depletion a week later (Escobedo et al., 2005). Although oxidative stress is a main cause of amphetamine-induced neurotoxicity, there are other contributing factors, such as metabolic compromise and mitochondrial dysfunction. As these factors are not directly related to dysregulation of the DA system, they will not be covered here (for review, see: Capela et al., 2009; Krasnova and Cadet, 2009; Yamamoto et al., 2010).

Thermal response

MA and MDMA-induced changes to body temperature play a significant role in neurotoxicity. A hyperthermic increase in core body temperature following amphetamine administration is strongly correlated with monoaminergic fluctuations, increased ROS, and striatal terminal degeneration (Docherty and Green, 2010; Bowyer and Hanig, 2014). Neurotoxicity is also exacerbated when drugs are administered at elevated ambient temperatures (≥ 27 °C) and hyperthermia is increased (Carvalho et al., 2002; Miller and O'Callaghan, 2003; Raineri et al., 2015). Conversely, neuroprotection can be provided by sustained hypothermia, induced at lowered ambient temperatures at (≤ 15 °C) (Miller and O'Callaghan, 1995; Mueller et al., 2013), as well as by pharmacological blockade of hyperthermia using D2R antagonists (haloperidol, sulpiride), 5HT2AR antagonists (ketanserin), and other agents (Albers and Sonsalla, 1995; Capela et al., 2006; Docherty and Green, 2010).

The majority of amphetamine-induced neurotoxicity studies report hyperthermia, which creates a feedback loop as increased body temperature enhances neurotoxicity. This difficulty in parsing the specific neurotoxic effects of amphetamines from those that are temperature-dependent. However, the relationship between body temperature and neurotoxicity is not always linear. MA and MDMA-induced neurotoxicity still occurs under hypothermic conditions. Pre-treatment with the VMAT2 inhibitor reserpine prior to MA (10 mg/kg, 4 inj, 2 h apart) causes severe hypothermia, but increases neurotoxicity measured 7 days later, indicated by decreases in DA and TH levels (Albers and Sonsalla, 1995). MDMA (20 mg/kg, 3 inj, 3 h apart) can also induce mild hypothermia by itself under normothermic conditions while decreasing striatal DA levels 7 days later (O'Shea et al., 2001). Finally, a higher dose of MA (15 mg, 4 inj, 2 h apart) administered at a lowered ambient temperature of 13 °C, in which animals remained hypothermic, still decreases striatal DA and TH levels 7 days later (Bowyer et al., 2001). These results demonstrate neurotoxicity can occur independently of temperature increases. Hyperthermia may exacerbate neurotoxicity, but it is not required.

Amphetamines can also decrease body temperature on their own. This effect typically occurs in a biphasic pattern, where core body temperature decreases immediately following administration, reaching a nadir within the first hour followed by a subsequent increase in temperature. Acute hypothermia is observed following MA and MDMA administration at normothermic temperatures (18-23 °C) and at lower doses of MA (1-5 mg/kg) and MDMA (5-10 mg/kg) (O'Shea et al., 2001; Johnson et al., 2002; Harkness et al., 2015). By studying MA and MDMA without increasing body temperature above baseline, it is possible to isolate their neurotoxic effects, independent of the synergistic effects of hyperthermia on neurotoxicity.

3. Substituted Methcathinones

The rise of new psychoactive substances (NPS) has skyrocketed over the past decade with over 700 new substances identified (UNODC, 2017). Although this catchall phrase includes synthetic cannabinoids and designer hallucinogens, perhaps none are as well-known as “Bath

Salts," the infamous moniker given to substituted methcathinones. Originally sold as legal alternatives to MDMA, in 2011, the U.S. Drug Enforcement Administration emergency classified three substituted methcathinones as Schedule I controlled substances: 3,4-methylenedioxymethcathinone (methylone), 3,4 -methylenedioxypyrovalerone (MDPV), and 4-methyl-methylmethcathinone (mephedrone) (Fig. 1)(DEA, 2013). The prevalence of MDMA, methylone, and MDPV in the U.S. is an interesting case study on the interaction of the illicit drug market and legislation. The National Forensic Laboratory Information System (NFLIS) annually reports the number of drug cases submitted for forensic analysis. MDMA reports (21,553) peaked in 2010, the first year MDPV reports (271) were included, though methylone was not yet reported (NFLIS, 2010). In 2013, methylone reports (12,067) reached their zenith, while MDMA reports (4,798) sharply declined and MPDV reports (1,051) increased (NFLIS, 2013). The latest report, from 2016, shows a mild rise in MDMA reports (5,768), while methylone reports (189) drastically decreased and MDPV is no longer reported (NFLIS, 2018). For context, MA reports dwarf MDMA and methcathinones and have doubled during the same period from over 145,000 in 2010 to more than 300,000 in 2016. The rapid decline in MDMA reports after 2010 is attributed to the increased international efforts to regulate traditional chemical precursors for MDMA manufacture, leading to a decrease in purity and availability (Mounteney et al., 2018). This coincided with the advent of substituted methcathinones, of which methylone is most similar to MDMA (Schifano et al., 2017). The drugs existed in a gray market, sold in gas stations, smoke shops, and online as "bath salts" or "plant food" to escape regulation by the Food and Drug Administration (Madras, 2017). As such, they were easily procured and readily substituted for MDMA. However, in 2011 a new unregulated chemical precursor began to be used for manufacturing MDMA, which has increased the production and purity of MDMA (UNODC, 2017). Thus, the combination of classifying methylone and MDPV as Schedule I controlled substances and the increased availability of high-purity MDMA has swung drug consumption back towards MDMA. User reports that MDMA has more positive effects in

comparison to methylone or MDPV are also a likely contributing factor to this shift (Matthews et al., 2017; Sutherland et al., 2017).

While methylone and MDPV are both substituted methcathinones, their psychostimulant profiles differ: methylone is typically described as MDMA-like and MDPV as cocaine-like (Karila et al., 2015). Both have effects similar to psychostimulants: increased euphoria, energy, and alertness, accompanied by elevated heart rate, blood pressure and body temperature, but methylone also increases empathogenic feelings in a manner similar to MDMA (Gregg and Rawls, 2014; Karila et al., 2015). This is reflected in discrimination tasks, where rats substitute both methylone and MDPV for MA and cocaine, while only methylone substitutes for MDMA (Dal Cason et al., 1997; Gatch et al., 2013; Dolan et al., 2018). Acute “bingeing” and chronic use of methylone and MDPV have serious health dangers similar to MA, including seizures, cardiac failure, rhabdomyolysis and death (Schifano et al., 2017). The dangers of methcathinones are reflected in emergency department visit statistics. In 2011, near their peak in popularity, 22,904 methcathinone-related visits were reported, 67% involving combinations with other drugs, exceeding the number of visits involving MDMA that year (DAWN, 2013)**.** Despite the greater number of methylone users, MDPV is disproportionately responsible for reports of psychosis and fatalities (Vallersnes et al., 2016; Zaami et al., 2018). This is in part due to the compulsive nature of MDPV use. Using an intra-venous self-administration paradigm in rats, the effect of MDPV on drug-reinforced behavior is more potent and efficacious than cocaine or MA (Aarde et al., 2013; Schindler et al., 2015). In comparisons between methylone and MDPV, animals self-administer both methcathinones, but acquisition of methylone self-administration takes longer and only MDPV leads to escalation of intake following extended access (Watterson et al., 2012; Watterson et al., 2014). These same studies investigated the ability of the drugs to directly stimulate reward pathways using intra-cranial self-stimulation of the medial forebrain bundle. Similar differential effects occurred: MDPV reduced self-stimulation thresholds at low doses whereas methylone only did so at very high doses.

The pharmacology of methylone and MDMA supports the differential effects of the two drugs. Like MA and MDMA, methylone is a transporter substrate, acting as an inhibitor of neurotransmitter uptake at DAT, SERT, and the NE transporter (NET), while also inducing release of neurotransmitters *via* these plasmalemmal transporters (Baumann et al., 2013; Eshleman et al., 2013). Methylone, similar to MDMA, is more potent in releasing 5HT than DA at the respective transporters. Conversely, MDPV is a transporter inhibitor only, with no effect on release, similar to cocaine. MDPV is an incredibly potent inhibitor of DAT and NET, with affinity for both transporters greater than 10X cocaine, but little effect on SERT (Simmler et al., 2013a). A primary difference between both methcathinones and MA or MDMA is their affinity and potency at VMAT2. Unlike the amphetamines, methylone and MDPV are not substrates of VMAT2 with low affinity and potency at VMAT2 (Cozzi et al., 1999; Eshleman et al., 2013).

Methylone and MDPV do not induce dopaminergic neurotoxicity by themselves. However, there are very few animal studies investigating the neurotoxicity of these drugs (Table 2). Methylone (10, 20, or 30 mg/kg, 4 inj, 2 h apart) does not alter striatal DA, TH, DAT levels or GFAP expression 2 days later (Anneken et al., 2015). Another study reported methylone (25 mg/kg, 4 inj, 3 h apart) does not alter striatal DAT or GFAP 3 or 7 days after administration, although it transiently decreases DAT in the frontal cortex 3 days later (Lopez-Arnau et al., 2014). Using a chronic paradigm of methylone (30 mg/kg, twice daily for 4 days), there is no depletion of DA, DOPAC, or HVA two weeks following treatment (den Hollander et al., 2013). There is less research on the neurotoxicity of MDPV with only one known study using a neurotoxic binge-like regimen. This study reported no changes in DA, TH, or GFAP expression two days following the final administration, despite using a very high dose of MDPV (30 mg/kg) (Anneken et al., 2015).

Table 2. Summary of studies: effects of methcathinones and combinations with amphetamines on biomarkers of neurotoxicity in a mouse model

Drug	Dose (mg/kg)	Time points (days)	Measures	Notes	Reference
Mephedrone	20,40	2,7	- DA,TH,DAT,GFAP	Only 40 mg/kg tested at 7 days	Angoa-Perez *et al*., 2012
Methylone	25[a]	3,7	- TH,DAT,GFAP		Lopez-Arnau *et al*., 2014
MA	2.5,5	2	↓DA,TH,DAT	TH: unchanged by 2.5 mg/kg	Angoa-Perez *et al*., 2013
MDMA	20		↓DA,TH,DAT		
MA+mephedrone	2.5,5+20,40		↓↓DA,TH,DAT	Mephedrone potentiated all measures	
MDMA+mephedrone	20+20		↓↓DA,TH,DAT	Mephedrone potentiated all measures	
Methylone	20,30	2	- DA,TH,DAT,GFAP		Anneken *et al*., 2015
MDPV	20,30		- DA,TH,DAT,GFAP		
MA	2.5,5,10		↓DA,TH,DAT; ↑GFAP	TH: unchanged by 2.5 mg/kg	
MDMA	20		↓DA,TH,DAT; ↑GFAP		
MA+methylone	2.5+20,30		↓↓DA,TH,DAT; ↑↑GFAP	Methylone potentiated all measures	
MA+MDPV	2.5,5,10+20,30		- DA,TH,DAT,GFAP	Unchanged at all dose combinations	
MDMA+MDPV	2.5+20,30		- DA,TH,DAT,GFAP		

All experiments were conducted using a dose regimen of 4 inj, 2 h apart, administered in a normothermic environment (20-23 °C), and quantified in striatal tissue, unless noted. Arrows indicate significant differences between drug-treated animals and saline-treated controls. ↓: decreased; ↑: increased; -: no difference.

[a] dose regimen: 3 inj, 3 h apart.

The Kuhn laboratory has conducted the few published studies on the combination of amphetamines with methcathinones. The group first reported pre-treatment with the transporter substrate mephedrone potentiates the neurotoxic effects of amphetamines. Pre-treatment with varying doses of mephedrone (10, 20, or 40 mg/kg) prior to each injection of MA (2.5 or 5 mg/kg, 4 inj, 2 h apart) decreases striatal DA, TH, and DAT levels when compared to administration of MA by itself (Angoa-Perez et al., 2013b). The study also found mephedrone (20 mg/kg) pre-treatment has the same effect on MDMA (20 mg/kg, 4 inj, 2 h apart) and AMPH (5 mg/kg, 4 inj, 2 h apart). Investigating other combinations, the same group reported co-administration of various doses of methylone (10, 20, or 30 mg/kg) with MA (2.5 mg/kg, 4 inj, 2 h apart) also potentiates neurotoxicity, decreasing striatal DA, TH and DAT levels, while increasing GFAP expression, beyond the effects of MA alone (Anneken et al., 2015). However, co-administration of MDPV (20 or 30 mg/kg) with MA (2.5, 5, or 10 mg/kg, 4 inj, 2 h apart) or MDMA (20 mg/kg, 4 inj, 2 h apart) diminishes neurotoxicity, mitigating the DA, TH, and DAT level decreases and GFAP expression increase that MA and MDMA elicit alone. This is supported by previous research on combinations of amphetamines and DAT inhibitors. Pre-treatment with cocaine or GBR 12909 attenuates MDMA-induced neurotoxicity (decreases in DA levels) 7 days after administration (O'Shea et al., 2001; Peraile et al., 2013). Supporting this is evidence from a cellular experiment where MDPV, as well as methylphenidate and bupropion, diminish MA-induced [^{3}H]DA release (Simmler et al., 2013b).

Methylone and MDPV differentially regulate body temperature. Acute administration of methylone at doses of 25 or 30 mg/kg induces hyperthermia 45 min later (den Hollander et al., 2013; Lopez-Arnau et al., 2014). Another study found methylone induces hyperthermia 30 min following administration, albeit using a high dose of 60 mg/kg (Yingshan et al., 2015). This paper also investigated the impact of SERT and DAT on thermal response to methylone using transgenic SERT- and DAT-KO mice. Methylone-induced hyperthermia is potentiated in SERT-KO compared to SERT-WT mice, whereas methylone-induced changes in body temperature is

unaltered in DAT-KO mice, indicating 5HT may play a more significant role than DA in thermal response to methylone. The effects of a single bolus of MDPV have also been compared at different ambient temperatures (Fantegrossi et al., 2013; Gannon et al., 2018). At a normothermic ambient temperature of 20 °C, body temperature over a period of 10 h does not differ in mice receiving MDPV (1, 3, 10, or 30 mg/kg) from mice receiving saline. However, at an elevated ambient temperature of 28°C, MDPV dose-dependently increases body temperature, albeit without statistical difference due to within-group variability. The Kuhn group also reported thermal response to methylone and MDPV. Both methcathinones and MA induce hyperthermia by themselves, evidenced by an increase in body temperature of 2-3 °C (Anneken et al., 2015). When co-administered, methylone (30 mg/kg) potentiates MA-induced hyperthermia. However, MDPV (30 mg/kg) did not alter MA-induced hyperthermia indicating the neuroprotective effects of MDPV were temperature-independent.

The frequent co-ingestion of MDMA and methcathinones, both intentionally and unknowingly, highlights the importance of studying these drug combinations (Caudevilla-Galligo et al., 2013; Palamar et al., 2016). Co-ingestion is attributed to the majority of MDMA users being poly-drug users and the content of “ecstasy” tablets and powder varying in purity and adulterants, which often include methcathinones (Vogels et al., 2009; Fernandez-Calderon et al., 2018). However, due to the complexities of studying drug interactions in a physiological environment, there is a paucity of research on the topic. As such, the neurotoxic effects of these drug combinations require additional study to better understand their concomitant dangers.

4. TAAR1

The trace amine-associated receptor 1 (TAAR1) is a promiscuous g-protein coupled receptor (GPCR) activated by endogenous trace amines, such as beta-phenethylamine (β-PEA), tyramine, and tryptamine, as well as many exogenous amines, including the psychostimulant class of substituted amphetamines, such as MA and MDMA (Bunzow et al., 2001). The TAAR family of receptors was first identified and cloned by two groups at the same

time, working independently (Borowsky et al., 2001; Bunzow et al., 2001). Nine mammalian receptors have been identified and classified into three sub groups of TAAR1-4, TAAR5, and TAAR6-9, found across four primary mammalian species: human, chimpanzee, rat, and mouse (Lindemann et al., 2005). Although located on different chromosomes and bands in different species, the *Taar* gene family is found on a single chromosome over a small single band ranging in size from 100 to 250 kb. Only TAAR1 and 4 respond to trace amines and TAAR4 is limited to activation by β-PEA and tyramine. TAAR1 is the only receptor of the TAAR family sensitive to amphetamines; therefore this review will be limited in scope to TAAR1.

TAAR1 is distributed in many areas of the CNS: ventral tegmental area (VTA), striatum, SN, NAc, dorsal raphe nucleus, locus coeruleus, frontal cortex, hypothalamus, preoptic area, amygdala, nucleus of the solitary tract, parahippocampal area region, and subiculum (Borowsky et al., 2001; Xie et al., 2007; Lindemann et al., 2008; Espinoza et al., 2015a), as well as several areas in the peripheral system: pancreas, small intestine, stomach, testes, and thyroid, (Chiellini et al., 2012; Szumska et al., 2015; Raab et al., 2016). TAAR1 is also expressed in astrocytes and leukocytes, such as B, T, NK, and polymorphonuclear cells, but not in macrophages, bone marrow, or dendritic cells, (Nelson et al., 2007; Wasik et al., 2012; Babusyte et al., 2013; Cisneros and Ghorpade, 2014). Uncharacteristic of most GPCRs, TAAR1 is not located on the cell membrane, but is primarily expressed intracellularly, appearing as intracellular puncta (Bunzow et al., 2001; Xie et al., 2007). Biotinylation assays have revealed TAAR1 expression is associated with the total cellular membrane fraction, including cytosol, nuclear, and cytoskeleton compartments, but is notably lacking in expression on the cell surface membrane (Xie et al., 2008a).

Mechanisms of action

TAAR1 signals through both G protein-dependent and -independent signaling pathways although the underlying mechanisms and effects of the receptor are still being determined. Figure 3 provides a general schematic of proposed TAAR1 signaling, with the caveat that some

effects are still debated. As a G_S coupled GPCR, activation of the receptor stimulates adenylyl cyclase, increasing the conversion of cytosolic adenosine triphosphate (ATP) to cyclic adenosine monophosphate (cAMP), and leading to the initiation of the protein kinase A and C (PKA and PKC) signaling cascades (Borowsky et al., 2001; Bunzow et al., 2001; Xie and Miller, 2007). Activation of the receptor is predominantly measured *via* quantification of cAMP levels (Espinoza et al., 2013; Shi et al., 2016). TAAR1 activation also generates an inwardly rectifying K^+ current and activates Kir3 channels (Bradaia et al., 2009). Finally, TAAR1 activation modulates the G protein-independent ß-arrestin2-dependent protein kinase B (Akt)/glycogen synthase kinase-3 (GSK3ß) signaling pathway (Espinoza et al., 2015a; Harmeier et al., 2015). Trace amines are distributed throughout the peripheral and central nervous systems at concentrations several hundred-fold lower than classic monoamine neurotransmitters (Berry, 2004). Despite their low concentrations, ß-PEA and tyramine have affinity and potency at TAAR1 in the nanomolar range, whereas DA, 5HT, and NE are in the micromolar range (Bunzow et al., 2001; Lindemann et al., 2005; Simmler et al., 2016). Activation of TAAR1 has an inhibitory effect on the firing of dopaminergic neurons. ß-PEA and *p*-tyramine and the selective TAAR1 agonist RO5166017 inhibit DA neuron firing in the VTA and SN, measured by electrophysiology recordings (Geracitano et al., 2004; Lindemann et al., 2008; Revel et al., 2011). Conversely, application of the selective TAAR1 antagonist EPPTB (*N*-(3-Ethoxyphenyl)-4-(1-pyrrolidinyl)-3-(trifluoromethyl) benzamide) increases DA firing in the VTA. Transgenic *Taar1*-KO mice also have elevated spontaneous DA firing rates indicating the blockade or absence of TAAR1 has an overall excitatory effect (Lindemann et al., 2008; Bradaia et al., 2009). Measured using fast-scan cyclic voltammetry (FSCV), evoked DA release is diminished in brain slices from the NAc and striatum treated with the selective agonist RO5166017 and potentiated in slices from the NAc treated with EPPTB (Leo et al., 2014). These ligands modulate DA release in tissue from *Taar1*-WT mice only, with no effect on *Taar1*-KO tissue,

indicating their selectivity for TAAR1. These results demonstrate the inhibitory effect of TAAR1 activation on the DA system.

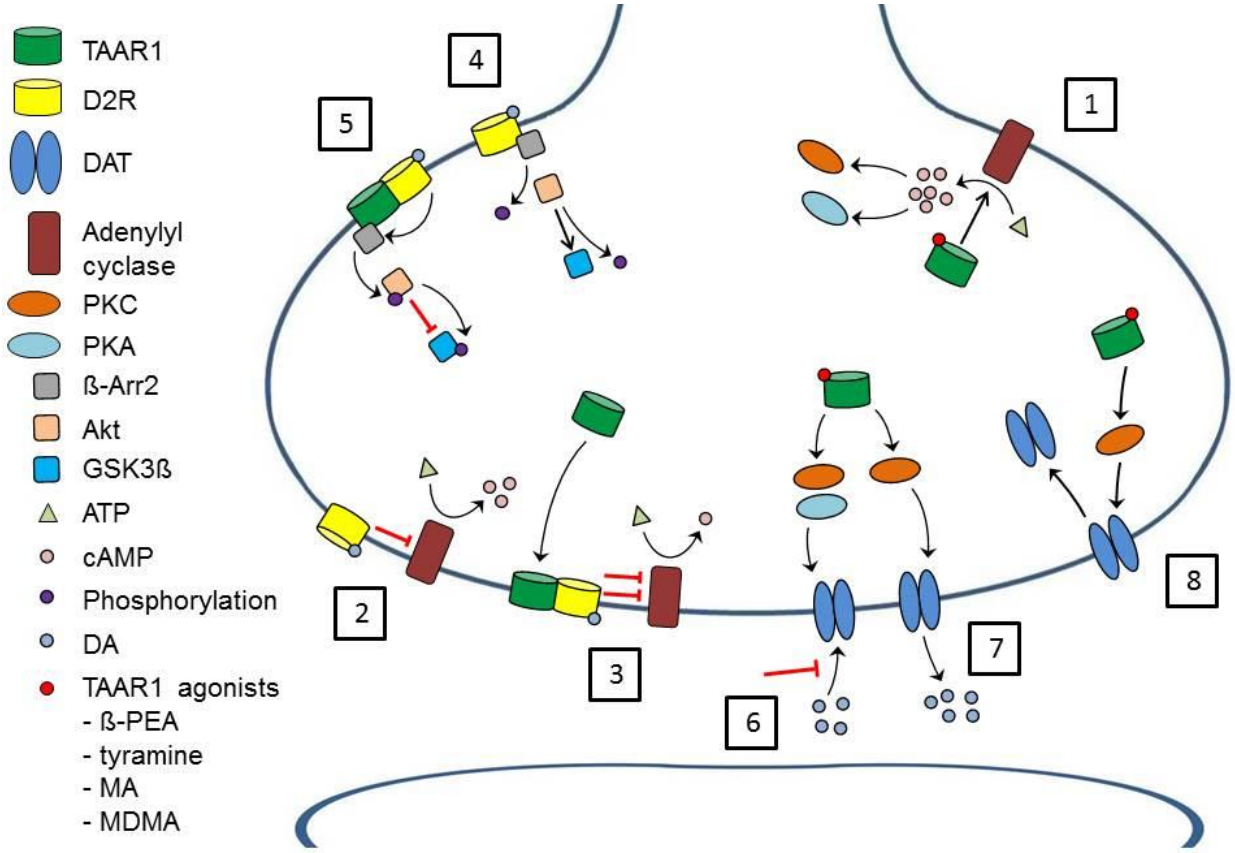

Figure 3. Schematic of TAAR1 signaling and related mechanisms within DA terminal. Activation of TAAR1 stimulates adenylyl cyclase increasing the conversion of ATP to cAMP and initiating the PKA and PKC signaling cascades (1). D2R activation inhibits adenylyl cyclase, decreasing cAMP production (2). TAAR1 translocates to the plasmalemmal membrane to form a heterodimer with D2R. Activation of the TAAR1-D2R heterodimer further inhibits adenylyl cyclase leading to less cAMP production (3). Active D2R recruits ß-Arr2, inactivating Akt through de-phosphorylation, leading to de-phosphorylation of GSK3ß and increased GSK3ß signaling (4). When TAAR1 and D2R form a heterodimer, TAAR1 recruits ß-Arr2 away from D2R, phosphorylating Akt, which inhibits GSK3ß signaling through phosphorylation (5). Activation of TAAR1 inhibits DA uptake by DAT, mediated by both the PKA and PKC signaling

pathways (6). Activation of TAAR1 increases DA release by DAT, mediated only by the PKC signaling pathway (7). Activation of TAAR1 leads to PKC-mediated internalization of DAT.

While TAAR1 modulation of the DA system is complex and not fully understood, much attention has focused on D2R, particularly pre-synaptic D2 autoreceptors. The D2R antagonist sulpiride blocks ß-PEA and tyramine inhibition of DA neuron hyperpolarization in the SN and VTA, whereas the DAT inhibitor cocaine does not, indicating specificity for the receptor and not the transporter (Geracitano et al., 2004). In an FSCV experiment using NAc brain slices, inhibition of DA release by the D2R agonist quinpirole is potentiated when combined with the TAAR1 agonist RO5166017, an effect absent in *Taar1*-KO mice (Leo et al., 2014). The D2R antagonist raclopride also inhibits striatal [^{3}H]DA uptake in *Taar1*-WT synaptosomes, an effect absent in *Taar1*-KO mice (Xie et al., 2008b). These results indicate not only are the inhibitory effects of TAAR1 D2R-dependent, but D2R autoinhibition is TAAR1-dependent.

Not all evidence supports the findings that TAAR1 activation increases D2R-mediated inhibition. In brain slices from *Taar1*-WT mice, application of quinpirole desensitizes DA neuron firing in the VTA and desensitization is blocked either in neurons pre-incubated with EPPTB or neurons from *Taar1*-KO mice (Bradaia et al., 2009). Additionally, the potency of quinpirole is increased in slices treated with EPPTB or from *Taar1*-KO mice. This implies D2R inhibition of DA neuron firing is increased in the absence of TAAR1. The authors postulate this may be a homeostatic method of DA firing regulation in the absence of TAAR1, but the results are not supported by other *in vitro* or *in vivo* findings and should be interpreted with caution.

In vitro cellular experiments have demonstrated a physical and functional interaction between TAAR1 and D2R. Although predominantly expressed intracellularly, TAAR1 and D2R can form a heterodimer, leading to increased cell membrane localization (Espinoza et al., 2011; Harmeier et al., 2015). Through G_i inhibitory signaling, activation of D2R decreases cAMP, in opposition to the effects of TAAR1. When TAAR1 and D2R are co-expressed, DA, ß-PEA, and

RO5166017 all produce less cAMP in comparison to when TAAR1 is expressed alone (Xie et al., 2008b; Espinoza et al., 2011; Harmeier et al., 2015). Co-application of the TAAR1 agonists with D2R antagonists, raclopride or sulpiride, results in equal cAMP production in TAAR1/D2R co-expressing and TAAR1 expressing cells, supporting G_i-dependent signaling. Besides the G_i-dependent pathway, TAAR1 also signals through the G protein-independent ß-arrestin2-dependent Akt/GSK3ß pathway. High levels of DA activate D2R leading to the recruitment of ß-Arr2, which inactivates Akt, disinhibiting GSK3ß (Beaulieu et al., 2011). Activation of TAAR1 in the presence of D2R diminishes GSK3ß by recruiting ß-Arr2 away from D2R (Harmeier et al., 2015). This study reported that in cells co-expressing TAAR1/D2R, tyramine and RO5166017 increases the recruitment of ß-Arr2 to activated TAAR1 with a concomitant decrease in recruitment to activated D2R. Conversely, recruitment of ß-Arr2 to TAAR1 is decreased when sulpiride is co-applied and in cells only expressing TAAR1, indicating recruitment is D2R-mediated. This translocation of ß-Arr2 from activated D2R to TAAR1 increases the phosphorylation of Akt and GSK3ß, silencing GSK3ß signaling. These findings indicate activation of TAAR1 not only enhances pre-synaptic D2R autoinhibition, but also prevents GSK3ß activation *via* dimerization with D2R. Enhanced GSK3ß signaling is associated with a hyperdopaminergic state, psychosis and increased locomotor activity (Li and Gao, 2011). Whether these findings from cellular experiments occur *in vivo* is yet to be determined.

An enhancement of post-synaptic D2R expression function also occurs in the absence of TAAR1. Basal striatal D2R levels are upregulated in *Taar1*-KO mice while pAkt and pGSK3ß levels are down-regulated (Espinoza et al., 2015a). Both of these factors enhance GSK3ß signaling at baseline in the absence of TAAR1. *Taar1*-KO mice also have an increased density of D2R in high-affinity states ($D2R^{High}$), which is correlated with DA supersensitivity, similar to GSK3ß signaling (Seeman et al., 2005; Wolinsky et al., 2007). To investigate the functional impact of this difference, locomotor activity (LMA) was measured following a high dose of quinpirole. Quinpirole has a biphasic locomotor response, diminishing locomotor activity through

activation of D2 autoreceptors at lower doses and promoting LMA through activation of post-synaptic D2R (Usiello et al., 2000; Gainetdinov et al., 2003). Quinpirole diminishes LMA in *Taar1*–WT mice and increases LMA in *Taar1*-KO mice (Espinoza et al., 2015a). These results illustrate the complex interaction between TAAR1 and D2R. While the inhibitory effects of pre-synaptic D2 autoreceptors are increased when TAAR1 is activated, the DA system is supersensitive in the absence of TAAR1. This is potentially due to post-synaptic D2R upregulation and signaling. It should be noted that D1R does not appear to interact with TAAR1. D1R levels are equivalent between *Taar1*-WT and –KO mice; LMA is equally increased in both genotypes by the D1R agonist SKF-82958; and the two receptors do not form a heterodimer (Espinoza et al., 2011; Espinoza et al., 2015a).

A significant body of *in vitro* research has investigated TAAR1 modulation of DAT, primarily by the Miller laboratory. The group demonstrated TAAR1 and DAT are co-expressed in a subset of DA neurons within the SN of both rhesus macaques and mice (Xie et al., 2007). Additionally, ß-PEA and tyramine release more cAMP in cells co-transfected with TAAR1 and DAT than in cells only transfected with TAAR1, indicating activation of the receptor is increased in the presence of DAT (Miller et al., 2005; Xie et al., 2007). As most TAAR1 agonists are transporter substrates and the receptor is predominantly expressed intracellularly, it is theorized the plasmalemmal transporters traffic agonists into cells, increasing TAAR1 activation. Functionality of DAT is also modulated by TAAR1 as application of DA inhibited [^{3}H]DA uptake and induced [^{3}H]DA release in TAAR1/DAT cells compared to cells only expressing DAT (Xie and Miller, 2007; Xie et al., 2008b). Downstream effects of TAAR1 activation may contribute to this impairment of DAT function. DA-evoked [^{3}H]DA uptake in TAAR1/DAT cells is PKA- and PKC-dependent as both PKA and PKC antagonists (H89 and RO-320432, respectively) block uptake inhibition (Xie and Miller, 2007). [^{3}H]DA release is specifically PKC-dependent as only the PKC inhibitor blocks release, indicating TAAR1 modulates the two DAT functions *via* separate pathways.

However, it has been argued the conduction of this research *in vitro* diminishes its validity. Administration of ß-PEA or the TAAR1 agonist RO5166017 diminishes hyperlocomotion in DAT-KO mice, indicating activation of TAAR1 functions independently of DAT (Sotnikova et al., 2004; Revel et al., 2011). This theory is bolstered by FSCV experiments. Evoked DA release and uptake, measured by Tau and half-life, are the same between genotypes. DA overflow is greater in the NAc of *Taar1*-KO than –WT mice, attributed to increased basal DA levels, but DA uptake is still the same between genotypes (Leo et al., 2014). Similarly, the partial TAAR1 agonist RO5203648 diminishes cocaine-induced DA overflow in the NAc without altering DA uptake, also indicating a DAT-independent mechanism (Pei et al., 2014). Further research is needed to better elucidate the interaction between TAAR1 and DAT.

Animal models

In 2007, two research groups independently created transgenic *Taar1*-KO mice: one using a mixed 129Sv x C57BL/6J genetic background (Wolinsky et al., 2007) and the other a congenic C57BL/6N background (Lindemann et al., 2008). The transgenic *Taar1*-KO mouse is the predominant animal model used to study TAAR1, as a TAAR1 antagonist that is viable for *in vivo* use has yet to be developed. *Taar1*-WT and -KO mice are equivalent on many baseline physiological and behavioral measures, such as body weight and temperature, viability, locomotor activity, elevated plus maze, and y-maze (Wolinsky et al., 2007; Lindemann et al., 2008). Biochemically, the two genotypes are equivalent in basal extracellular monoamine levels (DA, 5HT, and NE) in various regions of the brain (striatum, NAc, mPFC), measured by conventional *in vivo* microdialysis (Wolinsky et al., 2007; Lindemann et al., 2008; Di Cara et al., 2011). However, there are several baseline differences between genotypes, predominantly biochemical (Table 3). Using quantitative low perfusion rate (LPR) microdialysis, one study found basal DA levels in the NAc are elevated in *Taar1*-KO compared to *Taar1*-WT mice, though there are no differences in the striatum (Leo et al., 2014). Spontaneous firing of DA neurons in the VTA is decreased in *Taar1*-WT compared to –KO mice, indicating activation of

TAAR1 has an inhibitory effect on DA firing (Lindemann et al., 2008). Additional characterization, focusing on the corticolimbic DA system, found no differences between *Taar1*-WT and KO mice in mRNA expression of DAT, DA D1-5 type receptors, TH, and VMAT2 in the NAc, dorsal striatum, SN, VTA, and frontal cortex (Di Cara et al., 2011). An autoradiography experiment confirmed striatal DAT expression is equivalent across genotypes (Lindemann et al., 2008). However, another study found *Taar1*-KO mice have elevated D2R levels, most likely post-synaptic, in the striatum (Espinoza et al., 2015a). GluN1 (NMDAR subunit 1) is diminished in *Taar1*-KO compared to –WT mice in both the NAc and PFC (Espinoza et al., 2015b; Sukhanov et al., 2016). While there are few behavioral differences between the genotypes at baseline, *Taar1*-KO mice display a deficit in pre-pulse inhibition (PPI) accompanied by increased levels of D2R in a high affinity state, suggesting a potential model for positive symptoms of schizophrenia (Seeman et al., 2006; Wolinsky et al., 2007). However, the most notable difference between genotypes is that *Taar1*-KO mice, in comparison to their WT counterparts, have altered sensitive to many of the behavioral, physiological, and biochemical effects of amphetamines, as described in detail below. Besides *Taar1*-KO mice, a transgenic *Taar1* variation has been generated to overexpress TAAR1 (*Taar1*-OE) on a C57BL/6J background (Revel et al., 2012a). *Taar1*-OE mice have a similar baseline physiological and behavioral phenotype in comparison to *Taar1*-WT mice. However, basal levels of DA and NE in the NAc are elevated in *Taar1*-OE compared to *Taar1*-WT mice.

Table 3. Summary of studies: baseline differences within TAAR1 models.

Tissue	Measure	Method	*Taar1*-KO[a]	Reference
NAc	DA	microdialysis	↑	Leo *et al*., 2015
VTA	Spontaneous firing of DA neurons	Slice electrophysiology	↑	Lindemann *et al*., 2008
Striatum	D2R	mRNA/[^{3}H]spiperone saturation binding	↑	Espinoza *et al*., 2015
Striatum	$D2R^{high}$	[^{3}H]domperidone competition binding	↑	Wolinsky *et al*., 2007
-	PPI	Acoustic startle response	↓	
Striatum	GluN1 subunit of NMDA receptor	Immunoblot	↓	Suhkanov *et al*., 2015
PFC	GluN1 subunit of NMDA receptor	Immunoblot	↓	Espinoza *et al*., 2015a

Tissue	Measure	Method	*Taar1*-OE[a]	Reference
NAc	DA, NE	microdialysis	↑	Revel *et al*., 2012

Tissue	Measure	Method	MAHDR[b]	Reference
NAc	DA	microdialysis	↓	Lominac *et al*., 2014
	D2R	Immunoblot	↓	
	DAT	Immunoblot	↑	
	5HT	microdialysis	↑	
	SERT	Immunoblot	↑	
PFC	DA	microdialysis	↓	
	SERT	Immunoblot	↓	
NAc	GLU	microdialysis	↑	Szumlinsky *et al*., 2017
	EAAT3	Immunoblot	↓	
	mGlu5	Immunoblot	↑	
PFC	GLU	microdialysis	↑	Lominac *et al*., 2016
	mGlu2	Immunoblot	↓	
-	Total fluid intake	two-bottle choice	↑	Wheeler *et al*., 2009

This table reflects basal differences within TAAR1 models. All other traits measured are equivalent at baseline, for review, see Rutigliano et al., 2017 and Phillips et al., 2016. Arrows indicate significant differences between genotypes or lines, ↓: decreased, or ↑: increased.

[a] compared to *Taar1*-WT mice

[b] compared to MALDR mice

An alternative mouse model for studying TAAR1 is comprised of mice generated through bidirectional selective breeding for voluntary MA consumption. This model was developed by the Phillips laboratory as a means to investigate genetic effects on MA-related behaviors in a self-driven model, as opposed to operant self-administration or experimenter-administered models. Mice were selected from an F2 cross of C57BL/6J (B6) and DBA/2J (D2) mice using a two-bottle choice task to generate MA high drinking (MAHDR) and MA low drinking (MALDR) lines (Wheeler et al., 2009). The MA drinking (MADR) lines have been replicated 5 separate times with similar results (Phillips and Shabani, 2015). These replicate lines not only serve to avoid the increased inbreeding that occurs when a single line is maintained for a long period of time, but also demonstrate the robust and stable effects of selection for this trait. Using quantitative trait locus (QTL) mapping, a QTL was identified on chromosome 10 accounting for greater than 50% of the genetic variance between the MALDR and MAHDR lines (Belknap et al., 2013). Although the *Taar1* gene is expressed within the QTL on chromosome 10, the gene is equally expressed in both lines and was initially ignored. It was later discovered that the D2 progenitor mice possess a non-synonymous single-nucleotide polymorphism (SNP) that encodes a present, but non-functional TAAR1. MAHDR mice are homozygous for the D2 allele, whereas MALDR mice are either hetero- or homozygous for the dominant B6 allele that encodes a functional TAAR1 (Harkness et al., 2015; Shabani et al., 2016). The polymorphism found in the D2

mice was determined to originate from mice obtained from The Jackson Laboratory and arose sometime during 2001-2003 (Reed et al., 2018). Like the *Taar1* mouse model, MALDR and MAHDR mice have similar baseline physiological and behavioral phenotypes: body weight, temperature, locomotor activity, anxiety levels, and exploratory behavior, but with some differences (Table 3) (for review, see: Phillips and Shabani, 2015; Shabani et al., 2016). While conventional microdialysis found no difference in basal extracellular DA or 5HT levels in the NAc or mPFC, LPR microdialysis revealed DA levels are diminished in MAHDR compared to MALDR mice in both brain areas (Lominac et al., 2014). The same study also reported MAHDR mice have increased total DAT protein and decreased total D2R protein in the NAc. LPR microdialysis also found basal extracellular GLU levels in both the NAc and mPFC are elevated in MAHDR compared to MALDR mice indicating a hyperglutamatergic state at rest (Lominac et al., 2016; Szumlinski et al., 2017). The same studies investigated metabotropic glutamate receptors (mGlu), revealing the mGlu5 receptor is elevated in the NAc of MAHDR compared to MALDR mice, whereas in the PFC, mGlu2 is diminished in MAHDR mice. EAAT3 is also diminished in the NAc of MAHDR mice compared to MALDR mice, but not in the PFC.

The *Taar1* and MADR mouse models have distinct advantages and disadvantages. Transgenic *Taar1*-WT and –KO mice are isogenic lines differing only in the expression of the *Taar1* gene as the coding exon is either deleted or replaced in *Taar1*-KO mice (Wolinsky et al., 2007; Harkness et al., 2015). As a result, the TAAR1 protein is not expressed and the receptor is absent. Conversely, the selectively bred MADR mice are genetically heterogeneous lines developed for QTL mapping and the study of mechanisms associated with MA consumption and genetically associated traits. They possess greater genetic diversity, potentially associated with voluntary MA consumption (Belknap et al., 2013). As such, there are likely other genetic factors besides *Taar1* that contribute to differences in MA and other drug responses between the MALDR and MAHDR lines. There are also several

differences between models at baseline (Table 4): DA release in the NAc is increased in *Taar1*-KO compared to –WT mice, whereas it is decreased in MAHDR compared to MALDR mice and D2R is decreased, while DAT and SERT are increased, in the NAc of MAHDR compared to MALDR mice, but there is no difference between genotypes (Di Cara et al., 2011; Leo et al., 2014; Lominac et al., 2014).

Besides inter-model differences, there is also greater intra-model genetic variability in the MADR model, even for *Taar1*. While all *Taar1*-WT mice are genetically identical, their MALDR counterparts can be homozygous for the B6-*Taar1* allele or heterozygous for the B6- and D2-*Taar1* alleles. This is due to the dominant effect of the B6-*Taar1* allele on MA intake (Harkness et al., 2015). On the other hand, the *Taar1*-KO and counterpart MAHDR mice are all genetically identical at the *Taar1* locus, with the KO possessing the mutant KO allele, and the MAHDR mice homozygous for the D2-*Taar1* allele. However, the MADR model possesses greater face validity than the *Taar1* transgenic model. Similar to MAHDR mice, the *Taar1* gene is always present in humans, although some possess SNPs that render *Taar1* sub- or non-functional on a genetically heterogeneous background (Shi et al., 2015). This is in contrast to *Taar1*-KO mice where the gene and thus transporter are always absent. It should also be noted that while transgenic *Taar1* mice are genetically different only at the *Taar1* gene, there are several *Taar1*-KO mouse models in the literature that are generated from different backgrounds. Perhaps the most commonly used are *Taar1*-KO mice created from a 129Sv x C57BL/6J background, favored by the Miller and Gainetdinov labs (Wolinsky et al., 2007; Xie and Miller, 2009a; Espinoza et al., 2015a), and those created from a congenic C57BL/6N background used in most research by F. Hoffmann-La Roche (Lindemann et al., 2008; Revel et al., 2011). All experiments in this dissertation used *Taar1*-KO mice from the U.C. Davis Knockout Mouse Project (KOMP), generated from a C57BL/6N x BALBc background. These differences should be kept in mind when making comparisons with existing literature. Finally, like all models with genetic differences since

birth, there is the potential in both the transgenic and selected line model for developmental differences and compensation.

Pharmacological agents are also used to study TAAR1 in rodent models, both mice and rats. Several TAAR1 selective agonists and partial agonists have been developed, primarily by the pharmaceutical company F. Hoffmann-La Roche. Iterative structure modifications were made in search of ligands expressing high affinity and selectivity for TAAR1 with low metabolic turnover and favorable pharmacokinetic properties using a selective optimization of side activities approach originating with an α_{2a} adrenergic receptor agonist (Galley et al., 2016). This resulted in the identification of the selective TAAR1 selective agonists RO5166017 and RO5256390, as well as partial agonists RO5203648 and RO5263397, all with high affinity for mouse, rat, monkey, and human TAAR1 in the nanomolar range (Revel et al., 2011; Revel et al., 2012b; Revel et al., 2013). F. Hoffmann-La Roche employed a high throughput screening of their compound library to find a TAAR1 selective antagonist and identified benzanilides as a class of potential candidates before narrowing down to the compound EPPTB, technically an inverse agonist as it reduces cAMP levels (Stalder et al., 2011). While EPPTB has high affinity for the mouse TAAR1 (K_i = 0.9 nM), it has a lower affinity for rat TAAR1 (K_i = 0.9 µM) and weak affinity at the human TAAR1 (K_i > 5 µM). EPPTB is highly lipophilic with a high clearance rate. As such use of the TAAR1 antagonist has been predominantly limited to *in vitro* experiments in mouse tissue (Bradaia et al., 2009).

TAAR1 has been identified as a target for developing novel therapeutic agents to treat amphetamine abuse and addiction, as well as many other disorders. This is most evident in the amount of research the F. Hoffmann-La Roche has devoted to studying the receptor and developing TAAR1 agonists and antagonists. Scientists from F. Hoffmann-La Roche have collaborated with other researchers to publish over 40 TAAR1-related papers. Besides general characterization of the receptor, they have focused on TAAR1 interaction with

schizophrenia, bipolarity, depression, body weight control, pro-cognition, attention, nicotine, caffeine, and cocaine (Revel et al., 2011; Revel et al., 2012b; Revel et al., 2013; Pei et al., 2015; Schwartz et al., 2017; Liu et al., 2018).

Interaction with amphetamines

Substituted amphetamines were identified as potent activators TAAR1 during the initial characterization and cloning of the receptor (Bunzow et al., 2001). AMPH and MA have EC_{50} values in the nanomolar range and MDMA is in the low micromolar range (Simmler et al., 2016). The same study reported the rank order of affinity for TAAR1 is AMPH > MA > MDMA (K_i = 0.09, 0.55, 2.4 µM, respectively). Conversely, other psychostimulants, such as cocaine and substituted methcathinones, including methylone and MDPV, lack affinity for TAAR1 (K_i > 10 µM). Although amphetamines were identified as TAAR1 agonists, the modulatory role of TAAR1 on their effects remained undiscovered for several years until *in vitro* research revealed TAAR1 altered MA-induced [^{3}H]DA release and uptake (Xie and Miller, 2007; Xie et al., 2007). The advent of the *Taar1*-KO mouse model shortly thereafter reinforced the role of TAAR1 in modulating the effects of amphetamines: biochemical, physiological, and behavioral (Wolinsky et al., 2007; Lindemann et al., 2008).

Biochemical

Biochemical responses to amphetamines are altered when TAAR1 is activated (Table 4). Amphetamines elicit greater monoamine release when TAAR1 is not activated. Using *in vivo* microdialysis, a single dose of AMPH (2.5 and 2.9 mg/kg) increases DA, 5HT, and NE extracellular levels in the striatum of *Taar1*-KO mice compared to -WT mice (Wolinsky et al., 2007; Lindemann et al., 2008). MDMA (10 mg/kg) also increases extracellular levels of DA and 5HT levels in the striatum and NAc of *Taar1*-KO compared to –WT mice (Di Cara et al., 2011). However, these results have not been replicated in the MADR model using MA. In the NAc, MA (2 mg/kg) does not increase DA or 5HT levels in MALDR and MAHDR (Lominac et al., 2014). This is particularly surprising for DA levels, as lower doses of MA (1

mg/kg) increase DA levels in the NAc of C57BL/6 mice (Shin et al., 2009; Fujita et al., 2012). While MA increases DA levels in MAHDR compared to MALDR mice in the mPFC, MA does not increase DA levels above baseline in MALDR mice. Finally, MA does not increase NAc 5HT levels in either line and has an opposite effect in the mPFC where 5HT levels are increased in MALDR compared to MAHDR mice. While many of these results are at odds from findings in the *Taar1*-WT and –KO mice, they are potentially linked to differences in the biochemical basal phenotypes between the two models. MAHDR mice have lower basal DA levels and D2R expression in the NAc, whereas *Taar1*-KO mice have increased DA levels and D2R expression (Leo et al., 2014; Lominac et al., 2014; Espinoza et al., 2015a). MAHDR mice also have increased DAT levels in the NAc and decreased SERT in the mPFC, whereas there is no difference in transporter levels between *Taar1*-WT and –KO mice (Lindemann et al., 2008; Di Cara et al., 2011). Additionally, as MADR mice are selectively bred for MA consumption on a heterozygous background, there may be other genetic mutations affecting these biochemical characteristics outside of *Taar1*. The discrepancies may also be attributed to simple experimental factors, such as differences in drugs, dose, and brain regions. The *Taar1*-OE model provides an alternative perspective. At baseline, *Taar1*-OE mice have elevated basal DA and NE levels in the NAc compared to *Taar1*-WT mice (Revel et al., 2012a). Although a hyperdopaminergic state is typically associated with hyperlocomotion and other behavioral abnormalities, baseline behavioral phenotypes between *Taar1*-OE and –WT mice do not differ. When administered AMPH (2.5 mg/kg), extracellular DA or NE levels is increased in *Taar1*-WT mice as expected, but the levels are unaltered in *Taar1*-OE mice. Additionally, AMPH increases LMA in *Taar1*-WT more than the *Taar1*-OE mice, in which there is only a slight increase. As previous results indicate a hypersensitivity to amphetamines when TAAR1 is absent (Wolinsky et al., 2007; Lindemann et al., 2008), these results indicate there is a hyposensitivity to the effects of amphetamines when TAAR1 is overexpressed.

Table 4. Summary of studies: comparison within TAAR1 models of biochemical responses to amphetamines

Model	Drug	Dose (mg/kg)	Tissue	Measure	Method	WT	KO	Reference
Taar1-WT/KO	AMPH	2.9	Striatum	DA, NE	microdialysis	↑	↑↑	Wolinsky *et al*., 2007
	AMPH	2.5	Striatum	DA, NE	microdialysis	↑	↑↑	Lindemann *et al*., 2008
		2.5	Striatum	5HT		-	↑	
	MA	10^{-9}-10^{-5} M	Striatum	DA uptake	[^{3}H]DA uptake	↓	↓↓	Xie and Miller, 2009
		10^{-9}-10^{-4} M	Striatum	DA release	[^{3}H]DA release	↑	↑↑	
		10	PFC	DA		↑	↑↑	
	MDMA	7.5, 10	Striatum	DA, 5HT	microdialysis	↑	↑↑	Di Cara *et al*., 2011
		10	NAc	DA, 5HT		↑	↑↑	
		10	PFC	DA		↑	↑↑	

Model	Drug	Dose (mg/kg)	Tissue	Measure	Method	WT	OE	Reference
Taar1-WT/OE	MA	2.5	NAc	DA, NE	microdialysis	↑	-	Revel *et al*., 2012

Model	Drug	Dose (mg/kg)	Tissue	Measure	Method	MALDR	MAHDR	Reference
MALDR/MAHDR	MA	2	PFC	DA	microdialysis	-	↑	Lominac *et al*., 2014
		2	PFC	5HT		↑	-	
	MA	2	PFC	GLU	microdialysis	↓	-	Lominac *et al*., 2016
	MA	2	NAc	GLU	microdialysis	-	↑	Szumlinski *et al*., 2017

Model	Drug	Dose (mg/kg)	Tissue	Measure	Method	RO526337	Reference
Rats	MA	2	NAc	DA overflow	FSCV	↓	Pei *et al*., 2017

Arrows indicate significant differences between genotypes or lines. ↓: decreased; ↓↓: further decreased; ↑: increased; ↑↑ further increased; -: no difference.

The Miller laboratory has investigated TAAR1 modulation of MA effects at the DAT, similar to their *in vitro* research on TAAR1 and DAT. Supporting an interaction between TAAR1 and DAT, cells co-transfected with TAAR1 and DAT have greater activation of TAAR1 by AMPH, MA, and MDMA than cells only expressing TAAR1 (Miller et al., 2005; Xie et al., 2007). MA-induced [^{3}H]DA uptake inhibition and DA release are increased in both TAAR1/DAT co-transfected cells and *Taar1*-WT striatal synaptosomes in comparison to DAT transfected cells and *Taar1*-KO synaptosomes, respectively (Xie and Miller, 2007, 2009a). MA also induces DAT internalization in TAAR1/DAT cells and *Taar1*-WT mice, an effect absent in DAT cells and *Taar1*-KO mice, indicating the receptor is necessary for the trafficking of DAT from the cell membrane surface inward (Xie and Miller, 2009a). Acute DAT internalization following MA decreases [^{3}H]DA uptake and therefore may contribute to TAAR1 modulation of [^{3}H]DA uptake (Fleckenstein et al., 1997; Sandoval et al., 2001). The same study demonstrated TAAR1 mediation of MA impairment of DAT function is PKC-dependent, similar to previous work using DA as the TAAR1 agonist (Xie and Miller, 2007). The PKC inhibitor RO320432 blocks MA-induced inhibition of [^{3}H]DA uptake, [^{3}H]DA release, and DAT internalization. This is in accordance with previous research demonstrating PKC modulates these effects of MA (Zhang et al., 1997; Kantor and Gnegy, 1998; Boudanova et al., 2008). MA inhibition of [^{3}H]DA uptake is also blocked by the PKA inhibitor H89. While these findings indicate activation of TAAR1 modulates MA-induced impairment of DAT function, the same concerns raised above regarding *in vitro* results apply. Additionally, they suggest extracellular DA levels would increase following MA stimulation of TAAR1, whereas the opposite is true in microdialysis studies (Wolinsky et al.,

2007; Lindemann et al., 2008). Additional research is needed on the complex relationship between TAAR1 and DAT, particularly in the context of MA-induced neurotoxicity.

Although there is currently no published data confirming the interaction of TAAR1 with VMAT2, it has been speculated that TAAR1 resides on the vesicular membrane and may affect VMAT2 function (Bunzow et al., 2001; Xie et al., 2007; Rutigliano et al., 2017). This is predominantly due to the localization of TAAR1 on cytosolic membranes (Xie et al., 2008a). Intracellular localization of the receptor increases the likelihood of an interaction with VMAT2 and bypasses a common criticism of a TAAR1-DAT interaction: TAAR1 is only minimally expressed at the plasmalemmal membrane. MA impairment of VMAT2 function also increases extracellular DA levels, suggesting the transporter is a likely candidate for interaction with TAAR1 (Sulzer et al., 1995; Eiden and Weihe, 2011). TAAR1 mediation of VMAT2 function may also be indirectly mediated by D2R. In rats, D2R agonists quinpirole and pramipexole acutely increases striatal [^{3}H]DA uptake in the vesicular fraction and redistributes VMAT2, increasing immunoreactivity in the vesicular fraction without altering VMAT2 levels in the synaptosomal fraction (Truong et al., 2003; Truong et al., 2004). These effects were reversed when animals were pre-treated with the D2R antagonist eticlopride. Another potential link between TAAR1 and VMAT2 may occur by way of the PKC signaling cascade. MA-induced phosphorylation of PKA and PKC occurs in cells transfected with TAAR1, but is absent in the presence of EPPTB and in untransfected control cells (Panas et al., 2012). Pharmacological blockade of PKC by RO-320432 mitigates MA-induced inhibition of [^{3}H]DA uptake and [^{3}H]DA release in striatal synaptosomes from *Taar1*-WT mice, but not *Taar1*-KO mice, demonstrating an interaction between PKC and TAAR1 mediation of transporter function (Xie and Miller, 2009a). Independent of TAAR1 research, *in vitro* experiments demonstrated VMAT2 is phosphorylated at the N-terminus, selectively by PKC, but not PKA (Yao et al., 2004; Torres and Ruoho, 2014). PKC-dependent phosphorylation of VMAT2 also alters functionality of the transporter. 5HT sequestration is increased or decreased, dependent on phosphorylation site and serine

substitution (Torres and Ruoho, 2014). Based on these associations and the critical role of VMAT2 in MA-induced neurotoxicity, TAAR1 potentially modulates this neurotoxicity *via* VMAT2-dependent mechanisms.

Thermal response

While TAAR1 modulation of thermal response to amphetamines has not been widely investigated, existing research indicates activation of TAAR1 alters temperature response and contributes to amphetamine-induced acute hypothermia (Table 5). Under normothermic ambient conditions (20–23 °C), in both *Taar1*-WT and MALDR mice, MA (2 mg/kg) elicits hypothermia, reaching a nadir 30 min after administration, followed by an increase in body temperature (Harkness et al., 2015). This response is absent in both *Taar1*-KO and MAHDR mice, indicating activation of the receptor is necessary for MA-induced hypothermia. The same study examined the MA dose-response curve in MADR mice and found the hypothermic response to be most pronounced at lower doses. In MALDR mice, MA doses of 1, 2, and 4 mg/kg induces acute hypothermia 30 min following injection, but higher doses of MA (8 and 16 mg/kg) do not. All doses of MA induce hyperthermia in the MAHDR mice at this time point. Similar differences between genotypes are found in thermal response to MDMA (Di Cara et al., 2011). Thirty minutes following administration, the higher doses of MDMA (10 and 20 mg/kg) elicit hypothermia in *Taar1*-WT mice, while MDMA dose-dependently induces hyperthermia in *Taar1*-KO mice. MDMA (10 mg/kg) was also administered in an elevated temperature environment (27 °C). Under these conditions both genotypes exhibited hyperthermia, although the effect was more pronounced in *Taar1*-KO mice. These studies indicate the activation of TAAR1 is necessary for amphetamine-induced hypothermia and the absence of TAAR1 potentiates amphetamine-induced increases in body temperature. However, these experiments were all conducted using a single administration of drug. The effects of TAAR1 on changes in body temperature following a binge-like regimen of amphetamines remain to be explored.

Table 5. Summary of studies: comparison within TAAR1 models of acute thermal response to amphetamines

Model	Drug	Dose (mg/kg)	Ambient temp (°C)	WT	KO	Reference
Taar1-WT/KO	MDMA	10, 20	21	↓	↑	Di Cara *et al*., 2011
		10	27	↑	↑↑	
	MA	3	22	-	↑	Panas *et al*., 2012
	MDMA	25		↑	↑	
	MA	2	21	↓	-	Harkness *et al*., 2015

Model	Drug	Dose (mg/kg)	Ambient temp (°C)	MALDR	MAHDR	Reference
MALDR/MAHDR	MA	1, 2, 4	21	↓	-	Harkness *et al*., 2015
		8, 16	21	-	↑	

Arrows indicate significant differences in thermal response 30 min following first injection, relative to saline-treated control group. ↓: hypothermic decrease; ↑: hyperthermic increase; ↑↑ further hypothermic increase; -: no change in body temperature.

Behavior

TAAR1 modulates a variety of amphetamine-related behaviors (Table 6). Hyperlocomotion in response to a single dose of amphetamines is a traditional measure of psychomotor stimulant effects (Wise, 2004). Mitigation or enhancement of the effect, through genetic or pharmacological manipulation, provides insight into anatomical and underlying cellular mechanisms of psychostimulants, particularly with respect to the dopaminergic system, and the importance of DAT, D2R, and the mesolimbic pathway (Giros et al., 1996; Ikemoto, 2002; Kelly et al., 2008). The effect of TAAR1 activation on psychomotor stimulation is equivocal. Some research has reported low doses of AMPH, MA and MDMA elicit increased LMA in *Taar1*-KO compared to –WT mice (Wolinsky et al., 2007; Lindemann et al., 2008; Di Cara et al., 2011; Achat-Mendes et al., 2012). While these results indicate the absence of TAAR1 increases sensitivity to this effect of amphetamines, other studies report no difference in LMA between

Taar1-WT and –KO mice using similar doses and there are no reported differences between MALDR and MAHDR mice (Shabani et al., 2011; Sukhanov et al., 2016). A potential contributor to the discrepancies in results is the differences in backgrounds of the *Taar1*-KO vs. MADR mouse models. The lack of difference in MA effects on LMA between MALDR and MAHDR mice may be attributed to levels of MA-induced [^{3}H]DA release. Although DA levels have not been measured in the striatum, MA (2 mg/kg) does not increase DA levels in the NAc in either line (Lominac et al., 2014).

Table 6. Summary of studies: comparison within TAAR1 models of behavioral responses to amphetamines

Model	Drug	Dose (mg/kg)	Measure	Method	WT	KO	Reference
Taar1-WT/KO	AMPH	1	LMA	acute stimulation	↑	↑↑	Wolinsky *et al*., 2007
	AMPH	1, 2.5	LMA	acute stimulation	↑	↑↑	Lindemann *et al*., 2008
	MDMA	10	LMA	acute stimulation	↑	↑↑	Di Cara *et al*., 2011
	AMPH, MA	3	LMA	acute stimulation	↑	↑↑	Achat-Mendes *et al*., 201
		2, 3	LMA	repeated administration dose	↑	↑↑	
	MA	1	CPP	acquisition		sooner	
		1	CPP	retention during extinction	↑	↑↑	
	MA	2	CTA	acquisition	↑	-	Harkness *et al*., 2015
		20, 40 mg/l	2 bottle choice	voluntary drinking	-	↑	
	AMPH	2	LMA	behavioral sensitization: cue-induced and drug-primed	↑	↑↑	Sukhanov *et al*., 2016
		2	CPP	reinstatement	-	↑	

Model	Drug	Dose (mg/kg)	Measure	Method	WT	OE	Reference
Taar1-WT/OE	AMPH	2.5	LMA	acute stimulation	↑	-	Revel *et al*., 2012

Model	Drug	Dose (mg/kg)	Measure	Method	MALDR	MAHDR	Reference
MALDR/MAHDR	MA	0.5	CPP	acquisition	-	↑	Wheeler *et al*., 2009
		1, 2	CTA	acquisition	↑	-	
		20, 40 mg/l	2 bottle choice	voluntary drinking	-	↑	
	MA	0.5, 2, 4	CPP	acquisition	-	↑	Shabani *et al*., 2011
		0.5, 2, 4	CPA	acquisition (test day: drug-primed)	↑	-	
		4	LMA	behavioral sensitization	-	↑	
		20, 40 mg/l	2 bottle choice	voluntary drinking	-	↑	
	MA	2	CPA	acquisition (drug following conditioning)	↑	-	Shabani *et al*., 2012b
		1, 2	CTA	acquisition	↑	-	
	MA	20, 40 mg/l	oral SA	appetitive and consummatory behavior	↑	↑↑	Shabani *et al*., 2012a
		0.1-5 ug/infusion	ICV SA	consummatory behavior	↑	↑↑	
	MA	20, 40 mg/l	2 bottle choice	voluntary drinking	-	↑	Harkness *et al*., 2015

Table 6. Comparison within TAAR1 models behavioral responses to amphetamines (cont.)

Model	Drug	Dose (mg/kg)	Measure	Method	RO5203648	Reference
Rats	MA	0.75	LMA	behavioral sensitization	↓	Cotter *et al*., 2015
		0.05 infusion	SA, FR	consummatory behavior	↓	
					RO526337	
	MA	0.3, 1	LMA	behavioral sensitization	↓	Jing *et al*., 2014
		0.01, 0.03 infusion	SA, FR	consummatory behavior	↓	
		0.05 infusion	SA, FR	reinstatement: cue-induced and drug-primed	↓	
	MA	0.05 infusion	SA, PR	breakpoint	↓	Pei *et al*., 2017
		0.05 infusion	SA, PR	reinstatement	↓	

Arrows indicate significant differences between genotypes or lines. ↓: decreased; ↑: increased; ↑↑ further increased; -: no difference.

Behavioral sensitization to repeated administration of amphetamines is linked to the sensitization of incentive motivational properties, i.e. increased drug craving, as well as neuroadaptive changes (Vanderschuren and Kalivas, 2000). Following seven conditioning days of AMPH (2 mg/kg), AMPH-induced conditioned locomotion and context-dependent sensitization increases in *Taar1*-KO mice compared to *Taar1*-WT mice (Sukhanov et al., 2016). However, there are no differences in sensitization between genotypes during any of the 7 conditioning days. In the MADR model, where mice were administered the same dose of MA every other day for six trials, lower doses of MA (0.5 or 2 mg/kg) induce equal sensitization in both lines, while the highest dose of MA (4 mg/kg) elicits sensitization in MAHDR, but not MALDR mice (Shabani et al., 2011). As behavioral sensitivity to amphetamines is potentiated in *Taar1*-KO and MAHDR mice, the absence of TAAR1 activation may be correlated with increased drug-seeking behavior.

Drug-induced conditioned place preference (CPP), aversion (CPA), and conditioned taste aversion (CTA) are established behavioral methods used to measure the rewarding and aversive effects of amphetamines (Bardo and Bevins, 2000). Although specific methodologies vary, CPP is typically comprised of several conditioning days pairing administration of the drug with a particular context, such as a distinct flooring texture (e.g. grid), alternating with days where saline is administered and paired with a different floor texture (e.g. holes)(Cunningham and Noble, 1992; Cunningham et al., 2006; Davis and Riley, 2010). On the test day, following conditioning, animals are administered saline and provided access to both floor textures. CPP is acquired if more time is spent in the drug-associated context than the neutral context and indicates the rewarding effects of the drug. CPA is induced if significantly more time is spent in the neutral context and is indicative of the aversive effects of a drug. CPA can also be strengthened by administering a drug following conditioning sessions instead of prior (Fudala and Iwamoto, 1990). Another test of aversion, CTA typically pairs limited access to a novel tastant, such as NaCl, with administration of drug immediately following access (Cunningham

and Noble, 1992). Conditioning days are alternated with access to water. CTA is acquired if consumption of the novel tastant is significantly decreased over the conditioning trials. Both preference and aversion have been studied in the *Taar1*-KO model. In one study, AMPH (2 mg/kg) induced equal CPP in the 2 genotypes, but AMPH-induced reinstatement of CPP only occurred in *Taar1*-KO mice (Sukhanov et al., 2016). When conditioned with MA (1 mg/kg), *Taar1*-KO mice acquire MA-induced CPP earlier than *Taar1*–WT mice and retain MA-induced CPP longer during the extinction phase, although reinstatement occurrs in both genotypes (Achat-Mendes et al., 2012). In a CTA study, where MA was administered following a novel tastant, *Taar1*-WT mice readily acquire MA-induced CTA when conditioned with MA 2 mg/kg, whereas *Taar1*-KO mice do not exhibit MA-induced CTA and their consumption of the saline solution continued unabated (Harkness et al., 2015).

The rewarding and aversive effects of MA have been extensively studied in the MADR mouse model with robust differences. MA-induced CPP is exhibited by MAHDR mice at conditioning doses of MA (0.5, 2, and 4 mg/kg), but absent at all doses in MALDR mice (Wheeler et al., 2009; Shabani et al., 2011). In a CPA study, where MA was administered following each conditioning trial, MALDR mice conditioned with MA (2 or 4 mg/kg) exhibit MA-induced CPA, preferring the non-drug paired floor, while MA-induced CPA is only elicited by the higher conditioning dose of MA (4 mg/kg) in MAHDR mice (Shabani et al., 2012b). In CTA experiments, MALDR mice acquire MA-induced CTA when conditioned with MA (1 and 2) mg/kg. However, MAHDR mice fail to acquire MA-induced CTA at any conditioning dose of MA (1, 2, or 4 mg/kg) (Wheeler et al., 2009; Shabani et al., 2012b). These findings corroborate those in the *Taar1* mouse model, confirming the role of TAAR1 in modulation of MA rewarding and aversive effects.

Finally, true to their name, MAHDR mice orally and voluntarily consume more MA than MALDR mice (Wheeler et al., 2009; Shabani et al., 2011). Using a two-bottle choice task, MAHDR mice drink ~12x more MA than MALDR mice over an 18 h period. This disparity in MA

consumption has been replicated in the *Taar1* model, where *Taar1*-KO mice consume 6x more MA than *Taar1*-WT mice (Harkness et al., 2015). While the amount of MA consumed fluctuates between MAHDR and *Taar1*-KO mice, MALDR and *Taar1*-WT mice both drink similarly minimal amounts, rarely exceeding 0.5 mg/kg/18 h. Operant self-administration experiments have also been used to investigate the role of TAAR1 in MA reinforcement. In the MADR mouse model, this has been tested using both oral and intracerebroventricular (ICV) administration (Shabani et al., 2012a). MAHDR mice have higher appetitive and consummatory behavior than MALDR mice when orally presented with MA. Additionally, MAHDR mice acquire ICV MA self-administration, whereas MALDR mice do not, demonstrating increased sensitivity to the reinforcing effects of MA, while ruling out potential confounding effects of the taste of MA itself. As taste preference may influence oral consumption of MA, MALDR and MADR mice were also tested using tastant drinking tasks and there are no differences between lines for consumption of quinine (bitter) or saccharine (sweet) solutions (Wheeler et al., 2009).

MA self-administration has also been tested in rats using TAAR1 partial agonists: RO520648 (under a fixed ratio 1 (FR1) schedule) and RO5263397 (under an FR2 schedule) both block intravenous (IV) MA self-administration, but not saccharin (Jing et al., 2014; Cotter et al., 2015). RO526337 also reduces the break-point for MA self-administration using a progressive ratio schedule (Pei et al., 2017). Using multiple measures and methodologies, these studies demonstrate the rewarding, reinforcing, and motivational effects of amphetamines are potentiated when TAAR1 is not activated, while the aversive effects are diminished. This behavioral evidence indicates the risk of MA addiction is enhanced in the absence of TAAR1.

The summation of TAAR1 research indicates sensitivity to the effects of amphetamines is altered when TAAR1 is not activated: biochemically, physiologically, and behaviorally. Many of these findings are replicated in both *Taar1*-KO mice where the receptor is absent and MAHDR mice in which the receptor is present, but non-functional, in comparison to their *Taar1*-WT and MALDR mice counterparts. The convergence of these results strengthens the modulatory role of

TAAR1 as opposed to developmental differences. While there are discrepancies between certain findings, the majority of results point to an inhibitory effect of TAAR1 activation on underlying mechanisms and overt phenotypes associated with amphetamine abuse, addiction, and neurotoxicity.

However, the majority of research has examined the ability of TAAR1 to mediate the acute effects of amphetamines and there is no existing literature on the interaction between TAAR1 and neurotoxicity. To address this gap in research, my dissertation investigated the extent and underlying mechanisms through which TAAR1 mediates amphetamine-induced neurotoxicity. This novel research provides insight into the ability of TAAR1 to alter the effects of amphetamines at the molecular level after the drug has been cleared, investigating transient and sustained effects following administration. The ability of TAAR1 to modulate amphetamine-induced neurotoxicity indicates the receptor is a potential pharmacotherapeutic target for treatment of MA use disorder and addiction.

5. Dissertation studies

The overarching goal of this dissertation is to gain a better understanding of substituted amphetamine-induced neurotoxicity, with a focus on the TAAR1 receptor. I hypothesized activation of TAAR1 by amphetamines would diminish neurotoxicity. Using mouse models, I investigated induction of both transient and sustained neurotoxicity through quantification of neurotoxic biomarkers, modulation of neurotoxicity by activation of the TAAR1 receptor, and interactions of TAAR1 with monoaminergic transporters as potential mechanisms through which the receptor regulates amphetamine neurotoxicity. Finally, throughout all experiments, I examined the thermal response to these drugs and the effect of TAAR1 on this physiological measure.

First, I investigated the neurotoxic effects of MDMA and the substituted methcathinones, methylone and MDPV, alone or in combination (Chapter 2). In particular, I was interested in whether the combination of MDMA with different substituted methcathinones modulated MDMA-

induced neurotoxicity as these drugs are often co-ingested (Palamar et al., 2016). I chose two methcathinones based on their different mechanisms of action at DAT: methylone is a transporter substrate and MDPV is a transporter inhibitor (Eshleman et al., 2013). Previous work using similar drug combinations reported methcathinones that were transporter substrates potentiate amphetamine-induced neurotoxicity, whereas MDPV, a transporter inhibitor, ameliorates amphetamine-induced neurotoxicity (Angoa-Perez et al., 2013b; Anneken et al., 2015). I hypothesized the transient and sustained neurotoxic effects of MDMA would be increased when combined with the transporter substrate methylone and decreased when combined with the transporter inhibitor MDPV. I tested this hypothesis using a binge-like regimen of drug administration to mimic human drug use in a mouse model. I then quantified striatal biomarkers of neurotoxicity indicative of DA terminal degeneration (DA and TH levels) and astrocyte activation (GFAP expression) at time points indicative of transient and sustained neurotoxicity (2 and 7 days later). These markers, at these time points, are established indicators of amphetamine-induced neurotoxicity (O'Callaghan and Miller, 1994; McConnell et al., 2015). I was also interested in isolating any potential modulation of neurotoxicity independent of hyperthermia, which potently exacerbates neurotoxicity (Bowyer and Hanig, 2014). By administering the drugs in a normothermic temperature environment where hyperthermia was not induced, all neurotoxic effects, as well as modulation, were attributable to mechanisms independent of hyperthermia.

I next investigated TAAR1 modulation of MDMA-induced neurotoxicity and thermal response (Chapter 3). Activation of TAAR1 has an inhibitory effect on DA neuron firing (Lindemann et al., 2008). Additionally, sensitivity to many of the rewarding effects of amphetamines associated with drug use and addiction is increased when TAAR1 is not activated, such as AMPH- and MDMA-induced DA release, MA voluntary consumption, and MA-induced CPP (Wolinsky et al., 2007; Wheeler et al., 2009; Di Cara et al., 2011; Harkness et al., 2015). As such, I hypothesized MDMA-neurotoxicity would be increased when TAAR1 was not activated. Using the same

binge-like regimen, I quantified striatal DA levels and GFAP expression two days later as indicators of transient neurotoxicity. I used MALDR and MAHDR mice to examine the effects of TAAR1 activation on MDMA-neurotoxicity and methylone as a control due to its lack of affinity for TAAR1. Although *in vivo* AMPH-induced striatal DA release is increased in the absence of TAAR1 activation, *in vitro* MA-induced striatal DA release increases when TAAR1 is activated (Lindemann et al., 2008; Xie and Miller, 2009a). To determine whether the *in vitro* results were transferable to MDMA, I compared MDMA-induced DA release in *Taar1*-WT to –KO mice; hypothesizing release would also be greater when TAAR1 is activated. Finally, although I continued to pursue investigation of hyperthermia-independent neurotoxicity by conducting all experiments in a normothermic environment, I also wanted to investigate a thermal response pattern observed in Chapter 2. MDMA elicited a biphasic temperature pattern characterized by acute hypothermia after administration followed by an increase in body temperature. One study found this hypothermic response to MDMA is absent in *Taar1*-KO mice (Di Cara et al., 2011). Similar effects were also observed following MA administration where the hypothermic response is absent in *Taar1*-KO and MAHDR mice (Harkness et al., 2015). These results indicated TAAR1 activation may be responsible for the hypothermic response to amphetamines. As these studies all used a single dose of drug, I examined the effect 30 min following each of the four injections. I hypothesized the hypothermic response to MDMA would be absent when TAAR1 was not activated. I examined this in both the MADR and *Taar1* models to compare the effects of when the receptor is present, but inactive (MAHDR mice) and when the receptor is absent (*Taar1*-KO mice).

Due to difficulty inducing neurotoxicity with MDMA, the focus of my research pivoted to the more neurotoxic substance MA and TAAR1 modulation of its neurotoxic effects and thermal response (Chapter 4). MA robustly and consistently induces transient and sustained neurotoxicity (Angoa-Perez et al., 2013a; McConnell et al., 2015) in comparison to variable results with MDMA (Johnson et al., 2002; Fantegrossi et al., 2008). Similar to Chapter 3, I

hypothesized MA-neurotoxicity would be increased when TAAR1 was not activated. I used the same binge regimen with multiple doses of MA and expanded my biomarkers to include the monoamines and metabolites: DA, DOPA, HVA, 5HT, 5HIAA, and NE, as well as TH levels and GFAP expression, measuring them both 2 and 7 days later to investigate transient and sustained effects. I leveraged the *Taar1* mouse model to test whether MA-induced neurotoxicity would be increased when TAAR1 was not activated and absent, as opposed to when the receptor was activated. I also hypothesized the hypothermic response to MA would be absent when TAAR1 was not activated. Again, this was conducted in a normothermic environment to ensure all effects were hyperthermia-independent. I recorded thermal response and compared body temperature changes 30 min following each administration to examine the effect of TAAR1 activation on MA-induced acute hypothermia.

To better understand underlying mechanisms by which TAAR1 modulates MA-induced neurotoxicity, I examined how activation of the receptor altered biogenic amine transporters (Chapter 5). VMAT2 plays a significant role in the modulation of neurotoxicity as a regulator of intracellular DA levels (Fleckenstein et al., 2009). Impaired function and expression of VMAT2 increases MA-induced neurotoxicity (Fumagalli et al., 1999; Guillot et al., 2008). While there has been speculation of a TAAR1-VMAT2 interaction (Bunzow et al., 2001; Xie et al., 2007), there is currently no published data on their relationship. As a potential mechanism through which TAAR1 regulates MA-induced neurotoxicity, I hypothesized MA-induced impairment of VMAT2 function would be increased when TAAR1 was not activated.

Using the same binge-like regimen as previous chapters, I quantified VMAT2-mediated DA uptake in striatal tissue 24 h later in *Taar1*-WT and –KO mice. *In vivo* treatment with MA allowed for investigation of the interaction between TAAR1 and VMAT2 under physiological conditions following clearance of MA, but prior to terminal degeneration. VMAT2 experiments were conducted in fractionated tissue due to the heterogeneous distribution of VMAT2 across cellular compartments: synaptosomal, membrane-associated, and enriched vesicular fractions

(Scherman, 1986). VMAT2 found in whole synaptosomes can be separated into VMAT2 localized to membrane-associated vesicles and those found on cytosolic vesicles (Volz et al., 2007a). Transporter expression was also quantified following the same dosing regimen, using both TAAR1 mouse models: the transgenic *Taar1* and the selected line MAHDR models. VMAT2 binding is differentially expressed among fractions 24 h following MA administration, indicating trafficking of vesicles independent of terminal degeneration (Hogan et al., 2000; Ugarte et al., 2003). I hypothesized VMAT2 expression would be decreased when TAAR1 is not activated, but only in the vesicular fraction. To test this, I quantified VMAT2 expression in all three subcellular fractions of striatal tissue from *Taar1*-WT and KO mice and MALDR and MAHDR mice, 24 h following MA administration.

Not only does DAT regulate MA-induced neurotoxicity, but there is also evidence of a TAAR1 and DAT interaction, as the two are co-expressed in the SN (Xie et al., 2007).Several *in vitro* studies, predominantly using cellular models, indicate TAAR1 modulates DAT functionality as MA-induced striatal DA uptake inhibition and DA release is increased when TAAR1 is activated (Xie and Miller, 2007; Xie et al., 2008b; Xie and Miller, 2009b). However, these findings have not been replicated and other studies have reported amphetamines increase striatal extracellular DA release when TAAR1 is absent (Wolinsky et al., 2007; Lindemann et al., 2008; Di Cara et al., 2011). While VMAT2 function remains impaired 24 h following administration of MA, DAT function returns to baseline at this timepoint (Sandoval et al., 2001; Ugarte et al., 2003) and research on TAAR1 and DAT has been largely conducted *in vitro*. As such, I hypothesized *in vitro* treatment of MA would increase the impairment of DAT function when TAAR1 was not activated. To test this, I measured MA-induced DA uptake inhibition and DA release in striatal synaptosomes and homogenate from untreated*Taar1*-WT and -KO mice. I also quantified DAT expression in striatal synaptosomes from MA-treated *Taar1*-WT and –KO mice, as well as MALDR and MAHDR mice, using the same regimen used for VMAT2 expression. As MA decreases DAT expression 24 following administration, a measure that

corresponds with MA-induced neurotoxicity (Zhu et al., 2005; Bourque et al., 2012), I hypothesized DAT expression would be decreased when TAAR1 was not activated.

Finally, I investigated thermal response to MA in the MADR model to compare with *Taar1* mice. As both *Taar1* and MADR models responded similarly to MDMA in Chapter 2, and previous research reported similar responses in both models to a single administration of MA, I hypothesized I would replicate my findings from the *Taar1* model in the MADR model and the hypothermic response to MA would be absent when TAAR1 was not activated.

Chapter 2: The combined effects of MDMA and selected substituted methcathinones on measures of neurotoxicity

This chapter is adapted from the following publication:

Miner, N.B., O'Callaghan, J.P., Phillips, T.J., Janowsky, A (2017). The combined effects of 3,4 methylenedioxy-methamphetamine (MDMA) and selected substituted methcathinones on measures of neurotoxicity. Neurotoxicology and Teratology. 61, 74-81.

Acknowledgement: the analysis of striatal tissue for TH was conducted by James P. O'Callaghan.

1. Introduction

Co-ingestion of MDMA and methcathinones is common, due to poly-drug use and the practice of "cutting" street drugs with adulterants (Karila et al., 2016; Palamar et al., 2016). Although concurrent use of these drugs has been firmly substantiated through self-reporting, pill-testing, and emergency room visits (Caudevilla-Galligo et al., 2013; DAWN, 2013; Fernandez-Calderon et al., 2018), there remains a lack of research on the neurochemical effects of combining the two classes of substances. The goal of Chapter 2 was to investigate the neurotoxic profiles of two different substituted methcathinones, methylone and MDPV, both alone and in combination with MDMA. The two methcathinones have different mechanisms of action: methylone is a transporter substrate, whereas MDPV is a transporter inhibitor, and most selective for DAT. Both are not neurotoxic by themselves, but may modulate neurotoxicity in combination with amphetamines (Angoa-Perez et al., 2013b; Anneken et al., 2015). Following a binge-like regimen of the drugs by themselves or in combination, markers of neurotoxicity were

measured 2 days later to assess maximal, but transitory effects, as well as 7 days later to assess sustained effects. As MDMA is selective for damage to DA terminals in a mouse model and most severe in the striatum (O'Callaghan and Miller, 1994; Mueller et al., 2013), I quantified DA levels and its precursor enzyme TH in the striatal tissue of C57BL/6J mice. Additional indicators of neurotoxicity, markers of gliosis were also quantified: GFAP expression, an indicator of astrocyte activation, and [^{3}H]PK11195 binding to TSPO, an indicator of glial activation (O'Callaghan and Sriram, 2005; Chipana et al., 2006). [^{3}H]PK11195 binding was chosen to supplement GFAP protein quantification with a binding assay and investigate microglia activation as TSPO is expressed on both astrocytes and microglia (Kuhlmann and Guilarte, 2000).

MDMA-induced hyperthermia can confound the determination of the pharmacological effects of MDMA as it amplifies neurotoxicity (O'Shea et al., 2001; Miller and O'Callaghan, 2003). As such, the experiments were conducted in a normothermic environment, where hyperthermia was not induced, to assess temperature-independent effects of MDMA and its combination with methcathinones. Continuous monitoring of body temperature also provided thermal response data to each drug alone or in combination. I hypothesized that a combination of the two transporter substrates (MDMA and methylone) would have an additive neurotoxic effect, resulting in lower DA and TH levels and greater GFAP expression and [^{3}H]PK11195 binding, whereas a combination of a transporter substrate (MDMA) and a reuptake inhibitor (MDPV) would have a neuroprotective effect, mitigating the neurotoxic effect of MDMA.

2. Materials and Methods

2.1. Drugs and chemicals

Racemic MDMA, methylone, and MDPV hydrochloride were generously provided by the National Institute on Drug Abuse (NIDA) Research Resources Drug Supply program. All chemicals and reagents used to assay DA levels, as included in the Dopamine Research ELISA kit, were purchased from Rocky Mountain Diagnostics, Inc. (Colorado Springs, CO). The

materials used in the TH immunoassay have been described previously (Sriram et al., 2004; Sriram et al., 2006). All chemicals and reagents used to assay GFAP expression levels, as included in the GFAP ELISA kit, were purchased from EMD Millipore (Billerica, MA). [^{3}H]PK11195 (specific activity 82.7 Ci/mmol) was purchased from Perkin Elmer (Waltham, MA). All other reagents were obtained from standard commercial sources, unless otherwise noted.

2.2. Animal maintenance and housing

Adult female C57BL/6J mice were purchased from The Jackson Laboratory (Bar Harbor, ME), acclimated in the animal colony for a minimum of 7 days prior to experiments, and were tested at 11–15 weeks of age. Of the three most common mice strains (C57BL6, BALB/c and DBA/2), the C57BL/6 strain is most sensitive to the neurotoxic effects of amphetamines and frequently used in neurotoxicity research (Kita et al., 1998; Yu and Liao, 2000). Female mice are also often used in neurotoxic studies in order to avoid increased aggression and fights that occurs in males (Sokolov et al., 2004). The choice of female C57BL/6 mice also allowed for direct comparison to the amphetamine and methcathinone studies, which used the same gender and strain (Angoa-Perez et al., 2013b; Anneken et al., 2015).

Before experiment initiation, mice were group-housed in filtered acrylic plastic shoebox cages (28 cm×18 cm×13 cm; l ×w× h), fitted with wire tops. Cages were lined with either ECO-Fresh bedding (Absorption Corporation, Ferndale, WA) or Bed-O-Cob (The Andersons, Maumee, OH). Mice had free access to rodent chow (5LOD, 5.0% fat content, Purina Mills, St. Louis, MO) and water *ad libitum*. The colony room was maintained at an environmental temperature of 21 ± 1 °C with lights on a 12:12 h light:dark schedule, beginning at 0600 h. All procedures were approved by the VA Portland Health Care System's Institutional Animal Care and Use Committee and followed the requirements of the Guide for the Care and Use of Laboratory Animals. All efforts were made to minimize animal suffering, to reduce the number of animals used, and to use alternatives to *in vivo* techniques when available. All animals acclimated to the vivarium at least one week prior to testing.

2.4. Temperature recording

Two days prior to drug administration, mice were implanted with IPTT-300 temperature transponders from BioMedic Data Systems (Seaford, DE) to assess body temperature *via* telemetry. Animals were anesthetized with isoflurane (5% induction, 2.5% maintenance) and transponders were subcutaneously injected dorsally between the shoulders. On the day of drug administration, animals were weighed and transferred from group to individual cages to avoid temperature changes associated with interaction (e.g., huddling). After a 1 h acclimation period, temperature recording began and was measured every 15 min for 8 h. All experiments were conducted between 0700 and 1700 h. Temperatures were non-invasively recorded using the DAS-8001 reader console and smart probe from BioMedic Data Systems. Animals were removed from the cage and the smart probe placed within 5 cm of the embedded transponder to acquire temperature readings. The environmental temperature of the testing environment was 21 ± 1 °C. Although increased ambient temperature correlates with increased neurotoxicity, MDMA-induced neurotoxicity occurs at the temperature used (21 °C) (O'Shea et al., 2001; Peraile et al., 2013). This temperature was selected in order to differentiate neurotoxic effects of the drugs from those exacerbated by elevated environmental temperatures.

2.5. Drug treatment

Following the first temperature recording (baseline), each animal received four intra-peritoneal (i.p.) injections (same drug and dose for a particular animal) with a 2 h interval between injections. Fig. 4 outlines the protocol used in this and all neurotoxicity experiments. The seven treatment groups were: saline 0.9%, MDMA 15 mg/kg, methylone 20 mg/kg, MDPV 1 mg/kg, MDMA 30 mg/kg, methylone/MDMA 20/15 mg/kg combined, and MDPV/MDMA 1/15 mg/kg combined. An MDMA dose of 15 mg/kg was chosen for combination treatment groups as it decreases striatal DA levels without inducing fatalities (Sanchez et al., 2003; Johnson et al., 2004). MDMA is modestly more potent than methylone as a transporter substrate, whereas MDPV is 15 times more potent than MDMA as an uptake inhibitor at the DAT (Eshleman et al.,

2013). This rank order of potencies (MDPV>>MDMA> methylone) has been demonstrated behaviorally in rodents (Dal Cason et al., 1997; Gatch et al., 2013) and is reflected in estimates of human recreational doses: MDPV = 8-15 mg; MDMA = 75-[125] mg; methylone = 100-250 mg (Erowid, 2018). Single drug doses of methylone (20 mg/kg) and MDPV (1 mg/kg) were selected to approximate an equivalent dose to MDMA (15 mg/kg). Initial testing of drug doses on DA levels found MDMA 15 and 30 mg/kg decreased DA levels 2 days later, while methylone (20 mg/kg) and MDPV (1 mg/kg) did not (Supp. Fig. 1). All drugs were dissolved in 0.9% saline and injected in a final volume of 10 ml/kg. Mice were euthanized 2 or 7 days after the final drug treatment by cervical dislocation, followed by decapitation. The striatum was removed using blunt dissection, flash-frozen, and weighed prior to being stored at -70 °C until time of assay.

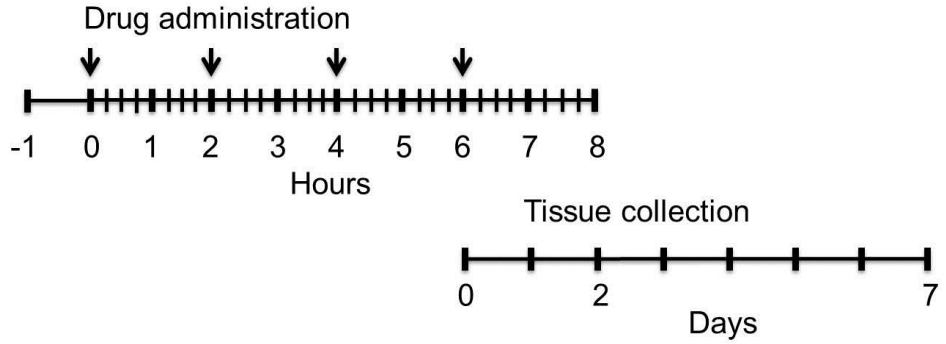

Figure 4. Binge-like model of neurotoxicity. Following 1 h habituation period, mice received 4 injections of the same drug and dose each time, spaced 2 h apart. Body temperature was collected *via* radio telemetry every 15 min for 8 h, beginning immediately prior to first injection. Animals were euthanized either 2 or 7 days following the final injection and striatal tissue collected, based on experiment.

2.6. Quantification of dopamine levels

Tissue was homogenized in a 1 mM EDTA, 4 mM metabisulfite, 0.01 N HCl solution**,** using a 5 mg/ml dilution, and sonicated for 30 s using a 2-mm ultra-sonification microprobe. Protein density was determined using the bicinchoninic acid (BCA) assay protocol (Thermo Fisher

Scientific, Waltham, MA). Striatal dopamine levels were quantified using a competitive enzyme-linked immunosorbent assay (ELISA) kit according to the manufacturer's instructions. 5 µl of tissue homogenate was used for DA analysis in duplicate. The amount of DA in the samples was calculated and expressed as nanograms DA per milligram total protein.

2.7. Quantification of tyrosine hydroxylase levels

Tissue was prepared as previously outlined (O'Callaghan, 2002). Striatal tissue was homogenized in 10 volumes of 1% hot (85-95 °C) sodium dodecyl sulfate (SDS) by sonification and the total protein concentration was determined by BCA assay. TH holoenzyme protein was assessed using a fluorescence-based ELISA developed in the laboratory (Sriram et al., 2004). In brief, a mouse anti-rat tyrosine hydroxylase monoclonal antibody (1:500; Sigma-Aldrich, St. Louis, MO) was coated on the wells of Immulon-2 microliter plates (Thermo Labsystems, Franklin, MA). The SDS homogenates and standards (prepared from control mouse striatum) were diluted in phosphate-buffered saline (pH 7.4) containing 0.5% Triton X-100. After blocking non-specific binding with 5% non-fat dry milk, aliquots of the homogenate and standards were added to the wells in duplicate and incubated. Following washes, a rabbit anti-rat TH polyclonal antibody (1:500; Calbiochem, San Diego, CA) was added to 'sandwich' the TH protein between the two antibodies. The amount of sandwich antibody bound to TH was then detected using a peroxidase-labeled antibody directed against rabbit IgG (1:3000; Artisan Technology Group, Champagne, IL. Peroxidase activity was detected using the fluorogenic substrate Quantablu (Thermo Fisher Scientific, Waltham, MA), which has excitation and emission maxima of 325 and 420 nm, respectively (read at 320/405 nm). The amount of TH in the samples was calculated and expressed as micrograms TH per milligram total protein.

2.8. Quantification of GFAP expression

Tissue homogenate for GFAP analysis was prepared in the same manner as for TH analysis. Striatal GFAP levels were quantified using a sandwich ELISA kit (EMD Millipore, Billerica, MA) according to the manufacturer's instructions. 100 µl of tissue homogenates, in

duplicate, were used for GFAP analysis against a standard curve using a GFAP standard provided by the manufacturer.

2.1. [^{3}H]PK11195 binding

A modified version of the [^{3}H]PK11195 saturation binding assay was conducted as previously described (Fantegrossi et al., 2008). Each sample consisted of pooled striata from 4 animals of a given treatment group homogenized with 20 ml of homogenizing buffer (5 mM Tris-HCl, 329 mM sucrose, and 1 µl/ml CalBioChem Protease Inhibitor Cocktail Set III (EMD Millipore), pH 7.4), using a Polytron homogenizer with a 7 mm dispersing unit, set at 1/3 maximum speed. Following homogenization, samples were centrifuged at 15,000 x *g* for 30 min at 4 °C. The supernatant was discarded and the pellet further refined by re-suspension in fresh homogenizing buffer followed by 10 strokes in a glass-glass homogenizer before being centrifuged again at 15,000 x *g* for 30 min at 4 °C. The supernatant was discarded, and the pellet was re-suspended in 6 ml of holding buffer (50 mM Tris–Base,120 mM NaCl, and 5 mM KCl, pH 7.4). The protein density of each sample was determined by BCA assay, followed by dilution to a final concentration of 1 µg of protein/2 µl, and then frozen at -70 °C until time of assay. A six-point saturation binding curve was generated for each treatment group in order to determine the B_{max} and K_D values. Concentrations of [^{3}H]PK11195 ranging from 0.1 to 9.0 nM were mixed in holding buffer. Specific binding was defined as the difference between binding observed in the presence (total binding) and absence (non-specific) of 10 µM RO5-4864 (4'-chlorodiazepam). Preliminary investigations indicated that optimal assay conditions included 75 µg of tissue protein and an incubation time of 2 hours (Supp. Fig. 2). In addition, a test of adherence of radioactivity to experimental surfaces (96 well plate, plastic Eppendorf tube, or a borosilicate glass test tube) over time was initially conducted using a low concentration of [3H]PK11195 of 0.08 nM (Supp. Fig. 3A). Radioactivity was added to the different containers and a 5 µl sample was withdrawn and added to a filter. Three hours later, another sample was removed and added similarly. Scintillation fluid was added and the filters counted. A later test

was conducted in plastic Eppendorf tubes using higher concentrations of 0.25 to 6 nM using the same 3 h interval (Supp. Fig. 3B).

[^{3}H]PK11195 binding, conducted with triplicate determinations, was characterized by at least three independent experiments. 50 µl of RO5-4864 were added to non-specific binding wells before 150 µl of protein were added to all wells and pre-incubated for 10 min. 50 µl of [^{3}H]PK11195 and holding buffer were added to bring all wells to a total volume of 500 µl. Samples were incubated for 120 min at 4 °C. Incubation was terminated by filtration using FiltermatA filters (Perkin Elmer) pre-soaked in 0.05% polyethyleneimine and a Tomtec 96-well cell harvester (Camden, CT), washed with ice-cold holding buffer. Scintillation fluid (25 µl) was added to each filter spot and radioactivity remaining on the filters was determined using a microbeta scintillation counter (Perkin Elmer).

2.9. Data analysis

One-way analysis of variance (ANOVA) was used to test the significance of drug treatment on striatal DA, TH levels, and GFAP expression at each time point, independently. Dunnett's multiple comparison test was used for follow-up mean comparisons with the saline group. Non-linear curve-fitting analysis was used to analyze the saturation curves of [^{3}H]PK11195 binding to determine the B_{max} and K_D values. One-way ANOVA was performed to test the significance of drug treatment on the B_{max} and K_D values of [^{3}H]PK11195 binding**,** using Dunnett's multiple comparison test for follow-up mean comparisons with the saline group. A two-way repeated measures ANOVA was performed to test the change in radioactivity counts over time with Bonferroni post-hoc tests. Mouse temperature data at each time point, grouped by drug treatment, were analyzed using a two-way repeated measures ANOVA. To follow up significant drug group x time interactions and examine the specific effects of each drug, data for each drug group were compared to the saline group data, using separate repeated measures ANOVAs, followed by Bonferroni's multiple comparison test for mean comparisons at individual time points. Overall temperature change for comparison of drug effects was assessed by subtracting

the mean temperature 15 min after the first injection (selected because maximal hypothermic effects were elicited at this time point) from the final mean temperature at the 8 h time point for each treatment group and analyzed by one-way ANOVA, using Dunnett's multiple comparison test for follow-up mean comparisons with the saline group. Data were analyzed for outliers using Dixon's Q test at 90% confidence. All statistical analyses were performed using Prism v.6.04 (GraphPad Software, La Jolla, CA). Differences were considered significant at $p < 0.05$.

3. Results

3.1. Dopamine levels

A main effect of drug group on DA levels (Fig. 5) was found in the striatum 2 days after drug treatment ($F_{6,48} = 4.09$, $p < 0.01$). *Post hoc* analysis revealed that only the MDMA 30 mg/kg group had significantly decreased DA levels in comparison to the saline group. There was also a main effect of drug 7 days after drug treatment ($F_{6,48} = 3.81$, $p < 0.01$), but none of the drug groups differed significantly from the saline group for DA level.

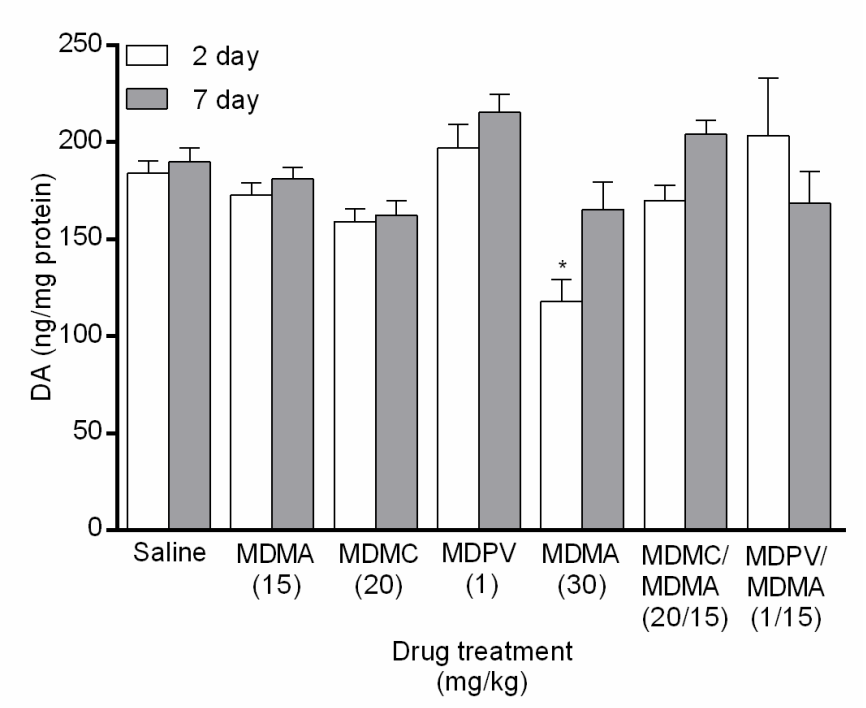

Figure 5. Striatal DA levels measured 2 and 7 days following treatment. Groups of mice received 4 i.p. injections of the same drug/dose (saline; MDMA 15 mg/kg; methylone (MDMC) 20 mg/kg; MDPV 1 mg/kg; MDMA 30 mg/kg; methylone (MDMC)/MDMA 20/15 mg/kg combined; or MDPV/MDMA 1/15 mg/kg combined), 2 h apart, and were euthanized either 2 or 7 days later for striatal tissue collection. DA values were normalized to the amount of protein in each tissue sample. Data represent mean ± SEM of 7-8 mice for each of the 14 treatment groups. *: $p < 0.05$ compared to the saline group (Dunnett's *post hoc* test).

3.2. Tyrosine hydroxylase levels

A main effect of drug group on TH levels (Fig. 6) was found in the striatum 2 days after drug treatment ($F_{6,39} = 2.40$, $p < 0.05$). *Post hoc* analysis revealed that only the MDMA 30 mg/kg group had significantly decreased TH levels in comparison to the saline group. There was also a main effect of drug 7 days after drug treatment ($F_{6,42} = 2.56$, $p < 0.01$), but none of the drug groups differed significantly from the saline group for TH level.

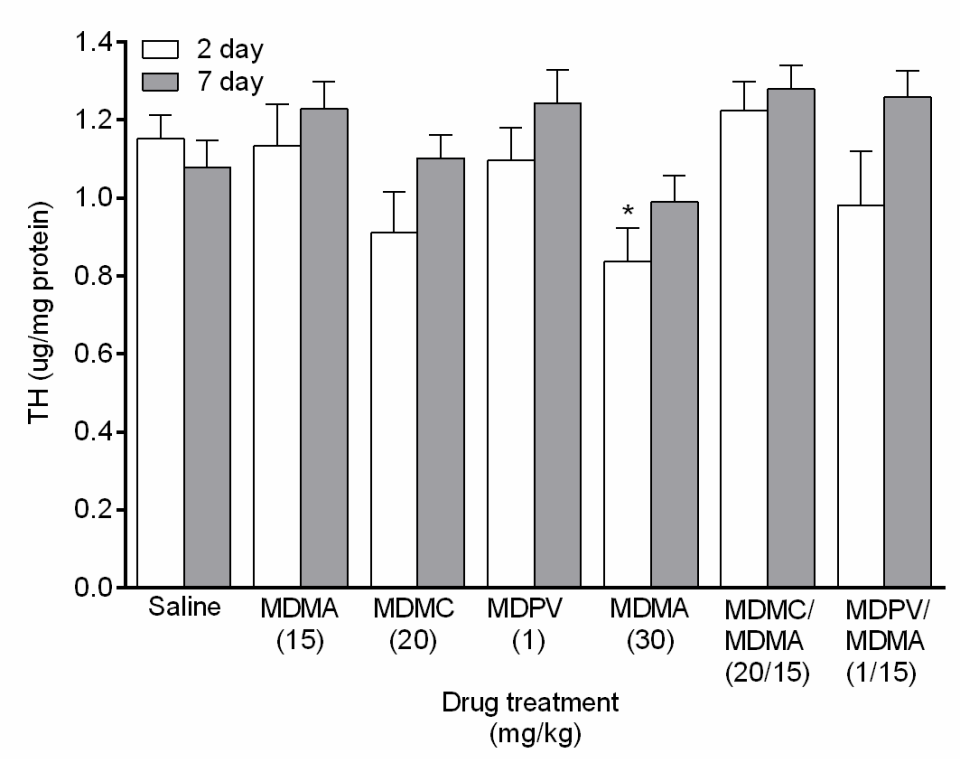

Figure 6. Striatal TH levels measured 2 and 7 days following treatment. Groups of mice received 4 i.p. injections of the same drug/dose (saline; MDMA 15 mg/kg; methylone (MDMC) 20 mg/kg; MDPV 1 mg/kg; MDMA 30 mg/kg; methylone (MDMC)/MDMA 20/15 mg/kg combined; or MDPV/MDMA 1/15 mg/kg combined), 2 h apart, and were euthanized either 2 or 7 days later for striatal tissue collection. TH values were normalized to the amount of protein in each tissue sample. Data represent mean ± SEM of 7-8 mice for each of the 14 treatment groups. *: $p < 0.05$ compared to the saline group (Dunnett's *post hoc* test).

3.3. GFAP expression

A main effect of drug group on GFAP expression (Fig. 7) was found in the striatum 2 days after drug treatment ($F_{6,49} = 11.78$, $p < 0.0001$). *Post hoc* analysis revealed that GFAP expression was significantly increased only in the two drug groups that received MDMA alone, compared to the saline group. There was also a main effect of drug 7 days after drug treatment ($F_{6,49} = 5.47$, $p < 0.001$), but again, none of the drug groups differed significantly from the saline group.

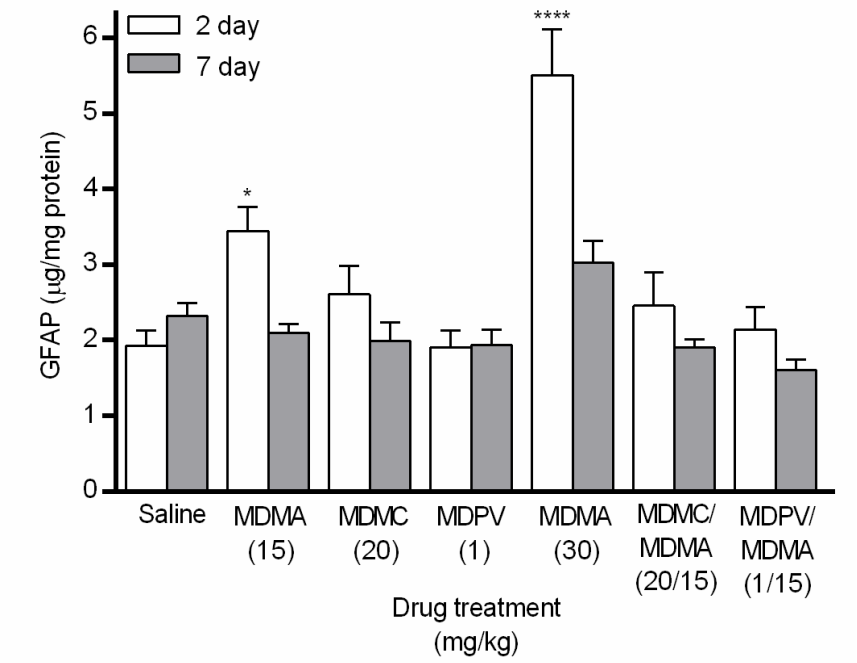

Figure 7. Striatal GFAP expression measured 2 and 7 days following treatment. Groups of mice received 4 i.p. injections of the same drug/dose (saline; MDMA 15 mg/kg; methylone (MDMC) 20 mg/kg; MDPV 1 mg/kg; MDMA 30 mg/kg; methylone (MDMC)/MDMA 20/15 mg/kg combined; or MDPV/MDMA 1/15 mg/kg combined), 2 h apart, and were euthanized either 2 or 7 days later for striatal tissue collection. GFAP values were normalized to the amount of protein present in each tissue sample. Data represent mean ± SEM of 8 mice for each of the 14 treatment groups. *: $p < 0.05$, ****: $p < 0.0001$ compared to the saline group (Dunnett's *post hoc* test).

3.1. [^{3}H]PK11195 binding

Saturation binding analysis was conducted in each fraction to determine the B_{max} and K_D values for [^{3}H]PK11195 binding (Fig. 8, Table 7). There was a main effect of drug group for K_D values of [^{3}H]PK11195 binding in the striatum 2 days following the final injection ($F_{6,16} = 2.85$, $p < 0.05$). *Post hoc* analysis revealed that K_D values 2 days after the final injection were significantly increased in the MDPV 1 mg/kg group ($p < 0.05$) in comparison to the saline group. None of the other drug groups differed significantly from the saline group for K_D values. There was no main effect of drug group for K_D values 7 days following injection or for the B_{max} at either 2 or 7 days later ($p > 0.05$).

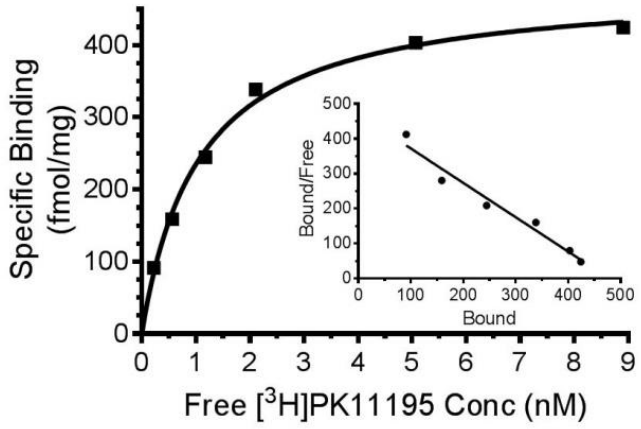

Figure 8. [^{3}H]PK11195 saturation binding in striatal tissue. Mice received 4 i.p. injections of saline or drug treatment, 2 h apart, and were euthanized 2 or 7 days following the final injection. Striatal tissue from 4 mice was pooled and values normalized to the amount of protein in each sample. Experiments were conducted as described in the text. Shown is a representative saturation curve. Inset: Scatchard transformation of [^{3}H]PK11195 binding data.

Table 7. [^{3}H]PK11195 binding in striatal tissue

Drug group (mg/kg)	B_{max} (fmol/mg protein) ± SEM		K_D (nM) ± SEM	
	2 day	7 day	2 day	7 day
Saline	385 ± 52	487 ± 98	0.94 ± 0.02	1.38 ± 0.25
MDMA (15)	500 ± 64	492 ± 45	1.56 ± 0.26	1.28 ± 0.22
MDMC (20)	451 ± 25	364 ± 64	1.79 ± 0.17	1.30 ± 0.52
MDPV (1)	501 ± 53	600 ± 69	2.79 ± 0.53[a]	2.86 ± 0.85
MDMA (30)	442 ± 88	440 ± 53	1.07 ± 0.37	1.40 ± 0.28
MDMC/MDMA (20/15)	492 ± 30	554 ± 28	2.38 ± 0.66	2.53 ± 0.73
MDPV/MDMA (1/15)	419 ± 38	413 ± 52	1.10 ± 0.13	1.49 ± 0.18

Data represent the mean ± SEM of 3-4 independent experiments. *a*: $p < 0.05$ compared to the saline group (Dunnett's *post hoc* test).

Thermal response

Following acclimation and immediately prior to the first injection, the mean baseline temperature of all animals was 38.4 °C (SEM = 0.04 °C**),** and there was no significant between-group difference. Temperature data (Fig. 9) analyzed using a two-way repeated measures ANOVA, revealed a significant drug group x time interaction ($F_{192,1568} = 19.31$, $p < 0.0001$). Examination of each drug group, in comparison to the saline group, revealed a significant drug group x time interaction for 5 of the 6 drug groups: MDMA 15 mg/kg ($F_{32,448} = 42.98$, $p < 0.0001$), MDMA 30 mg/kg ($F_{32,448} = 24.51$, $p < 0.0001$), methylone 20 mg/kg ($F_{32,448} = 32.01$, $p < 0.0001$), methylone/MDMA 20/15 mg/kg ($F_{32,448} = 32.32$, $p < 0.0001$), and MDPV/MDMA 1/15 mg/kg ($F_{32,448} = 39.38$, $p < 0.0001$). These five groups displayed a biphasic temperature pattern:

an acute temperature decrease immediately after drug injection followed by an increase in temperature until the next dose was administered. To statistically investigate the data, *post hoc* comparisons were performed between each drug group and the saline group, but only at the 15 min and 2 h time-points following each of the 4 injections (Table 8). Analyses were limited to these 8 time-points based on maximal temperature effects and to decrease error inflation associated with multiple comparisons. The MDPV 1 mg/kg group (Fig. 9E) did not display the temperature pattern elicited by other drug treatments (Fig. 9A-D and F), as it paralleled the saline group. No further analysis was conducted for this drug group, as there was no significant drug x time interaction.

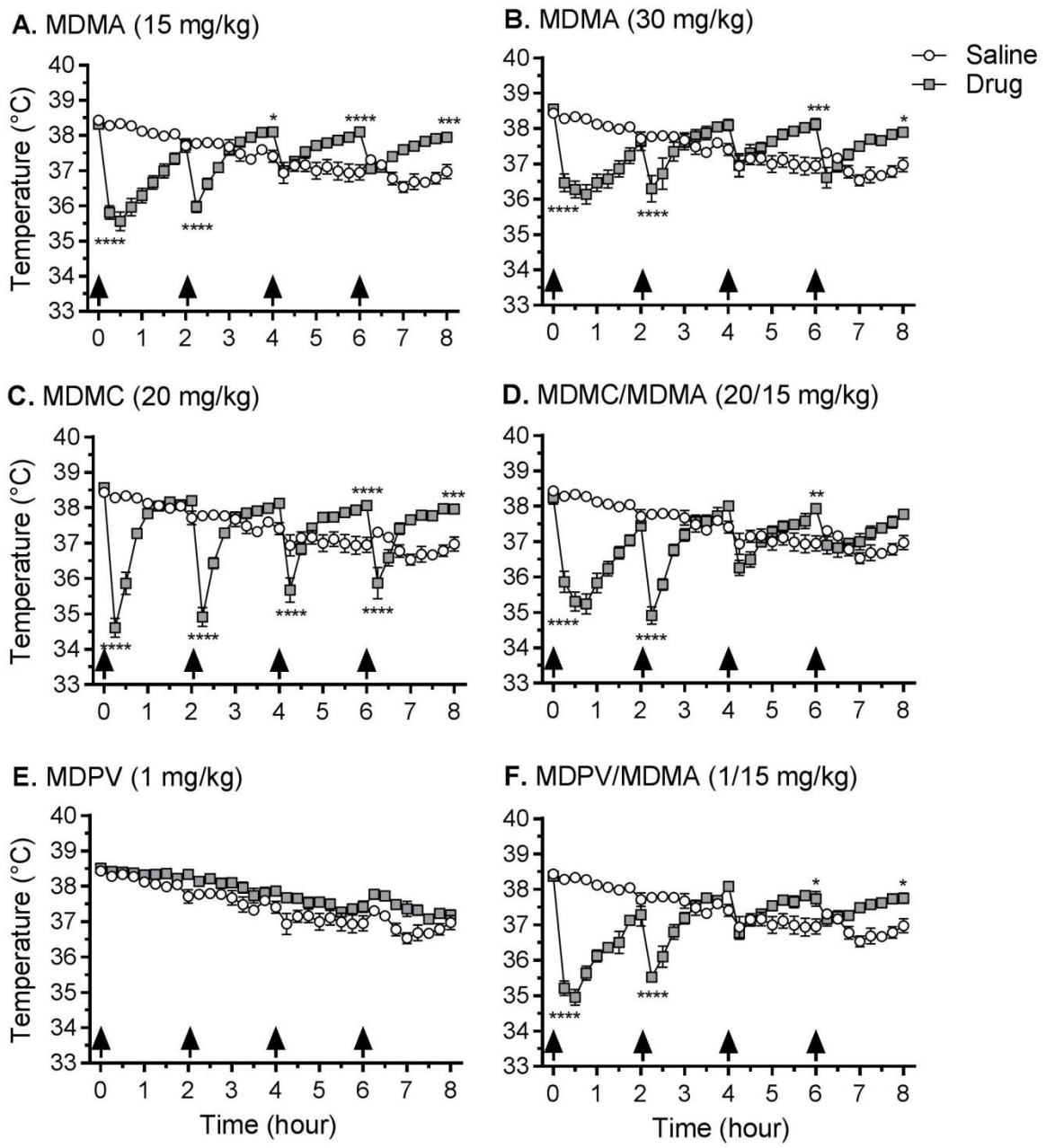

Figure 9. Effects of repeated drug injections on core body temperature. Groups of mice received 4 i.p. injections (arrows indicate time of drug injection) of the same drug/dose: MDMA (15 mg/kg) **(A)**; MDMA (30 mg/kg) (**B**); methylone (MDMC) (20 mg/kg) (**C**); Methylone (MDMC)/MDMA (20/15 mg/kg combined) (**D**); MDPV 1 mg/kg (**E**); or MDPV/MDMA (1/15 mg/kg combined) (**F**), and temperature was measured every 15 min *via* telemetry over 8 h. Data represent temperature for each saline and drug group (mean ± SEM) at that given time point, *n*

= 8 mice for each group. *: $p < 0.05$, **: $p < 0.01$, ***: $p < 0.001$, ****: $p < 0.0001$, compared to the saline group. Time points selected for comparison were 15 min and 2 h after each injection, with the 2 h measurement occurring just prior to the subsequent injection (Bonferroni *post hoc* test).

Table 8. Drug-induced change in body temperature relative to saline-treated mice

Drug	Dose (mg/kg)	15 min following injection (ΔT °C ± SEM)			
		1st	2nd	3rd	4th
MDMA	15	-2.48 ± 0.19[d]	-1.80 ± 0.17[d]	0.06 ± 0.13	-0.25 ± 0.13
MDMC	20	-3.68 ± 0.27[d]	-2.86 ± 0.27[d]	-1.26 ± 0.34[d]	-1.44 ± 0.44[d]
MDPV	1	0.14 ± 0.08	0.36 ± 0.11	0.74 ± 0.13	0.46 ± 0.06
MDMA	30	-1.83 ± 0.25[d]	-1.48 ± 0.37[d]	0.02 ± 0.33	-0.70 ± 0.29
MDMC/MDMA	20/15	-2.43 ± 0.30[d]	-2.86 ± 0.24[d]	-0.67 ± 0.22	-0.41 ± 0.24
MDPV/MDMA	1/15	-3.08 ± 0.21[d]	-2.25 ± 0.14[d]	-0.17 ± 0.17	-0.15 ± 0.20
Drug	Dose (mg/kg)	2 hr following injection (ΔT °C ± SEM)			
		1st	2nd	3rd	4th
MDMA	15	0.01 ± 0.15	0.69 ± 0.07[a]	1.15 ± 0.09[d]	0.98 ± 0.09[c]
MDMC	20	0.49 ± 0.06	0.71 ± 0.10	1.11 ± 0.09[d]	0.99 ± 0.12[c]
MDPV	1	0.63 ± 0.09	0.45 ± 0.10	0.47 ± 0.16	0.11 ± 0.14
MDMA	30	-0.07 ± 0.26	0.69 ± 0.16	1.18 ± 0.16[c]	0.92 ± 0.11[a]
MDMC/MDMA	20/15	-0.26 ± 0.14	0.60 ± 0.14	0.99 ± 0.10[b]	0.80 ± 0.09
MDPV/MDMA	1/15	-0.42 ± 0.32	0.67 ± 0.12	0.79 ± 0.21[a]	0.77 ± 0.15[a]

Data represent change in temperature (mean ± SEM) for drug- treated mice from saline controls at that given time point, $n = 8$ mice for each group. *a*: $p < 0.05$; *b*: $p < 0.01$; *c*: $p < 0.001$; *d*: $p < 0.00001$ compared to saline treated controls.

4. Discussion

The aim of this study was to investigate the combined effects of MDMA with selected and frequently abused substituted methcathinones. Body temperature was recorded during the drug administration day and measures of transient and sustained neurotoxicity were assessed 2 and

7 days following drug treatment. Methylone and MDPV were chosen for comparison based on their different mechanisms of action at monoamine transporters and their reported concomitant use with MDMA. Methylone and MDPV failed to affect striatal DA or TH levels (Fig. 5 and 6). These results support previous findings that by themselves, these methcathinones do not affect striatal dopaminergic markers of neurotoxicity (DA, DAT or TH expression) in mice 2-3 days following drug administration (Lopez-Arnau et al., 2014; Anneken et al., 2015). Another study in mice reported no change in striatal DA levels two weeks after drug administration (2 daily injections of methylone 30 mg/kg for 4 consecutive days), although there was a decrease in striatal DA levels in rats using the same dosing regimen, reinforcing inter-species response variability (den Hollander et al., 2013). However, I was surprised by the lack of methcathinone-induced changes in striatal DA and TH levels when combined with MDMA. This finding is discordant with similar amphetamine-methcathinone combination studies from a research group that found the administration of mephedrone and MDMA (4 injections of 20 mg/kg each) decreases striatal DA, DAT, and TH measured 2 days later as compared to effects of MDMA alone (Angoa-Perez et al., 2013b). The same group found the co-administration of methylone and MA (4 injections of 20 and 2.5 mg/kg, respectively) also decreases striatal DA, DAT, and TH measured 2 days later (Anneken et al., 2015). Alternatively, they found in the same study the combination of the transporter inhibitor MDPV and MDMA (4 injections of 30 and 20 mg/kg) mitigated MDMA-induced decreases in these markers.

It is possible that my findings differed from reported effects due to the use of a lower dose of MDMA (15 mg/kg), which did not decrease striatal DA or TH levels by itself, either 2 or 7 days following drug administration. These markers were decreased at the higher dose of MDMA (30 mg/kg), though only at 2 days following drug administration, indicating the effects were transient. The lower dose of MDMA was chosen as it was sufficient to elicit DA terminal degeneration in previous studies (Sanchez et al., 2003; Johnson et al., 2004), as well as decrease striatal DA levels 2 days later in the pilot study (Supp. Fig. 1), and in order to avoid a

potential floor effect when combined with the methcathinones. As there was no change in these markers when this dose of MDMA was combined with methylone and MDPV, it is possible these methcathinones only have modulatory effects on striatal DA and TH levels following an MDMA-induced decrease of these markers. Additionally, although the same dose of methylone was used in both studies, Anneken et al. (2015) administered a dose of MDPV 30x larger than in this experiment. I chose a dose of 1 mg/kg based on its increased potency at DAT in relation to MDMA, reflected in recreational doses reported by humans, where MDMA doses are estimated to be 20x greater than MDPV (Simmler et al., 2013a; Erowid, 2018). This dose (1 mg/kg) is also sufficient to induce conditioned place preference and significantly increase locomotor activity in mice (Fantegrossi et al., 2013; Karlsson et al., 2014).

MDMA increased GFAP expression 2 days following drug administration in a dose-dependent fashion, but not 7 days later (Fig. 7). This is in agreement with previous research demonstrating that GFAP expression in the striatum peaks 2-3 days following MDMA administration, correlating with localized decreased DA, DAT, and TH levels (Granado et al., 2008; Frau et al., 2013; O'Callaghan et al., 2014). Neither methcathinone increased GFAP expression 2 or 7 days following drug administration, also in accordance with previous research where methcathinones by themselves (methylone, MDPV, and mephedrone) do not alter striatal GFAP expression (Angoa-Perez et al., 2013b; Lopez-Arnau et al., 2014; Anneken et al., 2015). The increase in GFAP seen in response to the lower dose of MDMA was abolished when either methylone or MDPV were co-administered. Although Anneken et al. (2015) found the combination of MDMA and MDPV similarly decreases GFAP expression, they reported the combination of MA and methylone potentiates GFAP expression. This discrepancy in methylone-induced GFAP expression is potentially attributable to differences in drug combinations (MA vs. MDMA) or dose of MDMA (20 mg/kg vs. 15 mg/kg), though the same dose of methylone (20 mg/kg) was used in both studies. To further explore the effects of these drug combinations on reactive gliosis, other markers for astrogliosis such as activation of the

janus kinase 2 – signal transducer activator of transcription 3 (JAK2-STAT3) pathway, which precedes increased GFAP expression in models of neurotoxicity (O'Callaghan et al., 2014) could be characterized. Additionally, experiments could investigate microglial activation through quantification of microglial markers, such as CD11B, ILB4, or Mac-1.

[^{3}H]PK11195 binding is an indirect, yet sensitive measure of both astrocyte and microglia activation at axon terminals. It was hypothesized that [^{3}H]PK11195 binding to TSPO would be increased at least 2 days following drug administration in the MDMA groups, corresponding with increased GFAP expression. However, there was no difference in [^{3}H]PK11195 binding for any treatment group 2 or 7 days after drug administration (Table 8). This was particularly surprising for the two MDMA treatments, 2 days later, which increased GFAP expression. Since both assays indirectly measure astrocyte activation, an increase in GFAP expression should correlate with increased [^{3}H]PK11195 binding (Kuhlmann and Guilarte, 2000). Additionally, a lower dose of MDMA (25 mg/kg, 3 inj, 3 h apart) elicited increased binding 16 h later (Chipana et al., 2006). Although this is an earlier time point, a study using MA (10 mg/kg, 4 inj, 2 h apart) reported TSPO expression does not peak until 3 days following administration (Escubedo et al., 1998). While another study found no increase in [^{3}H]PK11195 binding 3 or 7 days following a different MDMA regimen (20 mg/kg, 2 inj per day, 4 days), there was also no increase in GFAP at either time point (Pubill et al., 2003). A potential explanation for the lack of increased TSPO expression is that the equipment used affected results as it was discovered that 10-40% of the radioactive material adhered to the sides of the assay wells, generating inter-experiment variability (Supp. Fig. 3).

Although DA terminal damage induces astrogliosis in neurotoxicity models, astrocyte activation can occur independently of terminal damage (O'Callaghan et al., 2014; McConnell et al., 2015). The absence of changes in DA and TH levels 2 days following the lower dose of MDMA (15 mg/kg dose), in contrast to the elicited increase in GFAP expression, suggests such a situation. The finding that both methylone and MDPV mitigated MDMA-induced astrogliosis

indicates the methcathinones may be competing with MDMA at the DAT, thereby preventing uptake of MDMA into the cell, subsequent dopaminergic damage, and the eventual induction of astrogliosis, whether they are transporter substrates or inhibitors. Both methcathinones have a higher affinity for DAT than MDMA (methylone, K_i = 5.02 µM; MDPV, K_i = 0.02 µM; MDMA, K_i = 22.00 µM (Eshleman et al., 2013)). At higher doses of MDMA, it is possible that MDMA is more readily taken up into the cell by DAT than is the transporter substrate methylone. Due to MDPV's substantially higher affinity for DAT and potency at inhibiting [^{3}H]DA uptake, it is likely that MDPV inhibits uptake of even high doses of MDMA by the DAT.

Another potential mechanism underlying the results is the difference between substituted amphetamine and substituted methcathinone effects at VMAT2. The vesicular transporter is recognized as a key modulator of neurotoxicity as interruption of its function leads to increased cytosolic DA levels, oxidative stress, and terminal degeneration (Fleckenstein et al., 2007). Substituted amphetamines, including MDMA, act as substrates at VMAT2 as well as DAT, depleting vesicular stores of monoamines and increasing cytosolic DA levels. Conversely, methylone and MDPV lack affinity for VMAT2 as well as potency at inhibiting monoamine uptake (Cozzi et al., 1999; Lopez-Arnau et al., 2012; Eshleman et al., 2013). As a DAT uptake inhibitor, MDPV's action is extracellular, inhibiting the uptake of DA and MDMA into the cell. As DAT substrates, both methylone and MDMA are taken into the cell and contact with VMAT2. The difference in affinity for VMAT2 between substituted amphetamines (MDMA and METH) and methcathinones (methylone and mephedrone) that are transporter substrates may underlie the different neurotoxic profiles of the two categories of drugs, providing an explanation for why methcathinones do not elicit DA terminal degeneration (Pifl et al., 1995; Angoa-Perez et al., 2013b). This may also contribute to the discrepancy between my findings and those of others that used differing doses of MDMA. As mentioned above, at the lower dose of MDMA, methylone may decrease the amount of MDMA that enters the cell, preventing MDMA-induced vesicular [^{3}H]DA release and leading to less neurotoxicity as reflected here by mitigation of

astrogliosis. At a higher dose, more MDMA may enter the cell, increasing cytosolic DA levels, as well as extracellular DA levels potentiated by the DAT substrate methylone. Thus, these drugs are excellent tools to investigate effects of drug combinations on VMAT2 function and expression to better understand the potential role of VMAT2 in the underlying mechanism of neurotoxicity.

None of the drugs, by themselves or in combination, elicited hyperthermia (> 40 °C) under these experimental conditions. Additionally, thermic response was not correlated with a drug's effects on markers of neurotoxicity. With the exception of MDPV, all drug treatments elicited a biphasic temperature response (Fig. 9). This pattern was characterized by an initial strong hypothermic reaction to drug administration followed by a steady increase in temperature. However, the increased temperature never exceeded 1.2 °C above the temperature of the saline group at that time point or rose above the initial baseline temperature of 38.4 °C, and therefore cannot be considered hyperthermia. As hypothermic conditions provide neuroprotection from MDMA (Miller and O'Callaghan, 1995; Fantegrossi et al., 2003; Mueller et al., 2013), it is possible that the hypothermic response to these drugs blunted their neurotoxic effects or that the normothermic environmental temperature (21 °C) and single-housing of animals during drug administration diminished hyperthermic effects (Carvalho et al., 2002; Fantegrossi et al., 2003; Gannon et al., 2016). The transporter substrate, methylone, both alone and in combination with MDMA, elicited the same biphasic pattern as MDMA alone, at either dose. As such, the differences in measures of neurotoxicity (DA, TH, and GFAP), both dose-dependently between MDMA doses and in comparison to methylone, must be considered independent of their elicited thermic responses. Although this agrees with findings that substituted methcathinones do not alter thermic response to MA or MDMA when combined (Angoa-Perez et al., 2013; Anneken et al., 2015), it should be noted that under the conditions of those studies, MA and MDMA administered alone elicited hyperthermia. Thus, a difference in findings may be driven by environmental factors, such as ambient temperatures, as even the

larger dose of MDMA 30 mg/kg did not elicit hyperthermia in contrast to their lower dose of MDMA 20 mg/kg. Further investigation of these drugs' combinatory effects under elevated environmental temperatures is needed to resolve this discrepancy.

The transporter inhibitor MDPV was the only drug that did not elicit the biphasic thermic pattern or produce a significant overall temperature change from the saline group. Previous reports indicate a similar lack of core temperature change following MDPV administration, despite doses up to 30 times greater than the dose used in my experiments (Aarde et al., 2013; Anneken et al., 2015; Gannon et al., 2016). MDPV is also a selective uptake inhibitor of DAT without effect on the serotonergic system, as opposed to methylone and MDMA which are non-selective transporter substrates. This finding indicates substituted methcathinones and amphetamines that act as transporter substrates alter body temperature through different mechanisms than transporter uptake inhibitors, potentially involving SERT. Though difficult to untangle the underlying mechanisms, the thermal response to MDMA appear to override those of MDPV, as the biphasic pattern re-emerged when the two drugs were co-administered.

The results from Chapter 2 provide new and additional insight into the neurotoxic profiles of methylone and MDPV. In comparison to MDMA, neither drug alone elicited changes to any of the measured neurotoxic markers in the striatum: DA and TH levels, or GFAP expression. They also did not have regulatory effects on DA or TH levels when combined with MDMA, although both methcathinones mitigated astrogliosis induced by MDMA, an effect previously only observed with MDPV. The methcathinones also modulated body temperature differentially, based on their mechanisms of action. While all transporter substrate treatment groups (alone or in combination) elicited a biphasic temperature response, only the transporter uptake inhibitor MDPV did not evoke this response. Though these results do not indicate a strong neurotoxic profile for either methylone or MDPV, caution must be exercised before drawing such conclusions. More research is needed on these substances both alone and in combination with MDMA at a higher dose in order to better determine their modulatory neurotoxic effects.

Stronger effects may be seen at elevated environmental temperatures, which more accurately reflect the environment in which these substances are often ingested.

Chapter 3: TAAR1 regulation of MDMA-induced neurotoxicity

The data presented in this chapter are unpublished.

1. Introduction

Activation of TAAR1 alters sensitivity to effects of substituted amphetamines, including MDMA. Most research has focused on the TAAR1 modulation of AMPH and MA acute effects, using either the transgenic *Taar1*-KO model, lacking TAAR1, or the MAHDR mouse model where the receptor is present, but non-functional (for review, see: Phillips and Shabani, 2015; Rutigliano et al., 2017). One paper (Di Cara et al., 2011) has investigated TAAR1 modulation on the acute effects of MDMA, finding similar effects following drug administration: locomotor activity increases, extracellular DA levels in the striatum increases, and core body temperature is higher in *Taar1*-KO mice relative to *Taar1*-WT mice. All effects which correspond with increased neurotoxicity (O'Shea et al., 2001; Camarero et al., 2002; Fantegrossi et al., 2003). Additionally, research on the modulatory effects of TAAR1 on thermal response to MA revealed the acute hypothermia observed *Taar1*-WT and MALDR mice is absent in *Taar1*-KO and MAHDR mice (Harkness et al., 2015).

DAT function plays a critical role in amphetamine-induced neurotoxicity. Impairment of [^{3}H]DA uptake or release is correlated with increased neurotoxicity and contributes to elevated extracellular DA levels (Fleckenstein et al., 2007). Previous research found *in vitro* treatment increases MA release in striatal synaptosomes from *Taar1*-WT compared to –KO mice (Xie and Miller, 2009a). This finding negatively corresponds with microdialysis experiments where MDMA and AMPH administration increases DA release in *Taar1*-KO compared to -WT mice (Wolinsky et al., 2007; Di Cara et al., 2011). However, it is possible that activation of TAAR1 may increase

DA release at a cellular level, while modulating the DA system at a physiological level, leading to increased extracellular DA release.

Based on these findings, I preliminarily investigated the effects of TAAR1 on MDMA-induced neurotoxicity. As MDMA 15 mg/kg did not significantly diminish striatal DA levels in Chapter 2, the dose was increased to 20 mg/kg, a common dose used to induce neurotoxicity (O'Callaghan and Miller, 1994; Angoa-Perez et al., 2013b). Methylone was used as a control as it is similar to MDMA, both in chemical structure and mechanism of action, but it lacks affinity for TAAR1 (Simmler et al., 2013a). The same binge-like regimen (4 inj, 2 h apart) was administered to MALDR and MAHDR mice. The experiment was originally intended to be conducted in *Taar1*-WT and –KO mice for continuity with the *in vitro* work and as an extension of MDMA research performed using the *Taar1* model (Di Cara et al., 2011). However, due to a lack of available transgenic *Taar1* mice at the time, MADR mice were used. Striatal DA levels and GFAP expression were measured 2 days later to capture peak effects. Temperature recordings in MADR mice were recorded along with a separate cohort of *Taar1*-WT and –KO mice for model comparison. MDMA-induced [^{3}H]DA release in striatal synaptosomes from untreated *Taar1*-WT and –KO mice was also included as a measure of TAAR1 modulation of impairment of DA function. I hypothesized MDMA would induce greater neurotoxicity, indicated by decreased DA levels and increased GFAP expression, in MAHDR mice lacking a functional TAAR1, compared to MALDR mice where TAAR1 is activated. Additionally, I hypothesized MALDR and *Taar1*-WT mice would exhibit the same biphasic thermal response to MDMA as the C57BL/6 mice did in Chapter 2, whereas the acute hypothermia would be blocked in MAHDR and *Taar1*-WT mice. As methylone lacks affinity for TAAR1, I did not expect the results to differ between line or genotype for any of the three measures. Finally, I hypothesized MDMA would increase [^{3}H]DA release in *Taar1*-WT compared to –KO mice.

2. Methods and Materials

2.1. Drugs and chemicals

Racemic MDMA and methylone were generously provided by the National Institute on Drug Abuse (NIDA) Research Resources Drug Supply program. All chemicals and reagents used to assay DA levels, as included in the Dopamine Research ELISA kit, were purchased from Rocky Mountain Diagnostics, Inc. (Colorado Springs, CO). All chemicals and reagents used to assay GFAP expression levels, as included in the GFAP ELISA kit, were purchased from EMD Millipore (Billerica, MA). [^{3}H]DA was purchased from Perkin Elmer (Boston, MA). All other reagents were obtained from standard commercial sources, unless otherwise noted.

2.2. Methamphetamine drinking selected mouse lines

Multiple pairs of MADR lines were consecutively, selectively bred from an F2 cross of the B6 and D2 inbred strains based on voluntary MA consumption during a two-bottle choice test. Details of this process and response to selection have been previously described (Wheeler et al., 2009; Shabani et al., 2011). Briefly, animals were provided access to a bottle containing a 20 mg/l MA solution for 18 h per day for 4 days, alongside continuous access to a water bottle. The concentration was increased to 40 mg/l MA for 4 additional days and mice were selected for breeding based on either high or low MA intake during this period. This breeding selection procedure was repeated for four generations to generate MALDR and MAHDR mice. The mice used in this experiment were MA-naïve offspring from second or later litters from replicates 2, selection generation 5, and replicate 3, selection generation 5.

2.3. Taar1−KO *mouse breeding and genotyping*

The *Taar1*-KO mice were obtained from the U.C. Davis Knockout Mouse Project (KOMP; www.komp.org) as previously described (Harkness et al., 2015). Briefly, chimeric mice were created using C57BL/6N ES cells in which the entire *Taar1* coding region was deleted by homologous recombination, using the Veloci-Gene Null Allele Bac vector, and then injected into BALB/c blastocysts. The chimeras were bred with wild-type C57BL/6N mice and their offspring

genotyped according to the strategy recommended by KOMP using the following primers: ACTCTTCACCAAGAATGTGG (forward); CCAACAGCGCTCAACAGTTC (reverse, wild-type allele); GTCGTCCTAGCTTCCTCACTG (reverse, null allele). Male and female siblings, identified as heterozygous for the targeted locus, were subsequently bred to produce *Taar1*-WT and *Taar1*-KO littermates.

2.4. Animal maintenance and housing

Mice of both sexes were used in all experiments and tested at 10–20 weeks of age. Before experiment initiation, mice were group-housed in filtered acrylic plastic shoebox cages (28 cm×18 cm×13 cm; l ×w× h), fitted with wire tops. Cages were lined with either ECO-Fresh bedding (Absorption Corporation, Ferndale, WA) or Bed-O-Cob (The Andersons, Maumee, OH). Mice had free access to rodent chow (5LOD, 5.0% fat content, Purina Mills, St. Louis, MO) and water *ad libitum*. The colony room was maintained at an environmental temperature of 21 ± 1 °C with lights on a 12:12 h light:dark schedule, beginning at 0600 h. All procedures were approved by the VA Portland Health Care System's Institutional Animal Care and Use Committee and followed the requirements of the Guide for the Care and Use of Laboratory Animals. All efforts were made to minimize animal suffering, to reduce the number of animals used, and to use alternatives to *in vivo* techniques when available. All animals acclimated to the vivarium at least one week prior to testing.

2.5. Temperature recording and drug treatment

Two days prior to drug administration, mice were implanted with IPTT-300 temperature transponders from BioMedic Data Systems (Seaford, DE) to assess body temperature *via* telemetry. Animals were anesthetized with isoflurane (5% induction, 2.5% maintenance) and transponders were subcutaneously injected dorsally between the shoulders. On the day of drug administration, animals were weighed and transferred from group to individual cages to avoid temperature changes associated with interaction (e.g., huddling). After a 1 h acclimation period, temperature recording began and was measured every 15 min for 8 h. All experiments were

conducted between 0700 and 1700 h. Temperatures were non-invasively recorded using the DAS-8001 reader console and smart probe from BioMedic Data Systems. Animals were removed from the cage and the smart probe placed within 5 cm of the embedded transponder to acquire temperature readings. The environmental temperature of the testing environment was 23 ± 1 °C. This temperature was selected in order to differentiate neurotoxic effects of the drugs from those exacerbated by elevated environmental temperatures.

2.6. Drug treatment

Following the first temperature recording (baseline), MADR mice received four i.p. injections (2 h apart) of saline, MDMA (20 mg/kg), or methylone (25 mg/kg). As MDMA is modestly more potent than methylone as a transporter substrate, a higher dose of methylone (25 mg/kg) was selected to approximate an equivalent dose to MDMA (20 mg/kg) (Eshleman et al., 2013). *Taar1* mice used for temperature experiments were only treated with saline or MDMA (20 mg/kg). All drugs were dissolved in 0.9% saline and injected in a final volume of 10 ml/kg. MADR mice were euthanized 2 days after the final drug treatment by cervical dislocation, followed by decapitation. The striatum was removed using blunt dissection, flash-frozen, and weighed prior to being stored at -70 °C until time of assay. Striatal tissue from each animal was dissected and each half used for either DA or GFAP assays (counterbalanced by side of brain).

2.7. Quantification of dopamine levels

Tissue was homogenized in a 1 mM EDTA, 4 mM metabisulfite, 0.01 N HCl solution**,** using a 5 mg/ml dilution, and sonicated for 30 s using a 2-mm ultra-sonification microprobe. Protein density was determined using the bicinchoninic acid (BCA) assay protocol. Striatal dopamine levels were quantified using a competitive enzyme-linked immunosorbent assay (ELISA) kit according to the manufacturer's instructions. 5 µl of tissue homogenate was used for DA analysis in duplicate. The amount of DA in the samples was calculated and expressed as nanograms DA per milligram total protein.

2.8. Quantification of GFAP expression

Tissue homogenate for GFAP analysis was prepared in the same manner as for TH analysis. Striatal GFAP levels were quantified using a sandwich ELISA kit (EMD Millipore, Billerica, MA) according to the manufacturer's instructions. 100 µl of tissue homogenates, in duplicate, were used for GFAP analysis against a standard curve using a GFAP standard provided by the manufacturer.

2.1. Synaptosomal preparation

Synaptosomal fractionation was performed as previously described (Rothman et al., 2001) with minor modifications. Striatal tissue from 5 naïve *Taar1*-WT or –KO mice were pooled and homogenized in ice-cold sucrose (0.32 M) and the inhibitors fluoxetine (50 nM), desipramine (100 nM), and reserpine (1 µM) with 12 strokes of a glass/teflon homogenizer before being centrifuged (1000 x *g*, 10 min, 4°C). The supernatant was decanted and diluted in Krebs-phosphate assay buffer (0.50 mM Na_2SO_4, 0.50 mM potassium tartrate, 126 mM NaCl, 2.40 mM KCl, 0.83 mM $CaCl_2x2H_2O$, 0.80 mM $MgCl_2x6H_2O$, 11.10 mM glucose, 1 mg/ml ascorbic acid, 50 µM pargyline, 100 µM tropolone; pH 7.4) with 1 µM reserpine to 0.25x volume of the original wet tissue weight (ml/mg) resulting in 5-6 µg total protein loaded. Protein density was determined by BCA assay.

2.2. [^{3}H]DA release assay

DA release was quantified using a similar protocol to that previously described (Rothman et al., 2001). In brief, synaptosomes (5 – 6 µg total protein) were incubated in [^{3}H]DA (10 nM) and assay buffer for 30 min in a 25 °C water bath until reaching a steady state. Preliminary experiments were conducted to optimize assay conditions (Supp. Fig. 4). The release assay was initiated by the addition of 850 µl of the synaptosomal preparation preloaded with [^{3}H]DA to 150 µl of MDMA (10 nM – 100 µM) in assay buffer supplemented with 1 mg/ml bovine serum albumin. Specific binding was defined as the difference in binding observed in the presence or absence of tyramine (10 µM) and the final assay volume was 1 ml. Incubation (10 min at 25 °C) was terminated using 10 mM Tris-HCl in saline (0.9% NaCl). Termination was performed by

filtration using a TomTec 96-well harvester (Hamden, CT) through Perkin Elmer filtermat A filters pre-soaked in 0.05% polyethlenimine. Scintillation fluid was added and radioactivity was determined using a Perkin Elmer microbeta plate counter. Assay was conducted in triplicate and results were normalized to the amount of total protein loaded.

2.9. Data analysis

DA and GFAP expression were analyzed by two-way analysis of variance (ANOVA) with selected line and dose as between-group factors, independently. Dunnett's multiple comparison test was used for follow-up mean comparisons with the saline group. Temperature data were analyzed using a repeated measures three-way ANOVA with time as a within-subject factor and selected line and dose as between-group factors. Due to the small size of animals run in this pilot study and lack of availability, sex was not included in the analyses. Significant two-way interactions were further investigated using simple main effect analyses and/or *post hoc* mean comparisons using the Newman-Keuls test, when appropriate. For temperature data, subsequent analyses were conducted at 30 min after each injection as, under the described conditions, the maximum hypothermic drop occurs 30 min following administration of MDMA (Harkness et al., 2015; Miner et al., 2017b). EC_{50} values were generated by analyzing the sigmoidal dose-response curves using a non-linear curve-fitting program and further analyzed using unpaired t-tests. Data were analyzed for outliers using Dixon's Q-test at 90% confidence. All statistical analyses were performed using Statistica version 13 software (StatSoft Inc., Tulsa, OK). Differences were considered significant at $p < 0.05$.

3. Results

3.1. Dopamine levels and GFAP expression

There were no significant interactions or main effects of selected line or dose 2 days following MDMA or methylone administration for striatal DA levels (Fig. 10A). While there was no significant interaction or main effect of line for striatal GFAP expression, there was a main

effect of drug treatment ($F_{2,29}$ = 4.64, p < 0.05) (Fig. 10B). MDMA increased GFAP expression, regardless of line, in comparison to saline-treated controls.

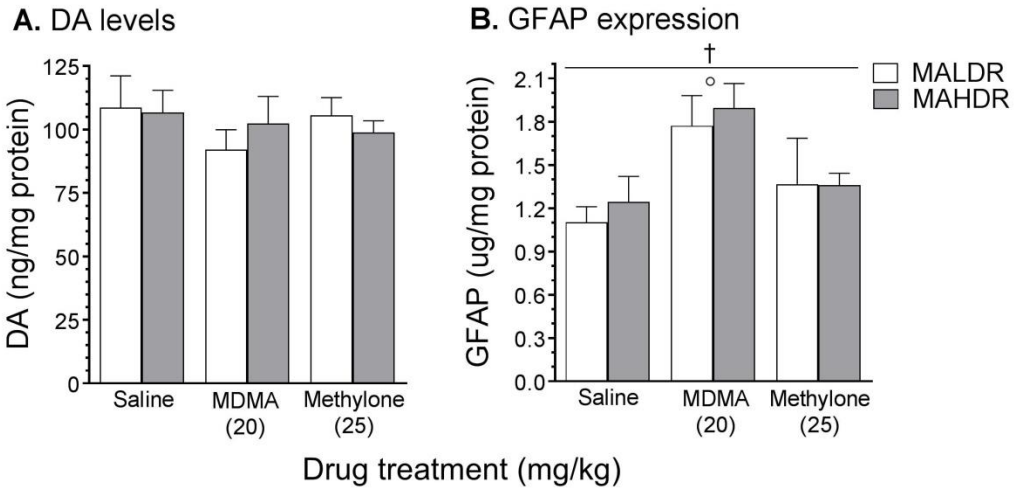

Figure 10. Striatal DA levels and GFAP expression measured 2 days following treatment. MALDR and MAHDR mice received 4 i.p. injections of saline, MDMA (20 mg/kg), or methylone (25 mg/kg), 2 h apart, and were euthanized two days following the final injection for striatal tissue collection. DA levels (**A**) were measured by competitive ELISA and GFAP expression (**B**) by sandwich ELISA. Values were normalized to the amount of protein in each tissue sample. Data represent means ± SEM of 7-9 mice per group. †: p < 0.05 for main effect of drug treatment; ◦: p < 0.01 compared to saline-treated controls, regardless of line.

3.2. [^{3}H]DA release

There was no significant difference in EC_{50} between striatal synaptosomes from *Taar1*-WT (0.375 ± 0.024 µM) and *Taar1*-KO (0.521 ± 0.057 µM) mice, p > 0.05 (Fig. 11).

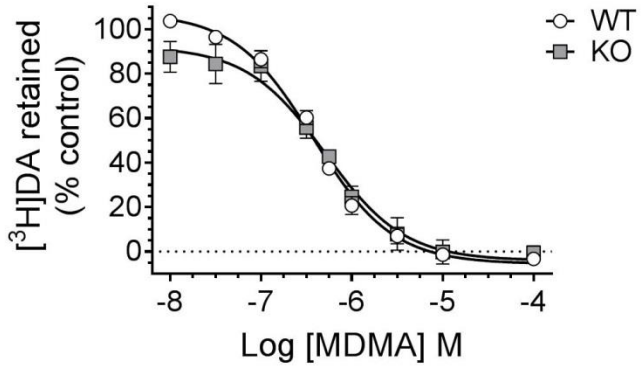

Figure 11. MDMA-induced [^{3}H]DA release in synaptosomes. Striatal synaptosomes from *Taar1*-WT and –KO mice were pre-loaded with [^{3}H]DA (10 nM) for 30 min before MDMA (10 nM – 100 µM) was added and incubated for 30 min. Values were normalized to the amount of protein in each sample. Data represent means ± SEM of 3 independent experiments, expressed as % of the *Taar1*-WT control group specific retention (63.9 ± 9.1 pmol/mg protein).

3.3. Thermal response

The mean baseline temperature of all *Taar1* mice was 38.4°C (SEM = 0.05°C), with no significant between-genotype or -treatment differences. MDMA elicited genotype-dependent hypothermia. Hyperthermia was not observed under any condition. A three-way repeated measures ANOVA revealed a significant genotype x treatment x time interaction ($F_{32,896}$ = 7.18, p < 0.0001). There was no difference in temperature between *Taar1*-WT and -KO mice receiving saline (Fig. 12A), although there was a main effect of time ($F_{32,448}$ = 38.60, p < 0.0001) as temperatures in these control groups decreased over the 8 h period, likely attributable to single housing. Examination of the effects of MDMA revealed a significant genotype x time interaction ($F_{32,448}$ = 12.07, p < 0.0001) (Fig. 12B). Analyses of genotype differences were conducted using simple main effect analyses at each 30 min post-injection time point to investigate the hypothermic drop in body temperature. The temperatures of *Taar1*-WT mice

receiving MDMA were significantly lower 30 min after each of the four MDMA injections compared to *Taar1*-KO counterparts.

Prior to the first injection, the mean baseline temperature of all MADR mice was 38.5°C (SEM = 0.11°C), with no significant between-line or -treatment differences. MDMA induced selected line-dependent acute hypothermia in MADR mice, whereas methylone induced hypothermia regardless of line. Neither drug elicited hyperthermia in any mice, defined as a 0.5°C increase in body temperature above the basal temperature. Temperature data for MADR mice, analyzed using a three-way repeated measures ANOVA, revealed a significant line x treatment x time interaction ($F_{64,1344} = 2.22$, $p < 0.0001$). There was no difference in temperature between selected lines for mice receiving saline (Fig. 12C), although there was a main effect of time ($F_{32,448} = 6.60$, $p < 0.0001$), again, as temperatures in the control groups decreased over the 8 h period. Examination of the effects of MDMA revealed a significant line x time interaction ($F_{32,448} = 2.91$, $p < 0.0001$) (Fig. 12D). Analyses of selected line differences were conducted using simple main effect analyses at each 30 min post-injection time point to investigate the hypothermic drop in body temperature. The temperatures of MALDR mice receiving MDMA were significantly lower 30 min after the first and second MDMA injection compared to MAHDR mice. There was no difference in temperature between selected lines for mice receiving methylone (Fig. 12E), although there was a main effect of time ($F_{32,448} = 3.30$, $p < 0.0001$).

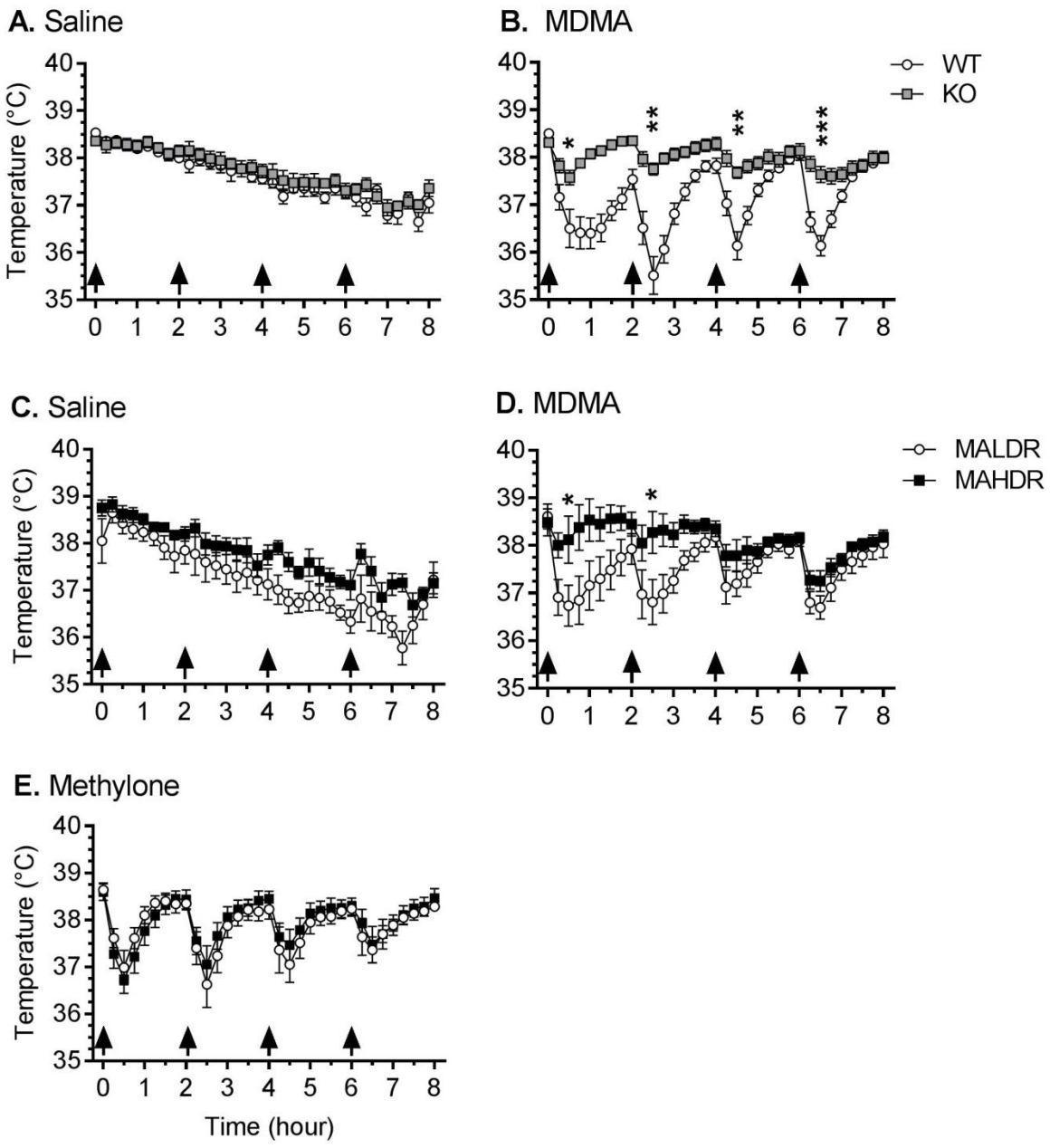

Figure 12. Effects of repeated saline, MDMA, or methylone injections on core body temperature. *Taar1*-WT, *Taar1*-KO, MALDR, or MAHDR mice received 4 i.p. injections (indicated by arrows) of saline, MDMA (20 mg/kg), or methylone (25 mg/kg), 2 h apart. Body temperature was measured every 15 min *via* telemetry over 8 h in an ambient temperature of 23 ± 1°C. Data represent temperature for each selected line or genotype and treatment group (mean ± SEM) at specified time points, n = 8 mice per group. Time points selected for detailed

analysis were 30 min after each injection. *: $p < 0.05$, **: $p < 0.001$, ***: $p < 0.0001$ compared between selected lines or genotypes.

Next, examination of the data for each *Taar1* genotype revealed a significant treatment x time interaction for both genotypes: *Taar1*-WT ($F_{32,448} = 24.27$, $p < 0.0001$) and *Taar1*-KO ($F_{32,448} = 9.86$, $p < 0.0001$). Simple main effects analyses revealed MDMA significantly decreased body temperature 30 min following all four injections in *Taar1*-WT mice compared to saline-treated control mice, while MDMA decreased temperatures only after the first injection in *Taar1*-KO mice (Table 9).

Examination of the data for each selected line revealed a significant treatment x time interaction for both lines: MALDR ($F_{64,672} = 8.8$, $p < 0.0001$) and MAHDR ($F_{64,672} = 7.5$, $p < 0.0001$). Simple main effects analysis was then used to statistically investigate MDMA and methylone effects within each line at the 30 min post-injection time points. MDMA significantly decreased body temperature 30 min following the first injection in MALDR mice, but not MAHDR mice, while methylone decreased temperature in both lines following the first injection.

Table 9. Drug-induced change in body temperature relative to saline treated mice

Line or Genotype	Drug (mg/kg)	30 min post-injection (ΔT °C ± SEM)			
		1st Inj	2nd Inj	3rd Inj	4th Inj
Taar1-WT	MDMA (20)	-1.88 ± 0.40[c]	-2.45 ± 0.40[d]	-1.05 ± 0.30[b]	-0.82 ± 0.21[a]
MALDR	MDMA (20)	-1.69 ± 0.43[b]	-0.79 ± 0.47	0.44 ± 0.27	0.15 ± 0.24
	Methylone (25)	-1.44 ± 0.37[b]	-0.98 ± 0.49	0.29 ± 0.38	0.81 ± 0.28
Taar1-KO	MDMA (20)	-0.75 ± 0.15[b]	-0.33 ± 0.13	0.15 ± 0.12	0.20 ± 0.17
MAHDR	MDMA (20)	-0.50 ± 0.50	0.29 ± 0.44	0.19 ± 0.34	-0.16 ± 0.22
	Methylone (25)	-1.89 ± 0.30[d]	-0.94 ± 0.40	-0.14 ± 0.34	0.06 ± 0.38

Data represent change in temperature (mean ± SEM) for each treatment group from saline-treated mice at specified time point, $n = 8$ mice per group. *a*: $p < 0.05$; *b*: $p < 0.01$; *c*: $p < 0.001$; *d*: $p < 0.0001$ in analysis compared to saline-treated controls.

4. Discussion

The modulatory effects of TAAR1 on MDMA-induced neurotoxicity are difficult to interpret based on the results of these experiments. Again, MDMA (20 mg/kg) did not decrease striatal DA levels two days following administration, a surprising result, given the ubiquity of this MDMA dose in neurotoxic experiments (O'Callaghan and Miller, 1994; Thomas et al., 2004a; Angoa-Perez et al., 2013b), although there is a report of this dose failing to elicit a decrease in DA three days later (Fantegrossi et al., 2008). MDMA did increase GFAP expression, which was expected as the lower dose of 15 mg/kg elicited an increase in Chapter 2, but there was no difference between selected lines. Although it could be speculated TAAR1 does not modulate MDMA-induced neurotoxicity, this would be premature, as without an observable decrease in DA levels, there is no indication neurotoxicity was actually induced under these conditions. While the higher dose of MDMA (30 mg/kg), used in Chapter 2, was not selected in order to avoid a potential floor effect, this may be a better dose to use for future experiments to induce a significant decrease in DA levels.

Following MDMA administration, striatal extracellular levels are increased in *Taar1*-KO compared to –WT mice (Di Cara et al., 2011). To determine whether this is mediated by genotypic differences in DAT function, MDMA-induced [^{3}H]DA release was measured *in vitro* in striatal synaptosomes from *Taar1*-WT and –KO mice. However, MDMA was equally potent at inducing [^{3}H]DA release in synaptosomes from both genotypes. This is in contrast to similar research measuring MA-induced [^{3}H]DA release which reported [^{3}H]DA release was significantly increased in *Taar1*-WT synaptosomes, whereas release was unaffected in *Taar1*-KO synaptosomes (Xie and Miller, 2009a). With the exception of swapping MDMA for MA, experimental procedures were replicated as best as possible. While the discrepancy in findings could be potentially attributed to the use of a different drug, this is unlikely. In the current experiment, [^{3}H]DA release was elicited in synaptosomes from *Taar1*-KO mice using the same

concentrations of MDMA and MA as used in the previous experiment. As MA is a more potent releaser of DA than MDMA, the effects should be greater in MA-treated mice when comparing within the *Taar1*-KO genotype. It remains unclear why [^{3}H]DA release was not observed in *Taar1*-KO mice in their experiment. Further research is warranted to determine whether a difference would be observed under different conditions.

However, activation of the receptor clearly modulates MDMA-induced changes to body temperature. This effect was most pronounced in *Taar1* mice, where MDMA decreased body temperatures of *Taar1*-WT mice 30 min after each injection significantly lower than saline and *Taar1*-KO mice. Di Cara et al. (2011) found a similar effect in *Taar1*-WT mice where the same dose of MDMA elicited a hypothermic drop 30 min following injection. However, they found body temperature was significantly increased in *Taar1*-KO mice at that time point, an effect absent in our *Taar1*–KO mice. Not as sustained, MDMA induced hyperthermia in MALDR mice following the first injection, but not subsequent administrations and MALDR mice differed from MAHDR mice only following the first and second injections. These findings indicate MDMA induces acute hypothermia when TAAR1 is activated, an effect mitigated when TAAR1 is either absent or present but non-functional. Validation of this effect in the two different mouse models of TAAR1 indicates developmental changes due to either model are unlikely. These results also replicate findings using MA in both models, albeit using a single dose paradigm (Harkness et al., 2015). MA (4 mg/kg) induced hypothermia 30 min following administration in both MALDR and *Taar1*-WT mice, an effect absent in MAHDR and *Taar1*-KO mice. Another paper investigating the effects of TAAR1 on thermal response to amphetamines found MDMA (25 mg/kg) and MA (3 mg/kg) induced hyperthermia in both *Taar1*-WT and –KO mice (Panas et al., 2010). The only difference between genotypes was hyperthermia was reached earlier in *Taar1*-KO compared to –WT mice. It is possible that the increased dose of MDMA shifted the response to hyperthermia in *Taar1*-WT mice as hyperthermia is observed at higher doses (O'Shea et al., 2001).

Additionally, it may be that activation of TAAR1 modulates the hypothermic response to MDMA at lower doses, at higher doses, this is masked or overwhelmed.

There was no difference in temperature response between MALDR and MAHDR mice administered methylone, indicating the drug's effect on body temperature is TAAR1-independent. While this was expected as the drug is not a TAAR1 agonist, it is intriguing that acute hypothermia and a biphasic temperature pattern is elicited. Taken together these findings indicate that for MDMA, a psychostimulant and TAAR1 agonist, to elicit acute hypothermia, TAAR1 activation is required, whereas for methylone, a psychostimulant that lacks affinity for TAAR1, activation of TAAR1 is not required to elicit acute hypothermia. Therefore, methylone-induced hypothermia must act, at least in part, through a separate mechanism from MDMA. Ethanol also induces hypothermia independently of TAAR1 activation. In both the *Taar1* and MADR model, ethanol administration (2 or 4 g/kg) induced hypothermia in both genotypes and lines (Harkness et al., 2015). Additional research is needed in both aspects of thermal response: TAAR1 modulation of amphetamine-induced changes in body temperature and the substituted methcathinones TAAR1-independent mechanism of action.

Based on the lack of changes observed for these markers of neurotoxicity, the question arises whether MDMA is a good model to study TAAR1 effects on neurotoxicity. To determine whether a biochemical target is a modulator of neurotoxicity, neurotoxicity must first be induced. Sustained MDMA use in humans causes cognitive deficits and decreased SERT binding (McCann et al., 1999; Reneman et al., 2001). However, it is difficult to discern to what degree this is caused by MDMA itself or due to poly-drug use (Schifano et al., 1998; Mohamed et al., 2011). The translational validity of rodent models of MDMA-induced neurotoxicity has also been called into question, particularly the issue of interspecies scaling of dose due to differential metabolism and pharmacokinetics (de la Torre and Farre, 2004; Easton and Marsden, 2006; Baumann et al., 2007). There is also a high degree of variability in neurotoxicity results reported using different doses of MDMA. In some experiments, such as the one above, a 20 mg/kg dose

of MDMA is insufficient to decrease DA levels 2 days later at peak effect, while in others 5 mg/kg can cause lasting depletion 7 days later (Fornai et al., 2005; Fantegrossi et al., 2008). In Chapter 2, only the highest dose of MDMA (30 mg/kg) diminished striatal DA levels and increased GFAP expression 2 days later, while both markers returned to baseline 7 days later. Finally, the primary mechanisms of action for TAAR1 are dopaminergic. Although there is a rationale for studying DA-related MDMA neurotoxicity in a mouse model (Colado et al., 2004), ultimately MDMA causes degeneration of 5HT terminals in humans, but not DA terminals, decreasing the validity of the model (Moratalla et al., 2017). MA is both a TAAR1 agonist and a highly abused substance. The neurotoxicity of MA is firmly established and reliably produces sustained DA terminal degeneration, similar to its action in humans. Based on this, the decision was made to pivot my research to TAAR1 modulation of MA-induced neurotoxicity.

Chapter 4: TAAR1 regulation of methamphetamine-induced neurotoxicity

This chapter is adapted from the following publication:

Miner, N.B., Elmore, J. S., Baumann, M. H., Phillips, T.J., Janowsky, A (2017). Trace amine-associated receptor 1 regulation of methamphetamine-induced neurotoxicity. Neurotoxicology. 63, 57-69.

Acknowledgements: the analyses of striatal tissue for monoamines and their metabolites (DA, DOPAC, HVA, 5HT, 5HIAA, and NE) were conducted by Josh S. Elmore and Michael H. Baumann.

1. Introduction

Based on the results of Chapter 3, the focus of my research turned to MA. MA has a robust neurotoxic profile across species. Neurotoxicity is most severe in the striatum, causing DA terminal degeneration. MA is taken into the cell *via* DAT and causes the depletion of vesicular stores of DA, reverse transport of DA and inhibits [^{3}H]DA uptake, all contributing to increases of intra- and extracellular DA levels (Sulzer et al., 2005; Fleckenstein et al., 2007). Increased cytosolic levels of DA are metabolized by MAO to produce H_2O_2 and superoxides, leading to the formation of hydroxyl radicals, as well as auto-oxidized to form harmful DA quinones, increasing oxidative stress and DA terminal degeneration (Cubells et al., 1994; LaVoie and Hastings, 1999). Neuroinflammation also occurs and sustained activation of astrocytes and microglia contribute to neurotoxicity (Loftis and Janowsky, 2014).

The GPCR receptor TAAR1 is a known modulator of amphetamine's effects. As discussed above, mice lacking the receptor (*Taar1*-KO) or mice possessing a non-functional TAAR1

(MAHDR) have altered sensitivity to the behavioral, physiological, and biochemical altering effects of AMPH and MA (Wolinsky et al., 2007; Wheeler et al., 2009; Achat-Mendes et al., 2012; Harkness et al., 2015). TAAR1 appears to act as a complex modulator of the DA system and its mechanisms remain to be fully elucidated. However, activation of the receptor does have an overall inhibitory effect, diminishing DA neuron firing, an effect diminished in *Taar1*-KO mice and when the TAAR1 antagonist EPPTB is applied (Lindemann et al., 2008; Bradaia et al., 2009). TAAR1 agonists also reduce [^{3}H]DA release *in vitro*, whereas EPPTB blocks this effect (Leo et al., 2014).

Increased sensitivity to certain neurochemical and behavioral effects of MA correspond with increased MA-induced neurotoxicity. Increased MA-induced striatal DA release and LMA are two such traits (Weinshenker et al., 2008; Ren et al., 2014). As both traits are also increased in response to AMPH and MDMA when TAAR1 is absent (Wolinsky et al., 2007; Lindemann et al., 2008), I hypothesized MA would induce increased neurotoxicity in *Taar1*-KO mice compared to –WT mice. The *Taar1* model was chosen as the above TAAR1 studies used this model. Additionally, MA (2 mg/kg) does not elicit a difference between MALDR and MAHDR mice in DA release in the NAc or differences in LMA (Shabani et al., 2011; Lominac et al., 2014). The following experiments continued to use the same neurotoxic regimen (4 inj, 2 h apart) and time points (2 and 7 days later) to assess transient and sustained MA-induced neurotoxicity in *Taar1*-WT and –KO mice. To investigate dose-dependent effects between genotypes, three separate doses of MA (2.5, 5, and 10 mg/kg) were administered. Striatal DA and TH levels are rarely altered following a MA dose below 4 mg/kg, whereas 5 mg/kg modestly decreases levels and 10 mg/kg robustly diminishes DA and TH (Thomas et al., 2004b; Fantegrossi et al., 2008; Angoa-Perez et al., 2013a; McConnell et al., 2015). Striatal astrocyte activation is dose-dependently increased as well, but more sensitive to MA than DA and TH levels, as GFAP expression can be increased at lower doses in the absence of DA depletion (McConnell et al., 2015).

While the same markers of neurotoxicity from Chapter 2 were assessed, the methodologies were changed to increase sensitivity. Instead of simply measuring striatal DA levels using a DA ELISA kit, the monoamines and their metabolites (DA, DOPAC, HVA, 5HT, 5HIAA, and NE) were quantified using high performance liquid chromatography with electrochemical detection (HPLC-ECD), the standard method in the field (Bergquist et al., 2002). GFAP expression quantification remained a sandwich ELISA, but shifted away from use of a kit as well. An established methodology (O'Callaghan, 2002) was adapted and optimized to allow for increased throughput and efficiency while reducing reliance on a commercial product. Finally, while TH levels were quantified by an outside collaborator in Chapter 2, their methodology, a similar sandwich ELISA for TH (Sriram et al., 2004) was adapted and employed to diminish outside reliance.

Body temperature data were collected to continue investigating the role TAAR1 plays in modulating amphetamine-induced body temperature using a binge-like regimen, specifically, acute hypothermia (see Chapter 2). In the *Taar1* mouse model, a single, low dose of MA (2 mg/kg) elicited hypothermia 30 min later in *Taar1*-WT mice, an effect absent in *Taar1*-KO mice (Harkness et al., 2015). The same study used a range of single MA doses in the MADR model, finding lower doses of MA (1, 2, and 4 mg/kg) induced acute hypothermia in MALDR, but not MAHDR mice. At higher doses of MA (8 and 16 mg/kg), there was no hypothermic response in MALDR mice, while hyperthermia was induced in MAHDR mice. Based on these results, I hypothesized the hypothermic effect would be dose-dependent in *Taar1*-WT mice, with the greatest decrease in temperature induced by the lowest dose of MA (2.5 mg/kg) and remain near baseline for *Taar1*-KO mice and perhaps hyperthermic at the highest dose (MA 10 mg/kg). The conditions of the experiment were again conducted in a normothermic environment to decrease the likelihood of hyperthermia and therefore investigate hyperthermic-independent neurotoxic effects.

2. Material and Methods

2.1. Drugs and chemicals

Racemic methamphetamine (MA) hydrochloride was generously provided by the National Institute on Drug Abuse (NIDA) Research Resources Drug Supply program (Bethesda, MD). The materials used in the TH and GFAP immunoassays have been described previously (O'Callaghan, 2002; Sriram et al., 2004). All other reagents were obtained from standard commercial sources, unless otherwise noted.

2.2. Taar1−KO *mouse breeding and genotyping*

The *Taar1*-KO mice were obtained from the U.C. Davis Knockout Mouse Project (KOMP; www.komp.org) as previously described (Harkness et al., 2015). Briefly, chimeric mice were created using C57BL/6N ES cells in which the entire *Taar1* coding region was deleted by homologous recombination, using the Veloci-Gene Null Allele Bac vector, and then injected into BALB/c blastocysts. The chimeras were bred with wild-type C57BL/6N mice and their offspring genotyped according to the strategy recommended by KOMP using the following primers: ACTCTTCACCAAGAATGTGG (forward); CCAACAGCGCTCAACAGTTC (reverse, wild-type allele); GTCGTCCTAGCTTCCTCACTG (reverse, null allele). Male and female siblings, identified as heterozygous for the targeted locus, were subsequently bred to produce *Taar1*-WT and *Taar1*-KO littermates.

2.3. Animal maintenance and housing

Mice of both sexes were used in all experiments and tested at 10–20 weeks of age. Before experiment initiation, mice were group-housed in filtered acrylic plastic shoebox cages (28 cm×18 cm×13 cm; l ×w× h), fitted with wire tops. Cages were lined with either ECO-Fresh bedding (Absorption Corporation, Ferndale, WA) or Bed-O-Cob (The Andersons, Maumee, OH). Mice had free access to rodent chow (5LOD, 5.0% fat content, Purina Mills, St. Louis, MO) and water *ad libitum*. The colony room was maintained at an environmental temperature of 21 ± 1 °C with lights on a 12:12 h light:dark schedule, beginning at 0600 h. All procedures were approved

by the VA Portland Health Care System's Institutional Animal Care and Use Committee and followed the requirements of the Guide for the Care and Use of Laboratory Animals. All efforts were made to minimize animal suffering, to reduce the number of animals used, and to use alternatives to *in vivo* techniques when available. All animals acclimated to the vivarium at least one week prior to testing.

2.4. Temperature recording

Two days prior to drug administration, mice were implanted with IPTT-300 temperature transponders from BioMedic Data Systems (Seaford, DE) to assess body temperature *via* telemetry. Animals were anesthetized with isoflurane (5% induction, 2.5% maintenance) and transponders were subcutaneously injected dorsally between the shoulders. On the day of drug administration, animals were weighed and transferred from group to individual cages to avoid temperature changes associated with interaction (e.g., huddling). After a 1 h acclimation period, temperature recording began and was measured every 15 min for 8 h. All experiments were conducted between 0700 and 1700 h. Temperatures were non-invasively recorded using the DAS-8001 reader console and smart probe from BioMedic Data Systems. Animals were removed from the cage and the smart probe placed within 5 cm of the embedded transponder to acquire temperature readings. The environmental temperature of the testing environment was 23 ± 1 °C. This temperature was selected in order to differentiate neurotoxic effects of the drugs from those exacerbated by elevated environmental temperatures.

2.5. Drug treatment

Following the first temperature recording (baseline), each animal received four i.p. injections (2 h apart) of saline or MA (2.5, 5, or 10 mg/kg). MA was dissolved in 0.9% saline and injected in a final volume of 10 ml/kg. These doses were selected based on preliminary experiments (Supp. Fig. 5). Mice were euthanized 2 or 7 days after the final drug treatment by cervical dislocation, followed by decapitation. The striatum was removed using blunt dissection, flash-frozen, and weighed prior to being stored at -70 °C until time of assay. Striatal tissue from each

animal was dissected and each half used for either monoamine and metabolite analyses or TH and GFAP assays (counterbalanced by side of brain).

2.6. Quantification of monoamines and metabolite levels

Striatal DA, DOPAC, HVA, 5HT, 5HIAA, and NE were quantified *via* high-performance liquid chromatography with electrochemical detection (HPLC-ECD). Tissue samples were weighed, homogenized in 0.1N $HClO_4$, and centrifuged at 16,600 *g* for 18 min at 4^{o}C. Concentrations of monoamines and their metabolites were quantified in the supernatant using HPLC-ECD. Aliquots were injected onto an HPLC column linked to a coulometric detector (ESA Model Coulochem III, Dionex, Chelmsford, MA). Mobile phase consisting of 50 mM sodium phosphate monobasic, 250 µM Na_2EDTA, 0.03% sodium octane sulfonic acid, and 25% methanol (pH = 2.75) was recirculated at 0.9 ml/min. Data were acquired by a Waters Empower software system, where peak heights of unknowns were compared with those of standards. The lower limit of assay sensitivity (3 x baseline noise) was 1 pg/20 µl sample.

2.7. Quantification of tyrosine hydroxylase levels

Tissue was prepared as previously outlined (O'Callaghan, 2002; Miller and O'Callaghan, 2003; Granado et al., 2011). Striatal tissue was homogenized in 10 volumes of 1% hot (85-95°C) sodium dodecyl sulfate (SDS) by sonification and total protein concentration determined by BCA assay. TH holoenzyme protein was assessed using a previously published ELISA with minor modifications (Sriram et al., 2004). In brief, an anti-TH monoclonal mouse antibody (1:500; Santa Cruz Biotechnology, Dallas, TX) was coated on the wells of Nunc MaxiSorp microplates (Thermo Fisher Scientific, Waltham, MA). The SDS homogenates and standards (prepared from control mouse striatum) were diluted in phosphate-buffered saline (pH = 7.4) containing 0.5% Triton X-100. After blocking non-specific binding with 5% non-fat dry milk, aliquots of the homogenate and standards were added to the wells in duplicate and incubated. Following washes, an anti-TH polyclonal rabbit antibody (1:500; EMD Millipore, Billerica, MA) was added to ‘sandwich’ the TH protein between the two antibodies, coupled with a horseradish

peroxidase (HRP) conjugated secondary anti-rabbit IgG antibody (1:3000; Santa Cruz Biotechnology, Dallas, TX). Peroxidase activity was detected using the substrate tetramethylbenzidine (Sigma-Aldrich, St. Louis, MO), followed by addition of a 1N sulfuric acid stop solution. Quantification was performed by measuring absorbance with a microplate reader (Bio-Rad Laboratories, Hercules, CA), at 450 nm. The amount of TH in the samples was calculated and expressed as TH (µg) per total protein (mg) loaded.

2.8. Quantification of GFAP expression

The same tissue homogenate used for TH analysis was also used for the GFAP assay. Striatal GFAP levels were quantified using a similar ELISA protocol (O'Callaghan, 2002) as described for TH quantification, with the following differences: an anti-GFAP polyclonal rabbit antibody (1:400; DAKO, Carpenteria, CA) was used as the capture antibody and an anti-GFAP monoclonal mouse antibody (1:250; EMD Millipore, Billerica, MA) was used as the detection antibody coupled with a secondary anti-mouse IgG-HRP antibody (1:3000; Santa Cruz Biotechnology, Dallas, TX).

2.9. Data analysis

Biochemical data were analyzed by three-way analysis of variance (ANOVA) with sex, genotype, and dose as between-group factors, at each time point, independently. Temperature data were analyzed using a repeated measures four-way ANOVA with time as a within-subject factor and sex, genotype, and dose as between-group factors. As there were no significant interactions involving sex in initial analyses, this factor was excluded from further analyses. Significant two-way interactions were further investigated using simple main effect analyses and/or *post hoc* mean comparisons using the Newman-Keuls test, when appropriate. For temperature data, subsequent analyses were conducted at 30 min after each injection as, under the described conditions, the maximum hypothermic drop occurs 30 min following administration of MA or MDMA (Harkness et al., 2015; Miner et al., 2017b). Data were analyzed for outliers using Dixon’s Q-test at 90% confidence. All statistical analyses were performed using Statistica

version 13 software (StatSoft Inc., Tulsa, OK). Differences were considered significant at $p < 0.05$.

3. Results

3.1. Monoamines and metabolite levels

MA dose-dependently decreased striatal levels of DA and DOPAC at both time points (2 and 7 days following the final injection) and HVA at 2 days (Fig. 13). Seven days later, levels of DA were lower in *Taar1*-KO mice compared to *Taar1*-WT mice after MA 2.5 and 5 mg/kg, but not 10 mg/kg, while DOPAC and HVA were lower in *Taar1*-KO mice compared to *Taar1*-WT mice, regardless of treatment. DA turnover rates (calculated by dividing DOPAC levels by DA) at both 2 and 7 days following the final treatment were higher in *Taar1*-KO compared to *Taar1*-WT mice, regardless of treatment. These characterizations are supported by the following statistical results. At 2 days following the final administration of saline or MA, a two-way ANOVA for DA level data identified a main effect of genotype ($F_{1,62} = 17.16$, $p < 0.001$) and dose ($F_{3,62} = 32.78$, $p < 0.0001$), but no significant interaction (Fig. 13A). DA levels were lower in *Taar1*-KO mice compared to *Taar1*-WT mice, regardless of treatment, and all doses of MA significantly decreased DA levels compared to saline-treated animals, regardless of genotype. At 7 days after saline or MA administration, there was a significant genotype x dose interaction ($F_{3,61} = 3.04$, $p < 0.05$) (Fig. 13B). Simple main effect analysis of the effect of genotype at each dose revealed no difference between genotypes for saline-treated animals, but *Taar1*-KO mice receiving either MA 2.5 or 5 mg/kg had significantly lower levels of striatal DA in comparison to *Taar1*-WT mice. There was no difference between genotypes at MA 10 mg/kg. Simple main effect analysis of the effect of dose within each genotype indicated significant dose-dependent effects in both *Taar1*-WT ($p < 0.0001$) and *Taar1*-KO ($p < 0.0001$) mice. In *Taar1*-WT mice, Newman-Keuls *post hoc* mean comparisons indicated that DA levels were significantly decreased by the MA 5 and 10 mg/kg doses compared to saline-treated animals, but not by MA

2.5 mg/kg. In *Taar1*-KO mice, DA levels were significantly decreased by all three MA doses compared to saline-treated animals.

Two days after the final administration of saline or MA, a two-way ANOVA for DOPAC level data revealed only a main effect of dose ($F_{3,62} = 12.94$, $p < 0.0001$) (Fig. 13C). DOPAC levels were significantly decreased by MA 5 and 10 mg/kg, but not 2.5 mg/kg, compared to saline-treated animals, regardless of genotype. At 7 days after MA administration, there was a main effect of genotype ($F_{1,61} = 13.43$, $p < 0.001$) and dose ($F_{3,61} = 35.34$, $p < 0.0001$), but no significant genotype x dose interaction (Fig. 13D). DOPAC levels were lower in *Taar1*-KO mice compared to *Taar1*-WT mice, regardless of treatment. Only the two higher doses of MA significantly decreased DOPAC levels compared to saline-treated animals, regardless of genotype.

There were no significant effects on HVA levels 2 days following the final administration of MA (Fig. 13E), but 7 days later there was a main effect of genotype ($F_{1,61} = 5.76$, $p < 0.05$) and dose ($F_{3,61} = 22.03$, $p < 0.0001$), though no significant interaction (Fig. 13F). HVA levels were lower in *Taar1*-KO mice compared to *Taar1*-WT mice, regardless of treatment. HVA levels were significantly increased by MA 2.5 mg/kg, but decreased by MA 5 and 10 mg/kg, in comparison to saline-treated animals, regardless of genotype.

At 2 days following the final injection of saline or MA, a two-way ANOVA for DA turnover data (expressed as a ratio of DOPAC/DA levels) identified a main effect of genotype ($F_{1,62} = 8.83$, $p < 0.01$) and dose ($F_{3,62} = 4.16$, $p < 0.01$), but no significant interaction (Fig. 13G). DA turnover was higher in *Taar1*-KO mice compared to *Taar1*-WT mice, regardless of treatment, and only MA 2.5 mg/kg significantly increased DA turnover compared to saline-treated animals, regardless of genotype. Seven days after the final administration of saline or MA, a two-way ANOVA for DA turnover data also found a main effect of genotype ($F_{1,61} = 12.30$, $p < 0.001$) and dose ($F_{3,61} = 20.09$, $p < 0.0001$), but no interaction (Fig. 13H). DA turnover was again higher in

Taar1-KO mice compared to *Taar1*-WT mice, regardless of treatment, and only MA 10 mg/kg significantly increased DA turnover compared to saline-treated animals, regardless of genotype.

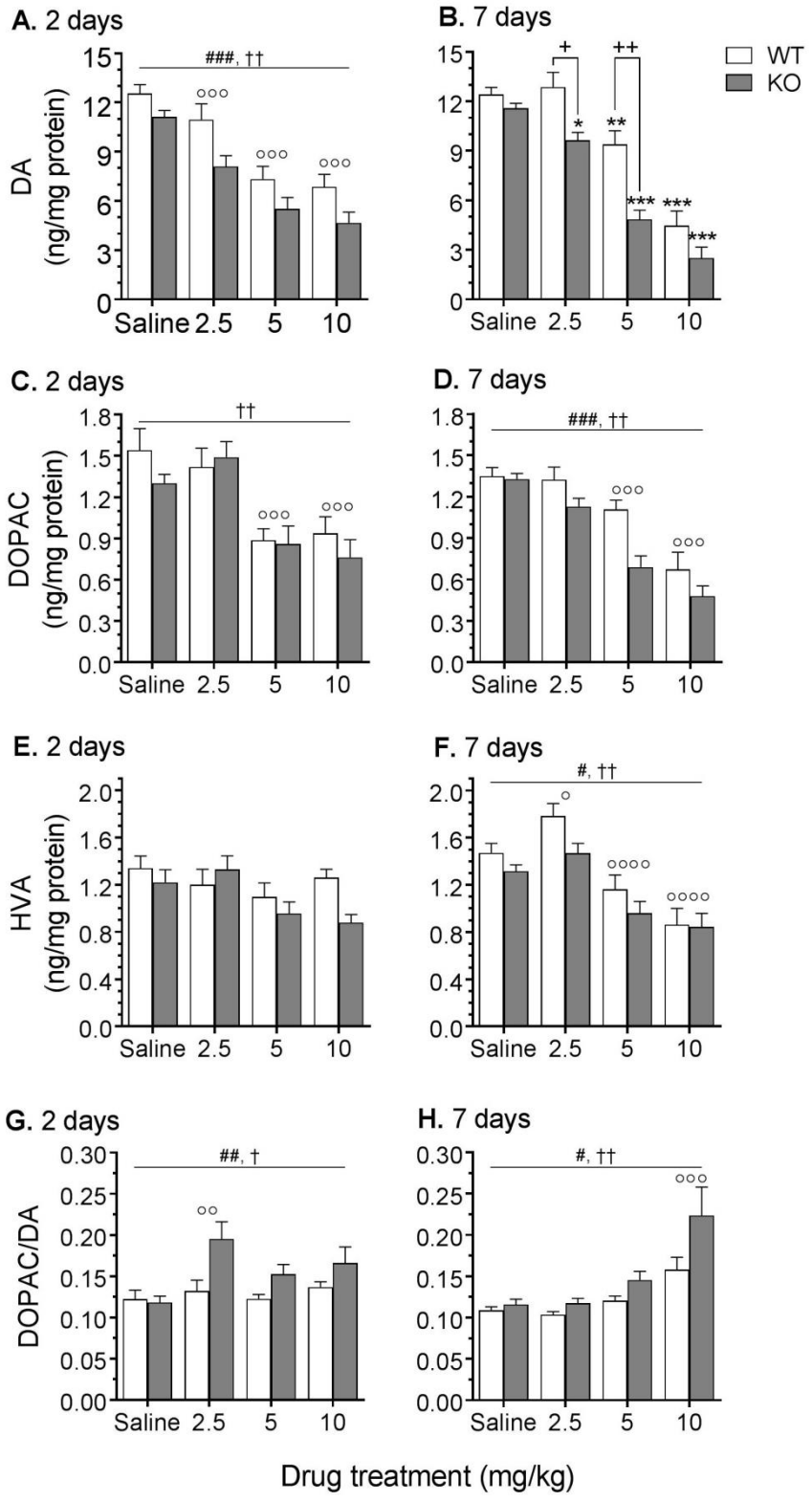

Figure 13. Striatal levels of DA, DOPAC, HVA and DA turnover measured 2 and 7 days following treatment. *Taar1*-WT and -KO mice received 4 i.p. injections of saline or MA (2.5, 5, or 10 mg/kg), 2 h apart, and were euthanized either 2 or 7 days following the final injection for striatal tissue collection. Values were normalized to the amount of protein in each tissue sample. Data represent means ± SEM of 7-11 mice per group. *: $p < 0.05$, **: $p < 0.01$, ***: $p < 0.001$ compared to saline-treated controls; +: $p < 0.001$, ++: $p < 0.0001$ between genotypes; #: $p < 0.05$, ##: $p < 0.01$, ###: $p < 0.001$ for main effect of genotype; †: $p < 0.01$, ††: $p < 0.0001$ for main effect of dose; ◦: $p < 0.05$, ◦◦: $p < 0.01$, ◦◦◦: $p < 0.001$,◦◦◦◦: $p < 0.0001$ compared to saline-treated controls, regardless of genotype.

There were no significant interactions or main effects of genotype at 2 or 7 days following MA administration for 5HT, 5HIAA, 5HT turnover, or NE (Fig. 14). A two-way ANOVA revealed a main effect of dose for 5HT levels both 2 days ($F_{3,62} = 7.34$, $p < 0.001$) and 7 days ($F_{3,61} = 13.14$, $p < 0.0001$) following the final treatment (Fig. 14A and B). Two days following administration, 5HT levels were significantly decreased by MA 5 and 10 mg/kg compared to saline-treated animals, whereas 7 days after administration MA 2.5 mg/kg significantly increased 5HT levels compared to saline-treated animals, regardless of genotype. There were no significant main effects for 5HIAA (Fig. 14C and D) or 5HT turnover (5HIAA/5HT levels) (Fig. 14E and F). A two-way ANOVA identified a main effect of dose for NE levels both 2 days ($F_{3,62} = 4.06$, $p < 0.01$) and 7 days ($F_{3,61} = 4.88$, $p < 0.01$) after the last treatment of saline or MA (Fig. 14G and H). Two days following administration, NE levels were significantly decreased by MA 10 mg/kg compared to saline-treated animals, whereas 7 days following administration, MA 5 and 10 mg/kg significantly decreased NE levels compared to saline-treated animals, regardless of genotype.

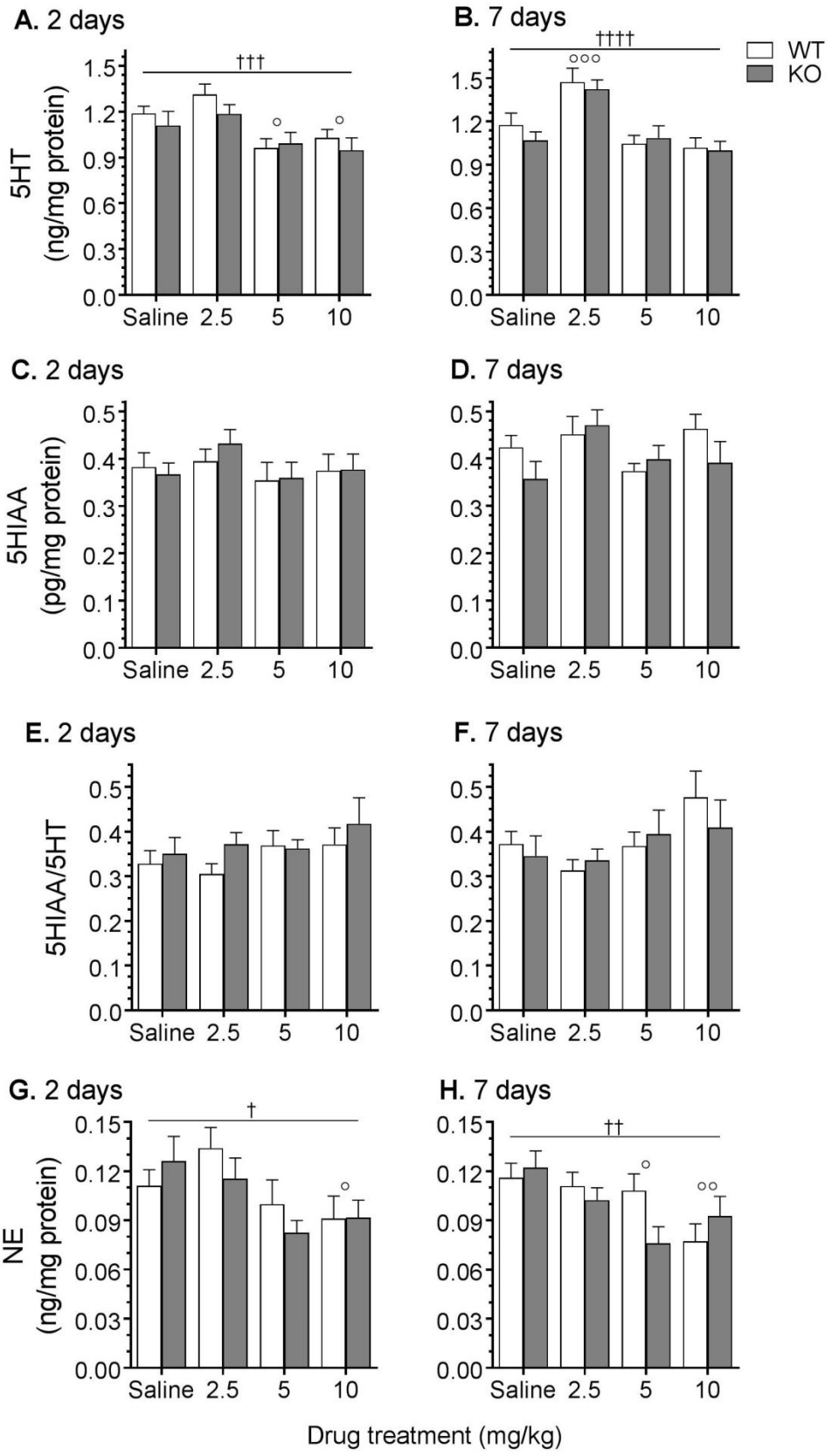
A. 2 days
B. 7 days
C. 2 days
D. 7 days
E. 2 days
F. 7 days
G. 2 days
H. 7 days
WT
KO
5HT (ng/mg protein)
5HIAA (pg/mg protein)
5HIAA/5HT
NE (ng/mg protein)
Saline
2.5
5
10
Drug treatment (mg/kg)

Figure 14. Striatal levels of 5HT, 5HIAA, 5HT turnover, and NE measured 2 and 7 days following treatment. *Taar1*-WT and -KO mice received 4 i.p. injections of saline or MA (2.5, 5, or 10 mg/kg), 2 h apart, and were euthanized either 2 or 7 days following the final injection for striatal tissue collection. Values were normalized to the amount of protein in each tissue sample. Data represent means ± SEM of 7-11 mice per group. †: $p < 0.05$, ††: $p < 0.01$, †††: $p < 0.01$, ††††: $p < 0.0001$ for main effect of dose; ◦: $p < 0.05$, ◦◦: $p < 0.01$, ◦◦◦: $p < 0.001$ compared to saline-treated controls, regardless of genotype.

3.2. Tyrosine hydroxylase levels

Overall, MA decreased striatal TH levels at each time point (2 and 7 days following final injection) and dose (2.5, 5, and 10 mg/kg). TH levels were also lower in *Taar1*-KO mice compared to *Taar1*-WT mice 2 days, but not 7 days, following final administration of saline or MA (Fig. 15). These characterizations are supported by the following statistical results. At 2 days following the final administration of saline or MA, a two-way ANOVA revealed a main effect of genotype ($F_{1,65} = 13.22$, $p < 0.001$) and dose ($F_{3,65} = 25.34$, $p < 0.0001$), but no significant interaction (Fig. 15A). TH levels were lower in *Taar1*-KO mice compared to *Taar1*-WT mice, regardless of treatment, and the two higher doses of MA (5 and 10 mg/kg), but not the 2.5 mg/kg dose, significantly decreased TH levels compared to saline-treated animals, regardless of genotype. At 7 days after MA administration, a two-way ANOVA revealed only a main effect of dose ($F_{3,59} = 25.12$, $p < 0.0001$) (Fig. 15B); all doses of MA decreased TH levels compared to levels in tissue from saline-treated controls, regardless of genotype.

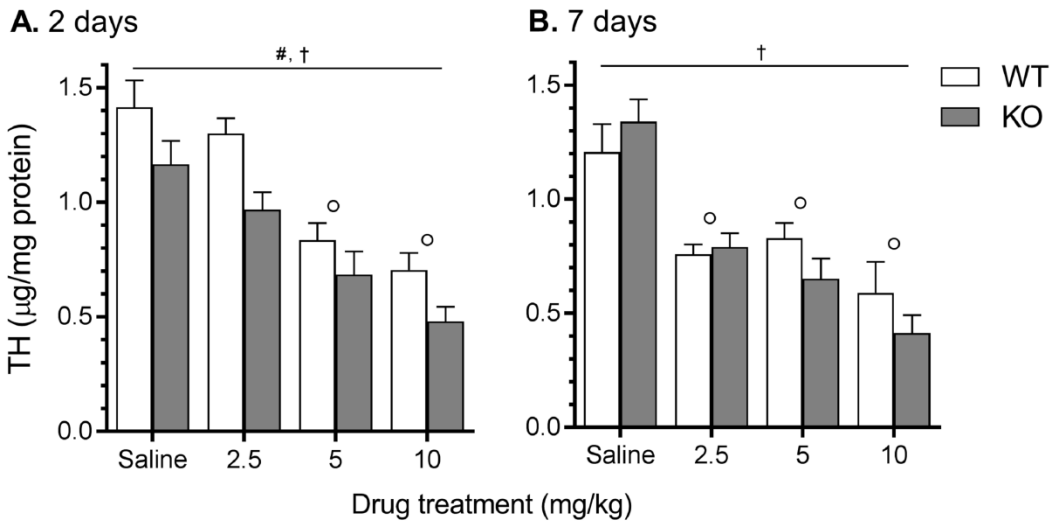

Figure 15. Striatal TH levels measured 2 and 7 days following treatment. *Taar1*-WT and -KO mice received 4 i.p. injections of saline or MA (2.5, 5, or 10 mg/kg), 2 h apart. Animals were euthanized either 2 (**A**) or 7 (**B**) days following the final injection for striatal tissue collection. TH values were normalized to the amount of protein in each tissue sample. Data represent means ± SEM of 7-11 mice per group. #: $p < 0.001$ for main effect of genotype, †: $p < 0.0001$ for main effect of dose; ◦: $p < 0.001$ compared to saline-treated controls, regardless of genotype.

3.3. GFAP expression

Overall, at both 2 and 7 days post MA administration, and at all doses (2.5, 5, or 10 mg/kg), MA increased striatal GFAP expression. GFAP was increased to a greater extent in striatal tissue from *Taar1*-KO compared to *Taar1*-WT mice by both the MA 2.5 and 5 mg/kg doses (Fig. 16). These characterizations are supported by the following statistical results. At 2 days following the final administration of saline or MA, a two-way ANOVA revealed a significant genotype x dose interaction ($F_{3,36} = 4.17$, $p < 0.01$) (Fig. 16A). Simple main effect analysis of genotype at each dose revealed no difference between genotypes for saline-treated animals, but *Taar1*-KO mice receiving either MA 2.5 or 5 mg/kg expressed significantly higher levels of striatal GFAP in comparison to *Taar1*-WT mice ($p < 0.01$ for both doses). There was no

difference between genotypes at MA 10 mg/kg. Simple main effect analysis of the effect of dose within each genotype indicated significant dose-dependent effects in both *Taar1*-WT ($p < 0.0001$) and *Taar1*-KO ($p < 0.0001$) mice. Newman-Keuls *post hoc* comparisons indicated all 3 doses of MA significantly increased levels of GFAP in both *Taar1*-WT and *Taar1*-KO mice compared to levels in saline-treated animals.

Similar results were obtained for striatal GFAP assessed 7 days after treatment. A two-way ANOVA revealed a significant genotype x dose interaction ($F_{3,58} = 5.38$, $p < 0.01$) (Fig. 16B). Again, simple main effect analyses of genotype at each dose revealed no difference between saline-treated *Taar1*-WT and -KO animals, but *Taar1*-KO mice receiving MA 2.5 or 5 mg/kg expressed significantly higher levels of GFAP than *Taar1*-WT mice, whereas there was no difference between genotypes administered the highest dose of MA. Simple main effect analysis of the effect of dose within each genotype indicated significant dose-dependent effects in both *Taar1*-WT ($p < 0.0001$) and *Taar1*-KO ($p < 0.0001$) mice. Newman-Keuls *post hoc* mean comparisons revealed that GFAP expression in *Taar1*-WT mice was only significantly elevated in mice treated with MA 5 mg/kg and 10 mg/kg compared to saline-treated animals, but all three doses of MA elevated GFAP expression in *Taar1*-KO mice compared to saline-treated mice.

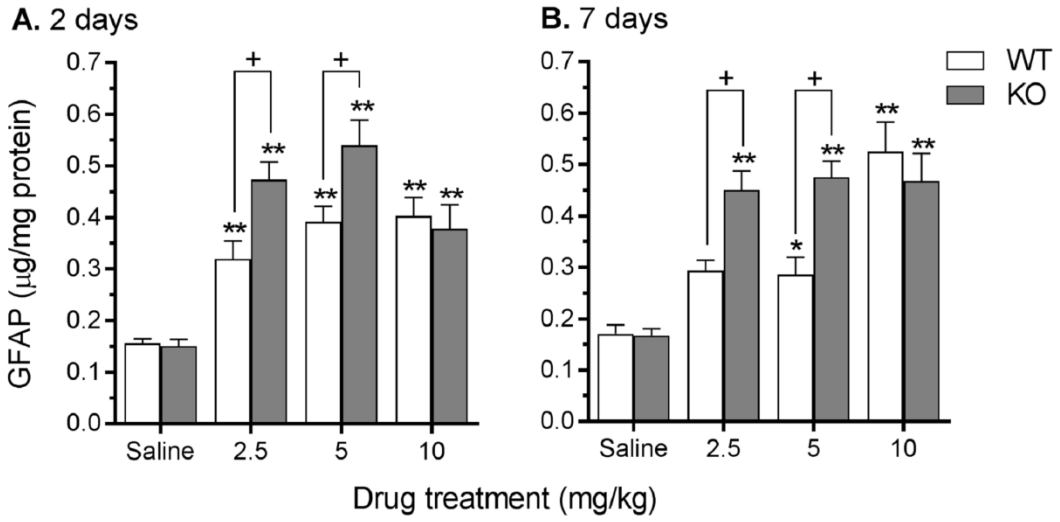

Figure 16. Striatal GFAP levels measured 2 and 7 days following treatment. *Taar1*-WT and -KO mice received 4 i.p. injections of saline or MA (2.5, 5, or 10 mg/kg), 2 h apart. Animals were euthanized either 2 (**A**) or 7 (**B**) days following the final injection for striatal tissue collection. GFAP values were normalized to the amount of protein in each tissue sample. Data represent means ± SEM of 7-11 mice per group. *: $p < 0.05$, **: $p < 0.001$ compared to saline-treated controls; +: $p < 0.001$ between genotypes.

3.4. Thermal response

Prior to the first injection, the mean baseline temperature of all animals was 38.3°C (SEM = 0.03°C), with no significant between-genotype or -group differences. Profound genotype-dependent MA-induced hypothermia was observed. MA did not elicit hyperthermia, defined as a 0.5°C increase in body temperature above the temperature of the untreated animal, in any group. Temperature data (Fig. 17), analyzed using a three-way repeated measures ANOVA, revealed a significant genotype x dose x time interaction ($F_{96, 4288} = 4.9$, $p < 0.0001$). There was no difference in temperature between genotypes for mice receiving saline (Fig. 17A), although there was a main effect of time ($F_{32, 1312} = 1.3$, $p < 0.0001$) as temperatures in these control groups decreased over the 8 h period, likely attributable to single housing.

Examination of the effects of each dose of MA revealed significant genotype x time interactions for all 3 doses: MA 2.5 mg/kg ($F_{32,672} = 9.4$, $p < 0.0001$) (Fig. 17B), MA 5 mg/kg ($F_{32,1120} = 15.3$, $p < 0.0001$) (Fig. 17C), and MA 10 mg/kg ($F_{32,1184} = 4.0$, $p < 0.0001$) (Fig. 17D). Analyses of genotype differences were conducted within each dose of MA using simple main effect analyses at each 30 min post-injection time point to investigate the hypothermic drop in body temperature. The temperatures of *Taar1*-WT mice receiving MA 2.5 mg/kg were significantly lower 30 min after each of the four MA injections compared to their *Taar1*-KO counterparts, whereas *Taar1*-WT mice administered either MA 5 or 10 mg/kg had significantly lower temperatures than *Taar1*-KO mice after the first three injections.

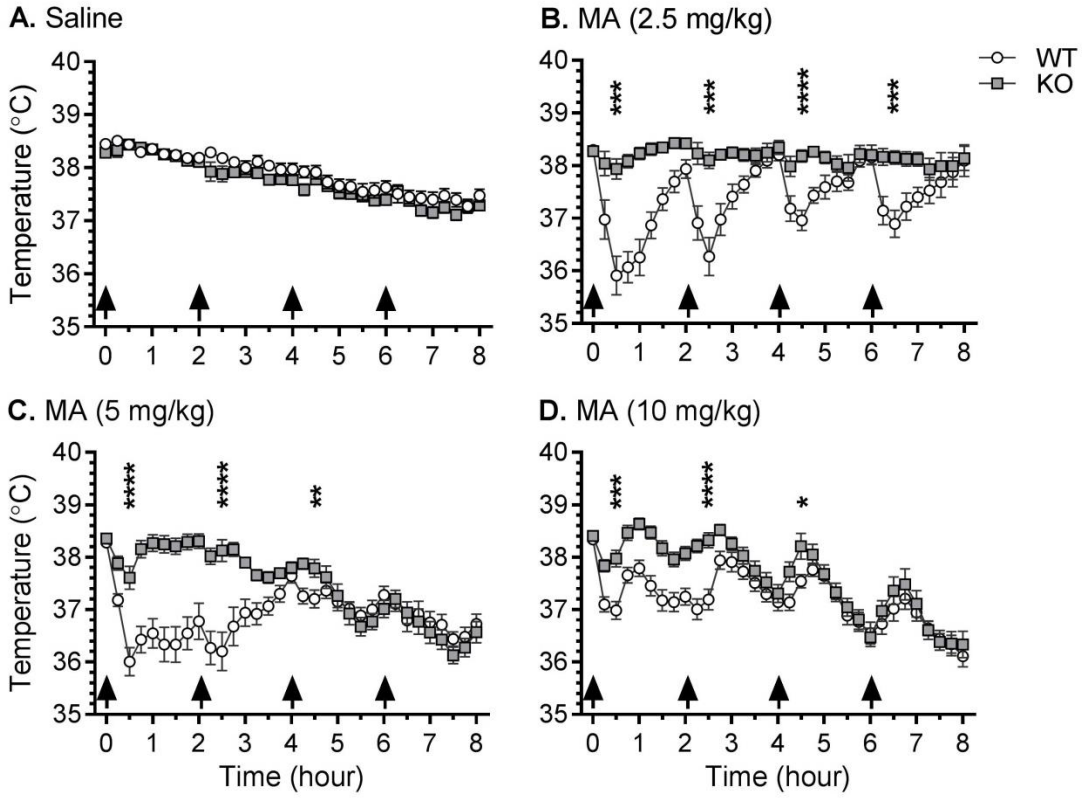

Figure 17. Effects of repeated saline or MA injections on core body temperature. *Taar1*-WT and -KO mice received 4 i.p. injections (indicated by arrows) of saline or MA (2.5, 5, or 10 mg/kg), 2 h apart. Body temperature was measured every 15 min *via* telemetry over 8 h in an ambient temperature of 23 ± 1°C. Data represent temperature for each genotype and treatment group (mean ± SEM) at specified time points, n = 11-21 mice per group. Time points selected for detailed analysis were 30 min after each injection. *: $p < 0.05$, **: $p < 0.01$, ***: $p < 0.001$, ****: $p < 0.0001$ compared between genotypes.

Next, examination of the data for each genotype revealed a significant dose x time interaction for both genotypes: *Taar1*-WT ($F_{96,2208} = 10.8$, $p < 0.0001$) and *Taar1*-KO ($F_{96,2080} = 7.5$, $p < 0.0001$). Simple main effects analysis was then used to statistically investigate MA effects within each genotype at the 30 min post-injection time points. There was a significant

effect of dose after the first, second and third injections in *Taar1*-WT mice (all $p < 0.0001$) and after the first and fourth injections in *Taar1*-KO mice (both $p < 0.001$ and $p < 0.01$). Newman-Keuls *post hoc* mean comparisons indicated that 30 min following the first and second injection *Taar1*-WT mice treated with all MA doses had lower body temperatures than *Taar1*-WT mice receiving saline (Table 10). Thirty min after the third injection, the difference was significant in *Taar1*-WT mice receiving MA 2.5 or 5 mg/kg, but not 10 mg/kg, and there were no significant effects of MA 30 min after the fourth injection. In *Taar1*-KO mice, body temperature was significantly reduced by MA 5 and 10 mg/kg 30 min after the first injection. There were no other significant hypothermic responses to MA in *Taar1*-KO mice, though body temperature was significantly increased 30 min following the fourth injection in mice receiving MA 2.5 mg/kg. However, this increase of 0.8°C for *Taar1*-KO mice at this dose and time resulted in a mean body temperature of 38.5°C compared to the initial basal temperature of 38.3°C, providing little evidence of MA-induced hyperthermia.

Table 10. MA-induced change in body temperature relative to saline-treated mice

Taar1	MA	30 min post-injection (ΔT°C ± SEM)			
	(mg/kg)	1st Inj	2nd Inj	3rd Inj	4th Inj
WT	2.5	-2.53 ± 0.37[c]	-1.91 ± 0.36[c]	-0.96 ± 0.19[b]	-0.56 ± 0.26
	5	-2.44 ± 0.27[c]	-1.98 ± 0.36[c]	-0.71 ± 0.17[a]	-0.65 ± 0.22
	10	-1.45 ± 0.17[c]	-0.99 ± 0.20[b]	-0.37 ± 0.12	-0.43 ± 0.24
KO	2.5	-0.50 ± 0.20	0.22 ± 0.16	0.40 ± 0.11	0.78 ± 0.13[b]
	5	-0.83 ± 0.22[a]	0.24 ± 0.21	0.01 ± 0.17	-0.44 ± 0.21
	10	-0.47 ± 0.16[a]	0.44 ± 0.14	0.42 ± 0.25	-0.02 ± 0.26

Data represent change in temperature (mean ± SEM) for each treatment group from saline-treated mice at specified time point, n = 11-21 mice per group. *a*: $p < 0.05$; *b*: $p < 0.01$; *c*: $p < 0.001$ in analysis compared to saline-treated controls.

4. Discussion

In Chapter 4, I report for the first time that activation of TAAR1 by a binge-like regimen of MA altered thermal response and decreased markers of neurotoxicity both 2 and 7 days following administration. Activation of TAAR1 inhibits DA firing in the striatum, the locus of MA-induced neurotoxicity, and mice lacking TAAR1 have altered sensitivity to the acute effects of amphetamines, biochemically and behaviorally (Lindemann et al., 2008; Revel et al., 2011; Harkness et al., 2015). Based on these findings, I administered MA to *Taar1*-WT and *Taar1*-KO mice and measured acute thermal response, as well as transient and sustained effects of MA on markers of DA terminal degeneration and astrogliosis.

At 2 days post-treatment, DA and TH levels were dose-dependently diminished and levels were lower when TAAR1 was absent, regardless of treatment. However, this should not be interpreted as differences in basal levels as 7 days following treatment there was no significant difference in saline-treated animals. The findings from 7 days post-treatment indicate sustained MA-induced decreases in DA levels are dose-dependently diminished when TAAR1 is activated: the lowest dose of MA did not decrease DA levels when TAAR1 was activated, but did when TAAR1 was absent; the middle MA dose (5mg/kg) further decreased DA levels when TAAR1 was not activated; and the highest dose of MA did not differentially decrease DA when the receptor was activated or not. However, TH levels were not differentially affected across genotype at this later time point, indicating activation of TAAR1 transiently altered TH levels, but the effects were not sustained. The difference in levels of DA and metabolites between genotypes coupled with equally diminished TH levels at this time point suggests the sustained effects of TAAR1 activation take place post-DA synthesis. Although amphetamines acutely increase striatal levels of 5HT and NE, measured by microdialysis, in *Taar1*-KO compared to *Taar1*-WT mice (Lindemann et al., 2008; Di Cara et al., 2011), here there were no significant differences in striatal levels of 5HT, 5HIAA, or NE between genotypes 2 or 7 days following MA administration. This indicates that, while TAAR1 modulates acute MA-induced release of 5HT

and NE, the modulatory effects of the receptor on striatal monoamine levels at later time points are DA specific, reflective of the selectivity of MA for DA terminal degeneration in mice (Krasnova and Cadet, 2009).

Astrocyte activation, a glial reaction to neuronal injury, is an established marker of MA-induced neurotoxicity. An increase in GFAP expression peaks 2-3 days after MA administration and correlates with increased neurotoxicity, inflammatory response, and ROS (O'Callaghan and Miller, 1994; Lau et al., 2000; McConnell et al., 2015), though it can also increase independently of decreases in markers such as TH and DA (Pu and Vorhees, 1993; Miner et al., 2017b). I report the novel finding that astrocyte activation in response to MA is increased when TAAR1 is not activated. At both time points, the two lower doses of MA increased GFAP expression in *Taar1*-KO compared to *Taar1*-WT mice (though not at the highest dose). Additionally, at 7 days following the last administration, the lowest dose of MA significantly increased GFAP expression in *Taar1*-KO mice compared to saline-treated mice, while there was no significant increase when TAAR1 was activated in *Taar1*-WT mice. This corresponds with the DA data, indicating activation of TAAR1 is neuroprotective at lower doses, but the effect is suppressed at the highest dose of MA.

When using a binge-like regimen in a mouse model, MA 10 mg/kg is a common dose based on its strong neurotoxic effects (O'Callaghan and Miller, 1994; Zhu et al., 2006; Fantegrossi et al., 2008; Grace et al., 2010). In my experiments, this dose caused the largest changes in DA, TH, and GFAP, but abolished differences between genotypes. Comparing the two lower doses of MA, decreases in DA and TH levels were less than two-fold in *Taar1*-WT mice, though DA and TH levels were decreased more than two-fold in *Taar1*-KO mice receiving MA 5 mg/kg, indicating increased neurotoxicity. At peak astrocyte activation (2 days post-administration), increases in GFAP expression were even larger with MA 2.5 and 5 mg/kg increasing GFAP expression greater than two-fold in *Taar1*-WT mice and three-fold in *Taar1*-KO mice. This magnitude of change is commensurate with previous research using MA doses less than 10

mg/kg (Thomas et al., 2004a; McConnell et al., 2015) and indicates that TAAR1 may play an even more significant role in astroglial activation than DA terminal degeneration.

The temperature findings present a novel insight into the effects of TAAR1 on regulation of thermal response to MA and associated neurotoxicity. MA elicited hypothermia in *Taar1*-WT, but not *Taar1*-KO mice. In *Taar1*-WT mice, hypothermia was inversely dose-dependent: the largest change in temperature and longest persisting effects were elicited by the two lower doses of MA, whereas hypothermia and genotype differences were attenuated at the highest dose. In *Taar1*-KO mice, MA elicited only mild fluctuations from the initial basal temperature. These findings indicate the hypothermic response to MA is dependent on activation of TAAR1. Direct stimulation of TAAR1, using the selective agonist RO5166017, has produced differing results: in C57BL/6 mice, a single dose of 1 mg/kg induced hypothermia 45 min later (Revel et al., 2011), while in Sprague-Dawley rats, doses of 3.2 – 10 mg/kg did not alter body temperature one hour post-injection (Siemian et al., 2017). It is unclear whether this is a species and/or dose dependent effect. Although previous TAAR1 research support my finding of TAAR1-dependent MA-induced hypothermia (Harkness et al., 2015), Panas et al. (2010) found a single dose of MA (3 mg/kg) elicited an equal hyperthermic response in *Taar1*-WT and –KO mice. It is difficult to explain the disparity in these results as experimental conditions (ambient temperature and housing) were similar and elicited hypothermia and genotype differences using MA doses less and greater than their dose. However, there is always the possibility that differences in the backgrounds from which the *Taar1*-KO mice were generated may account for differential results. Additionally, similarly to the same discrepancy between the thermal response to MDMA (Chapter 3) and the findings reported in this paper, it may be that once hyperthermia is induced in *Taar1*-WT mice, the ability for TAAR1 activation to modulate body temperature is masked and any differences between genotypes disappears.

However, MA did not induce hyperthermia in animals of either genotype, similar to my findings with MDMA. When studying MA-induced neurotoxicity, hyperthermia can confound the

ability to distinguish neurotoxicity attributable to the direct actions of MA versus the indirect effects of inducing hyperthermia, which leads to increased ROS production and permeability of the blood brain barrier (Kiyatkin and Sharma, 2009; Bowyer and Hanig, 2014). As body temperatures only reached a maximum increase of 0.2°C from the initial baseline temperature, the increase in MA-induced markers of neurotoxicity in *Taar1*-KO mice cannot be attributed to hyperthermic effects. Conversely, hypothermia can confer neuroprotection against MA. Typically, this is induced by lowering the ambient temperature to 15 or 4 °C or by leveraging pharmacological agents to decrease temperature (Miller and O'Callaghan, 1994; Albers and Sonsalla, 1995; Ali et al., 1996; Metzger et al., 2000; Sharma et al., 2015), whereas in the current study all animals received the same drugs under the same conditions. Therefore, it is possible that the increased MA-induced neurotoxicity in *Taar1*-KO mice is attributable to the absence of MA-induced hypothermia. This theory is supported by the connection between temperature data and neurotoxicity with regard to dose. Significant differences between genotypes in DA levels and GFAP expression occurred only at the two lower doses of MA, corresponding with the greatest hypothermic responses.

However, the neuroprotective effects of TAAR1 activation and its modulation of thermal response may occur in tandem or independently. The intent of this study was to separate the hyperthermic influence from drug-dependent effects to better understand the effect of TAAR1 on both drug-induced changes in body temperature and neurotoxicity. However, studies are needed to determine whether the activation of TAAR1 diminishes MA-induced neurotoxicity due to its hypothermic effects or other mechanisms, potentially through pharmacologically equalizing temperature fluctuations. Additional research is also warranted under environmental conditions where hyperthermia occurs to further explore TAAR1 regulation of temperature and MA-induced neurotoxicity.

While the effects of TAAR1 activation on the DA system are complex and its mechanism still not fully understood, significant attention has been focused on D2R. Compared to *Taar1*-WT

mice*, Taar1*-KO mice over-express D2R, possess increased density of D2R in high-affinity states for DA ($D2R^{High}$) , and express super-sensitivity to activation of post-synaptic D2R (Wolinsky et al., 2007; Espinoza et al., 2015a), traits associated with increased behavioral sensitivity to amphetamines (Seeman et al., 2005; Shuto et al., 2008). Additionally, inhibition of TAAR1 increases potency of D2R agonists and reduces D2R desensitization rates (Bradaia et al., 2009). Finally, TAAR1 and D2R can form a heterodimer and the D2R antagonist raclopride increases TAAR1 activation (Espinoza et al., 2011). MA-induced neurotoxicity is D2R-mediated and D2R antagonists, such as raclopride and eticlopride, diminish MA-induced neurotoxicity (DA, TH, DAT levels, and GFAP expression) and attenuate MA-induced hyperthermia (Albers and Sonsalla, 1995; Broening et al., 2005; Xu et al., 2005; Hadlock et al., 2010). These markers of neurotoxicity are also lower in D2R-KO mice receiving MA, which exhibit MA-induced hypothermia as well, in comparison to D2R-WT mice (Granado et al., 2011). It is possible that the absence of MA-induced hypothermia and increased neurotoxicity in *Taar1*-KO mice can be attributed to increased D2R activation compared to when TAAR1 is activated in *Taar1*-WT mice. Future research on the intersection of TAAR1 and D2R effects on MA-induced neurotoxicity are warranted. Additionally, as neurotoxicity is primarily attributed to increased cytosolic levels of DA (Fleckenstein et al., 2007) and TAAR1 is predominantly localized intracellularly (Borowsky et al., 2001), future research of TAAR1 regulation of MA-induced neurotoxicity could investigate acute intracellular markers of neurotoxicity, such as impaired VMAT2 expression and function (Fumagalli et al., 1999; Guillot et al., 2008), and increased DA quinone and ROS production (Cubells et al., 1994; LaVoie and Hastings, 1999; Yamamoto and Raudensky, 2008).

TAAR1 mediation of excitotoxicity is another potential contributor to MA-induced neurotoxicity. The expression and phosphorylation of the GluN1 subunit of the NMDA GLU receptors, in both the striatum and the prefrontal cortex (PFC), is lower in *Taar1*-KO mice compared to *Taar1*-WT mice (Espinoza et al., 2015b; Sukhanov et al., 2016). However, when amphetamine is administered, striatal expression and phosphorylation of GluN1 are increased

only in *Taar1*-KO mice. This suggests amphetamines elicit an increased GLU response when TAAR1 is not activated, potentially contributing to increased neurotoxicity. Supporting a GLU system regulatory role for TAAR1, another study, using 6-hydroxydopamine (6-OHDA) to induce an animal model of Parkinson's disease, found the intrastriatal application of the selective TAAR1 agonist, RO5166017, blocked 6-OHDA-induced increased striatal GLU release (Alvarsson et al., 2015). This same study also evaluated the effects of intrastriatal administration of 6-OHDA on DA markers using the *Taar1*-KO mouse model. Surprisingly, four weeks following 6-OHDA treatment, *Taar1*-WT mice had lower levels of striatal TH and DAT compared to *Taar1*-KO mice. While counter to my findings that activation of TAAR1 is neuroprotective against MA-induced neurotoxicity, it is important to note 6-OHDA lesioning destroys cell bodies in the substantia nigra pars compacta (SNpc) as well as terminals in the striatum (Bove and Perier, 2012). Although there is evidence MA causes DA cell body death in the SNpc, MA primarily causes degeneration of striatal neuron terminals (Sonsalla et al., 1996; Ares-Santos et al., 2014). It is plausible TAAR1 has different modulatory roles in these two models of neuronal injury, as they differ in underlying mechanism, time course, and severity.

Astrocytes also decrease excitotoxicity *via* clearance of synaptic GLU by the excitatory amino acid transporter 2 (EAAT2) (Anderson and Swanson, 2000). Cisneros and Ghorpade (2014) investigated TAAR1 regulation of this function using cultured astrocytes. The authors found that knockdown of TAAR1 using RNA interference mitigates MA-induced down-regulation of EAAT2 and increases GLU clearance, while overexpression of TAAR1 increases MA-induced EAAT2 down-regulation and decreases GLU clearance. These findings imply MA activation of TAAR1 increases excitotoxicity, acting as a contributing factor to neurotoxicity (Burrows and Meshul, 1997). It is possible that MA activation of TAAR1 impairs astrocytic GLU function *in vitro*, but this effect is overshadowed by the increase in MA-induced astrocyte activation in *Taar1*-KO mice compared to *Taar1*-WT mice under physiological conditions. Additional research is warranted to explore TAAR1 regulation of other markers of gliosis, namely microglia.

MA induces neuroinflammation and microgliosis, other contributors to neurotoxicity, through the production of harmful cytokines and chemokines, which is also ameliorated at lower temperatures (LaVoie et al., 2004; Thomas et al., 2004a; O'Callaghan et al., 2014).

While TAAR1 research has focused on the acute effects of single doses of amphetamines, the results presented in Chapter 4 indicate a regulatory role for TAAR1 on the effects of a binge-like dosing regimen of MA, persisting up to 7 days later. Activation of TAAR1 elicited an acute hypothermic response to MA, similar to MDMA, and decreased MA-induced neurotoxicity. For the first time, I demonstrate MA-induced neurotoxicity is increased in animals lacking TAAR1; indicating activation of the receptor confers neuroprotection.

Chapter 5: The role of biogenic amine transporters on TAAR1 regulation of methamphetamine-induced neurotoxicity

The data presented in this chapter are unpublished.

1. Introduction

The findings from Chapter 4 demonstrate TAAR1 modulates MA-induced neurotoxicity, but do not provide an explanation or mechanism through which this occurs. Although TAAR1 modulation of the thermal response to MA may contribute, there are undoubtedly additional factors at play. As previously discussed, the origin of the neurotoxic effects of MA reside in its ability to impair striatal VMAT2 and DAT function, resulting in elevated cytosolic DA levels (Fleckenstein et al., 2007). DAT function is rapidly impaired by MA, reflected by decreases in DA uptake inhibition and release that quickly return to baseline. MA (10 mg/kg, 4 inj, 2 h apart) inhibits [^{3}H]DA uptake 1 h following administration, but not 24 h later (Sandoval et al., 2000). In rats, a single dose of MA (15 mg/kg) decreases [^{3}H]DA uptake 30 min later, similarly returning to baseline at 24 h (Fleckenstein et al., 1997). However, MA does not diminish DAT expression until 24 h following administration and reaches a maximal decrease 3 days later (Zhu et al., 2005; McConnell et al., 2015). While MA decreases DAT expression and is a biomarker of neurotoxicity, decreased basal DAT expression also mitigates MA-induced neurotoxicity. DAT-knockout mice are resistant to the neurotoxic effects of MA, measured by DA levels, GFAP expression, and free radical production (Fumagalli et al., 1998). When DAT levels are decreased, less DA and MA enter the terminal resulting in a smaller intracellular DA pool and diminished effects on vesicular DA storage.

TAAR1 is predominantly localized in the cytoplasm, but there is evidence that TAAR1 and DAT co-localize in the SN (Xie et al., 2007). However, a functional connection between TAAR1

and DAT has been difficult to establish. In striatal synaptosomes from rats, activation of TAAR1 by a partial agonist (RO5203648) does not alter *in vitro* MA-induced striatal [^{3}H]DA uptake or release (Cotter et al., 2015). An alternative study reported *in vitro* treatment with MA increases [^{3}HDA uptake inhibition and [^{3}H]DA release in striatal synaptosomes from *Taar1*-WT compared to –KO mice (Xie and Miller, 2009a). This study, indicating activation of TAAR1 increases MA-induced impairment of DAT function, is seemingly at odds with my results from Chapter 4, as well as *in vivo* microdialysis findings that amphetamine-induced DA release is increased in *Taar1*-KO mice (Wolinsky et al., 2007; Di Cara et al., 2011). Additional research is needed on the interaction between TAAR1 and DAT.

The functionality and expression of VMAT2 are perhaps even more critical to neurotoxicity than DAT. While DAT transports MA into the cell, it predominantly increases extracellular DA, whereas VMAT2 increases intracellular DA leading to the formation of ROS and oxidative stress (Sulzer et al., 1995; Volz et al., 2007b). Diminished basal VMAT2 expression also increases MA-induced neurotoxicity. A transgenic VMAT2 knockout mouse model was developed, creating mice heterozygous for transporter (VMAT2-HET) with low VMAT2 expression, and used to study MA-induced neurotoxicity (Fumagalli et al., 1999). As to be expected, MA (15 mg/kg, 4 inj, 2 h apart) decreases striatal DA levels 2 days following administration and DAT levels 7 days later in VMAT2-HET compared to VMAT2-WT mice. However, MA acutely increases extracellular DA levels in VMAT2-WT compared to -HET mice. This indicates the observed neurotoxicity is preferentially due to intracellular rather than extracellular DA, presumably due to the diminished ability of the VMAT2-HET mice to sequester cytosolic DA. Vesicular VMAT2 function is diminished at both 1 and 24 h following MA (10 mg/kg, 4 inj, 2 h apart) administration, corresponding with DA terminal degeneration 6 days later (Hogan et al., 2000; Ugarte et al., 2003). While VMAT2 function is typically solely measured in this enriched vesicular fraction consisting of cytosolic vesicles, Fleckenstein and coworkers examined VMAT2-mediated DA uptake in membrane-associated vesicles (Volz et al., 2007a). Similar to

the vesicular fraction, they reported MA inhibits VMAT2-mediated [^{3}H]DA uptake in the membrane-associated fraction 1, 24, and 72 h following administration (Chu et al., 2010). VMAT2 expression is also decreased by MA at these time points, but the effect is localized to the purified vesicular fraction, as VMAT2 expression in the synaptosomal and membrane-associated fractions is unchanged, indicative of vesicular trafficking (Hogan et al., 2000; Riddle et al., 2002; Ugarte et al., 2003). Although there is currently no published data on an interaction between TAAR1 and VMAT2, , their intracellular localization suggests a link. TAAR1 is associated with the total cellular membrane fraction, including cytosol, nuclear, and cytoskeletal compartments, but is notably lacking in expression on the cell surface membrane (Bunzow et al., 2001; Xie et al., 2008a). TAAR1 activation of the PKC signaling cascade is also a potential bridge as PKC phosphorylates VMAT2 and modulating the ability of the transporter to sequester and release monoamines (Panas et al., 2012; Torres and Ruoho, 2014).

Based on the key roles VMAT2 and DAT play in the regulation of neurotoxicity and my finding that TAAR1 modulates neurotoxicity, I investigated potential interactions between TAAR1 and the transporters VMAT2 and DAT. In particular, the impact of TAAR1 activation on MA-induced dysregulation of striatal VMAT2 function and expression on membrane-associated and cytosolic vesicles, separately, as well as DAT function and expression in striatal synaptosomes. I conducted VMAT2 function and expression experiments using *in vivo* treated tissue in order to more closely resemble a physiological environment and investigate the effects of MA after it has been cleared from the CNS. Using the binge-like regimen of MA (5 mg/kg, 4 inj, 2 h apart), VMAT2-mediated [^{3}H]DA uptake was quantified 24 h following final administration in striatal tissue from *Taar1*-WT and –KO mice. The intermediary dose of MA (5 mg/kg) was chosen as it elicited changes in neurotoxic markers in both genotypes, as well as between genotypes (Chapter 4). Although both VMAT2 function and expression are diminished 1 h following MA administration, I chose to measure the effects 24 h later as MA concentration

levels in the brain return to baseline by this time (Fleckenstein et al., 1997; Hogan et al., 2000; Ugarte et al., 2003).

Due to the heterogeneous expression of VMAT2 among cell compartments, I separated striatal homogenate into synaptosomal, membrane-associated, and vesicular fractions *via* subcellular fractionation. As VMAT2 expression is differentially trafficked between fractions, this is likely reflected in VMAT2 function, but has not been widely examined. Investigation in the other fractions would also aid in determining whether expression matches function. VMAT2 function in all fractions was quantified by [^{3}H]DA uptake and the VMAT2 selective inhibitor reserpine was used to determine non-specific binding. As reserpine does not bind to DAT, SERT, or NET (Pristupa et al., 1994; Rudd et al., 2005; Mandela et al., 2010), all specific uptake was considered VMAT2-mediated. I hypothesized [^{3}H]DA uptake inhibition would be increased in *Taar1*-KO compared to -WT mice following MA administration, indicating VMAT2 function is impaired when TAAR1 is not activated. Since the ability of MA to elevate cytosolic DA levels *via* VMAT2 is primarily attributed to transporters expressed on the vesicles and MA does not alter VMAT2 expression in the other fractions, I hypothesized the difference would only be observed in the vesicular fraction. To further my investigation of DAT function from Chapter 3, I quantified time-dependent [^{3}H]DA release using a superfusion apparatus and [^{3}H]DA uptake in striatal tissue homogenate and synaptosomes from *Taar1*-WT and –KO mice. This was performed *in vitro* as DAT function returns to baseline 24 h following MA administration (Sandoval et al., 2000). I hypothesized DA uptake inhibition and release would be increased in tissue from *Taar1*-KO compared to –WT mice, indicating TAAR1 acutely modulates DAT function.

Besides VMAT2 function, TAAR1 modulation of VMAT2 and DAT expression was also quantified 24 h following MA (5 mg/kg, 4 inj, 2 h apart) administration. Quantification of transporter expression was performed in both the *Taar1* and MADR mouse models. VMAT2 expression was measured in whole synaptosomes, as well as isolated membrane-associated vesicles and cytosolic vesicles. I hypothesized MA would diminish VMAT2 expression in the

vesicular fraction and be decreased in *Taar1*-KO and MAHDR compared to *Taar1*-WT and MALDR mice, but would remain unchanged in the synaptosomal and membrane-associated fractions. These results would support earlier research that VMAT2 is redistributed by MA at this early time point, while total VMAT2 expression in synaptosomes remains the same (Hogan et al., 2000; Ugarte et al., 2003). A decrease in baseline VMAT2 expression in *Taar1*-KO and MAHDR mice would contribute to decreased VMAT2 functionality and indicate an interaction with TAAR1, potentially mediating MA-induced neurotoxicity. I hypothesized MA would decrease synaptosomal DAT expression in *Taar1*-KO and MAHDR compared to *Taar1*-WT and MALDR mice as another marker of neurotoxicity.

Finally, to continue my investigation of TAAR1 modulation of thermal response to MA, I recorded body temperature in MADR and *Taar1* mice for inter-model comparison. I hypothesized both models would produce similar results: MA would elicit acute hypothermia in both MALDR and *Taar1*-WT mice, in which TAAR1 was activated, but not in MAHDR and *Taar1*-KO mice, in which the receptor was not activated as it was either non-functional or absent.

2. Material and Methods

2.1. Drugs and chemicals

Racemic MA hydrochloride was generously provided by the National Institute on Drug Abuse (NIDA) Research Resources Drug Supply program (Bethesda, MD). [^{3}H]DA and [^{125}I]RTI-55 were purchased from Perkin Elmer (Boston, MA). [^{3}H]DHTB and DHTB were purchased from American Radiolabeled Chemicals (St. Louis, MO). All other reagents were obtained from standard commercial sources, unless otherwise noted.

2.2. Taar1−KO mouse breeding and genotyping

The *Taar1*-KO mice were obtained from the U.C. Davis Knockout Mouse Project (KOMP; www.komp.org) as previously described (Harkness et al., 2015). Briefly, chimeric mice were created using C57BL/6N ES cells in which the entire *Taar1* coding region was deleted by

homologous recombination, using the Veloci-Gene Null Allele Bac vector, and then injected into BALB/c blastocysts. The chimeras were bred with wild-type C57BL/6N mice and their offspring genotyped according to the strategy recommended by KOMP using the following primers: ACTCTTCACCAAGAATGTGG (forward); CCAACAGCGCTCAACAGTTC (reverse, wild-type allele); GTCGTCCTAGCTTCCTCACTG (reverse, null allele). Male and female siblings, identified as heterozygous for the targeted locus, were subsequently bred to produce *Taar1*-WT and *Taar1*-KO littermates.

2.3. Methamphetamine drinking selected mouse lines

Multiple pairs of MADR lines were consecutively, selectively bred from an F2 cross of the B6 and D2 inbred strains based on voluntary MA consumption during a two-bottle choice test. Details of this process and response to selection have been previously described (Wheeler et al., 2009; Shabani et al., 2011). Briefly, animals were provided access to a bottle containing a 20 mg/l MA solution for 18 h per day for 4 days, alongside continuous access to a water bottle. The concentration was increased to 40 mg/l MA for 4 additional days and mice were selected for breeding based on either high or low MA intake during this period. This breeding selection procedure was repeated for four generations to generate MALDR and MAHDR mice. The mice used in these experiments were MA-naïve offspring from second or later litters from replicate 4, selection generations 3, 4, and 5, and replicate 5, selection generation 3, 4, and 5.

2.4. Animal maintenance and housing

Mice of both sexes were used in all experiments and tested at 10–20 weeks of age. Before experiment initiation, mice were group-housed in filtered acrylic plastic shoebox cages (28 cm×18 cm×13 cm; l ×w× h), fitted with wire tops. Cages were lined with either ECO-Fresh bedding (Absorption Corporation, Ferndale, WA) or Bed-O-Cob (The Andersons, Maumee, OH). Mice had free access to rodent chow (5LOD, 5.0% fat content, Purina Mills, St. Louis, MO) and water *ad libitum*. The colony room was maintained at an environmental temperature of 21 ± 1 °C with lights on a 12:12 h light:dark schedule, beginning at 0600 h. All procedures

were approved by the VA Portland Health Care System's Institutional Animal Care and Use Committee and followed the requirements of the Guide for the Care and Use of Laboratory Animals. All efforts were made to minimize animal suffering, to reduce the number of animals used, and to use alternatives to *in vivo* techniques when available. All animals acclimated to the vivarium at least one week prior to testing.

2.5. Temperature recording

Two days prior to drug administration, mice were implanted with IPTT-300 temperature transponders from BioMedic Data Systems (Seaford, DE) to assess body temperature *via* telemetry. Animals were anesthetized with isoflurane (5% induction, 2.5% maintenance) and transponders were subcutaneously injected dorsally between the shoulders. On the day of drug administration, animals were weighed and transferred from group to individual cages to avoid temperature changes associated with interaction (e.g., huddling). After a 1 h acclimation period, temperature recording began and was measured every 15 min for 8 h. All experiments were conducted between 0700 and 1700 h. Temperatures were non-invasively recorded using the DAS-8001 reader console and smart probe from BioMedic Data Systems. Animals were removed from the cage and the smart probe placed within 5 cm of the embedded transponder to acquire temperature readings. The environmental temperature of the testing environment was 23 ± 1 °C. This temperature was selected in order to differentiate neurotoxic effects of the drugs from those exacerbated by elevated environmental temperatures.

2.6. Drug treatment

Following the first temperature recording (baseline), each animal received four i.p. injections (2 h apart) of saline or MA (5 mg/kg). This regimen and dose were selected based on ability to elicit differences between *Taar1*-WT and –KO mice on neurotoxicity measures (Miner et al., 2017a). MA was dissolved in 0.9% saline and injected in a final volume of 10 ml/kg. MA was dissolved in 0.9% saline and injected in a final volume of 10 ml/kg. Mice were euthanized 24 h after treatment by cervical dislocation, followed by decapitation. The striatum was removed

using blunt dissection and either kept on ice to be immediately used for the [^{3}H]DA uptake assay or flash-frozen and stored at -70°C until time of use for [^{3}H]DHTB or [^{125}I]RTI-55 binding.

2.7. Subcellular fractionation of striatal tissue for VMAT2-mediated [^{3}H]DA uptake and [^{3}H]DHTB binding

Three separate subcellular fractions (crude synaptosomal, membrane-associated, and enriched vesicular) were isolated as previously described (Teng et al., 1998; Hogan et al., 2000) with minor modifications (Fig. 18). Striata were homogenized in ice-cold sucrose (0.32 M, with protease inhibitors) using 12 strokes of a glass/teflon homogenizer before being centrifuged (800 x *g*, 12 min, 4°C). The supernatant (S1) was removed and centrifuged (22,000 x *g*, 15 min, 4°C). The resulting pellet (P2) was osmotically shocked with ice-cold water to disrupt the synaptosomes and release membrane-associated structures, followed by homogenization with 6 strokes of a glass/teflon homogenizer. Osmolarity was restored by addition of Tris (25 mM, pH 7.4) and potassium tartrate (100 mM). A sample was removed to be used for the crude synaptosomal fraction and the remaining P2 fraction was centrifuged (20,000 x *g*, 20 min, 4°C). The resulting supernatant (S3) was removed and saved. The pellet (P3) was re-suspended in VMAT2 assay buffer (25 mM Tris, 100 mM potassium tartrate, 2 mM $MgSO_4$, 4mM KCl, 0.5 mM EGTA, 0.1 mM EDTA, 1.7 mM ascorbic acid, 10 µM pargyline, and 100 µM tropolone; pH 7.4) and homogenized with 6 strokes of a glass/teflon homogenizer to generate the plasmalemmal membrane-associated fraction. $MgSO_4$ (final: 0.9 mM) was added to the supernatant (S3) and centrifuged (100,000 x *g*, 45 min, 4°C). The supernatant was discarded and the pellet (P4) re-suspended in assay buffer and homogenized with 6 strokes of a glass/teflon homogenizer to generate the enriched vesicular fraction. Protein concentrations from all three fractions were determined using the Bio-Rad protein assay (Bio-Rad Laboratories, Hercules, CA).

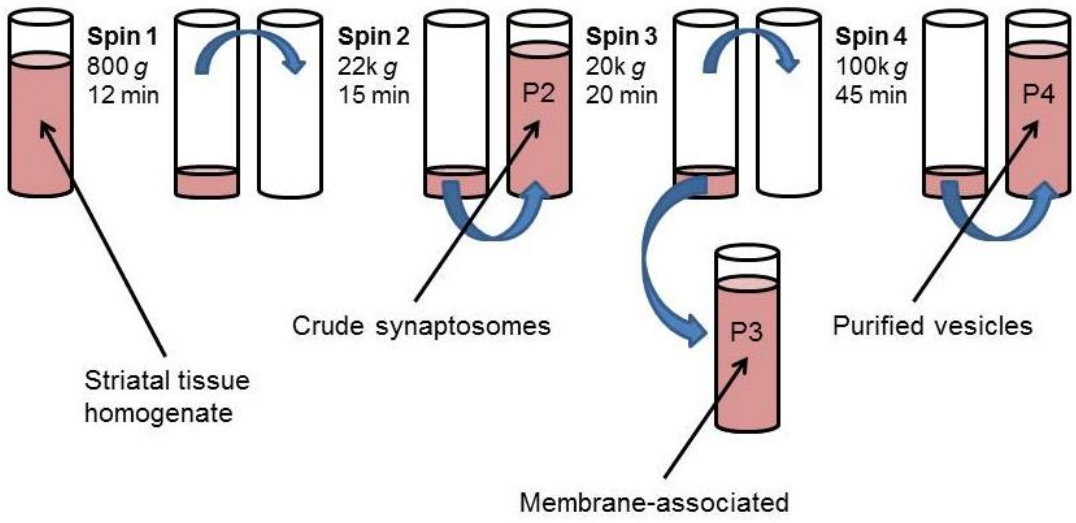

Figure 18. Subcellular fractionation of striatal tissue homogenate through centrifugation. Striatal tissue undergoes several centrifugation spins to separate the tissue into subcellular fractions: synaptosomal, membrane-associated, and vesicular fractions.

2.8. Tissue homogenate preparation for DAT-mediated [^{3}H]DA uptake and release assays

Striatal tissue from untreated mice was minced into 100 µm^2 squares using a McIlwain tissue chopper (Mickle Laboratory Engineering, Surrey, UK) and re-suspended in 0.15X ml/mg wet tissue of DAT assay buffer (Krebs-HEPES buffer: 25 mM HEPES, 122 mM NaCl, 5 mM KCl, 1.2 mM $MgSO_4$, 2.5 mM $CaCl_2$, 0.2% glucose, 0.02% ascorbic acid, 10 µM pargyline, 100 µM tropolone; pH 7.4) supplemented with inhibitors fluoxetine (1 µM), and desipramine (500 nM). Protein density was determined by BCA protein assay.

2.9. Synaptosome preparation for DAT-mediated [^{3}H]DA uptake

Synaptosomes for DAT-mediated [^{3}H]DA uptake were isolated as previously described (Janowsky et al., 2001a) with minor modifications. Striatal tissue from untreated mice was homogenized in ice-cold sucrose (0.32 M, with protease inhibitors) using 12 strokes of a glass/teflon homogenizer before being centrifuged (800 x *g*, 12 min, 4°C). The supernatant (S1) was removed and centrifuged (22,000 x *g*, 15 min, 4°C). The resulting pellet (P2) was re-

suspended in 0.1X ml/mg wet tissue of DAT assay buffer supplemented with inhibitors fluoxetine (1 µM), and desipramine (500 nM). Protein density was determined using the BCA protein assay.

2.10. Synaptosome preparation for [^{125}I]RTI-55 binding

Synaptosomes for [^{125}I]RTI-55 binding were isolated as previously described (Janowsky et al., 2001a) with minor modifications. Striata were homogenized in ice-cold sucrose (0.32 M, with protease inhibitors) using 12 strokes of a glass/teflon homogenizer before being centrifuged (1200 x *g*, 10 min, 4°C). The supernatant (S1) was removed and centrifuged (33,000 x *g*, 20 min, 4°C). The resulting pellet (P2) was brought up in 3 ml of ice-cold sucrose (0.32 M) and homogenized with 6 strokes of a glass/teflon homogenizer. Protein density was determined by BCA assay.

2.11. Radioligand binding assays

Radioligand binding assays were terminated by filtration using a Wallac 96-well harvester through Perkin Elmer filtermat A filters pre-soaked in 0.05% polyethlenimine (PEI), unless noted. Scintillation fluid was added and radioactivity was determined using a Perkin Elmer microbeta plate counter. Assays were conducted in duplicate or triplicate, and data from three or more independent experiments were analyzed. All results were normalized to the amount of total protein loaded.

2.12. VMAT2: [^{3}H]DA uptake

The *in vivo* drug-treated [^{3}H]DA uptake assay was adapted from a previously described protocol (Hogan et al., 2000). [^{3}H]DA uptake was performed using pooled striatal tissue from 4-5 *Taar1*-WT or –KO mice. Uptake was measured in each fraction preparation separately: synaptosomal (~5 µg protein), membrane-associated (~5 µg protein), and vesicular (~2.5 µg protein) (Supp. Fig. 8). Preparations were supplemented with MgATP (2 mM) and the assay initiated with the addition of [^{3}H]DA (50 nM). Specific uptake was defined as the difference in uptake observed in the presence or absence of reserpine (1 µM). The final assay volume was

250 µl. Incubation (6 min, 30 °C) was terminated using ice-cold saline (0.9% NaCl) and radioactivity was measured as described above.

2.13. VMAT2: [^{3}H]DHTB saturation binding

The *in vivo* drug-treated [^{3}H]DHTB binding assay was adapted from a previously described protocol (Teng et al., 1998). [^{3}H]DHTB binding was performed using pooled striatal tissue from 12-15 *Taar1* mice or 9-10 MADR mice with minor differences between models. Binding was measured in each subcellular fraction separately: synaptosomal (~15 µg protein), membrane-associated (~15 µg protein, *Taar1*; ~25 µg protein, MADR), and vesicular (~10 µg protein) (Supp. Fig. 9). Preliminary experiments were conducted to optimize assay conditions (Supp. Fig. 10 and 11). The assay was initiated with the addition of [^{3}H]DHTB (1 – 16 nM, *Taar1*; 1 - 20 nM, MADR). Specific binding was defined as the difference in binding observed in the presence or absence of cold tetrabenazine (10µM, *Taar1*) or DHTB (20 µM, MADR). The final assay volume was 1 mL. Incubation (60 min, 25 °C) was terminated using ice-cold Tris buffer (50 mM) and radioactivity remaining on the filters was measured as described above.

2.14. DAT: in vitro MA-induced [^{3}H]DA uptake assay

The drug-induced [^{3}H]DA uptake assay was adapted from a previously described protocol (Janowsky et al., 2001b). Preliminary experiments were conducted to optimize assay conditions (Supp. Fig. 7). Striatal synaptosomes (~10 µg protein) from untreated *Taar1*-WT and –KO mice were pre-incubated with MA (1 nM – 10 µM) for 10 min at 37 °C and the uptake assay was initiated with the addition of [^{3}H]DA (8 nM). Striatal tissue homogenate (~25 µg protein) from untreated *Taar1*-WT and –KO mice was pre-incubated with MA (10 nM – 10 µM) for 10 min at 37 °C and the uptake assay was initiated with the addition of [^{3}H]DA (20 nM). Specific binding was defined as the difference in binding observed in the presence or absence of mazindol (5 µM) and the final assay volume was 500 µl. Incubation (10 min, 37 °C) was terminated using ice-cold saline (0.9% NaCl) and radioactivity was measured as described above.

2.15. DAT: in vitro MA-induced [^{3}H]DA release (homogenate)

The drug-induced [^{3}H]DA superfusion release assay was adapted from a previously described protocol (Eshleman et al., 2013). Preliminary experiments were conducted to optimize assay conditions (Supp. Fig. 6). Striatal tissue homogenate (~200 µg protein) from *Taar1*-WT and –KO mice was pre-incubated with [^{3}H]DA (120 nM) for 30 min at 37 °C and added to a Brandel superfusion device (Gaitherburg, MD). [^{3}H]DA release was performed in tissue homogenate only. DAT assay buffer without inhibitors was perfused for 15 min as a washout period to establish stable efflux and then collection began for 45 min (18 fractions, 2.5 min each). The first 7.5 min (3 fractions) established baseline, then MA (10 nM – 100 µM) was perfused for 5 min (2 fractions), followed by buffer for 22.5 minutes (9 fractions), and finally 10 minutes (4 fractions) of SDS (1%) to lyse the homogenate. Radioactivity was determined using a Beckman liquid scintillation counter (Fullerton, CA). Fractional release was calculated by dividing the amount of radioactivity in each fraction by the total radioactivity in the remaining fractions.

2.16. DAT: [^{125}I]RTI-55 saturation binding

The *in vivo* drug-treated [^{125}I]RTI-55 binding assay was adapted from a previously described protocol (Eshleman et al., 1999). [^{125}I]RTI-55 binding was performed using striatal tissue from *Taar1* and MADR mice with minor differences between models. Preliminary experiments were conducted to optimize assay conditions (Supp. Fig. 12). Saturation binding was measured in synaptosomes only (~15 µg protein). DAT assay buffer was supplemented with fluoxetine (50 nM) and the assay initiated with the addition of [^{125}I]RTI-55. The specific activity of [^{125}I]RTI-55 was diluted with unlabeled [^{125}I]RTI-55 ranging in concentrations from 0.02 to 20 nM (*Taar1*) or 0.04 to 16.6 nM (MADR) and specific binding was defined as the difference in binding observed in the presence or absence of mazindol (5 µM). The final assay volume was 250 µl. Incubation (90 min, 25 °C) was terminated using ice-cold saline (0.9% NaCl) and radioactivity was measured as described above, with the exception that filters were not soaked in PEI. A preliminary experiment was also conducted to compare DAT expression between all three

fractions using pooled striatal tissue from 6 untreated *Taar1*-HET mice, due to availability. This was performed using [^{125}I]RTI-55 (40 pM) diluted with a single concentration of unlabeled RTI-55 (4 nM), under the same conditions outlined above.

2.17. Data analysis

The IC_{50} and EC_{50} values for the drug-induced uptake and release assays were calculated by analyzing the sigmoidal dose-response curves using a non-linear curve-fitting program and further analyzed using unpaired tests (Prism version 7, GraphPad Software, La Jolla, CA).. For the release assay, area under the curve (AUC) for fractional release over time by each drug concentration was generated. Saturation binding data were analyzed by non-linear regression to generate K_D and B_{max}. Radioligand data were analyzed by two-way analysis of variance (ANOVA) with treatment and either selected line or genotype as between-group factors. Temperature data were analyzed using a repeated measures four-way ANOVA with time as a within-subject factor and sex, genotype, and treatment as between-group factors. Significant two-way interactions were further investigated using *post hoc* mean comparisons using the Newman-Keuls test, when appropriate. For temperature data, subsequent analyses were conducted at 30 min after each injection as, under the described conditions, the maximum hypothermic drop occurs 30 min following administration of MA (Harkness et al., 2015; Miner et al., 2017a). Data were analyzed for outliers using Dixon's Q-test at 90% confidence. Statistical analyses were performed using Statistica version 13 software (StatSoft Inc., Tulsa, OK) and Prism version 7 (GraphPad Software, La Jolla, CA). Differences were considered significant at $p < 0.05$.

3. Results

3.1. VMAT2: [^{3}H]DA uptake

VMAT2-mediated DA uptake was evaluated in *Taar1* mice 24 h following MA treatment. DA uptake was pharmacologically limited to VMAT2 function as reserpine was to used define non-specific binding. Specific [^{3}H]DA uptake was assessed separately in each of the three

subcellular fractions. In the synaptosomal fraction, MA inhibited [^{3}H]DA uptake compared to saline treatment and inhibition of uptake was increased in *Taar1*-KO compared to -WT mice. A two-way ANOVA revealed a significant genotype x treatment interaction ($F_{1,23} = 6.26$, $p < 0.05$) (Fig. 19A). Simple main effect analysis of genotype for each treatment revealed no difference between genotypes for saline-treated animals, but MA-induced [^{3}H]DA uptake inhibition was significantly greater in *Taar1*-KO compared to *Taar1*-WT mice ($p < 0.01$). Simple main effect analysis of treatment for each genotype found MA significantly inhibited [^{3}H]DA uptake in both *Taar1*-WT and *Taar1*-KO mice compared to levels in saline-treated animals ($p < 0.0001$). In the membrane-associated fraction, a two-way ANOVA for [^{3}H]DA uptake revealed only a main effect of treatment ($F_{1,19} = 164.5$, $p < 0.0001$) (Fig. 19B). MA inhibited [^{3}H]DA uptake compared to saline-treated controls, collapsed across genotype. In the vesicular fraction, a two-way ANOVA revealed a main effect of genotype ($F_{1,19} = 9.14$, $p < 0.01$) and treatment ($F_{1,19} = 81.56$, $p < 0.0001$), but no significant interaction (Fig. 19C). MA inhibited [^{3}H]DA uptake compared to saline-treated controls, collapsed across genotype, and [^{3}H]DA uptake was decreased in *Taar1*-KO compared to -WT mice, collapsed across treatment.

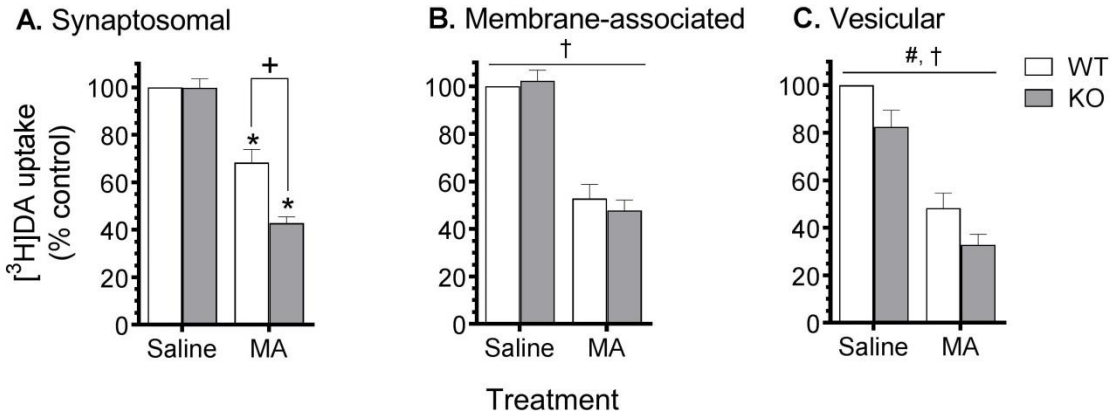

Figure 19. VMAT2: MA-induced [^{3}H]DA uptake in subcellular fractions. *Taar1*-WT and -KO mice received 4 i.p. injections of saline or MA (5 mg/kg), 2 h apart, and were euthanized 24 h following the final injection. Striatal tissue from 4-5 mice was pooled and values normalized to the amount of protein in each sample. Experiments were conducted as described in the text.

Data represent means ± SEM of 5-7 independent experiments, expressed as % of the *Taar1*-WT control group uptake for each fraction: synaptosomal (13.4 ± 3.1 pmol/mg protein), membrane-associated (15.0 ± 3.1 pmol/mg protein), vesicular (72.9 ± 21.6 pmol.mg) *: $p < 0.0001$ compared to saline-treated controls; +: $p < 0.05$ between genotypes; #: $p < 0.0001$ for main effect of treatment; †: $p < 0.01$ for main effect of genotype.

3.2. VMAT2: [^{3}H]DHTB saturation binding

Saturation binding analysis was conducted in both TAAR1 models (*Taar1* and MADR) and in each of the three fractions to determine the B_{max} and K_D values for [^{3}H]DHTB binding (Fig. 20). In the *Taar1* model, there were no significant interactions or main effects of genotype for B_{max} or K_D values within any of the tissue fractions (Table 11). A two-way ANOVA of B_{max} revealed a main effect of treatment in the vesicular fraction only ($F_{1,8} = 6.97$ $p < 0.05$). MA decreased B_{max} in the vesicular fraction compared to saline-treated animals, regardless of genotype. A two-way ANOVA of K_D values also revealed a main effect of treatment in the vesicular fraction only ($F_{1,8} = 9.82$ $p < 0.05$) where K_D values were decreased in MA-treated animals compared to saline-treated controls. Baseline [^{3}H]DHTB binding was compared between fractions in saline-treated animals, collapsed across genotype. A one-way ANOVA revealed a significant difference in B_{max} between the three fractions ($F_{2,15} = 5.29$ $p < 0.05$). B_{max} was highest in the membrane-associated fraction (1.92 ± 0.25 pmol/mg protein), followed by the synaptosomal fraction (1.43 ± 0.13 pmol/mg protein), and vesicular fraction (1.10 ± 0.12 pmol/mg protein). There were no significant differences in baseline K_D values between the three fractions: synaptosomal (2.31 ± 0.27 nM), membrane-associated (2.31 ± 0.38 nM), and vesicular (2.79 ± 0.53 nM) fractions.

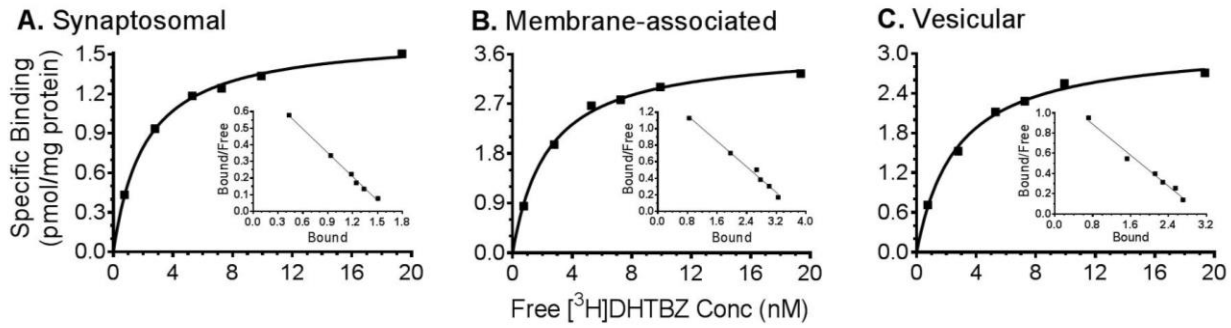

Figure 20. [^{3}H]DHTB saturation binding in subcellular fractions. *Taar1* and MADR mice received 4 i.p. injections of saline or MA (5 mg/kg), 2 h apart, and were euthanized 24 h following the final injection. Striatal tissue from 12-15 (*Taar1*) or 9-10 (MADR) mice was pooled and values normalized to the amount of protein in each sample. Experiments were conducted as described in the text. Shown are representative saturation curves from each fraction. Inset: Scatchard transformation of [^{3}H]DHTB binding data.

Table 11. [^{3}H]DHTB binding in subcellular fractions

Fraction	Treatment	Genotype	B_{max} (pmol/mg protein) ± SEM	K_D (nM) ± SEM
Synaptosomal	Saline	*Taar1*-WT	1.41 ± 0.23	2.27 ± 0.45
		Taar1-KO	1.45 ± 0.19	2.36 ± 0.40
	MA	*Taar1*-WT	1.32 ± 0.24	2.25 ± 0.41
		Taar1-KO	1.27 ± 0.22	2.26 ± 0.18
Membrane-associated	Saline	*Taar1*-WT	1.89 ± 0.34	2.30 ± 0.45
		Taar1-KO	1.96 ± 0.45	2.32 ± 0.71
	MA	*Taar1*-WT	1.58 ± 0.27	2.26 ± 0.63
		Taar1-KO	1.54 ± 0.27	2.37 ± 0.52
Vesicular	Saline	*Taar1*-WT	1.04 ± 0.23	2.20 ± 0.25
		Taar1-KO	1.17 ± 0.11 *a*	3.38 ± 1.00 *a*
	MA	*Taar1*-WT	0.80 ± 0.15	1.17 ± 0.12
		Taar1-KO	0.60 ± 0.06	1.14 ± 0.10

Data represent mean ± SEM for each treatment group from three independent experiments, using pooled tissue from 12-15 mice per groups. *a*: $p < 0.05$ for main effect of treatment.

Similar to the *Taar1* model, analysis of [^{3}H]DHTB saturation binding in the MADR model did not find any significant interactions or main effects of selected line for B_{max} or K_D values within any of the tissue fractions (Table 10). A two-way ANOVA revealed a main effect of treatment, in the vesicular fraction only, for B_{max} ($F_{1,8}$ = 13.76 p < 0.01). MA decreased B_{max} in the vesicular fraction compare to saline-treated animals, regardless of selected line (Table 12). Baseline [^{3}H]DHTB binding was compared between fractions in saline-treated animals, collapsed across selected line. A one-way ANOVA revealed a significant difference in B_{max} between the three fractions ($F_{2,15}$ = 32.27 p < 0.0001). B_{max} was highest in the membrane-associated fraction (3.61 ± 0.22 pmol/mg protein), followed by the vesicular fraction (2.75 ± 0.15 pmol/mg protein), and synaptosomal fraction (1.79 ± 0.08 pmol/mg protein). There were no significant differences in K_D values between the three fractions: synaptosomal (2.94 ± 0.27 nM), membrane-associated (2.68 ± 0.21 nM), and vesicular (2.75 ± 0.30 nM) fractions.

Table 12. [^{3}H]DHTB binding in subcellular fractions

Fraction	Treatment	Selected line	B_{max} (pmol/mg protein) ± SEM	K_D (nM) ± SEM
Synaptosomal	Saline	MALDR	1.76 ± 0.16	3.17 ± 0.33
		MAHDR	1.83 ± 0.08	2.72 ± 0.45
	MA	MALDR	1.45 ± 0.11	2.43 ± 0.23
		MAHDR	1.23 ± 0.35	2.1 ± 0.20
Membrane-associated	Saline	MALDR	3.53 ± 0.44	2.58 ± 0.45
		MAHDR	3.69 ± 0.21	2.78 ± 0.13
	MA	MALDR	3.37 ± 0.51	2.49 ± 0.08
		MAHDR	3.42 ± 0.89	3.35 ± 0.30
Vesicular	Saline	MALDR	2.55 ± 0.24	2.75 ± 0.56
		MAHDR	2.94 ± 0.11	2.75 ± 0.37
	MA	MALDR	2.21 ± 0.14	2.40 ± 0.46
		MAHDR	1.60 ± 0.34	2.41 ± 0.40

Data represent mean ± SEM for each treatment group from three independent experiments, using pooled tissue from 9-10 mice per group. *a*: p < 0.01 for main effect of treatment.

3.3. DAT: in vitro MA-induced changes in [^{3}H]DA uptake

[^{3}H]DA uptake was measured in both striatal synaptosomes and minced striatal tissue (homogenate) from *Taar1*-WT and –KO mice. Following incubation with MA, there was no significant difference in IC_{50} values for DAT-mediated [^{3}H]DA uptake between striatal synaptosomes from *Taar1*-WT (362.8 ± 54.8 nM) and *Taar1*-KO (416.4 ± 38.9 nM) mice, $p > 0.05$ (Fig. 21A). There was also no significant difference in IC_{50} values for DAT-mediated [^{3}H]DA uptake between striatal tissue homogenates from *Taar1*-WT (90.4 ± 6.9 nM) and *Taar1*-KO (102.6 ± 40.3 nM) mice, $p > 0.05$ (Fig. 21B).

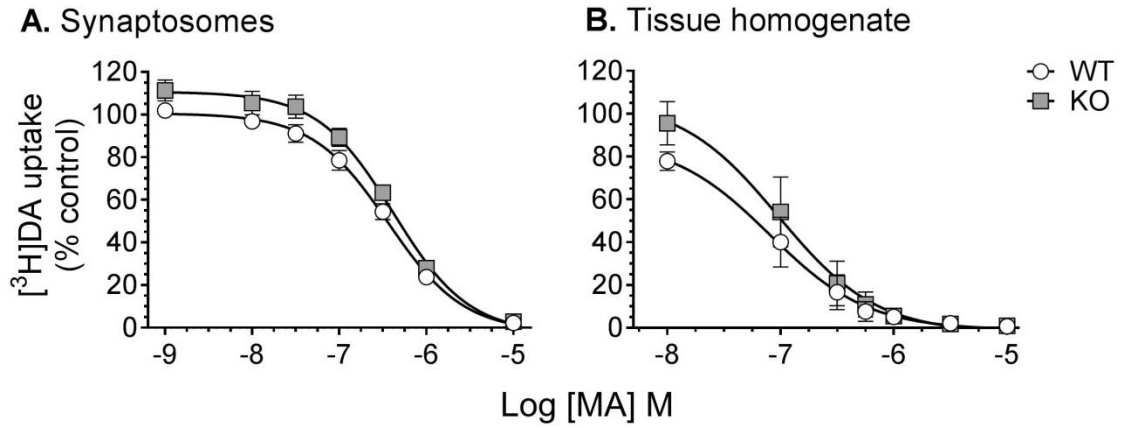

Figure 21. DAT: MA-induced [^{3}H]DA uptake in synaptosomes and tissue homogenate. Striatal synaptosomes from untreated *Taar1*-WT and –KO mice were pre-incubated with MA (1 nM – 10 µM) for 10 min before [^{3}H]DA (8 nM) was added and incubated for 10 min (**A**). Values were normalized to the amount of protein in each sample. Two independent sets of each genotype were run per experiment. Data represent mean ± SEM for each genotype from three independent experiments (n = 6), expressed as % of the *Taar1*-WT control group specific uptake (39.9 ± 5.2 pmol/mg protein). Striatal tissue homogenate from *Taar1*-WT and –KO mice were pre-incubated with MA (10 nM – 10 µM) for 10 min before [^{3}H]DA (20 nM) was added and incubated for 10 min (**B**). Values were normalized to the amount of protein in each sample. Data

represent means ± SEM of 3 independent experiments, expressed as % of the *Taar1*-WT control group specific uptake (27.9 ± 2.2 pmol/mg protein).

3.4. DAT: in vitro MA-induced changes in [^{3}H]DA release superfusion

There was no significant difference in EC_{50} values for [^{3}H]DA release as measured by superfusion between minced striatal tissue homogenate from *Taar1*-WT (1.29 ± 0.27 µM) and *Taar1*-KO (2.34 ± 0.49 µM) mice, $p > 0.05$ (Fig. 22).

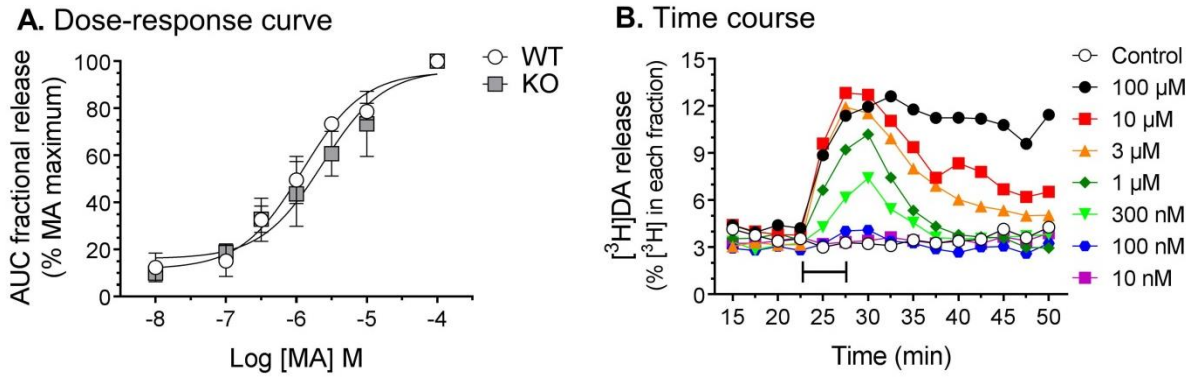

Figure 22. DAT: MA-induced [^{3}H]DA release in tissue homogenate. The area under the curve (AUC) for each drug concentration was normalized to maximal effect of MA for that experiment (**A**). Data shown are the mean ± SEM of 3 independent experiments. Representative superfusion time course of % [^{3}H]DA in each fraction: after washout and before lysing (**B**). MA was present for 5 min (2 fractions), indicated by bar. Data from each fraction are normalized to the total amount of [^{3}H]DA in remaining fractions.

3.5. DAT: [^{125}I]RTI-55 binding

Subcellular fractionation analyses of DAT expression was conducted at a single concentration of RTI-55 (4 nM) in untreated *Taar1*-HET mice and compared between fractions. A one-way ANOVA revealed a significant difference in binding between the three fractions ($F_{2,15}$ = 23.53 $p < 0.0001$). [^{125}I]RTI-55 binding was highest in the isolated membrane-associated

fraction, followed by the overall synaptosomal fraction, with negligible binding in the vesicular fraction (Table 13).

Table 13. [^{125}I]RTI-55 specific binding in subcellular fractions

Fraction	[^{125}I]RTI-55 binding (pmol/mg protein) ± SEM
Synaptosomal	3.94 ± 0.40
Membrane-associated	6.23 ± 0.45
Vesicular	0.57 ± 0.14

Striatal tissue was pooled from 6-8 *Taar1*-HET mice and values normalized to the amount of protein. Two independent sets of pooled tissue were run per experiment. Data represent mean ± SEM for each subcellular fraction from three independent experiments (n = 6).

Subsequent [^{125}I]RTI-55 binding saturation binding analysis was conducted in the synaptosomal fraction of *Taar1* and MADR mice to determine B_{max} and K_D values (Fig. 23). In *Taar1* mice, a two-way ANOVA revealed a main effect of treatment for B_{max} ($F_{1,12}$ = 10.83 p < 0.01), but no significant interaction or main effect of genotype (Table 14). MA decreased the B_{max} in comparison to saline-treated animals, regardless of genotype. There was no significant interaction or main effects of treatment or genotype on K_D values. In MADR mice, a two-way ANOVA revealed a main effect of treatment for B_{max} ($F_{1,20}$ = 9.98 p < 0.01), but there was no significant interaction or main effect of selected line (Table 15), similar to *Taar1* mice. MA decreased the B_{max} in comparison to saline-treated animals, regardless of selected line. There was no interaction or main effects on K_D values.

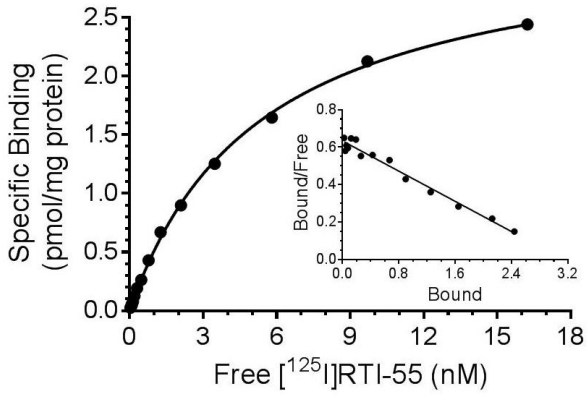

Figure 23. MA-induced [^{125}I]RTI-55 saturation binding in synaptosomes. *Taar1* and MADR mice received 4 i.p. injections of saline or MA (5 mg/kg), 2 h apart, and were euthanized 24 h following the final injection. Values were normalized to the amount of protein in each sample. Experiments were conducted as described in the text. Shown is a representative saturation curve. Inset: Scatchard transformation of [^{125}I]RTI-55 binding data.

Table 14. [^{125}I]RTI-55 binding in synaptosomes

Treatment	Genotype	B_{max} (pmol/mg protein) ± SEM		K_D (nM) ± SEM
Saline	*Taar1*-WT	10.34 ± 0.76		3.68 ± 0.18
	Taar1-KO	11.68 ± 1.25	*a*	4.28 ± 0.37
MA	*Taar1*-WT	8.45 ± 0.36		3.59 ± 0.35
	Taar1-KO	7.57 ± 1.03		3.84 ± 0.72

Data represent mean ± SEM for each treatment group from four independent experiments.

a: $p < 0.01$ for main effect of treatment.

Table 15. [^{125}I]RTI-55 binding in synaptosomes

Treatment	Selected line	B_{max} (pmol/mg protein) ± SEM	K_D (nM) ± SEM
Saline	MALDR	3.33 ± 0.28	3.65 ± 0.63
	MAHDR	3.54 ± 0.41	3.43 ± 0.56
MA	MALDR	2.45 ± 0.26	3.23 ± 0.48
	MAHDR	2.29 ± 0.37	4.06 ± 0.80

a

Two independent sets of each treatment group were run per experiment. Data represent mean ± SEM for each treatment group from three independent experiments (n = 6).

a: $p < 0.01$ for main effect of treatment.

3.6. Thermal response

Prior to the first injection, the mean baseline temperature of all MADR mice was 38.4°C (SEM = 0.04°C), with no significant between-line or -treatment differences. Profound selected line-dependent MA-induced hypothermia was observed as well as a sex effect. MA did not elicit hyperthermia in any mice, defined as a 0.5°C increase in body temperature above the basal temperature. Temperature data (Fig. 24), analyzed using a repeated measures four-way ANOVA with sex, line, and treatment as between-group factors and time as a within-subject factor found a significant effect of sex ($F_{32,3264} = 5.03$, $p < 0.0001$) and thus data for each sex was analyzed separately.

Temperature data for male MADR mice, analyzed using a three-way repeated measures ANOVA, revealed a significant line x treatment x time interaction ($F_{32,1536} = 21.20$, $p < 0.0001$). There was no difference in temperature between selected lines for male mice receiving saline (Fig. 24A), although there was a main effect of time ($F_{32,768} = 45.40$, $p < 0.0001$) as temperatures in these control groups decreased over the 8 h period, likely attributable to single housing. Examination of the effects of MA revealed a significant line x time interaction ($F_{32,768} = 27.24$, $p < 0.0001$) (Fig. 24B). Analyses of selected line differences were conducted using simple main effect analyses at each 30 min post-injection time point to investigate the

hypothermic drop in body temperature. The temperatures of male MALDR mice receiving MA were significantly lower 30 min after each of the four MA injections compared to their MAHDR counterparts.

Temperature data for female MADR mice, analyzed using a three-way repeated measures ANOVA, also revealed a significant line x treatment x time interaction ($F_{32,1728} = 9.18$, $p < 0.0001$). Again, there was no difference in temperature between selected lines for female mice receiving saline (Fig. 24C), although there was a main effect of time ($F_{32,832} = 34.30$, $p < 0.0001$), as temperatures decreased over time. Examination of MA treatment revealed a significant line x time interaction ($F_{32,896} = 10.52$, $p < 0.0001$) (Fig. 24D). Simple main effect analyses at 30 min post-injection time point revealed the body temperatures of female MALDR mice receiving MA were significantly lower compared to their MAHDR counterparts.

The mean baseline temperature of all *Taar1* mice was 38.0°C (SEM = 0.06°C), with no significant between-genotype or -treatment differences. Similar to MADR mice, significant genotype-dependent MA-induced hypothermia was observed and MA did not elicit hyperthermia in any mice. Temperature data were analyzed using a repeated measures four-way ANOVA with time as a within-subject factor and sex, genotype, and dose as between-group factors. However, as there were no significant interactions involving sex in initial analyses of *Taar1* mice, this factor was excluded from further analyses. Temperature data for *Taar1* mice, analyzed using a three-way repeated measures ANOVA, revealed a significant genotype x treatment x time interaction ($F_{32,1376} = 5.15$, $p < 0.0001$). There was no difference in temperature between *Taar1*-WT and -KO mice receiving saline (Fig. 24E), although there was a main effect of time ($F_{32,704} = 30.20$, $p < 0.0001$) similar to saline-treated MADR mice. Examination of the effects of MA revealed a significant genotype x time interaction ($F_{32.672} = 7.60$, $p < 0.0001$) (Fig. 24F). Analyses of genotype differences were conducted using simple main effect analyses at each 30 min post-injection time point to investigate the hypothermic drop in body temperature.

The temperatures of *Taar1*-WT mice receiving MA were significantly lower 30 min after the first and second injection MA injections compared to their *Taar1*-KO counterparts.

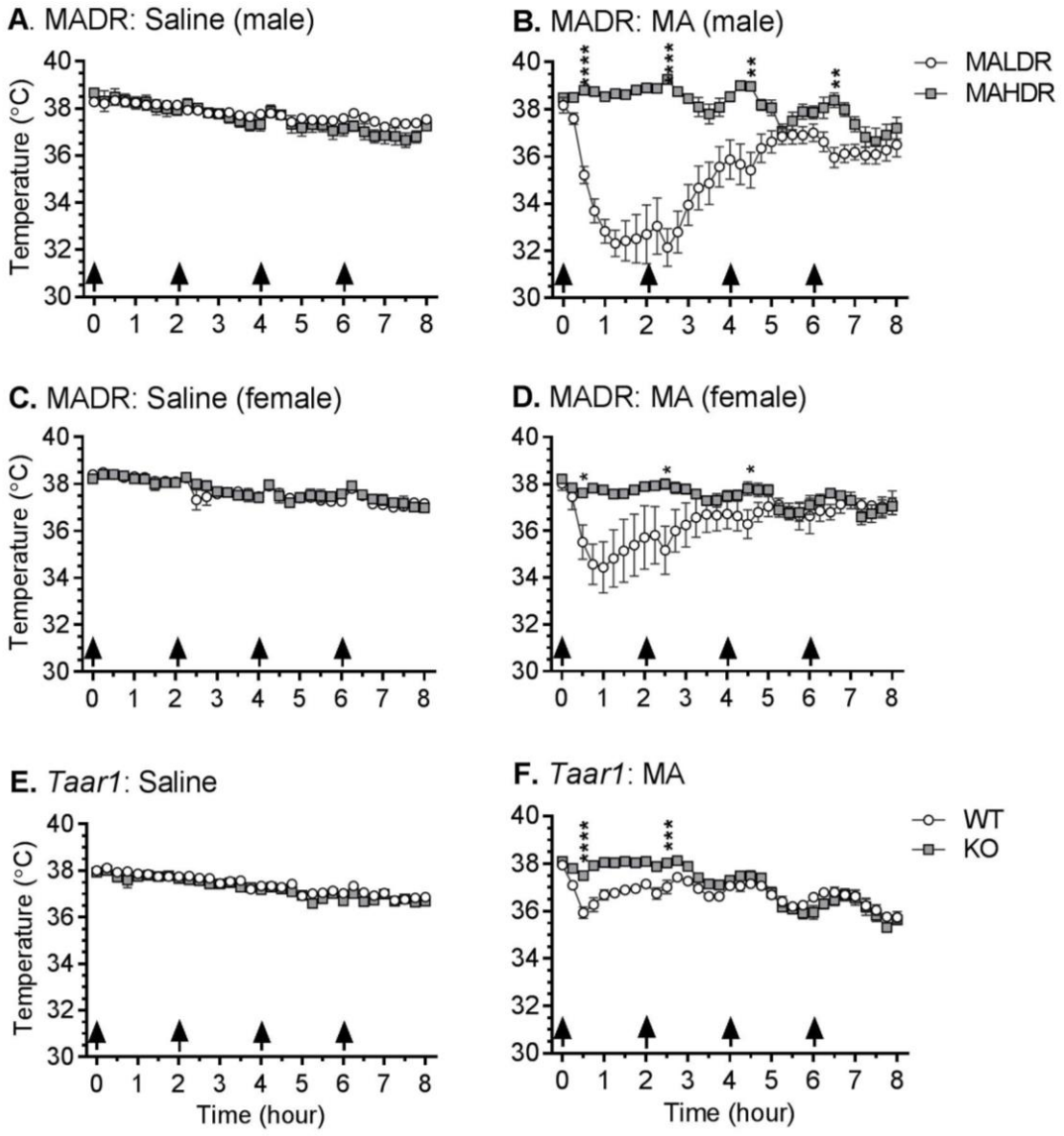

Figure 24. Effects of repeated saline or MA injections on core body temperature. *Taar1* and MADR mice received 4 i.p. injections (indicated by arrows) of saline or MA (5 mg/kg), 2 h apart. Body temperature was measured every 15 min *via* telemetry over 8 h in an ambient temperature of 23 ± 1°C. Data represent temperature for each selected line or genotype and treatment group (mean ± SEM) at specified time points, *n* = 11-15 mice per group. Time points

selected for detailed analysis were 30 min after each injection. *: $p < 0.05$, **: $p < 0.01$, ***: $p < 0.001$, ****: $p < 0.0001$ compared between selected lines or genotypes.

Next, the data were analyzed by selected line for each gender, revealing a significant treatment x time interaction for both selected lines and sexes: male MALDR ($F_{32,768} = 31.66$, $p < 0.0001$), male MAHDR ($F_{32,768} = 1.95$, $p < 0.01$), female MALDR ($F_{32,896} = 14.43$, $p < 0.0001$), and female MAHDR ($F_{32,832} = 2.35$, $p < 0.0001$). Simple main effects analysis was then used to statistically investigate MA effects within each selected line at 30 min post-injection. MA significantly decreased body temperature in male MALDR mice after all four injections, while MA significantly increased body temperature in male MAHDR mice compared to saline-treated controls (Table 16). MA also significantly decreased body temperature in female MALDR mice following all four injections. Body temperature was significantly decreased in female MAHDR mice 30 min following the first injection compared to saline controls, but MA significantly increased body temperature following the final injection. Examination of the data for each genotype revealed a significant treatment x time interaction for both genotypes: *Taar1*-WT ($F_{32,704} = 5.63$, $p < 0.0001$) and *Taar1*-KO ($F_{32,672} = 6.82$, $p < 0.0001$). Simple main effects analyses revealed MA significantly decreased body temperature 30 min following the first and second injection in *Taar1*-WT mice, while MA significantly increased temperatures in *Taar1*-KO mice following the second injection, compared to saline-treated control mice.

Table 16. MA-induced change in body temperature relative to saline-treated mice

Line or Genotype	Sex	30 min post-injection (ΔT °C ± SEM)			
		1st Inj	2nd Inj	3rd Inj	4th Inj
MALDR	M	-3.11 ± 0.32[d]	-4.75 ± 0.76[d]	-1.38 ± 0.49[b]	-0.76 ± 0.35[a]
	F	-2.53 ± 0.37[d]	-1.94 ± 0.54[b]	-0.66 ± 0.31	-0.46 ± 0.19[a]
Taar1-WT	M/F	-2.00 ± 0.24[b]	-0.66 ± 0.29[a]	-0.13 ± 0.20	-0.26 ± 0.21
MAHDR	M	-0.03 ± 0.18	1.00 ± 0.21[c]	0.96 ± 0.32[a]	0.77 ± 0.31
	F	-0.51 ± 0.11[b]	0.16 ± 0.10	0.36 ± 0.15	0.51 ± 0.13[a]
Taar1-KO	M/F	-0.23 ± 0.16	0.47 ± 0.14[a]	0.26 ± 0.23	-0.21 ± 0.22

Data represent change in temperature (mean ± SEM) for each treatment group from saline-treated mice at specified time point, n = 11-15 mice per group. *a*: $p < 0.05$; *b*: $p < 0.01$; *c*: $p < 0.001$; *d*: $p < 0.0001$ in analysis compared to saline-treated controls.

4. Discussion

This chapter investigated potential mechanisms underlying TAAR1 regulation of MA-induced neurotoxicity, specifically VMAT2 and DAT function and expression. As criticism of previous TAAR1 research has been directed at reliance on *in vitro* methods, my experiments were conducted using *in vivo* treated tissue, with the exception of DAT function. Twenty-four hours following treatment with MA (5 mg/kg, 4 inj, 2 h apart), VMAT2-mediated [^{3}H]DA uptake was decreased in all three fractions: synaptosomal, membrane-associated, and vesicular. In the synaptosomal fraction, MA-induced [^{3}H]DA uptake inhibition was increased in *Taar1*-KO compared to –WT mice, indicating VMAT2 function is impaired overall when TAAR1 is not activated. Although MA inhibited DA uptake in the membrane-associated fraction, there was no difference between genotypes. This is logical due to the predominantly intracellular localization of TAAR1 (Xie et al., 2008a). In the enriched vesicular fraction consisting of cytoplasmic vesicles, [^{3}H]DA uptake was diminished in *Taar1*-KO compared to –WT mice, but decreased regardless of treatment. These findings indicate MA-induced impairment of VMAT2 function is increased when TAAR1 is not activated and impairment of VMAT2 function is both a biomarker and potential cause of increased MA-induced neurotoxicity. Additionally, TAAR1 activation does not modulate the function of VMAT2 located on membrane-associated vesicles, but does affect VMAT2 located on vesicles in the cytoplasm, as measured in the purified vesicular fraction.

Conducted in both the transgenic *Taar1* and selected line MADR mouse models, there were no differences in VMAT2 expression between genotypes or selected lines in any of the three fractions. MA did not alter [^{3}H]DHTB binding in the synaptosomal and membrane-associated fractions, but diminished binding in the vesicular fraction in both models. This differential

pattern of VMAT2 expression is in agreement with previous findings (Brown et al., 2000; Hogan et al., 2000). While TAAR1 does not appear to affect VMAT2 expression under these conditions, these findings, in combination with the results from the VMAT2 function experiment, have novel implications. It is often difficult to separate impairment in VMAT2 function from decreased function due to diminished expression as they typically coincide. This is true in the vesicular fraction where VMAT2 function is most often measured (Sandoval et al., 2003). Here, independent of the effects of TAAR1, MA inhibited [^{3}H]DA uptake in both the synaptosomal and membrane-associated fractions where [^{3}H]DHTB binding did not change, indicating MA impaired VMAT2 function independent of a change in VMAT2 expression. Although only VMAT2 expression was quantified in the MADR model, both VMAT2 function and expression assessment were completed in the *Taar1* model. However, without VMAT2 function data from MADR mice, caution should be exerted in conflating the transporter function and expression results as they were obtained from different TAAR1 mouse models and there are basal biochemical differences between *Taar1* and MADR mice to consider (Table 3). In relevance to these transporters: DAT and VMAT2 are equally expressed in *Taar1*-WT and –KO mice in the striatum, NAc, SN, VTA, and cortex (Lindemann et al., 2008; Di Cara et al., 2011), DAT is elevated in the NAc of MAHDR compared to MALDR mice, (Lominac et al., 2014). DAT has yet to be quantified in MADR mice in the striatum, and VMAT2 levels have not been examined in any region.

Previous *in vitro* research on TAAR1 modulation of DAT function has produced equivocal findings. One study reported MA-induced [^{3}H]DA uptake inhibition and [^{3}H]DA release is increased in striatal tissue from *Taar1*-WT compared to –KO mice (Xie and Miller, 2009a). Similar findings were found in cellular experiments, where MA-induced [^{3}H]DA uptake inhibition and release is increased in cells co-transfected with TAAR1 and DAT compared to cells only transfected with DAT. While these findings indicates MA-induced impairment of DAT function is increased when TAAR1 is activated, the co-administration of MA and the TAAR1 partial agonist

RO523648 does not alter [^{3}H]DA uptake and release in striatal synaptosomes from rats (Cotter et al., 2015). Using *in vitro* treatment with MA, similar to previous radioligand assays, I was unable to find differences between *Taar1*-WT and –KO mice in DAT function. Following incubation with MA, time-dependent [^{3}H]DA release produced equivalent EC_{50} values in striatal synaptosomes from both *Taar1*-WT and –KO mice. Additionally, there was no difference in IC_{50} values of MA to inhibit [^{3}H]DA uptake between genotypes. Similar to VMAT2 expression, analysis of DAT expression 24 h following *in vivo* treatment with MA (5 mg/kg, 4 inj, 2 h apart) in *Taar1* and MADR mice also revealed no differences between genotypes or selected lines. MA diminished [^{125}I]RTI-55 binding in synaptosomes in both models, indicating this was not due to a lack of an effect of MA. Taken together, these findings indicate TAAR1 and DAT do not interact and DAT is an unlikely mediator of TAAR1 regulation of MA-induced neurotoxicity. The absences of an interaction is not altogether unsurprising, based on an FSCV experiment reporting activation of TAAR1 does not alter DAT function (Leo et al., 2014) and behavioral research demonstrating activation of TAAR1 diminishes hyperlocomotion independently of DAT (Revel et al., 2011; Leo et al., 2018).

Although the overall pattern of thermal response to MA was similar between the MADR and *Taar1* mouse models, there were some unexpected differences. A sex difference was found in MALDR mice treated with MA, an effect absent in MALDR mice treated with saline and MAHDR mice following either treatment. The hypothermic response to MA in male MALDR mice was exacerbated in both degree and duration, peaking 30 min after the second injection at 4.75 degrees below saline-treated mice, more than double the peak hypothermic response of *Taar1*-WT mice. There were no sex differences in *Taar1*-WT or –KO mice. There was no difference between MAHDR and *Taar1*-KO mice, indicating thermal response to MA is similar when TAAR1 is not activated, whether the receptor is non-functional or absent. The sex difference in thermal response to MA is surprising, given the lack of sex difference in MALDR mice in reaction to MDMA and the similar bi-phasic pattern observed in both MALDR and *Taar1*-WT

mice in Chapter 3. Additionally, a previous study comparing MADR and *Taar1* models in response to a single dose of MA (2 mg/kg), found MALDR and *Taar1*-WT mice reacted similarly with no observed sex differences in 2 different replicate sets of the MADR lines (Harkness et al., 2015). The same study also tested MADR mice with single administrations of MA at various doses (1, 2, 4, 8, 16 mg/kg) with no sex differences reported. These findings suggest a potential role for genetic variation within the MALDR mice. Selected from an F2 cross of B6 and D2 mice, MAHDR mice are homozygous for the D2 allele, while MALDR mice are either homozygous for the dominant B6 allele or heterozygous (Wheeler et al., 2009). It is possible that variations between homozygous and heterozygous MALDR mice may account for some of the thermal differences. This would also account for the stability of the MAHDR thermal response as they lack the genetic variation. Additionally, mice from the different experiments came from different replicates of the MADR mice selected lines. Those used here in Chapter 5 were obtained from replicates 4 and 5, whereas MADR mice from Chapter 3 were from replicates 2 and 3, the same replicates used in Harkness et al. (2015). Due to the large number of animals required for the saturation binding assays, sex differences were unable to be tested for in the transporter expression assays. However, as the selected lines did not differ in transporter expression, MA-induced decreases in synaptosomal DAT and vesicular VMAT2 expression occurred independently of the differences in thermal response between lines.

In conclusion, these findings demonstrate for the first time an interaction between TAAR1 and VMAT2, as activation of TAAR1 modulated VMAT2 function, independent of expression. Additionally, this interaction is localized to VMAT2 on cytosolic vesicles and activation of TAAR1 does not modulate VMAT2 function on membrane-associated vesicles. While this interaction may be a potential underlying mechanism by which TAAR1 regulates MA-induced neurotoxicity, more research is necessary to further understand and characterize this relationship. The results also demonstrate MA diminishes VMAT2 function in all subcellular fractions, potentially independent of a change in VMAT2 expression. However, there was no indication TAAR1

interacts with DAT, as activation of the receptor did not modulate *in vitro* MA-impairment of DAT function or alter DAT expression. Finally, the temperature data demonstrated MA elicits a similar thermal response to MA in MAHDR and *Taar1*-KO mice, an absence of the hypothermic response, but the degree of hypothermia induced in MALDR and *Taar1*-WT mice differed.

Chapter 6: General discussion

1. Overview

The overarching goal of this dissertation was to examine the role of TAAR1 in regulating substituted amphetamine-induced neurotoxicity. My research began with investigation of the neurotoxic effects of MDMA and substituted methcathinones, methylone and MDPV, alone and in combination. I measured transient and sustained neurotoxicity, as well as thermal effects of the drugs. As activation of TAAR1 alters sensitivity to many of amphetamine's effects, I next examined the role of TAAR1 in modulating MDMA-induced neurotoxicity and thermal response, before shifting my focus to TAAR1 regulation of MA-induced neurotoxicity (Tables 17 and 18). Finally, I examined potential mechanisms through which TAAR1 modulates MA-induced neurotoxicity, specifically VMAT2 and DAT function and expression (Table 19). Taken together, these studies aimed to determine the impact of TAAR1 on the neurotoxic effects of amphetamines in order to better understand underlying mechanisms of neurotoxicity.

Table 17. Summary of results: TAAR1 regulation of amphetamine-induced neurotoxicity

					MALDR	MAHDR
Chapter	Drug	Dose (mg/kg)	Biomarker	Method	2 days	
3	MDMA	20	DA	ELISA	no difference	
	Methylone	25			no difference	
	MDMA	20	GFAP	ELISA	increased	
	Methylone	25			no difference	

					WT	KO	WT	KO
Chapter	Drug	Dose (mg/kg)	Measure	Method	2 days		7 days	
4	MA	2.5	DA	HPLC-ECD	decreased		-	↓
		5			decreased		↓	↓↓
		10			decreased		decreased	
	MA	2.5	5HT	HPLC-ECD	no difference		increased	
		5			decreased		no difference	
		10			decreased		no difference	
	MA	2.5	TH	ELISA	no difference		decreased	
		5			decreased		decreased	
		10			decreased		decreased	
	MA	2.5	GFAP	ELISA	↑	↑↑	↑	↑↑
		5			↑	↑↑	↑	↑↑
		10			increased		increased	

All results are in comparison to saline-treated control group. No difference, decreased, and increased indicate similar effects across genotypes or lines, whereas arrows indicate significant differences between genotypes or lines. ↓: decreased; ↓↓: further decreased; ↑: increased; ↑↑: further increased; -: no difference. For clarity, monoamine metabolites and NE levels have been omitted.

Table 18. Summary of results: TAAR1 mediation of acute hypothermic response to amphetamines

			WT	KO
Chapter	Drug	Dose (mg/kg)	Body temperature	
3	MDMA	20	↓↓	↓

			MALDR	MAHDR
	MDMA	20	↓	-
	Methylone	25	decreased	

			WT	KO
Chapter	Drug	Dose (mg/kg)	Body temperature	
4	MA	2.5	↓	-
		5	↓↓	↓
		10	↓↓	↓

			MALDR	MAHDR
Chapter	Drug (sex)	Dose (mg/kg)	Body temperature	
5	MA (m)	5	↓	-
	MA (f)		↓↓	↓

		WT	KO
	MA (m/f)	↓	-

All results represent a decrease in body temperature, 30 min following first injection, relative to saline-treated control group. Decreased indicates similar effects across line, whereas arrows indicate significant differences between genotypes or lines. ↓: decreased; ↓↓: further decreased; -: no difference.

Table 19. Summary of results: TAAR1 interaction with DAT and VMAT2

Chapter	Transporter	Measure	Fraction	Drug	Dose (mg/kg)	24 h later WT	24 h later KO
5	VMAT2	DA uptake	synaptosomal	MA	5	↓	↓↓
			membrane			decreased	
			vesicular			↓	↓↓
						WT/MALDR	KO/MAHDR
		VMAT2 expression	synaptosomal	MA	5	no difference	
			membrane			no difference	
			vesicular			decreased	

Chapter	Transporter	Measure	Fraction	Drug	Dose (M)	*in vitro* WT	*in vitro* KO
3	DAT	DA release	synaptosomal	MDMA	10^{-8} - 10^{-4}	increased	
5		DA uptake	synaptosomal	MA	10^{-9} - 10^{-5}	decreased	
		DA uptake	homogenate	MA	10^{-8} - 10^{-5}	decreased	
		DA release	homogenate	MA	10^{-8} - 10^{-4}	increased	

	Measure	Fraction	Drug	Dose (mg/kg)	24 h later WT/MALDR	24 h later KO/MAHDR
	DAT expression	synaptosomal	MA	5	decreased	

All results are in comparison to saline-treated control group. No difference, increased, and decreased indicate similar effects across genotypes or lines, whereas arrows indicate significant differences between genotypes or lines. ↓: decreased; ↓↓: further decreased.

2. Summary of major findings

In Chapter 2, I examined the neurotoxic profiles of MDMA and the popular methcathinones, methylone and MDPV. As MDMA and methcathinones are frequently co-ingested (Palamar et al., 2016), the drugs were administered alone or in combination. This allowed for investigation of combining amphetamines with similar or different mechanisms as both MDMA and methylone are transporter substrates, while MDPV is a transporter inhibitor (Eshleman et al., 2013). I hypothesized MDMA-induced neurotoxicity would be increased when combined with methylone and decreased when combined with MDPV. All drugs were administered using a binge-like dosing regimen, a paradigm employed throughout the rest of my studies, and all neurotoxicity markers were quantified in striatal tissue where the effects of amphetamine-induced neurotoxicity are the greatest (Kuhn et al., 2011), as in all subsequent studies. Two days following administration, the highest dose of MDMA (30 mg/kg) transiently decreased DA and TH levels, markers of DA terminal injury, and increased GFAP expression, a marker of astrocyte activation and neuroinflammation. However, these markers returned to baseline 7 days following administration indicating the neurotoxic effects were not sustained. This finding was unexpected given lower doses of MDMA (20 mg/kg and greater) regularly induce long-term neurotoxicity (O'Callaghan and Miller, 1994; Granado et al., 2011). The lower dose of MDMA (15 mg/kg) did not alter striatal DA or TH at any time point, in contrast to my pilot study and previous research using the same or lower doses (Sanchez et al., 2003; Johnson et al., 2004). This dose did transiently increase GFAP expression, which can occur independently of decreases in DA or TH levels (McConnell et al., 2015).

Administered alone, methylone (20 mg/kg) and MDPV (1 mg/kg) did not alter DA and TH levels or GFAP expression at either time point. These results confirm previous findings that methcathinones are not neurotoxic by themselves (Baumann et al., 2012; Anneken et al., 2015). While these findings might indicate the substances are benign, both substances induce higher levels of self-administration and escalating intake as compared to MDMA (Watterson et al.,

2014; Schindler et al., 2015). This type of compulsive use can lead to serious peripheral health complications, such as cardiac arrest, hyperthermia, and rhabdomyolysis (Schifano et al., 2017). The difference in neurotoxicity is particular striking between methylone and MDMA as both are transporter substrates and differ in chemical structure by only a ketone group. One potential cause for the weak neurotoxic profile of the methcathinones is their low affinity and potency at VMAT2 (Eshleman et al., 2013; Pifl et al., 2015; Anneken et al., 2018). Lacking the ability to disrupt vesicular sequestration of DA, it is possible that methylone by itself may not sufficiently elevate intracellular levels necessary to cause terminal damage.

The co-administration of either methcathinone with MDMA returned levels of GFAP expression to baseline 2 days later, indicating both have a negative modulatory effect on astrocyte expression when combined with MDMA. A previous study reported the combination of MDMA and MDPV attenuates GFAP expression 2 days later (Anneken et al., 2015). Although they did not study the combination of MDMA and methylone, they found the combination of MA and methylone potentiates MDMA-induced GFAP expression. A possible explanation is they used a larger dose of MDMA (20 mg/kg), inducing neurotoxicity and hyperthermia. I assessed an additional measure of gliosis using radioligand saturation analyses of [^{3}H]PK11195 binding to the glial-specific protein TSPO. However, there was no difference in TSPO expression between any drug treatments at either time point. This result was surprising as [^{3}H]PK11195 binding correlates with astrocyte and microglial activation (Kuhlmann and Guilarte, 1999), and both doses of MDMA increased GFAP expression. While other studies have reported similar doses of MDMA do not increase TSPO expression, either GFAP expression also did not increase or it was not included as a measure (Pubill et al., 2003; Fantegrossi et al., 2008). This discrepancy in results may also be attributed to issues with the radioligand itself, discovered post-experiment.

Core body temperature did not increase above baseline in any of the treatment groups indicating any changes in neurotoxicity biomarkers occurred independently of hyperthermia. As hyperthermia exacerbates MDMA-induced neurotoxicity, it can be difficult to discern the

neurotoxic effects from the synergistic effect of hyperthermia (Docherty and Green, 2010). While hyperthermia is a commonly reported response, it is not required for MDMA-induced neurotoxicity, although the resulting neurotoxicity is then not as drastic (O'Shea et al., 2001; Johnson et al., 2002). As such, this factor may have contributed to the absence of MDMA-induced neurotoxicity reported. However, mechanistic differences emerged in thermal response to the different drugs. Administration of transporter substrates, MDMA and methylone, alone or in combination, elicited a similar bi-phasic pattern of acute hypothermia followed by an increase in temperature. In contrast, the transporter inhibitor, MDPV, did not elicit this pattern or differ from saline-treated control animals. These findings corroborate previous evidence of different thermal responses to transporter substrates and inhibitors. MDMA and methylone elicit similar changes in body temperatures, different from MDPV, which is similar to cocaine (Fantegrossi et al., 2013; Anneken et al., 2015; Wakabayashi et al., 2015). Although MDPV alone exerted no change in body temperature, when it was co-administered with MDMA, the bi-phasic thermal response re-emerged. This is supported by previous literature demonstrating DAT inhibitors, such as cocaine or GBR 12909, do not affect temperature by themselves or alter the thermal response to transporter substrates when co-administered (O'Shea et al., 2001; Peraile et al., 2010).

While the results did not substantiate my hypothesis that these methcathinones would modulate MDMA-induced neurotoxicity, caution must be exercised before drawing conclusions as MDMA did not induce neurotoxicity by itself. Since these methcathinones are not neurotoxic by themselves, the modulatory properties of methylone and MDPV can only be assessed following the induction of neurotoxicity. Further research is warranted under conditions where MDMA produces robust neurotoxicity.

In Chapter 3, I began to investigate the role of TAAR1 in regulating amphetamine-induced neurotoxicity. I hypothesized MDMA-induced neurotoxicity would be increased when TAAR1 was not activated; DA release would be increased when TAAR1 was activated; and the acute

hypothermic response to MDMA was induced by TAAR1 activation. Using a similar model and measures as in Chapter 2, I investigated transient MDMA-induced neurotoxicity in the selected line MADR mouse model. I chose a larger dose of MDMA (20 mg/kg) commonly used to induce neurotoxicity (O'Callaghan and Miller, 1994; Angoa-Perez et al., 2013b), to avoid the lack of neurotoxicity in Chapter 2. Methylone was included as a control as it lacks affinity for TAAR1, but is similar to MDMA in chemical structure and mechanism of action (Simmler et al., 2013a). Although the dose was increased, results similar to Chapter 2 were obtained: GFAP expression increased, but DA levels remained unchanged. Additionally, there were no differences for either measure between MALDR and MAHDR mice. I also examined the effect of TAAR1 activation on MDMA-induced [^{3}H]DA release. This was performed in striatal synaptosomes from *Taar1*-WT and –KO mice to determine if activation of the receptor modulated DAT function. Similar *in vitro* research has only been performed using MA, reporting DA release is greater in striatal synaptosomes from *Taar1*-WT compared to –KO mice (Xie and Miller, 2009a). Conversely, microdialysis results have shown MDMA-induced striatal DA release is greater in *Taar1*-KO than –WT mice (Di Cara et al., 2011). I found no differences in EC_{50} values between the two genotypes indicating activation of TAAR1 does not modulate *in vitro* MDMA-induced [^{3}H]DA release.

Although there was no evidence of TAAR1 mediation of dopaminergic effects measured, activation of TAAR1 modulated thermal response to MDMA. In MALDR mice, a strong biphasic temperature pattern emerged in response to MDMA, similar to C57BL/J mice in Chapter 2. However, in MAHDR mice, where TAAR1 is non-functional, the biphasic pattern was severely attenuated and the temperature modestly fluctuated from baseline. While it is possible that non-TAAR1 related genetic variation in MAHDR mice contributed to the difference between lines in thermal response to MA, this is unlikely as the effects were replicated in the transgenic *Taar1* model where only TAAR1 is absent. MDMA elicited acute hypothermia when TAAR1 was activated in *Taar1*-WT mice whereas the effect was absent in *Taar1*-KO mice. Although TAAR1

temperature research has only been previously conducted following a single administration, the same dose of MDMA (20 mg/kg) elicits a similar hypothermic reaction 30 min later in *Taar1*-WT mice, although it elicits a hyperthermic response in *Taar1*-KO mice at that point (Di Cara et al., 2011). While TAAR1 regulates MDMA-induced changes in body temperature, this effect did not correspond with astrocyte activation as GFAP expression was increased by MDMA in both lines, regardless of temperature changes. When administered methylone, which lacks affinity for TAAR1, there was no difference between MALDR and MAHDR mice in thermal response, but a strong biphasic response was elicited in both lines. This indicates similar psychostimulants, such as methcathinones, that do not signal through TAAR1 affect thermal response through alternate pathways. This would explain why amphetamines elicit hypothermia only when TAAR1 is present and activated, but methylone elicits hypothermia whether TAAR1 is functional or not.

While my hypothesis that MDMA-induced neurotoxicity would be increased in the absence of TAAR1 activation was not supported, I encountered the same issue as in Chapter 2: I was unable to induce any neurotoxicity to modulate. Therefore, the modulatory effect of TAAR1 on MDMA-induced neurotoxicity remains undetermined. My hypothesis that TAAR1 activation would increase MDMA-induced DA release was also not substantiated as there was no difference between genotypes. While this may simply indicate activation of TAAR1 does not affect DA release, there remains the potential that a difference may emerge with MA, a drug with increased potency at the DAT and greater efficacy as a DA releasing agonist. Finally, my data supported my hypothesis that the hypothermic response to MDMA was induced by TAAR1 activation. MDMA elicited hypothermia in both MALDR and *Taar1*-WT mice, in which TAAR1 was activated, and was absent in MAHDR and *Taar1*-KO mice, in which the receptor was not activated.

I shifted my focus to TAAR1 modulation of MA-induced neurotoxicity in Chapter 4 due to the difficulty I experienced using MDMA to elicit neurotoxicity in Chapters 2 and 3. My hypotheses were similar: I hypothesized MA-induced neurotoxicity would be increased when TAAR1 was

not activated and the hypothermic response to MA would be induced only when TAAR1 was activated. Using the more potent neurotoxin MA, I was able to clearly elicit both transient and sustained MA-induced neurotoxicity and the effects were dose-dependent. While MA decreased striatal DA levels 2 days following administration, they were decreased in *Taar1*-KO compared to –WT mice regardless of treatment. Seven days following administration, the lower doses of MA (2.5 and 5 mg/kg) decreased DA levels in *Taar1*-KO compared to –WT mice. An interpretation of this finding is that at the peak of neurotoxic effects, the ability of TAAR1 to modulate these transient and maximal decreases is at least partially eclipsed. The receptor may exert more influence on sustained DA terminal degeneration, as evidenced 7 days later. Although there were no genotype differences 7 days following the highest dose of MA (10 mg/kg), it is unlikely this is due to a floor effect as higher doses of MA (15 mg/kg) further decrease DA levels (Fumagalli et al., 1999; Guillot et al., 2008). It is probable that as the dose of MA increases, a point is reached at which TAAR1 can no longer regulate MA-induced neurotoxicity.

While the difference in striatal DA levels was greatest between genotypes at the intermediate dose of MA, the difference observed following the lowest dose is of particular importance. MA does not diminish striatal DA levels at doses below 4 mg/kg, either 2 or 7 days following administration (Thomas et al., 2004b; McConnell et al., 2015). This lack of neurotoxicity was replicated here in *Taar1*-WT mice, but when TAAR1 was not activated, the lower dose of MA significantly decreased DA levels 7 days following the final injection. This indicates not only is MA-induced neurotoxicity potentiated when TAAR1 is not activated, but MA also induces neurotoxicity in the absence of TAAR1 under conditions where neurotoxicity does not occur. Additionally, the two lower doses of MA diminished DA levels in *Taar1*-KO mice to approximately the same degree as the next higher MA dose affected *Taar1*-WT mice. That is to say DA levels in *Taar1*-KO mice administered MA (2.5 mg/kg) were equivalent to DA levels in *Taar1*-WT mice that received MA (5 mg/kg) and DA levels in *Taar1*-KO mice administered MA

(5 mg/kg) were similar to *Taar1*-WT mice given MA (10 mg/kg). This step-wise decrease indicates that when TAAR1 is absent, the effects of MA (2.5 and 5 mg/kg) on striatal DA levels are equivalent to 2x that dose of MA when TAAR1 is activated.

TAAR1 differentially mediated DA metabolite levels 2 and 7 days following MA. There was no effect of genotype on DOPAC or HVA levels 2 days later, while they were diminished in *Taar1*-KO compared to –WT mice 7 days later, regardless of treatment. This lack of a TAAR1 effect on the metabolites at 2 days, coupled with a decrease in DA levels in *Taar1*-KO mice at the same time indicates DA metabolism was increased, as evidenced by the elevated DA turnover rate in *Taar1*-KO mice. Seven days following treatment, changes in DOPAC and HVA levels paralleled DA levels and all were decreased in *Taar1*-KO compared to –WT mice. Although there was still a main effect of genotype, this was predominantly driven by the group of *Taar1*-KO that received MA (10 mg/kg). When DA is metabolized to DOPAC by MAO it produces ROS and increases oxidative stress (Cadet and Brannock, 1998). It is possible that DA metabolism is transiently increased when TAAR1 is not activated, leading to increased oxidative stress, contributing to increased DA terminal degeneration at the later time point.

While MA had minor effects on 5HT and NE levels, there were no differences between genotypes at any dose. The higher doses of MA transiently diminished 5HT levels, a common effect at these doses (McConnell et al., 2015). While there were transient and sustained decreases in NE, the levels of NE are much less than DA and 5HT in the striatum and MA does not damage the NE system as it does the other monoamines (Battaglia et al., 1987; Fleckenstein et al., 2000). This demonstrates TAAR1 selectively modulates the sustained effects of MA on the dopaminergic system, whereas microdialysis studies have demonstrated a non-selective effect of TAAR1 on acute monoamine release: AMPH increases striatal DA, 5HT, and NE levels in *Taar1*-KO compared to –WT mice and MDMA similarly increases striatal DA and 5HT (Wolinsky et al., 2007; Lindemann et al., 2008; Di Cara et al., 2011).

Striatal TH levels were diminished 2 days following MA administration. TH levels were also decreased in *Taar1*-KO compared to –WT mice, but this occurred regardless of treatment. While MA decreased TH levels 7 days following administration, there was no effect of genotype. Examination of the data revealed this was driven by the group of *Taar1*-WT mice that received MA (2.5 mg/kg) as the other groups follow the patterns of DA levels at this time. It is unclear why this group would have a significant drop in TH, when their DA levels are not altered. Additionally, MA does not decrease striatal TH levels at doses below 5 mg/kg, tested at 2, 3, or 7 days following administration (Angoa-Perez et al., 2013a; McConnell et al., 2015).

GFAP expression was increased both 2 and 7 days following MA administration in *Taar1*-KO compared to –WT mice. Similar to DA levels, genotype differences were only observed using the two lower doses of MA (2.5 and 5 mg/kg), supporting the hypothesis that TAAR1 no longer modulates neurotoxic effects at the highest dose of MA (10 mg/kg). While decreased DA markers and increased astrocyte activation serve as markers of MA-induced neurotoxicity, the early emergent genotype difference in MA-induced astrogliosis reinforces the separate trajectory of the two indicators of neuronal injury. Astrocyte activation is also more sensitive to MA than DA or TH levels and occurs at lower doses in the absence of changes to these DA-related markers (O'Callaghan and Sriram, 2005; McConnell et al., 2015). TAAR1 is localized on astrocytes and activation by MA decreases EAAT2 and GLU clearance (Cisneros and Ghorpade, 2014). In cultured astrocytes, the siRNA knockdown of TAAR1 increases EAAT2 expression and GLU uptake indicating activation of TAAR1 increases excitotoxicity. MA also diminishes potassium channel function in human fetal astrocytes through TAAR1-mediated PKA and PKC signaling pathways (Dave et al., 2018). However, based on the results of my experiments, other TAAR1-mediated effects in a physiological environment either overcome or negate the increased impairment of astrocyte function when TAAR1 is activated by MA in these *in vitro* experiments.

Activation of TAAR1 modulated thermal response to MA in a dose-dependent manner. In *Taar1*-WT mice, the lowest dose of MA produced the greatest degree of acute hypothermia, followed closely by the intermediary dose, while the highest dose produced significantly less hypothermia. In the absence of TAAR1 activation, there were modest MA-induced fluctuations in body temperature in *Taar1*-KO mice, but they were rarely significant and hyperthermia was not induced. A previous study reported a similar effect: MA induces acute hypothermia (30 min later) in *Taar1*-WT mice, but no significant change in body temperature in *Taar1*-KO mice (Harkness et al., 2015). The biphasic temperature pattern was clearly present following each administration of the lowest dose of MA in *Taar1*-WT mice. The thermal response to the middle dose of MA in both genotypes began to converge following the third injection, while it converged following the second administration of the highest dose of MA. Under these normothermic ambient conditions, hypothermia was only induced when TAAR1 is activated. As hyperthermia did not occur at any dose or in either genotype, all neurotoxicity can be deemed hyperthermia-independent. Although the dose-dependent MA-induced neurotoxicity inversely corresponds with hypothermia in *Taar1*-WT mice, it remains to be determined whether any observed neuroprotective effects are hypothermia-dependent. Thirty min following the first administration of MA (2.5, 5, and 10 mg/kg) the body temperature of *Taar1*–WT mice fell 2.5, 2.4, and 1.5 °C, respectively. This may have contributed to the neuroprotection in *Taar1*-WT mice at the two lower doses where there was a larger temperature drop. As there were no dose-dependent temperature changes in *Taar1*-KO mice; thermal response to MA did not modulate neurotoxicity in the absence of TAAR1.

These findings and others support a role of TAAR1 in modulating amphetamine-induced hypothermia under normothermic conditions (Di Cara et al., 2011; Harkness et al., 2015). Administered at 27 °C, MDMA (10 mg/kg) elicits hyperthermia in both genotypes and is potentiated in *Taar1*-KO mice (Di Cara et al., 2011). This indicates not only does the activation of TAAR1 elicit amphetamine-induced hypothermia, but the absence of TAAR1 can increase

body temperature in response to amphetamines. This may be another mechanism through which TAAR1 mediates amphetamine-induced neurotoxicity. However, once hyperthermia is induced, underlying mechanisms of neurotoxicity become much more difficult to disentangle as diminished neurotoxicity often correlates with decreases in hyperthermia (Miller and O'Callaghan, 1994; Albers and Sonsalla, 1995). Additional research is needed on TAAR1 mediation of thermal response to amphetamines and the effect this has on amphetamine-induced neurotoxicity.

The findings from Chapter 4 substantiated both my stated hypotheses. MA-induced neurotoxicity was increased when TAAR1 was not activated and the hypothermic response to MA was induced only when TAAR1 was activated (Fig. 25).

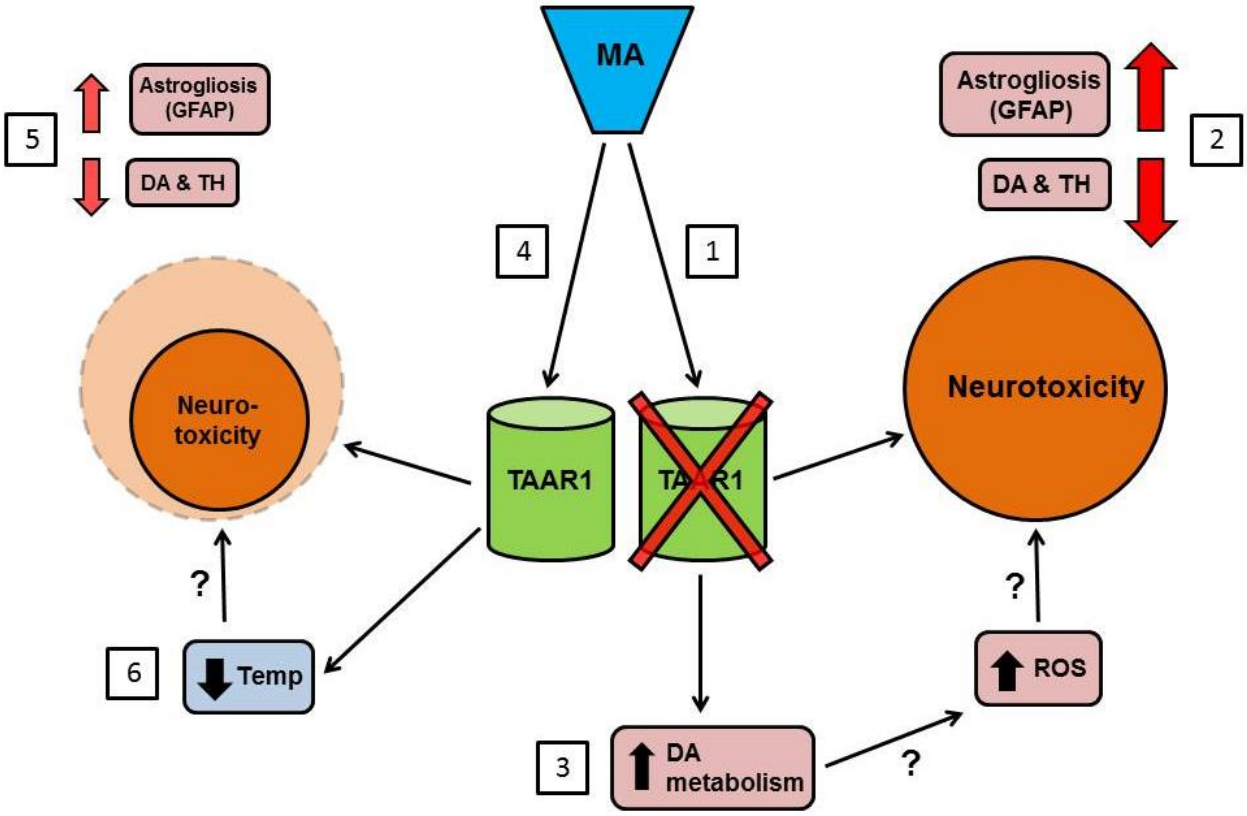

Figure 25. Schematic of TAAR1 regulation of MA-induced neurotoxicity. MA-induced neurotoxicity was increased when TAAR1 was absent (**1**): striatal DA and TH levels decreased and astrogliosis increased (**2**). DA metabolism was increased and may contribute to

neurotoxicity by increasing the formation of ROS (**3**). MA induced neurotoxicity to a lesser degree when TAAR1 was activated (**4**): DA and TH levels were less diminished and astrogliosis was not as enhanced (**5**). Activation of TAAR1 induced acute hypothermia which may have neuroprotective qualities (**6**).

In Chapter 5, I investigated interactions between TAAR1 and the monoaminergic transporters VMAT2 and DAT as potential mechanisms through which TAAR1 regulates MA-induced neurotoxicity. Based on the primary role of these transporters in modulating neurotoxicity (Fleckenstein et al., 2007), I hypothesized the ability of MA to impair VMAT2 and DAT function, as well as decrease VMAT2 and DAT expression, would be exacerbated when TAAR1 was not activated. Transporter function was measured only in *Taar1*-WT and KO mice, while transporter expression was quantified in both the *Taar1* and MADR mouse models. Additionally, I hypothesized I would replicate my previous effects of TAAR1 modulation of thermal response to MA, observed in the *Taar1* model, using the MADR model: MA-induced hypothermia would be induced only when TAAR1 was activated.

I was especially interested in examining the interaction of VMAT2 and TAAR1 as a potential mechanism of MA-induced neurotoxicity. As a regulator of cytosolic DA levels, VMAT2 is a critical modulator of MA-induced neurotoxicity (Hanson et al., 2004). Using subcellular fractionation, the effects of TAAR1 activation on VMAT2 were quantified in whole synaptosomes, but were also differentiated between VMAT2 localized to membrane-associated vesicles and transporters found on cytosolic vesicles. While [^{3}H]DHTB binding was robust in all three fractions, indicating the ubiquitous presence of VMAT2, [^{125}I]RTI-55 binding was robust only in the synaptosomal and membrane-associated fractions, reflecting both the purity of the enriched vesicular fraction and the restricted localization of DAT to plasmalemmal membranes. The same results have been previously reported in similar subcellular fractions using immunoreactivity assays of VMAT2 and DAT expression (Volz et al., 2007a). Twenty-four hours

following a neurotoxic regimen of MA (5 mg/kg, 4 inj, 2 h apart), VMAT2-mediated [^{3}H]DA uptake was decreased in synaptosomes and both of the isolated fractions. In the synaptosomal fraction, MA-induced [^{3}H]DA uptake inhibition was increased in *Taar1*-KO compared to –WT mice. MA equally inhibited [^{3}H]DA uptake among genotypes in the membrane-associated fraction, while in the vesicular fraction [^{3}H]DA uptake was diminished in *Taar1*-KO compared to –WT mice, regardless of treatment. These novel findings provide the first evidence of an interaction between TAAR1 and VMAT2, indicating TAAR1 activation has an overall protective effect against MA-induced impairment of VMAT2 function. This effect is localized to VMAT2 found on cytosolic vesicles as TAAR1 activation does not modulate the VMAT2 function on membrane-associated vesicles. The absence of this effect in the membrane-associated fraction is presumably due to the intracellular localization of TAAR1 (Bunzow et al., 2001; Xie et al., 2008a; Harmeier et al., 2015). As impairment of VMAT2 function is both a biomarker and potential cause of increased MA-induced neurotoxicity (Fleckenstein et al., 2009), this interaction may be responsible for the increased MA-induced neurotoxicity in *Taar1*-KO mice using the same dose and regimen, as reported in Chapter 4. MA diminishes the ability of VMAT2 to sequester DA, leading to elevated cytosolic DA levels, which in turn results in increased formation of reactive oxygen species, oxidative stress, and finally terminal degeneration (Kita et al., 2009). The observed further impairment of VMAT2 function, when TAAR1 was not activated, may increase intracellular DA levels leading to increased MA-induced neurotoxicity.

To assess VMAT2 expression, [^{3}H]DHTB binding was quantified in all three subcellular fractions from *Taar1* and MADR mice. As diminished VMAT2 expression increases MA-induced neurotoxicity (Fumagalli et al., 1999; Guillot et al., 2008), we hypothesized *Taar1*-KO and MAHDR mice would express less VMAT2 than *Taar1*-WT and MALDR mice, a potential contributing factor to the increased sensitivity to the neurotoxic effects of MA when TAAR1 is not activated . However, there was no difference in VMAT2 expression in either model between

the genotypes or the selected lines in any of the fractions. This confirms previous research reporting equal baseline mRNA expression of VMAT2 in in the SN, striatum, VTA, and NAc of *Taar1*-WT and –KO mice (Di Cara et al., 2011). There is currently no published data on VMAT2 in the MADR model. Although MA diminished [^{3}H]DHTB binding 24 h later in the purified vesicular fraction, it did not alter binding in the synaptosomal and membrane-associated fractions. This differential pattern of VMAT2 expression among subcellular compartments has been previously reported, indicating intracellular trafficking of the transporter (Hogan et al., 2000; Ugarte et al., 2003; Chu et al., 2008). Decreased VMAT2 function has been attributed to trafficking of VMAT2 out of the vesicles (Riddle et al., 2002; Sandoval et al., 2003). However, it is difficult to separate impairment in VMAT2 function from decreased function due to diminished expression when changes in both measures occur concurrently. Although TAAR1 activation did not alter VMAT2 expression under these conditions, examining the findings in the context of the VMAT2 function experiment has novel implications. Genotype differences in [^{3}H]DA uptake within the vesicular fraction, but not [^{3}H]DHTB binding, suggest that VMAT2 function is impaired when TAAR1 is not activated, as opposed to being decreased due to trafficking. Another study has also demonstrated that a decrease in vesicular VMAT2 function can occur without diminished expression by investigating regional differences of the effects of MA (Chu et al., 2008). One hour following MA administration, [^{3}H]DA uptake is diminished in the vesicular fraction from both the striatum and NAc, but VMAT2 immunoreactivity is decreased only in the striatum and remains unchanged in the NAc. Coupled with our findings, this suggests other effects than trafficking may be responsible for the decreased function of VMAT2 found on cytosolic vesicles. Additionally, independent of the effects of TAAR1 activation in the synaptosomal and vesicular fractions, the separation of VMAT2 function and expression was also observed in the membrane-associated fraction, where MA inhibited [^{3}H]DA uptake, but did not alter [^{3}H]DHTB binding. While most studies of VMAT2 function have focused on cytosolic vesicles, one study has reported that MA diminishes VMAT2-mediated DA uptake 24 h later in

membrane-associated vesicles as well (Chu et al., 2010). These results, in conjunction with previous research demonstrating VMAT2 expression is unchanged in membrane-associated vesicles following MA administration (Riddle et al., 2002; Ugarte et al., 2003), further indicate MA can impair VMAT2 function independently of decreasing VMAT2 expression.

DAT function was measured *in vitro* due to the swift return of DAT function to baseline within 24 h of MA administration (Sandoval et al., 2000). Incubation of striatal homogenates from *Taar1*-WT and –KO mice with MA revealed no difference in DAT-mediated [^{3}H]DA release or [^{3}H]DA uptake. This corroborated my findings from Chapter 3 using MDMA, where TAAR1 activation also did not alter [^{3}H]DA release. Supporting these findings, activation of TAAR1 by a partial TAAR1 agonist in rat striatal synaptosomes does not alter MA-induced [^{3}H]DA release or uptake (Cotter et al., 2015). My results and the above study find no evidence that activation of TAAR1 by amphetamines directly modulates striatal DAT function, refuting the report that activation of TAAR1 enhances MA impairment of striatal DAT function (Xie and Miller, 2009a). There is also behavioral evidence of dissociation between the receptor and transporter. Spontaneous hyperlocomotion in DAT-KO mice and rats is diminished by TAAR1 agonists, indicating TAAR1 mediation of DA-dependent hyperactivity occurs independently of DAT (Revel et al., 2011; Leo et al., 2018).

To determine whether TAAR1 activation alters DAT expression, I quantified [^{125}I]RTI-55 binding using saturation binding analyses in both the *Taar1* and MADR mouse models 24 h following treatment with MA (5 mg/kg, 4 inj, 2 h apart). As expected, MA reduced [^{125}I]RTI-55 binding in striatal synaptosomes, but, similar to VMAT2 expression, there were no differences in DAT expression between either *Taar1*-WT and –KO mice or MALDR and MAHDR mice. Although there is no previous published data on the effects of TAAR1 on DAT following MA administration, my findings are in alignment with previous research in the *Taar1* model demonstrating basal striatal DAT expression is equivalent in *Taar1*-WT and –KO mice (Lindemann et al., 2008; Di Cara et al., 2011). Although MAHDR mice have a higher

expression of DAT in the NAc at baseline than MALDR mice, DAT levels have not been previously quantified in the striatum in the MADR model (Lominac et al., 2014). While decreased DAT expression at 24 h is indicative of MA-induced neurotoxicity, it is not representative of permanent striatal DA terminal loss until later time points, such as 7 days later (Granado et al., 2010; Bourque et al., 2012). As TAAR1 activation did not significantly modulate DA biomarkers 2 days following MA administration, but did 7 days later, it is possible a similar effect would emerge at that time point and DAT expression would be decreased in the *Taar1*-KO or MAHDR mice.

Finally, TAAR1 mediation of thermal response to MA was assessed in both TAAR1 models for direct comparison. Again, MA only induced hypothermia when TAAR1 was activated, in both the MALDR and *Taar1*-WT mice. Conversely, the effect was absent in MAHDR mice and *Taar1*-KO mice demonstrating the hypothermic response to MA was TAAR1-dependent. Replication of thermal response to MA in the MAHDR and *Taar1*-KO mice indicate the effects are due to a lack of activation of TAAR1 versus developmental effects or compensation in MAHDR or *Taar1*-KO mice. However, the thermal response to MA was markedly different in MALDR compared to *Taar1*-WT mice, although the overall pattern was similar. There was a sex difference in thermal response to MA among MALDR mice. MA elicited a stronger hypothermic response in male MALDR mice compared to female MALDR mice or *Taar1*-WT mice. There was no sex difference in thermal response to MA in MAHDR or *Taar1*-WT/KO mice. Additionally, hypothermia was sustained in MALDR mice compared to *Taar1*-WT mice and peaked following the second injection of MA, whereas hypothermia in *Taar1*-WT always peaked immediately following the first injection, here and in Chapter 4. These differences in MALDR mice were surprising given the lack of a sex difference in MALDR mice receiving MDMA in Chapter 3 and the similar response to MDMA between MALDR and *Taar1*-WT mice. This may be attributed to genetic variation within MALDR mice, heterozygous for the B6 and D2 allele, as opposed to MAHDR mice, homozygous for the D2 allele, and the isogenic *Taar1*-WT/KO mice. Another

possibility is variance between replicate sets of the generated selected lines, as MALDR and *Taar1*-WT mice did not differ in thermal response to MA in experiments using mice from earlier replicate sets (Harkness et al., 2015).

The results from Chapter 5 substantiated my hypothesis that MA-induced impairment of VMAT2 function would be increased when TAAR1 was not activated, potentially contributing to the ability of TAAR1 to regulate MA-induced neurotoxicity. This effect was not restricted to cytosolic vesicles as suspected and was found in whole synaptosomes as well, but absent in the membrane-associated fraction. My hypothesis that MA-induced decreases in VMAT2 expression would be exacerbated in the absence of TAAR1 activation was not substantiated, suggesting the receptor does not modulate transporter expression, at least under the given conditions. Contrary to my hypotheses, activation of TAAR1 did not alter *in vitro* MA-induced impairment of DAT function or *in vivo* MA-induced changes in DAT expression. These findings, coupled with similar *in vitro* results from Chapter 3 using MDMA, indicate TAAR1 does not directly interact with DAT. Finally, while the body temperature data supported my hypothesis that MA-induced hypothermia only occurs when TAAR1 is activated, the hypothermic response to MA varied between models. This discrepancy is most likely attributable to genetic differences between *Taar1*-WT and MALDR mice.

Conjointly, these findings indicate for the first time that TAAR1 regulates MA-induced neurotoxicity. Activation of TAAR1 had a greater influence on DA markers of terminal degeneration 7 days following MA administration indicating TAAR1 is more potent at modulating the sustained neurotoxic effects of MA. TAAR1 regulation of MA-induced astrocyte activation was robust at both early and later time points. The results also provide strong evidence that activation of TAAR1 is necessary for the hypothermic response to amphetamines as this effect was replicated in both the transgenic *Taar1* and selected line MADR mouse models using MDMA and MA. Finally, activation of TAAR1 protects against MA-induced impairment of VMAT2 function, but this effect is localized to cytosolic vesicles, a potential mechanism for regulation of

MA-induced neurotoxicity. My negative results are also informative and fill in several gaps in the literature between TAAR1 models. My *in vitro* experiments bolster current theories that TAAR1 does not directly mediate DAT function. The results also provide the first evidence that striatal DAT and VMAT2 expression are equivalent in MALDR and MAHDR mice, both at baseline and 24 h following MA administration. Together they strengthen the case that TAAR1 does not interact with transporters at the plasma membrane surface. These results will hopefully inform future TAAR1 research.

3. Clinical implications

Since 2001 when TAAR1 was simultaneously cloned and identified as potently activated by amphetamines, TAAR1 has been an area of interest for the treatment of drug addiction (for review, see Grandy et al., 2016; Liu and Li, 2018a). The receptor has also been implicated in a variety of other disorders and afflictions, such as schizophrenia, Parkinson's disease, depression, cancer, sleep disorders, and obesity (for review, see Pei et al., 2016; Berry et al., 2017). These findings have driven the search for TAAR1 agonists and antagonists in hopes of identifying and developing novel pharmacological agents to treat these disorders (Stalder et al., 2011; Galley et al., 2016). F. Hoffmann-La Roche is currently evaluating the TAAR1 partial agonist RG7351 in a phase I clinical trial to treat major depression and Sunovion Pharmaceuticals is testing SEP-363856, a dual agonist at the 5HT 1A-type receptor and TAAR1, for treatment of schizophrenia in phase II clinical trials (Liu and Li, 2018b).

As activation of TAAR1 diminishes the biochemical and behavior changes associated with amphetamine reward, reinforcement, and craving (Lindemann et al., 2008; Shabani et al., 2011; Achat-Mendes et al., 2012; Shabani et al., 2012a), research has focused on mediating these properties of amphetamine use and addiction. Two different TAAR1 partial agonists, RO520648 and RO5263397, have already been shown to diminish the rewarding properties of MA (Cotter et al., 2015; Pei et al., 2017). Hopefully, based on my research, exploration of the effects of TAAR1 agonists will expand to include MA-induced neurotoxicity. Future TAAR1 research could

lead to the development of novel pharmacological therapies with neuroprotective properties to ameliorate the harmful impact of MA in active or recovering addicts. This research may also have broader implications to other DA-related pathologies, such as Parkinson's disease and schizophrenia.

While my results imply the activation of TAAR1 is protective against the harms of MA, the flipside is the harmful effects of MA may be enhanced when the receptor is not activated. Just as MAHDR mice possess a non-synonymous SNP that encodes a non-functional TAAR1 (Reed et al., 2018), there are similar mutations in the human *Taar1* gene that alter functionality. Over 250 non-synonymous SNPs have been identified in h*Taar1* (dbSNP database, NCBI, accessed July 19th, 2018). In a cellular model, several non-synonymous SNPs were substituted into h*Taar1* and receptor response to the TAAR1 agonist ß-PEA was tested (Shi et al., 2016). SNP substitutions varied, resulting in a fully functional TAAR1 response, a sub-functional response, and a non-functional response. While the effect of SNP variants in h*Taar1* has yet to be determined on MA-related changes and behaviors, SNP variants have other reported effects. A survey of SNPs in h*Taar1* was conducted in a schizophrenic patient population (John et al., 2017). Seven rare SNPs of h*Taar1* were identified as protein disturbing variants, potentially elevating the risk for development of schizophrenia. There is precedence for this finding in TAAR1 animal research as *Taar1*-KO mice display a PPI deficit and possess an increased density of $D2R^{High}$ at baseline, traits that are both associated with schizophrenia (Wolinsky et al., 2007). Another survey of h*Taar1* SNPs, conducted in patients with obesity and/or impaired glucose regulation, identified two SNPs resulting in sub-functional and non-functional receptor response (Muhlhaus et al., 2017). This corresponds with an animal study reporting TAAR1 modulates food intake and glucose homeostasis in mice (Raab et al., 2016). The study also found human TAAR1 co-localized with insulin in pancreatic ß-cells. Finally, TAAR1 expression negatively correlates with malignant breast tumor grade and TAAR1 over-expression correlates with longer overall survival from breast cancer (Vattai et al., 2017; Kovács et al., 2019). These

preliminary clinical studies reflect the positive effects of the presence of TAAR1 and deleterious effects when the receptor is sub- or non-functional.

From an epidemiological standpoint, this indicates a subset of the population may be at greater risk of physical and cognitive harm resulting from enhanced MA-induced neurotoxicity due to decreased TAAR1 activation. As rewarding properties of MA are increased and aversive properties decreased when TAAR1 is non-functional, this same population may also be at greater risk for MA use disorder, exacerbating neurotoxicity through increased use.

4. Limitations

There are certain limitations inherent to the chosen components and specific findings of these experiments. In Chapter 2, the lower dose of MDMA (15 mg/kg) did not have any sustained effects on biomarkers of neurotoxicity and only transiently increased GFAP expression. As this was the MDMA dose used in combination with methylone and MDPV, I was unable to draw conclusions on the regulatory role of these methcathinones on MDMA-induced neurotoxicity, although they may affect neuroinflammation, as combination of MDMA with either methylone or MDPV ameliorated astrocyte activation. Investigating the interaction of TAAR1 and MDMA neurotoxicity in Chapter 3, a higher dose of MDMA (20 mg/kg) also failed to diminish transient DA levels in both selected lines. This was surprising as both doses of MDMA (15 and 20 mg/kg) typically decrease striatal DA and TH levels when measured at 2,3, and 7 days later (O'Callaghan and Miller, 1994; Johnson et al., 2004; Angoa-Perez et al., 2013b). While MDMA increased GFAP expression, the effect was equivalent in both MALDR and MAHDR mice. Although the lack of differences between MALDR and MAHDR mice may indicate TAAR1 activation does not mediate MDMA-induced changes in these markers, the same confound exists as from Chapter 2: neurotoxicity of a drug (MDMA) must first be demonstrated before the modulatory role of an agent (methcathinones or TAAR1) can be assessed.

The activation of TAAR1 in *Taar1*-WT mice mitigated MA-induced neurotoxicity in Chapter 4, as compared to *Taar1*-KO mice. However, interpreting the results of Chapter 5 to investigate the potential underlying mechanisms is more challenging due to the mixed use of TAAR1 mouse models. Both transporter function and expression were quantified in the *Taar1*-WT and –KO mice, allowing for extrapolation to findings in Chapter 4 using the same model. Due to animal availability and time constrictions, only VMAT2 expression was able to be measured in the selected line MADR mouse model. Quantification of VMAT2 function would not only provide a more holistic profile of a TAAR1/VMAT2 interaction within the MADR model, but would also allow for between model comparisons with transgenic *Taar1* mice.

The results from Chapters 3-5 clearly demonstrate activation of TAAR1 (in both models) modulates thermal response to amphetamines (MDMA and MA). However, it remains uncertain if the diminished MA-induced neurotoxicity in *Taar1*-WT mice is hypothermia-independent. As the dose-dependent MA-induced neurotoxicity in *Taar1*-WT mice inversely corresponded with hypothermic response this may have contributed to the increased neuroprotection in *Taar1*-WT mice. In comparison, the neurotoxicity observed in *Taar1*-KO mice is temperature-independent as MA did not elicit hyper- or hypothermia. Additionally, there were other results that were not influenced by changes in temperature. In Chapter 3, MDMA elicited the same divergent temperature patterns in MALDR and MAHDR mice, yet equally increased GFAP expression. In Chapter 5, MA equally decreased DAT and VMAT2 expression in MALDR and MAHDR mice, while only eliciting hypothermia in MALDR mice. These findings call into question whether activation of TAAR1 provides neuroprotection *via* induction of hypothermia or if the receptor simply regulates thermal response to amphetamines without an effect on neurotoxicity.

5. Future directions

I have demonstrated TAAR1 modulates MA-induced neurotoxicity and thermal response. Additional research is needed to investigate the extent of TAAR1 regulation of MA-induced neurotoxicity. As my results indicate the TAAR1 effects on DA biomarkers do not emerge until

later, time course studies are necessary during the first week following administration to create a temporal outline of TAAR1 modulatory effects. Though resource intensive, papers that have studied the same biomarkers of MA neurotoxicity (monoamine, TH, and DAT levels, and GFAP expression) at multiple time points (1, 2, 3, 5, 7, and 14 days) have provided invaluable information to the field of neurotoxicity (O'Callaghan and Miller, 1994; McConnell et al., 2015). A study of this breadth, in either or both TAAR1 mouse models, would provide a temporal map of TAAR1 mediation of MA-induced neurotoxicity. While these markers are the most commonly quantified biomarkers of neurotoxicity, the use of direct methodologies of observation, such as silver staining, Fluor-Jade C labeling, and EM, would verify DA terminal degeneration, independent of transient fluctuations in these markers.

Oxidative stress, the byproduct of MA-induced elevation of intracellular DA levels, is a primary cause of DA terminal degeneration. Cytosolic DA is metabolized by MAO to produce ROS: H_2O_2, superoxides, and hydroxyl radicals. DA is also auto-oxidized to form reactive DA quinones. Both ROS and DA quinones increase oxidative stress leading to lipid peroxidation and the breakdown of terminal proteins (Krasnova and Cadet, 2009). Although I did not measure any markers of oxidative stress, my finding that DA metabolism is increased in *Taar1*-KO mice indicates another potential mechanism through which TAAR1 mediates MA-induced neurotoxicity. Due to temporal differences in turnover rate, conducting a time course of hydroxyl formation or protein carbonyl would provide insight into this potential mechanism. DA quinones reflect cytosolic-specific oxidative stress (LaVoie and Hastings, 1999; Miyazaki et al., 2006). Acute measurement of quinones following MA would provide additional insight into whether TAAR1 modulates MA-induced neurotoxicity *via* intra- or extracellular mechanisms.

My research and the proposed studies focused on the extent to which TAAR1 mediates neurotoxicity through comparison of one system in which TAAR1 is activated to another in which it is not. While this begins to provide an understanding on how TAAR1 regulates MA-induced neurotoxicity, the logical progression is to investigate the modulatory effects of the

receptor within a TAAR1-intact organism. The development of full and partial TAAR1 agonists provides the pharmacological tools to begin this work. Testing the ability of these drugs to mediate MA-induced neurotoxicity in *Taar1*-WT or MALDR mice would allow for direct comparison to my dissertation research. Additionally, administration of the TAAR1 agonists to *Taar1*-KO or MAHDR mice would provide another control to ensure there are no off-target effects. However, these substances could also be tested in a rat model to validate cross-species efficacy. As amphetamines are already TAAR1 agonists, assessment of modulating TAAR1 activation, instead of the comparison of activation versus inactivation, is necessary for the development of tools to ameliorate MA-induced neurotoxicity.

6. Conclusions

My findings demonstrate for the first time that activation of TAAR1 confers neuroprotection against MA-induced neurotoxicity with sustained effects one week following drug administration. The absence of TAAR1 not only potentiated MA-induced neurotoxicity, but also induced neurotoxicity at lower doses. Modulation was specific for markers of DA terminal degeneration as other monoamines were unaltered. MA-induced astrogliosis was particularly sensitive to TAAR1 regulation as both transient and sustained astrocyte activation was diminished when TAAR1 was activated. As MDMA failed to induce neurotoxicity under current conditions, the ability for TAAR1 to modulate MDMA-neurotoxicity should not be speculated. TAAR1 also modulated thermal response to both MDMA and MA. Acute hypothermia was induced only when TAAR1 was activated by the amphetamines. This effect was replicated in separate TAAR1 mouse models and was absent when the receptor was either knocked down in *Taar1*-KO mice or non-functional in MAHDR mice. Confirming selectivity for the receptor, thermal response to methylone, a non-TAAR1 agonist, was equivalent when TAAR1 was activated or not. The regulatory effects of TAAR1 on MA-induced neurotoxicity and thermal response were most pronounced at lower doses. It is likely that once MA levels increase past a certain point, the modulatory effects of TAAR1 are overshadowed. My investigation into monoaminergic

transporters provides the first evidence of an interaction between TAAR1 and VMAT2. MA-induced impairment of VMAT2 function was increased when TAAR1 was not activated, but only on cytosolic vesicles. I found no evidence that activation of TAAR1 alters DAT functionality following *in vitro* treatment with MA or MDMA. TAAR1 activation also did not modulate either VMAT2 or DAT expression. These results indicate TAAR1 does not interact with transporters near the plasma membrane. TAAR1 does mediate VMAT2 function localized to cytosolic vesicles, a potential mechanism underlying TAAR1 regulation of MA-induced neurotoxicity.

The involvement of TAAR1 in MA-induced neurotoxicity provides a new avenue of research to pursue in order to better understand the complexities of the neurotoxic profiles of amphetamines. Additionally, it suggests the receptor is a potential target for novel pharmacotherapeutic agents to treat MA use disorder and addiction.

Appendices

Appendix 1: additional experiments associated with Chapter 2

A1.1. DA ELISA and drug dose

Drug dose

To determine the optimal drug dose to use for experiments conducted in Chapter 2, various concentrations of MDMA , methylone (MDMC), and MPDV were administered to C57BL/6 mice using a binge-like regimen (4 inj, 2 h apart) and mice were euthanized 2 days later. A one-way ANOVA revealed a main effect of drug dose on DA levels 2 days following drug administration ($F_{10,27}$ = 18.77 , p < 0.0001) (Supp. Fig. 1). *Post hoc* analysis revealed DA levels were significantly decreased by the MDMA 15, 20, and 30 mg/kg treatment, but not MDMA 10 mg/kg or any of the methylone or MDPV treatments. MDMA 15 and 30 mg/kg were selected as drug doses for experiments in Chapter 2 due to their differential effects on DA depletion. As there was no difference between methylone doses, the higher dose (20 mg/kg) was selected as it is less potent a transporter substrate than MDMA (Eshleman et al., 2013). As there were no differences between MDPV doses, the intermediary dose (1.0 mg/kg) was selected. Due to the potency of MDPV, the drug elicits increased LMA at doses as low as 0.3 mg/kg, but 1.0 mg/kg is a commonly used dose (Fantegrossi et al., 2013; Marusich et al., 2014).

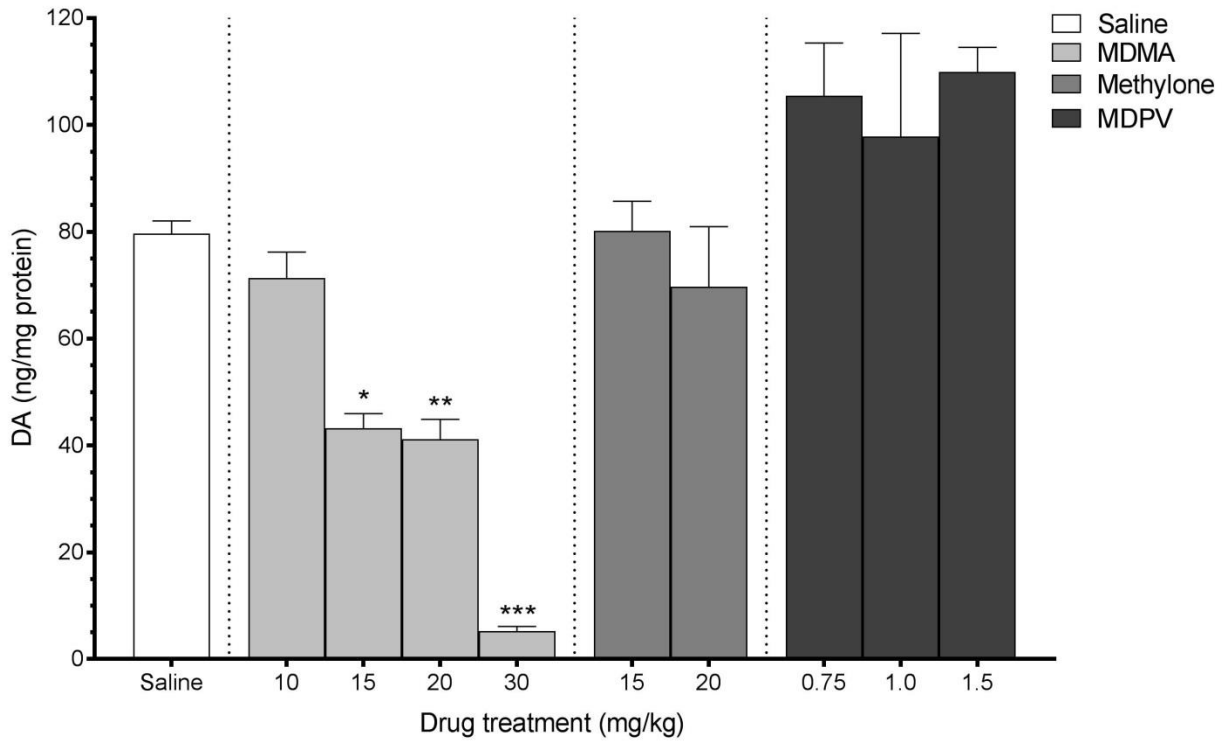

Supplementary Figure 1. Dose response curve for DA ELISA kit. C57BL/6 mice received 4 i.p. injections of saline, MDMA (10, 15, 20, or 30 mg/kg), methylone (MDMA, 15 or 20 mg/kg), or MDPV (0.75, 1.0, or 1.5 mg/kg), 2 h apart, and were euthanized 2 days later for striatal tissue collection. DA values were normalized to the amount of protein in each tissue sample. Data represent mean ± SEM of 3-4 independent experiments. *: $p < 0.05$, **: $p < 0.01$, ***: $p < 0.0001$ compared to the saline group (Dunnett's *post hoc* test).

A1.2. Temperature recordings

Core body temperature reading: rectal vs. radio telemetry

To test the accuracy of the DAS-8001 radio telemetry temperature recording device, 5 mice were implanted with telemetry transponders as described in Chapter 2 and temperatures were recorded every hour for 4 h, first using a standard rectal glycerol-lubricated probe (Sensortek, Clifton, NJ), immediately followed by a telemetry measurement. The mean difference in temperature difference between the two types of measurement, from all mice at each time point,

was 0.15 ± 0.03 °C. As there was no significant difference in temperature between the two methods, the telemetry method of body temperature was considered validated and used henceforth.

A1.3. [^{3}H]PK11195 binding to TSPO

[3H]PK11195 optimization experiments

To determine the optimal conditions to perform the PK11195 binding assay, a protein curve and a time course were conducted. First, various amounts of protein (25 – 200 µg) were loaded (Supp. Fig. 2A). The experiment was conducted as described in Chapter 2, using a [^{3}H]PK11195 concentration of 1.5 nM and an incubation time of 2 h. Second, a time course was conducted at various incubation times (15 min – 3 h) using a [^{3}H]PK11195 concentration of 1.4 nM and 0.75 µg protein loaded (Supp. Fig. 2B). It was determined that 75 µg of protein provided optimal binding while remaining within the linear range, avoiding saturation. An incubation time of 2 h was selected as sufficient to reach equilibrium.

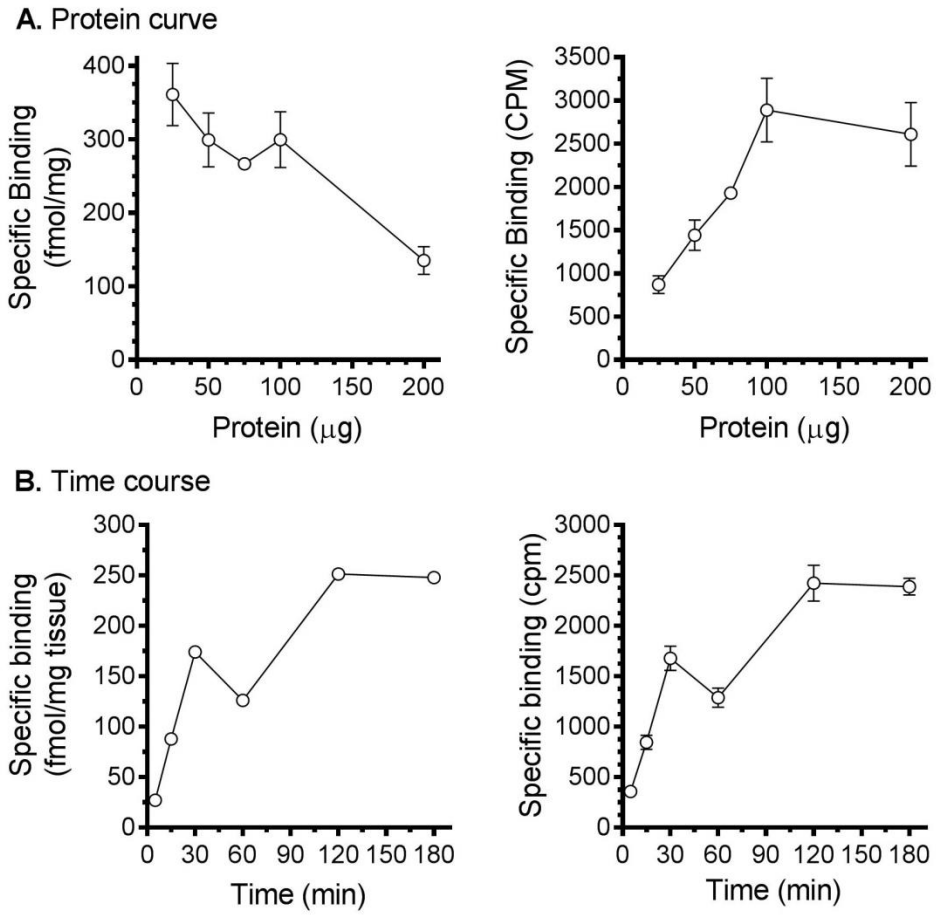

Supplementary Figure 2. [^{3}H]PK11195 binding assay optimization. A protein curve (**A**) and incubation time course (**B**) were evaluated. Data shown are mean ± SEM of 3 independent experiments (**A**) or mean ± SEM from a single experiment, in triplicate (**B**).

[3H]PK11195 adherence

It was discovered at the end of the [^{3}H]PK11195 binding assays that 10-40% of the radioactive material was adhering to the sides of the assay wells. This only occurred at [^{3}H]PK11195 concentrations 1 nM and above. Preliminary adherence tests used a low concentration of 0.08 nM [^{3}H]PK11195 that did not reveal any difference in CPMs after 3 h for any of three surfaces (Supp. Fig. 3A). However, based on the variability in final results, a post-experiment was conducted using higher concentrations and found CPMs were lower 3 h after

being added (Supp. Fig. 3B). A two-way repeated measures ANOVA for PK11195 radioactivity counts identified a significant interaction of concentration and time ($F_{4,10}$ = 118.6, p < 0.0001) and a main effect of concentration ($F_{4,10}$ = 467.5, p < 0.0001) and time ($F_{1,10}$ = 3043, p < 0.0001). Radioactivity counts were lower 3 h later compared to initial counts at all concentrations. Post-hoc analysis Bonferroni at each concentration revealed counts were significantly lower 3 h later at 6, 3, and 1 nM, but not 0.5 or 0.25 nM.

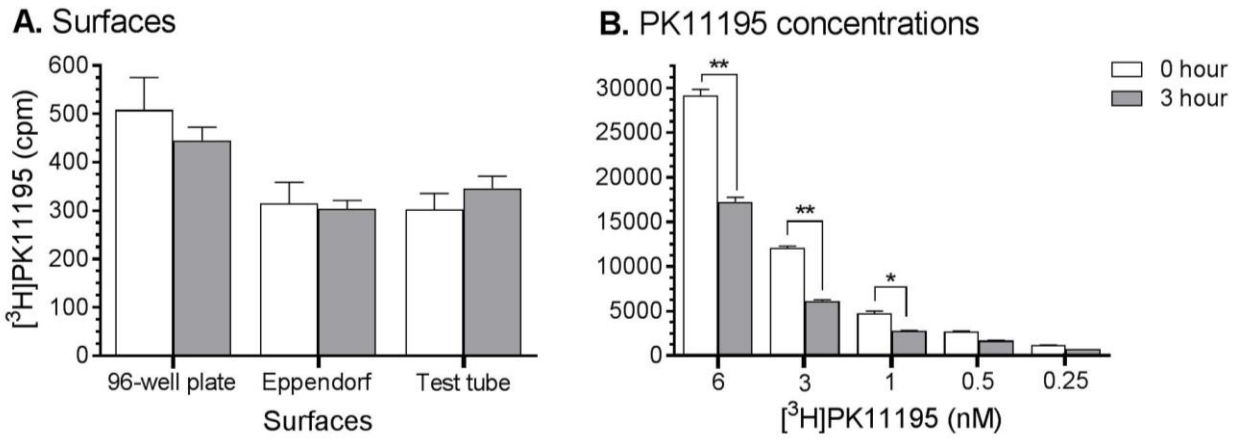

Supplementary Figure 3. Test of radioactivity adherence over time. [^{3}H]PK11195 (0.08 nM) was added to a well of a plastic 96-well plate, a plastic Eppendorf vial, and a glass test tube (**A**). [^{3}H]PK11195 (0.25 - 6 nM) was added to a plastic Eppendorf vial (**B**). In both assays, radioactivity was spotted on a filter immediately and then 3 hours later. Data shown are mean ± SEM from separate, single experiments, in triplicate *: p < 0.01, **: p < 0.0001 compared between time points.

Appendix 2: additional experiments associated with Chapter 3

A2.1. MDMA-induced [^{3}H]DA release optimization experiments

[^{3}H]DA release: time, temperature, protein

To optimize the release assay, an incubation time curve was conducted under two different temperature conditions. Synaptosomes (4 µg protein) were preloaded with [^{3}H]DA (10 nM) for

30 min in a 25 °C water bath. The release assay was initiated by the addition of 850 µl of the synaptosomal preparation preloaded with [^{3}H]DA to 150 µl of cocaine (100 nM), MA (1 µM) or assay buffer as control, and incubated for 5, 10, or 30 min in either a 25 or 37 °C water bath. Additionally, synaptosomes of various protein concentrations, prepared using 0.25, 0.33, 0.5, 1.0, and 2.0x dilutions of assay buffer (ml/mg wet weight of tissue), were preloaded with [^{3}H]DA (10 nM) for 30 min in a 25 °C water bath until reaching a steady state. The release assay was initiated similarly, at 25 °C, and incubation was terminated 30 min later. Cocaine and MA were chosen for comparison as a DAT inhibitor and DAT substrate, respectively.

Incubation at 25 °C elicited a greater difference in DA retention between cocaine and MA and was used onward (Supp. Fig. 4A and 4B). As 10 and 20 min were equally optimal in DA retention, a 10 min incubation period was selected. Dilution of synaptosomes by 0.25X (ml/mg wet weight tissue) yielded 5-6 µg of total protein and was also deemed optimal and used onward (Supp. Fig. 4C).

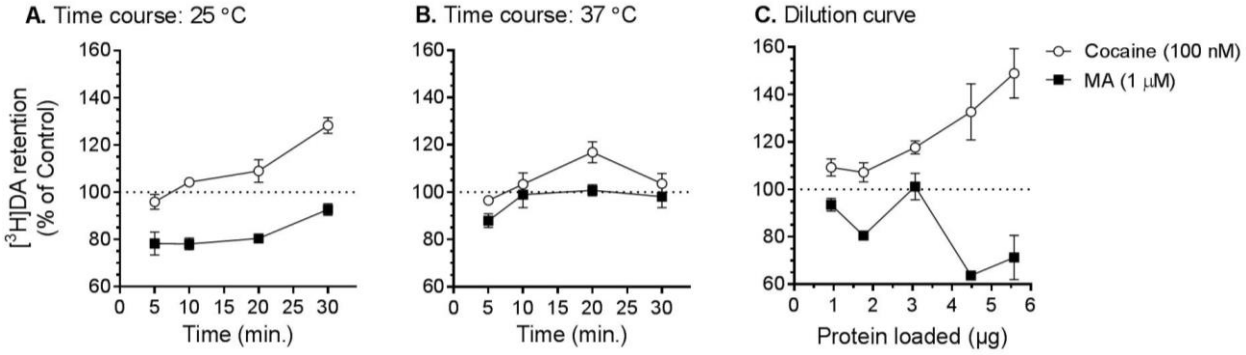

Supplementary Figure 4. [^{3}H]DA release assay optimization. An incubation time course (**A** and **B**) and protein curve (**C**) were evaluated. Data shown are mean ± SEM from a single experiment, in triplicate (**A** and **B**) or the mean ± SEM of 3 independent experiments (**C**).

Appendix 3: additional experiments associated with Chapter 4

A3.1. TAAR1 modulation of DA and dose response curve pilot

Dose pilot

An initial pilot experiment was conducted to determine whether there was a difference in MA-induced decreases in striatal DA levels between *Taar1*-WT and –KO mice and to test different doses of MA. *Taar1*-WT and –KO mice were treated with the same binge regimen (4 inj, 2 h apart) of saline or MA (5 or 10 mg/kg), euthanized 2 or 7 days following final injection and striatal tissue removed and frozen, as described in Chapter 4. Tissue was analyzed for DA content using the same DA ELISA kit and protocol used in Chapter 2.

MA dose-dependently decreased striatal levels of DA at both time points (2 and 7 days following the final injection). Additionally, at both time points DA levels were lower in *Taar1*-KO mice compared to *Taar1*-WT mice after MA 5 mg/kg, but not 10 mg/kg. These characterizations are supported by the following statistical results. At 2 days after saline or MA administration, a two-way ANOVA for DA level revealed a significant genotype x dose interaction ($F_{2,29} = 3.97$, $p < 0.05$) (Supp. Fig. 5A). Simple main effect analysis of the effect of genotype at each dose revealed no difference between genotypes for saline-treated animals, but *Taar1*-KO mice receiving MA 5 mg/kg had significantly lower levels of striatal DA in comparison to *Taar1*-WT mice. There was no difference between genotypes at MA 10 mg/kg. Simple main effect analysis of the effect of dose within each genotype indicated significant dose-dependent effects in both *Taar1*-WT and -KO mice. Follow up analyses within each genotype using Newman-Keuls *post hoc* mean comparisons indicated that DA levels in *Taar1*-WT and –KO mice were significantly decreased by both doses of MA compared to saline-treated animals. Seven days following administration, there was also a significant genotype x dose interaction ($F_{2,30} = 3.41$, $p < 0.05$) (Supp. Fig. 5B). Further analysis revealed similar results to those at 2 days later. Simple main effect analysis of the effect of genotype at each dose revealed no difference between genotypes

for animals administered saline or MA 10 mg/kg, but *Taar1*-KO mice receiving either MA 5 mg/kg had significantly lower levels of striatal DA in comparison to *Taar1*-WT mice. Simple main effect analysis of the effect of dose indicated significant dose-dependent effects in both genotypes. However, in *Taar1*-WT mice, Newman-Keuls *post hoc* mean comparisons indicated that DA levels were significantly decreased by the MA 10 mg/kg dose compared to saline-treated animals, but not by MA 5 mg/kg. In *Taar1*-KO mice, DA levels were significantly decreased by both MA doses compared to saline-treated animals. Based on these results, both doses were selected for ongoing experiments based on the significant difference between genotypes at both time points using the MA 5 mg/kg dose. The MA 10 mg/kg dose was retained for comparison as it indicated a floor effect was achieved where differences between the genotypes disappeared. A lower dose of MA (2.5 mg/kg) was added to investigate differences between genotypes at an additional dose.

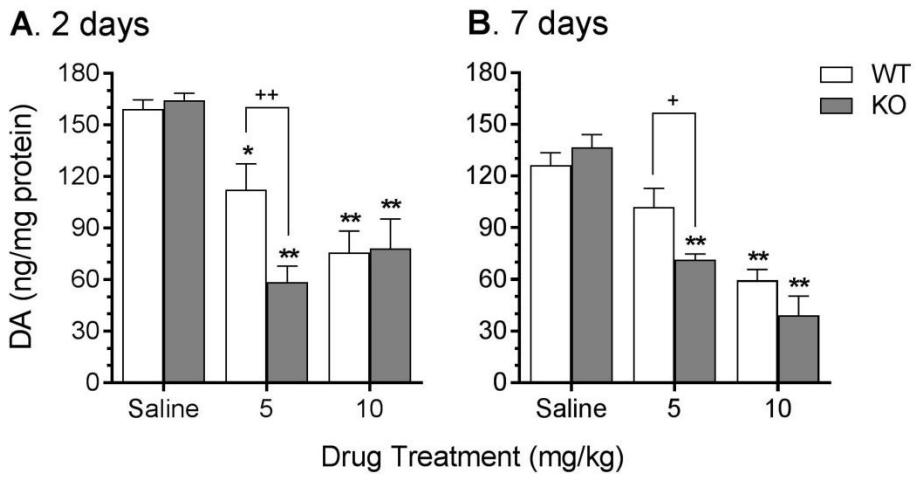

Supplementary Figure 5. MA dose response curve for DA ELISA kit. Striatal levels of DA were measured 2 and 7 days following saline or MA treatment. *Taar1*-WT and -KO mice received 4 i.p. injections of saline or MA (5, or 10 mg/kg), 2 h apart, and were euthanized either 2 or 7 days following the final injection for striatal tissue collection. Values were normalized to the amount of protein in each tissue sample. Data represent means ± SEM of 6 mice per group.

*: $p < 0.05$, **: $p < 0.0001$ compared to saline-treated controls; +: $p < 0.05$, ++: $p < 0.01$ between genotypes.

Appendix 4: Additional experiments associated with Chapter 5

A4.1. MA-induced [^{3}H]DA release (superfusion) optimization experiments

[3H]DA release: protein

To optimize the release assay, a superfusion experiment was conducted loading various amounts of protein. The experiment was similar to that described in Chapter 5 with the following modifications. Striatal tissue was minced into 300 µm^2 squares and homogenized. Samples containing 50, 100, or 200 µg of protein were pre-loaded with [^{3}H]DA (120 nM) for 30 min at 37 °C and added to the superfusion device. Assay buffer without inhibitors was perfused for 30 min as a washout period to establish stable efflux and then collection began for 36 min (18 fractions, 2 min each). The first 6 min (3 fractions) established baseline, then MA (10 µM) was continuously perfused for 18 min (9 fractions), and finally 8 minutes (4 fractions) of SDS (1%) to lyse the homogenate. Although MA elicited similar % release across the different amounts of protein loaded, CPM values were significantly lower when 100 and 50 µg was loaded, compared to 200 µg (Supp. Fig. 6A). While 200 µg of protein appeared optimal, it was decided to continue testing 100 µg in additional experiments.

[3H]DA release: wash time

To optimize the release assay, the length of washout period was evaluated. The experiment was similar to that described in Chapter 5 with the following modifications. Striatal tissue was minced into 300 µm^2 squares and homogenized. Samples containing 100 or 200 µg of protein were pre-loaded with [^{3}H]DA (120 nM) for 30 min at 37 °C and added to the superfusion device. Assay buffer without inhibitors was perfused for 30 min as a washout period and 10 fractions (3

min each) were collected. As [^{3}H]DA release, both % and CPM (Supp. Fig. 6B) reached a stable state after 15 min, it was decided to decrease the washout period to 15 min.

[3H]DA release: drug perfusion

To optimize the release assay, the method of drug perfusion: continuous or pulsed, was evaluated. The experiment was similar to that described in Chapter 5 with the following modifications. Striatal tissue was minced into 300 µm^2 squares and homogenized. Samples containing 100 or 200 µg of protein were pre-loaded with [^{3}H]DA (120 nM) for 30 min at 37 °C and added to the superfusion device. Assay buffer without inhibitors was perfused for 15 min as a washout period to establish stable efflux and then collection began for 45 min (18 fractions, 2.5 min each). The first 7.5 min (3 fractions) established baseline. For the continuous condition: MA (10 µM) was perfused for 27.5 min (11 fractions), followed by 10 minutes (4 fractions) of SDS (1%) to lyse the homogenate. For the pulsed condition, MA (10 µM) was perfused for 5 min (2 fractions), followed by buffer for 22.5 minutes (9 fractions), and finally 10 minutes (4 fractions) of SDS (1%) to lyse the homogenate. When MA was continuously administered, [^{3}H]DA release did not return to baseline by the end of the collection period, whereas when MA was administered for a pulse of 5 min, release returned to baseline at the end of the hour, allowing for better comparison (Supp. Fig. 6C). The 200 µg of protein continued to produce higher % release and CPMs. It was decided to conduct ongoing experiments using pulsed drug perfusion and loading a total amount of 200 µg of protein.

[3H]DA release: slice thickness

To optimize the release assay, the width of slice thickness was evaluated. The McIlwain tissue chopper allows for variable slice thickness. Once sliced, the plate is rotated 90 degrees to create minced squares instead of slices. The experiment was similar to that described in Chapter 5 with the following modifications. Striatal tissue was minced into either 300 or 100 µm^2 squares and homogenized. Samples containing 100 µg of protein were pre-loaded with [^{3}H]DA (120 nM) for 30 min at 37 °C and added to the superfusion device. Assay buffer without

inhibitors was perfused for 15 min as a washout period to establish stable efflux and then collection began for 45 min (18 fractions, 2.5 min each). The first 7.5 min (3 fractions) established baseline. Mincing the tissue into 100 µm slices increased [^{3}H]DA release (% and CPM) compared to 300 µm slices, most likely due to the increase in surface area (Supp. Fig. 6D). It was decided to conduct ongoing experiments using 100 µm slices.

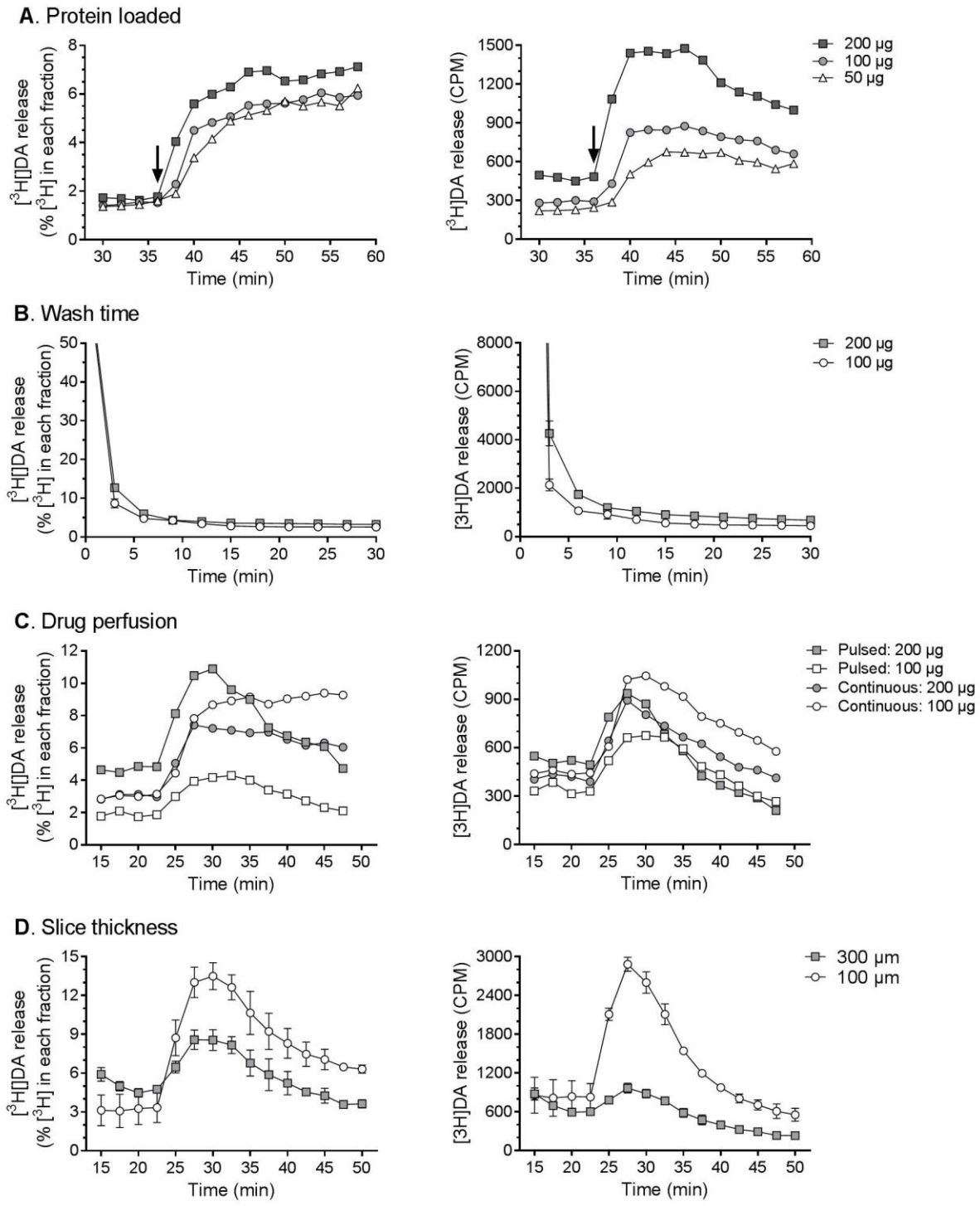

Supplementary Figure 6. [^{3}H]DA release superfusion assay optimization. The amount of protein loaded (**A**), the washout period (**B**), drug perfusion method (**C**), and slice thickness (**D**) were evaluated for optimization. MA (10 µM) was either perfused continuously after baseline,

indicated by arrow, or pulsed for 5 min (2 fractions), indicated by bar. Data shown are from separate, single experiments. Data from each fraction are normalized to the total amount of [^{3}H]DA in remaining fractions or represent the radioactivity counted in each fraction.

A4.2. MA-induced [^{3}H]DA uptake optimization experiments

[^{3}H]DA uptake assay: time course

To optimize the uptake assay, an incubation time course experiment was conducted. The experiment was similar to that described in Chapter 5 with the following modifications. Striatal tissue homogenate (~25 µg protein) was pre-incubated with in assay buffer with inhibitors for 10 min at 37 °C. The uptake assay was initiated with the addition of [^{3}H]DA (10 nM). Specific binding was defined as the difference in binding observed in the presence or absence of mazindol (5 µM) and the final assay volume was 500 µl. Incubation at 37 °C was terminated at various time points (1, 2, 4, 5, 8, 10, 15, and 20 min) using ice-cold saline (0.9% NaCl) and radioactivity was measured as described above. An incubation time of 10 min was selected as this time point resulted in the highest specific uptake while remaining within the linear range of the time course (Supp. Fig. 7A).

[^{3}H]DA uptake assay: protein curve

To optimize the uptake assay, a protein curve experiment was conducted. The experiment was similar to that described in Chapter 5 with the following modifications. Striatal tissue homogenates of various protein concentrations, prepared using 0.05, 0.1, 0.15 and 0.2x dilutions of assay buffer (ml/mg wet weight of tissue), were pre-incubated with either assay buffer (control) or MA (1 µM) for 10 min at 37 °C. The uptake assay was initiated with the addition of [^{3}H]DA (20 nM). Specific binding was defined as the difference in binding observed in the presence or absence of mazindol (5 µM) and the final assay volume was 500 µl. Incubation (10 min, 37 °C) was terminated using ice-cold saline (0.9% NaCl) and radioactivity was measured as described above. The protein curves for both buffer and MA-induced [^{3}H]DA

uptake were linear, although there was indication of saturation at the highest protein concentration (Supp. Fig. 7B and C). The two lower protein concentrations were also dismissed due to the low level of specific uptake in homogenate pre-loaded with MA. As such, the 0.15x dilution (equivalent to ~ 25 µg protein loaded) was selected for ongoing experiments.

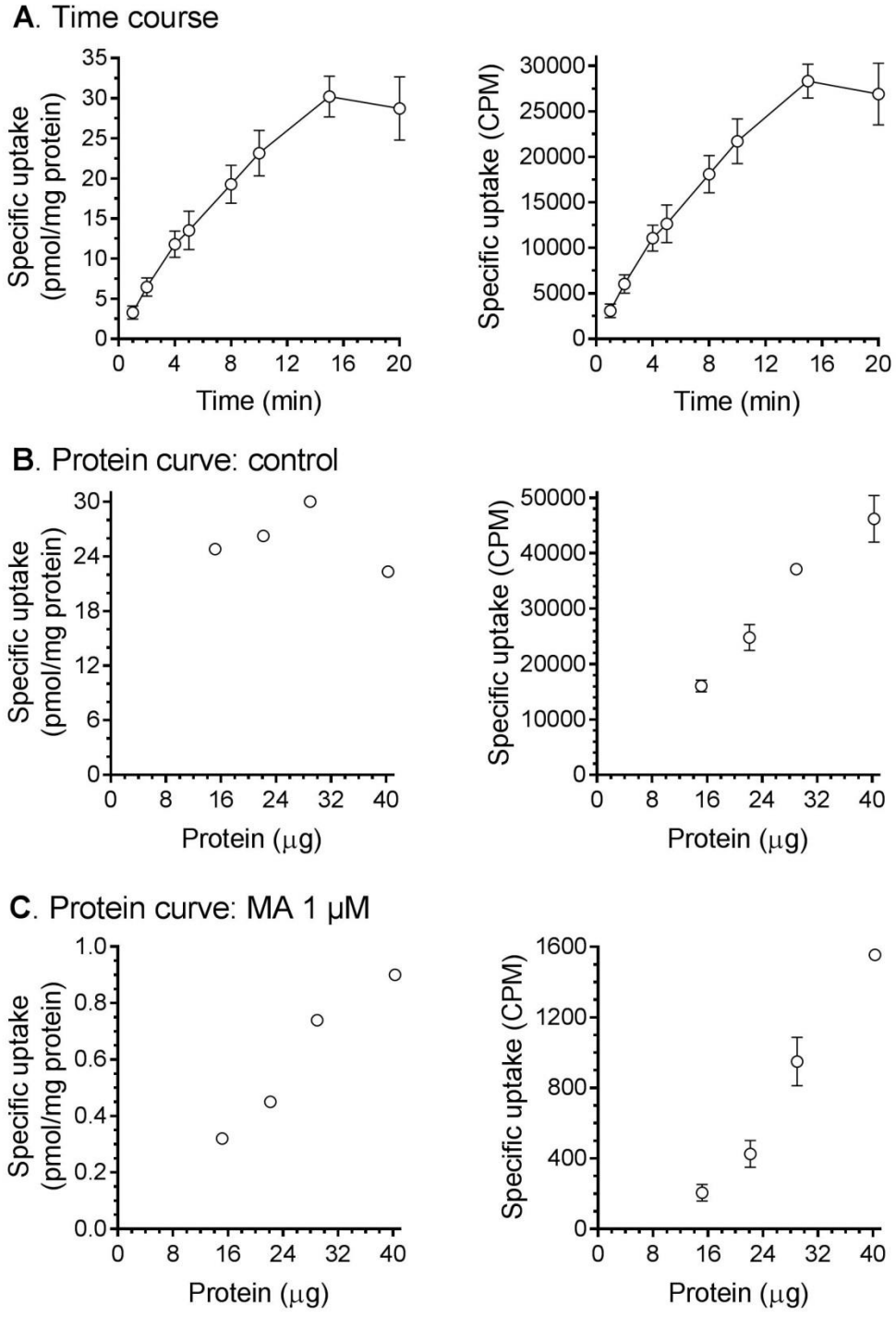

Supplementary Figure 7. [^{3}H]DA uptake assay optimization. An incubation time course (**A**) and protein curve in homogenate pre-loaded with assay buffer (**B**) or MA (1 µM) (**C**) were evaluated. Data shown are the mean ± SEM of 3 independent experiments (**A**) or from a single

experiment in triplicate (**B** and **C**). Data are normalized to the total amount of protein loaded (left) or are the specific radioactivity counts (right).

A4.3. *In vivo* treated [^{3}H]DA uptake pilot

[^{3}H]DA uptake pilot

The number of animals required per [^{3}H]DA uptake experiment is dependent on the amount of protein loaded from the vesicular fraction. To minimize the number of animals used (4-5 mice pooled), only the lowest amount of total protein cited in previous research (2.5 µg) was tested in the pilot (Hogan et al., 2000; Hansen et al., 2002). The experiment was similar to that described in Chapter 5. [^{3}H]DA uptake was performed using pooled striatal tissue from 4-5 mice. Uptake was measured in each fraction preparation separately: P2 - synaptosomal (~5 µg protein), P3 - membrane-associated (~5 µg protein), and P4 - vesicular (~2.5 µg protein). The assay initiated with the addition of [^{3}H]DA (30 nM). Specific uptake was defined as the difference in uptake observed in the presence or absence of reserpine (1 µM). The final assay volume was 250 µl. Incubation (6 min, 30 °C) was terminated using ice-cold saline (0.9% NaCl) and radioactivity was measured as described above. The results demonstrate the amount of 2.5 µg of protein from the vesicular fraction (P2) is sufficient for the assay, as is 5 µg in the synaptosomal and membrane-associated fractions (P2 and P3) (Supp. Fig. 8).

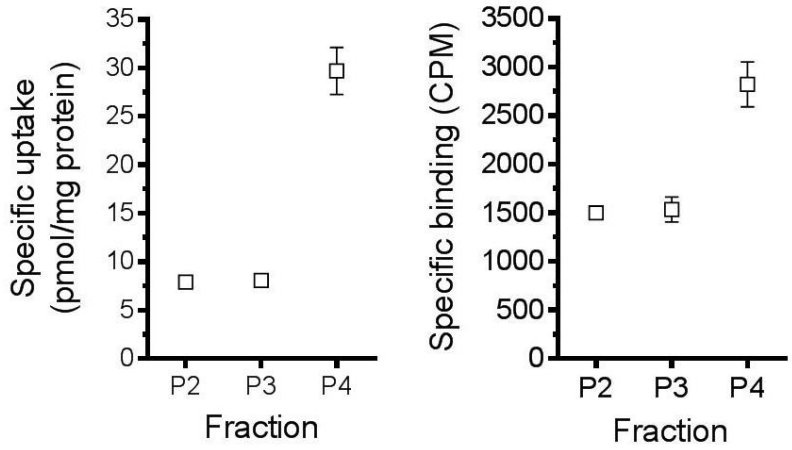

Supplementary Figure 8. [^{3}H]DA uptake assay pilot. Uptake was measured in each fraction preparation separately: P2 - synaptosomal (~5 µg protein), P3 - membrane-associated (~5 µg protein), and P4 - vesicular (~2.5 µg protein). Data shown are the mean ± SEM of 3-4 pooled samples. Data are normalized to the total amount of protein loaded (left) or are the specific radioactivity counts (right).

A4.4. *In vivo* treated [^{3}H]DHTB saturation binding optimization

[^{3}H]DHTB binding: protein

The number of animals required per [^{3}H]DHTB binding experiment is again dependent on the amount of protein loaded from the vesicular fraction. Previous studies typically use 2.5 – 5 µg of protein in the vesicular fraction for [^{3}H]DHTB binding (Teng et al., 1998; Brown et al., 2000; Staal et al., 2000). As such, 2.5 and 5 µg of protein in the vesicular fraction (P4) was tested along with 5 µg in the synaptosomal (P2) and 5 and 10 µg of protein in the membrane-associated fraction (P3). The experiment was similar to that described in Chapter 5, except it was carried out at a single concentration of [^{3}H]DHTB (2 nM), similar to the previously reported K_D value (Scherman, 1986; Hogan et al., 2000). [^{3}H]DHTB binding was performed using pooled striatal tissue from 4-5 untreated mice. Binding was measured in each subcellular fraction separately and the assay was initiated with the addition of [^{3}H]DHTB (2 nM). Specific binding

was defined as the difference in binding observed in the presence or absence of [^{3}H]DHTB (20 µM). The final assay volume was 1 mL. Incubation (60 min, 25 °C) was terminated using ice-cold Tris buffer (50 mM) and radioactivity was measured as described above. Based on the radioactivity counts, it was decided 2.5 µg of protein in the vesicular fraction did not provide adequate specific binding (111 ± 13 CPM) or 5 µg of protein in the synaptosomal fraction (126 ± 11 CPM) as this was nearing a lack of binding (Supp. Fig. 9).

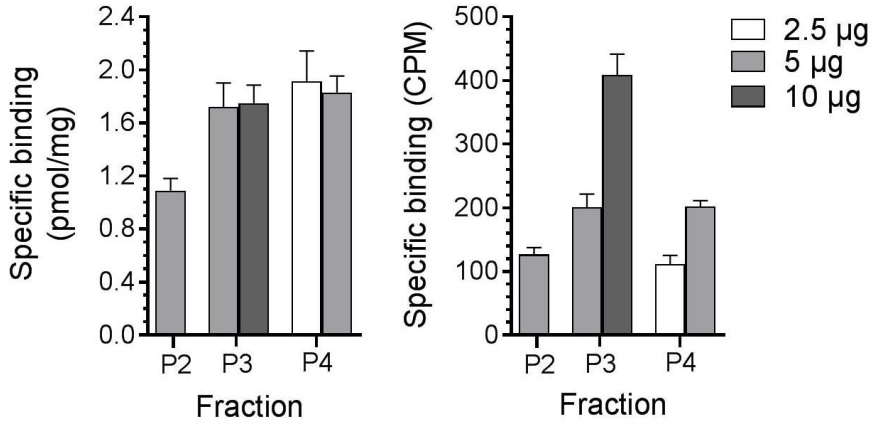

Supplementary Figure 9. [^{3}H]DHTB binding protein assay. Binding was measured in each fraction preparation separately: P2 - synaptosomal (5 µg protein), P3 - membrane-associated (5 or 10 µg protein), and P4 - vesicular (2.5 or 5 µg protein). Data shown are the mean ± SEM of 5-8 pooled samples. Data are normalized to the total amount of protein loaded (left) or are the specific binding radioactivity counts (right).

[^{3}H]DHTB binding pilot: treated tissue

In a follow-up experiment, [^{3}H]DHTB binding was evaluated using tissue from *Taar1*-WT and –KO mice receiving a binge-like regimen (4 inj, 2 h apart) of saline or MA (5 or 10 mg/kg) and euthanized 24 h later (Supp. Fig. 10). The total amount of protein loaded from the synaptosomal and membrane-associated fractions ranged from 8–10 µg and the vesicular fraction ranged from 4–5 µg. [^{3}H]DHTB binding was performed using pooled striatal tissue from 5 mice of each

group. Binding was measured in each subcellular fraction separately and the assay was initiated with the addition of [^{3}H]DHTB (2 nM). Specific binding was defined as the difference in binding observed in the presence or absence of [^{3}H]DHTB (20 µM). The final assay volume was 1 mL. Incubation (60 min, 25 °C) was terminated using ice-cold Tris buffer (50 mM) and radioactivity was measured as described above. While the pilot yielded promising results: specific binding was decreased in the vesicular fraction in *Taar1*-KO mice receiving MA 5 mg/kg compared to *Taar1*-WT mice (Supp. Fig. 10C), the low radioactivity counts in the MA treated groups were problematic (Supp. Fig. 10G). In the vesicular, 3 or the 4 groups receiving MA had specific binding radioactivity counts below 100: *Taar1*-KO mice receiving MA 5 mg/kg (70 ± 17 CPM), and both genotypes receiving MA 10 mg/kg: *Taar1*-WT (59 ± 2 CPM) and *Taar1*-KO (45 ± 4 CPM). These counts, at the estimated K_D of [^{3}H]DHTB (2 nM) were deemed too low to investigate differences in genotypes following MA treatment. It was decided to increase the amount of protein loaded from the vesicular fraction to 10 µg.

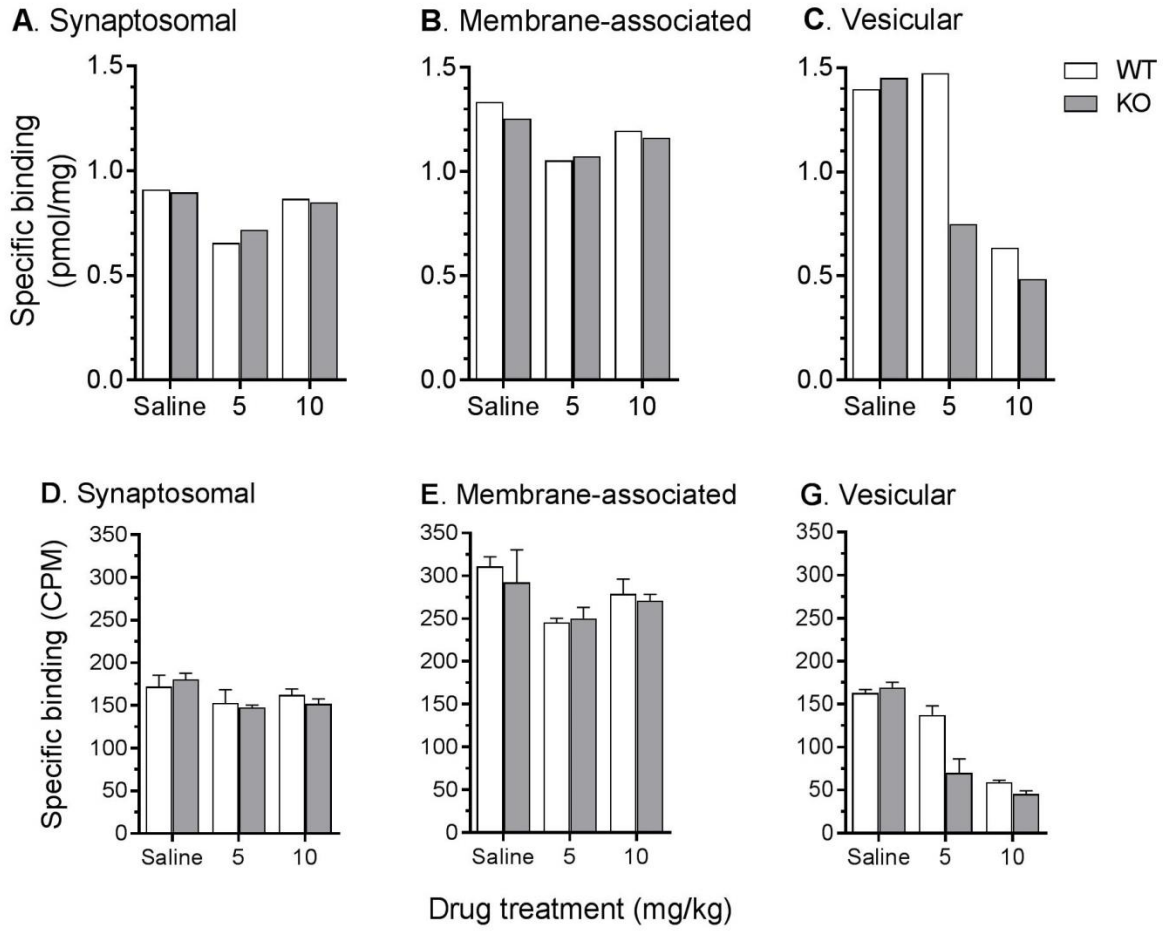

Supplementary Figure 10. [^{3}H]DHTB binding pilot in treated tissue. Binding was measured in each fraction preparation separately: synaptosomal (8-10 µg protein) (**A** and **D**), membrane-associated (8-10 µg protein) (**B** and **E**), and vesicular (4-5 µg protein) (**C** and **F**). Data shown are from a single experiment in triplicate. Data are normalized to the total amount of protein loaded (**A**, **B**, **C**) or are the specific radioactivity counts (**D**, **E**, **F**).

[^{3}H]DHTB saturation binding pilot

Due to the surfeit of membrane-associated fraction, a [^{3}H]DHTB saturation binding pilot was conducted in the remaining membrane-associated fraction from the treated *Taar1*-WT and –KO mice used in the [^{3}H]DHTB binding pilot. The experiment was similar to that described in Chapter 5. Binding was measured in the membrane-associated fraction only, using 4-6 µg of

protein. The assay was initiated with the addition of [^{3}H]DHTB (0.5 - 22 nM). Specific binding was defined as the difference in binding observed in the presence or absence of [^{3}H]DHTB (20 µM). The final assay volume was 1 ml. Incubation (60 min, 25 °C) was terminated using ice-cold Tris buffer (50 mM) and radioactivity was measured as described above. There was no difference between genotypes or treatment groups in B_{max} or K_D values (Supp. Table 1), similar to previous research in the membrane fraction (Riddle et al., 2002). B_{max} and K_D values were within range of previously established values (Scherman, 1986; Staal et al., 2000). This experiment validated the [^{3}H]DHTB saturation binding protocol and the described parameters were used in future experiments.

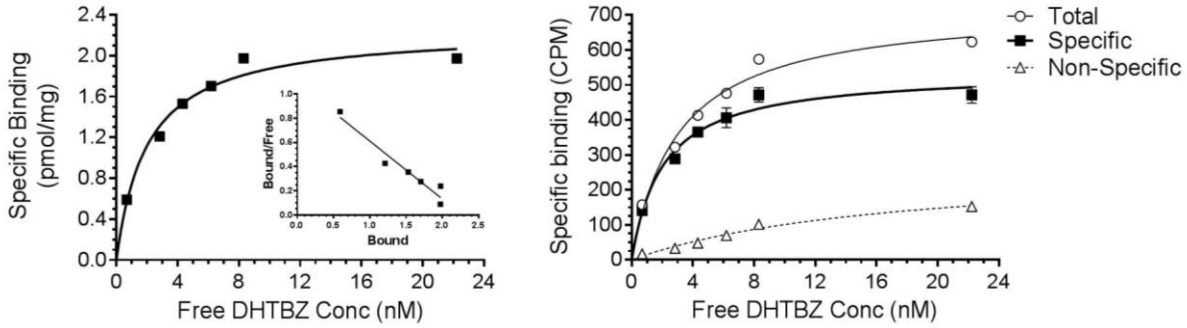

Supplementary Figure 11. [^{3}H]DHTB saturation binding pilot. *Taar1*-WT and -KO mice received 4 i.p. injections of saline or MA (5 or 10 mg/kg), 2 h apart, and were euthanized 24 h following the final injection. Striatal tissue from 4-5 mice was pooled and the membrane-associated fraction analyzed. Experiments were conducted as described in the text. Shown is a representative saturation curve normalized to protein in each sample (left) and saturation curve of the radioactivity counts. Inset: Scatchard transformation of [^{3}H]DHTB binding data.

Supplementary Table 1. [^{3}H]DHTB binding in membrane-associated fraction

Treatment (mg/kg)	Genotype	B_{max} (pmol/mg protein) ± SEM	K_D (nM) ± SEM
Saline	*Taar1*-WT	1.8 ± 0.2	6.3 ± 1.0
	Taar1-KO	2.1 ± 0.3	6.6 ± 0.3
MA (5)	*Taar1*-WT	2.0 ± 0.3	4.1 ± 0.1
	Taar1-KO	2.1 ± 0.4	6.3 ± 0.5
MA (10)	*Taar1*-WT	2.2 ± 0.3	7.0 ± 0.9
	Taar1-KO	2.1 ± 0.6	6.7 ± 0.8

Data represent mean ± SEM for each treatment group from six independent experiments, using pooled tissue from 4-6 mice per group.

[^{125}I]RTI-55 saturation binding pilot

The experiment was similar to that described in Chapter 5. [^{125}I]RTI-55 binding was performed using striatal tissue from 4 untreated mice. Binding was measured in synaptosomes only (~20 µg protein) with one mouse per assay. Assay buffer (Krebs-HEPES buffer) was supplemented with fluoxetine (50 nM) and the assay initiated with the addition of [^{125}I]RTI-55. The specific activity of [^{125}I]RTI-55 was diluted with unlabeled [^{125}I]RTI-55 ranging in concentrations from 0.036 to 16.6 nM and specific binding was defined as the difference in binding observed in the presence or absence of mazindol (5 µM). The final assay volume was 250 µl. Incubation (90 min, 25 °C) was terminated using ice-cold saline (0.9% NaCl) and radioactivity was measured as described above, with the exception that filters were not soaked in PEI. The B_{max} (4.67 ± 0.17 pmol/mg protein) and K_D values (3.32 ± 0.41 nM) were similar to previously reported values (Eshleman et al., 2001). This experiment validated the [^{125}I]RTI-55 saturation binding protocol and the described parameters were used in future experiments.

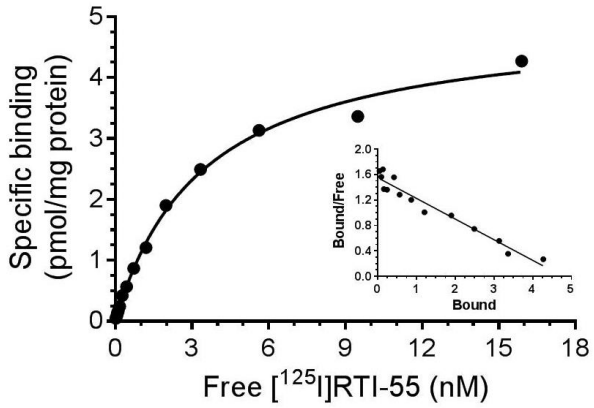

Supplementary Figure 12. [^{125}I]RTI-55 saturation binding pilot. Experiment was conducted as described in text. Shown is a representative saturation curve. Inset: Scatchard transformation of [^{125}I]RTI-55 binding data.

References

Aarde, S. M., Huang, P. K., Creehan, K. M., Dickerson, T. J., Taffe, M. A., 2013. The novel recreational drug 3,4-methylenedioxypyrovalerone (MDPV) is a potent psychomotor stimulant: self-administration and locomotor activity in rats. Neuropharmacology 71, 130-140.

Achat-Mendes, C., Lynch, L. J., Sullivan, K. A., Vallender, E. J., Miller, G. M., 2012. Augmentation of methamphetamine-induced behaviors in transgenic mice lacking the trace amine-associated receptor 1. Pharmacol. Biochem. Behav 101, 201-207.

Albers, D. S., Sonsalla, P. K., 1995. Methamphetamine-induced hyperthermia and dopaminergic neurotoxicity in mice: pharmacological profile of protective and nonprotective agents. J. Pharmacol. Exp. Ther 275, 1104-1114.

Ali, S. F., Newport, G. D., Slikker, W., Jr., 1996. Methamphetamine-induced dopaminergic toxicity in mice. Role of environmental temperature and pharmacological agents. Ann. N. Y. Acad. Sci 801, 187-198.

Alvarsson, A., Zhang, X., Stan, T. L., Schintu, N., Kadkhodaei, B., Millan, M. J., Perlmann, T., Svenningsson, P., 2015. Modulation by Trace Amine-Associated Receptor 1 of Experimental Parkinsonism, l-DOPA Responsivity, and Glutamatergic Neurotransmission. J. Neurosci 35, 14057-14069.

Alves, E., Summavielle, T., Alves, C. J., Gomes-da-Silva, J., Barata, J. C., Fernandes, E., Bastos Mde, L., Tavares, M. A., Carvalho, F., 2007. Monoamine oxidase-B mediates ecstasy-induced neurotoxic effects to adolescent rat brain mitochondria. J Neurosci 27, 10203-10210.

Anderson, C. M., Swanson, R. A., 2000. Astrocyte glutamate transport: review of properties, regulation, and physiological functions. Glia 32, 1-14.

Anderson, K. L., Itzhak, Y., 2006. Methamphetamine-induced selective dopaminergic neurotoxicity is accompanied by an increase in striatal nitrate in the mouse. Ann N Y Acad Sci 1074, 225-233.

Angoa-Perez, M., Kane, M. J., Briggs, D. I., Francescutti, D. M., Sykes, C. E., Shah, M. M., Thomas, D. M., Kuhn, D. M., 2013a. Mephedrone does not damage dopamine nerve endings of the striatum, but enhances the neurotoxicity of methamphetamine, amphetamine, and MDMA. J Neurochem 125, 102-110.

Angoa-Perez, M., Kane, M. J., Herrera-Mundo, N., Francescutti, D. M., Kuhn, D. M., 2013b. Effects of combined treatment with mephedrone and methamphetamine or 3,4-methylenedioxymethamphetamine on serotonin nerve endings of the hippocampus. Life Sci.

Anneken, J. H., Angoa-Perez, M., Kuhn, D. M., 2015. 3,4-Methylenedioxypyrovalerone (MDPV) prevents while methylone enhances methamphetamine-induced damage to dopamine nerve endings: beta-ketoamphetamine modulation of neurotoxicity by the dopamine transporter. J. Neurochem.

Anneken, J. H., Angoa-Perez, M., Sati, G. C., Crich, D., Kuhn, D. M., 2018. Assessing the role of dopamine in the differential neurotoxicity patterns of methamphetamine, mephedrone, methcathinone and 4-methylmethamphetamine. Neuropharmacology 134, 46-56.

Ares-Santos, S., Granado, N., Espadas, I., Martinez-Murillo, R., Moratalla, R., 2014. Methamphetamine causes degeneration of dopamine cell bodies and terminals of the nigrostriatal pathway evidenced by silver staining. Neuropsychopharmacology 39, 1066-1080.

Babusyte, A., Kotthoff, M., Fiedler, J., Krautwurst, D., 2013. Biogenic amines activate blood leukocytes via trace amine-associated receptors TAAR1 and TAAR2. J. Leukoc. Biol 93, 387-394.

Barbosa, D. J., Serrat, R., Mirra, S., Quevedo, M., de Barreda, E. G., Avila, J., Ferreira, L. M., Branco, P. S., Fernandes, E., Lourdes, B. M., Capela, J. P., Soriano, E., Carvalho, F., 2014. The mixture of "ecstasy" and its metabolites impairs mitochondrial fusion/fission equilibrium and trafficking in hippocampal neurons, at in vivo relevant concentrations. Toxicol Sci 139, 407-420.

Bardo, M. T., Bevins, R. A., 2000. Conditioned place preference: what does it add to our preclinical understanding of drug reward? Psychopharmacology (Berl) 153, 31-43.

Battaglia, G., Yeh, S. Y., O'Hearn, E., Molliver, M. E., Kuhar, M. J., De Souza, E. B., 1987. 3,4-Methylenedioxymethamphetamine and 3,4-methylenedioxyamphetamine destroy serotonin terminals in rat brain: quantification of neurodegeneration by measurement of [3H]paroxetine-labeled serotonin uptake sites. J Pharmacol Exp Ther 242, 911-916.

Baumann, M. H., Ayestas, M. A., Jr., Partilla, J. S., Sink, J. R., Shulgin, A. T., Daley, P. F., Brandt, S. D., Rothman, R. B., Ruoho, A. E., Cozzi, N. V., 2012. The designer methcathinone analogs, mephedrone and methylone, are substrates for monoamine transporters in brain tissue. Neuropsychopharmacology 37, 1192-1203.

Baumann, M. H., Partilla, J. S., Lehner, K. R., 2013. Psychoactive "bath salts": not so soothing. Eur. J Pharmacol 698, 1-5.

Baumann, M. H., Wang, X., Rothman, R. B., 2007. 3,4-Methylenedioxymethamphetamine (MDMA) neurotoxicity in rats: a reappraisal of past and present findings. Psychopharmacology (Berl) 189, 407-424.

Beardsley, P. M., Hauser, K. F., 2014. Glial modulators as potential treatments of psychostimulant abuse. Advances in Pharmacology, pp. 1-69.

Beaulieu, J. M., Del'guidice, T., Sotnikova, T. D., Lemasson, M., Gainetdinov, R. R., 2011. Beyond cAMP: The Regulation of Akt and GSK3 by Dopamine Receptors. Front Mol. Neurosci 4, 38.

Belknap, J. K., McWeeney, S., Reed, C., Burkhart-Kasch, S., McKinnon, C. S., Li, N., Baba, H., Scibelli, A. C., Hitzemann, R., Phillips, T. J., 2013. Genetic factors involved in risk for methamphetamine intake and sensitization. Mamm. Genome 24, 446-458.

Benavides, J., Dubois, A., Scatton, B., 2001. Peripheral type benzodiazepine binding sites as a tool for the detection and quantification of CNS injury. Curr Protoc. Neurosci Chapter 7, Unit7.

Bergquist, J., Sciubisz, A., Kaczor, A., Silberring, J., 2002. Catecholamines and methods for their identification and quantitation in biological tissues and fluids. J Neurosci Methods 113, 1-13.

Bernheim, A., See, R. E., Reichel, C. M., 2016. Chronic methamphetamine self-administration disrupts cortical control of cognition. Neuroscience & Biobehavioral Reviews 69, 36-48.

Berry, M. D., 2004. Mammalian central nervous system trace amines. Pharmacologic amphetamines, physiologic neuromodulators. J. Neurochem 90, 257-271.

Berry, M. D., Gainetdinov, R. R., Hoener, M. C., Shahid, M., 2017. Pharmacology of human trace amine-associated receptors: Therapeutic opportunities and challenges. Pharmacol Ther 180, 161-180.

Block, M. L., Zecca, L., Hong, J. S., 2007. Microglia-mediated neurotoxicity: uncovering the molecular mechanisms. Nat Rev Neurosci 8, 57-69.

Borowsky, B., Adham, N., Jones, K. A., Raddatz, R., Artymyshyn, R., Ogozalek, K. L., Durkin, M. M., Lakhlani, P. P., Bonini, J. A., Pathirana, S., Boyle, N., Pu, X., Kouranova, E., Lichtblau, H., Ochoa, F. Y., Branchek, T. A., Gerald, C., 2001. Trace amines: identification of a family of mammalian G protein-coupled receptors. Proc. Natl. Acad. Sci. U. S. A 98, 8966-8971.

Boudanova, E., Navaroli, D. M., Melikian, H. E., 2008. Amphetamine-induced decreases in dopamine transporter surface expression are protein kinase C-independent. Neuropharmacology 54, 605-612.

Bourque, M., Dluzen, D. E., Di Paolo, T., 2012. Sex and temporally-dependent effects of methamphetamine toxicity on dopamine markers and signaling pathways. Neuropharmacology 62, 2363-2372.

Bove, J., Perier, C., 2012. Neurotoxin-based models of Parkinson's disease. Neuroscience 211, 51-76.

Bowyer, J. F., Hanig, J. P., 2014. Amphetamine- and methamphetamine-induced hyperthermia: Implications of the effects produced in brain vasculature and peripheral organs to forebrain neurotoxicity. Temperature. (Austin.) 1, 172-182.

Bowyer, J. F., Holson, R. R., Miller, D. B., O'Callaghan, J. P., 2001. Phenobarbital and dizocilpine can block methamphetamine-induced neurotoxicity in mice by mechanisms that are independent of thermoregulation. Brain Res 919, 179-183.

Bowyer, J. F., Robinson, B., Ali, S., Schmued, L. C., 2008. Neurotoxic-related changes in tyrosine hydroxylase, microglia, myelin, and the blood-brain barrier in the caudate-putamen from acute methamphetamine exposure. Synapse 62, 193-204.

Bradaia, A., Trube, G., Stalder, H., Norcross, R. D., Ozmen, L., Wettstein, J. G., Pinard, A., Buchy, D., Gassmann, M., Hoener, M. C., Bettler, B., 2009. The selective antagonist EPPTB reveals TAAR1-mediated regulatory mechanisms in dopaminergic neurons of the mesolimbic system. Proc. Natl. Acad. Sci. U. S. A 106, 20081-20086.

Broening, H. W., Morford, L. L., Vorhees, C. V., 2005. Interactions of dopamine D1 and D2 receptor antagonists with D-methamphetamine-induced hyperthermia and striatal dopamine and serotonin reductions. Synapse 56, 84-93.

Brown, J. M., Hanson, G. R., Fleckenstein, A. E., 2000. Methamphetamine rapidly decreases vesicular dopamine uptake. J. Neurochem 74, 2221-2223.

Bunzow, J. R., Sonders, M. S., Arttamangkul, S., Harrison, L. M., Zhang, G., Quigley, D. I., Darland, T., Suchland, K. L., Pasumamula, S., Kennedy, J. L., Olson, S. B., Magenis, R. E., Amara, S. G., Grandy, D. K., 2001. Amphetamine, 3,4-methylenedioxymethamphetamine, lysergic acid diethylamide, and metabolites of the catecholamine neurotransmitters are agonists of a rat trace amine receptor. Mol. Pharmacol 60, 1181-1188.

Burrows, K. B., Meshul, C. K., 1997. Methamphetamine alters presynaptic glutamate immunoreactivity in the caudate nucleus and motor cortex. Synapse 27, 133-144.

Cadet, J. L., Brannock, C., 1998. Free radicals and the pathobiology of brain dopamine systems. Neurochem. Int 32, 117-131.

Cadet, J. L., Krasnova, I. N., Jayanthi, S., Lyles, J., 2007. Neurotoxicity of substituted amphetamines: molecular and cellular mechanisms. Neurotox. Res 11, 183-202.

Cadet, J. L., Ladenheim, B., Hirata, H., Rothman, R. B., Ali, S., Carlson, E., Epstein, C., Moran, T. H., 1995. Superoxide radicals mediate the biochemical effects of methylenedioxymethamphetamine (MDMA): evidence from using CuZn-superoxide dismutase transgenic mice. Synapse 21, 169-176.

Camarero, J., Sanchez, V., O'Shea, E., Green, A. R., Colado, M. I., 2002. Studies, using in vivo microdialysis, on the effect of the dopamine uptake inhibitor GBR 12909 on 3,4-methylenedioxymethamphetamine ('ecstasy')-induced dopamine release and free radical formation in the mouse striatum. J. Neurochem 81, 961-972.

Capela, J. P., Carmo, H., Remiao, F., Bastos, M. L., Meisel, A., Carvalho, F., 2009. Molecular and cellular mechanisms of ecstasy-induced neurotoxicity: an overview. Mol Neurobiol 39, 210-271.

Capela, J. P., Ruscher, K., Lautenschlager, M., Freyer, D., Dirnagl, U., Gaio, A. R., Bastos, M. L., Meisel, A., Carvalho, F., 2006. Ecstasy-induced cell death in cortical neuronal cultures is serotonin 2A-receptor-dependent and potentiated under hyperthermia. Neuroscience 139, 1069-1081.

Carvalho, M., Carvalho, F., Remiao, F., de Lourdes, P. M., Pires-das-Neves, R., de Lourdes, B. M., 2002. Effect of 3,4-methylenedioxymethamphetamine ("ecstasy") on body temperature and liver antioxidant status in mice: influence of ambient temperature. Arch Toxicol 76, 166-172.

Caudevilla-Galligo, F., Ventura, M., Indave Ruiz, B. I., Fornis, I., 2013. Presence and composition of cathinone derivatives in drug samples taken from a drug test service in Spain (2010-2012). Hum Psychopharmacol 28, 341-344.

Cervinski, M. A., Foster, J. D., Vaughan, R. A., 2005. Psychoactive substrates stimulate dopamine transporter phosphorylation and down-regulation by cocaine-sensitive and protein kinase C-dependent mechanisms. J. Biol. Chem 280, 40442-40449.

Chiellini, G., Erba, P., Carnicelli, V., Manfredi, C., Frascarelli, S., Ghelardoni, S., Mariani, G., Zucchi, R., 2012. Distribution of exogenous [125I]-3-iodothyronamine in mouse in vivo: relationship with trace amine-associated receptors. J. Endocrinol 213, 223-230.

Chipana, C., Camarasa, J., Pubill, D., Escubedo, E., 2006. Protection against MDMA-induced dopaminergic neurotoxicity in mice by methyllycaconitine: involvement of nicotinic receptors. Neuropharmacology 51, 885-895.

Chu, P.-W., Seferian, K. S., Birdsall, E., Truong, J. G., Riordan, J. A., Metcalf, C. S., Hanson, G. R., Fleckenstein, A. E., 2008. Differential regional effects of methamphetamine on dopamine transport. Eur J Pharmacol 590, 105-110.

Chu, P. W., Hadlock, G. C., Vieira-Brock, P., Stout, K., Hanson, G. R., Fleckenstein, A. E., 2010. Methamphetamine alters vesicular monoamine transporter-2 function and potassium-stimulated dopamine release. J Neurochem 115, 325-332.

Cisneros, I. E., Ghorpade, A., 2014. Methamphetamine and HIV-1-induced neurotoxicity: role of trace amine associated receptor 1 cAMP signaling in astrocytes. Neuropharmacology 85, 499-507.

Colado, M. I., Camarero, J., Mechan, A. O., Sanchez, V., Esteban, B., Elliott, J. M., Green, A. R., 2001. A study of the mechanisms involved in the neurotoxic action of 3,4-methylenedioxymethamphetamine (MDMA, 'ecstasy') on dopamine neurones in mouse brain. Br. J Pharmacol 134, 1711-1723.

Colado, M. I., Green, A. R., 1994. A study of the mechanism of MDMA ('ecstasy')-induced neurotoxicity of 5-HT neurones using chlormethiazole, dizocilpine and other protective compounds. Br. J. Pharmacol 111, 131-136.

Colado, M. I., Green, A. R., 1995. The spin trap reagent alpha-phenyl-N-tert-butyl nitrone prevents 'ecstasy'-induced neurodegeneration of 5-hydroxytryptamine neurones. Eur J Pharmacol 280, 343-346.

Colado, M. I., O'Shea, E., Green, A. R., 2004. Acute and long-term effects of MDMA on cerebral dopamine biochemistry and function. Psychopharmacology (Berl) 173, 249-263.

Cotter, R., Pei, Y., Mus, L., Harmeier, A., Gainetdinov, R. R., Hoener, M. C., Canales, J. J., 2015. The trace amine-associated receptor 1 modulates methamphetamine's neurochemical and behavioral effects. Front Neurosci 9, 39.

Cozzi, N. V., Sievert, M. K., Shulgin, A. T., Jacob, P., III, Ruoho, A. E., 1999. Inhibition of plasma membrane monoamine transporters by beta-ketoamphetamines. Eur. J Pharmacol 381, 63-69.

Cruickshank, C. C., Dyer, K. R., 2009. A review of the clinical pharmacology of methamphetamine. Addiction 104, 1085-1099.

Cubells, J. F., Rayport, S., Rajendran, G., Sulzer, D., 1994. Methamphetamine neurotoxicity involves vacuolation of endocytic organelles and dopamine-dependent intracellular oxidative stress. J. Neurosci 14, 2260-2271.

Cunningham, C. L., Gremel, C. M., Groblewski, P. A., 2006. Drug-induced conditioned place preference and aversion in mice. Nat. Protoc 1, 1662-1670.

Cunningham, C. L., Noble, D., 1992. Methamphetamine-induced conditioned place preference or aversion depending on dose and presence of drug. Ann N Y Acad Sci 654, 431-433.

Dal Cason, T. A., Young, R., Glennon, R. A., 1997. Cathinone: an investigation of several N-alkyl and methylenedioxy-substituted analogs. Pharmacol Biochem Behav 58, 1109-1116.

Dambinova, S. A., Maroon, J. C., Sufrinko, A. M., Mullins, J. D., Alexandrova, E. V., Potapov, A. A., 2016. Functional, Structural, and Neurotoxicity Biomarkers in Integrative Assessment of Concussions. Frontiers in Neurology 7.

Darke, S., Duflou, J., Lappin, J., Kaye, S., 2017. Clinical and Autopsy Characteristics of Fatal Methamphetamine Toxicity in Australia. J Forensic Sci.

Darke, S., Kaye, S., McKetin, R., Duflou, J., 2008. Major physical and psychological harms of methamphetamine use. Drug Alcohol Rev 27, 253-262.

Dave, S., Chen, L., Yu, C., Seaton, M., Khodr, C. E., Al-Harthi, L., Hu, X.-T., 2018. Methamphetamine decreases K+ channel function in human fetal astrocytes by activating the trace amine-associated receptor type-1. Journal of Neurochemistry 0.

Davis, C. M., Riley, A. L., 2010. Conditioned taste aversion learning: implications for animal models of drug abuse. Ann N Y Acad Sci 1187, 247-275.

DAWN, 2013. Drug Abuse Warning Network, 2011: National Estimates of Drug-Related Emergency Department Visits. Substance abuse and mental health services addministration., http://www. samhsa. gov/data/2k13/DAWN2k11ED/DAWN2k11ED. htm.

de la Torre, R., Farre, M., 2004. Neurotoxicity of MDMA (ecstasy): the limitations of scaling from animals to humans. Trends Pharmacol Sci 25, 505-508.

de la Torre, R., Farre, M., Ortuno, J., Mas, M., Brenneisen, R., Roset, P. N., Segura, J., Cami, J., 2000. Non-linear pharmacokinetics of MDMA ('ecstasy') in humans. Br. J Clin. Pharmacol 49, 104-109.

De Robertis, E., Rodrigues De Lores, G., Peligrino De Iraldi, A. L., 1962. Isolation of synaptic vesicles from nerve endings of the rat brain. Nature 194, 794-795.

DEA, 2013. Drug Enforcement Administration, Federal Register Notice, Rules - 2013, Establishment of Drug Codes for 26 Substances., http://www. deadiversion. usdoj. gov/fed_regs/rules/2013/fr0104. htm.

den Hollander, B., Rozov, S., Linden, A. M., Uusi-Oukari, M., Ojanpera, I., Korpi, E. R., 2013. Long-term cognitive and neurochemical effects of "bath salt" designer drugs methylone and mephedrone. Pharmacol. Biochem. Behav 103, 501-509.

Deng, X., Ladenheim, B., Tsao, L. I., Cadet, J. L., 1999. Null mutation of c-fos causes exacerbation of methamphetamine-induced neurotoxicity. J Neurosci 19, 10107-10115.

Di Cara, B., Maggio, R., Aloisi, G., Rivet, J. M., Lundius, E. G., Yoshitake, T., Svenningsson, P., Brocco, M., Gobert, A., De, G. L., Cistarelli, L., Veiga, S., De, M. C., Rodriguez, M., Galizzi, J. P., Lockhart, B. P., Coge, F., Boutin, J. A., Vayer, P., Verdouw, P. M., Groenink, L., Millan, M. J., 2011. Genetic deletion of trace amine 1 receptors reveals their role in auto-inhibiting the actions of ecstasy (MDMA). J. Neurosci 31, 16928-16940.

Docherty, J. R., Green, A. R., 2010. The role of monoamines in the changes in body temperature induced by 3,4-methylenedioxymethamphetamine (MDMA, ecstasy) and its derivatives. Br. J. Pharmacol 160, 1029-1044.

Dolan, S. B., Chen, Z., Huang, R., Gatch, M. B., 2018. "Ecstasy" to addiction: Mechanisms and reinforcing effects of three synthetic cathinone analogs of MDMA. Neuropharmacology 133, 171-180.

Easton, N., Marsden, C. A., 2006. Ecstasy: are animal data consistent between species and can they translate to humans? J. Psychopharmacol 20, 194-210.

Eiden, L. E., Weihe, E., 2011. VMAT2: a dynamic regulator of brain monoaminergic neuronal function interacting with drugs of abuse. Ann. N. Y. Acad. Sci 1216, 86-98.

Erowid, 2018. Psychoactive chemicals. https://www.erowid.org/chemicals/.

Escobedo, I., O'Shea, E., Orio, L., Sanchez, V., Segura, M., de la Torre, R., Farre, M., Green, A. R., Colado, M. I., 2005. A comparative study on the acute and long-term effects of MDMA and 3,4-dihydroxymethamphetamine (HHMA) on brain monoamine levels after i.p. or striatal administration in mice. Br. J. Pharmacol 144, 231-241.

Escubedo, E., Guitart, L., Sureda, F. X., Jimenez, A., Pubill, D., Pallas, M., Camins, A., Camarasa, J., 1998. Microgliosis and down-regulation of adenosine transporter induced by methamphetamine in rats. Brain Res 814, 120-126.

Eshleman, A. J., Carmolli, M., Cumbay, M., Martens, C. R., Neve, K. A., Janowsky, A., 1999. Characteristics of drug interactions with recombinant biogenic amine transporters expressed in the same cell type. J Pharmacol Exp Ther 289, 877-885.

Eshleman, A. J., Wolfrum, K., Mash, D. C., Christensen, K., Janowsky, A., 2001. Drug interactions with the dopamine transporter in cryopreserved human caudate. J. Pharmacol. Exp. Ther 296, 442-449.

Eshleman, A. J., Wolfrum, K. M., Hatfield, M. G., Johnson, R. A., Murphy, K. V., Janowsky, A., 2013. Substituted methcathinones differ in transporter and receptor interactions. Biochem Pharmacol 85, 1803-1815.

Espinoza, S., Ghisi, V., Emanuele, M., Leo, D., Sukhanov, I., Sotnikova, T. D., Chieregatti, E., Gainetdinov, R. R., 2015a. Postsynaptic D2 dopamine receptor supersensitivity in the striatum of mice lacking TAAR1. Neuropharmacology 93, 308-313.

Espinoza, S., Lignani, G., Caffino, L., Maggi, S., Sukhanov, I., Leo, D., Mus, L., Emanuele, M., Ronzitti, G., Harmeier, A., Medrihan, L., Sotnikova, T. D., Chieregatti, E., Hoener, M. C., Benfenati, F., Tucci, V., Fumagalli, F., Gainetdinov, R. R., 2015b. TAAR1 Modulates Cortical Glutamate NMDA Receptor Function. Neuropsychopharmacology.

Espinoza, S., Masri, B., Salahpour, A., Gainetdinov, R. R., 2013. BRET approaches to characterize dopamine and TAAR1 receptor pharmacology and signaling. Methods Mol. Biol 964, 107-122.

Espinoza, S., Salahpour, A., Masri, B., Sotnikova, T. D., Messa, M., Barak, L. S., Caron, M. G., Gainetdinov, R. R., 2011. Functional interaction between trace amine-associated receptor 1 and dopamine D2 receptor. Mol. Pharmacol 80, 416-425.

Esteban, B., O'Shea, E., Camarero, J., Sanchez, V., Green, A. R., Colado, M. I., 2001. 3,4-Methylenedioxymethamphetamine induces monoamine release, but not toxicity, when administered centrally at a concentration occurring following a peripherally injected neurotoxic dose. Psychopharmacology (Berl) 154, 251-260.

Eyerman, D. J., Yamamoto, B. K., 2005. Lobeline attenuates methamphetamine-induced changes in vesicular monoamine transporter 2 immunoreactivity and monoamine depletions in the striatum. J. Pharmacol. Exp. Ther 312, 160-169.

Eyerman, D. J., Yamamoto, B. K., 2007. A rapid oxidation and persistent decrease in the vesicular monoamine transporter 2 after methamphetamine. J. Neurochem 103, 1219-1227.

Fallon, J. K., Shah, D., Kicman, A. T., Hutt, A. J., Henry, J. A., Cowan, D. A., Forsling, M., 2002. Action of MDMA (ecstasy) and its metabolites on arginine vasopressin release. Ann N Y Acad Sci 965, 399-409.

Fantegrossi, W. E., Ciullo, J. R., Wakabayashi, K. T., De La Garza, R., Traynor, J. R., Woods, J. H., 2008. A comparison of the physiological, behavioral, neurochemical and microglial effects of methamphetamine and 3,4-methylenedioxymethamphetamine in the mouse. Neuroscience 151, 533-543.

Fantegrossi, W. E., Gannon, B. M., Zimmerman, S. M., Rice, K. C., 2013. In vivo effects of abused 'bath salt' constituent 3,4-methylenedioxypyrovalerone (MDPV) in mice: drug discrimination, thermoregulation, and locomotor activity. Neuropsychopharmacology 38, 563-573.

Fantegrossi, W. E., Godlewski, T., Karabenick, R. L., Stephens, J. M., Ullrich, T., Rice, K. C., Woods, J. H., 2003. Pharmacological characterization of the effects of 3,4-methylenedioxymethamphetamine (''ecstasy'') and its enantiomers on lethality, core

temperature, and locomotor activity in singly housed and crowded mice. Psychopharmacology (Berl) 166, 202-211.

Fernandez-Calderon, F., Cleland, C. M., Palamar, J. J., 2018. Polysubstance use profiles among electronic dance music party attendees in New York City and their relation to use of new psychoactive substances. Addict Behav 78, 85-93.

Fischer, J. F., Cho, A. K., 1979. Chemical release of dopamine from striatal homogenates: evidence for an exchange diffusion model. J. Pharmacol. Exp. Ther 208, 203-209.

Fleckenstein, A. E., Gibb, J. W., Hanson, G. R., 2000. Differential effects of stimulants on monoaminergic transporters: pharmacological consequences and implications for neurotoxicity. Eur J Pharmacol 406, 1-13.

Fleckenstein, A. E., Metzger, R. R., Gibb, J. W., Hanson, G. R., 1997. A rapid and reversible change in dopamine transporters induced by methamphetamine. Eur. J. Pharmacol 323, R9-10.

Fleckenstein, A. E., Volz, T. J., Hanson, G. R., 2009. Psychostimulant-induced alterations in vesicular monoamine transporter-2 function: neurotoxic and therapeutic implications. Neuropharmacology 56 Suppl 1, 133-138.

Fleckenstein, A. E., Volz, T. J., Riddle, E. L., Gibb, J. W., Hanson, G. R., 2007. New insights into the mechanism of action of amphetamines. Annu. Rev. Pharmacol. Toxicol 47, 681-698.

Fornai, F., Lenzi, P., Ferrucci, M., Lazzeri, G., di Poggio, A. B., Natale, G., Busceti, C. L., Biagioni, F., Giusiani, M., Ruggieri, S., Paparelli, A., 2005. Occurrence of neuronal inclusions combined with increased nigral expression of alpha-synuclein within dopaminergic neurons following treatment with amphetamine derivatives in mice. Brain Res Bull 65, 405-413.

Fornai, F., Lenzi, P., Frenzilli, G., Gesi, M., Ferrucci, M., Lazzeri, G., Biagioni, F., Nigro, M., Falleni, A., Giusiani, M., Pellegrini, A., Blandini, F., Ruggieri, S., Paparelli, A., 2004. DNA damage and ubiquitinated neuronal inclusions in the substantia nigra and striatum of mice following MDMA (ecstasy). Psychopharmacology (Berl) 173, 353-363.

Frau, L., Simola, N., Plumitallo, A., Morelli, M., 2013. Microglial and astroglial activation by 3,4-methylenedioxymethamphetamine (MDMA) in mice depends on S(+) enantiomer and is associated with an increase in body temperature and motility. J Neurochem 124, 69-78.

Fricks-Gleason, A. N., German, C. L., Hoonakker, A. J., Friend, D. M., Ganesh, K. K., Carver, A. S., Hanson, G. R., Fleckenstein, A. E., Keefe, K. A., 2016. An acute, epitope-specific modification in the dopamine transporter associated with methamphetamine-induced neurotoxicity. Synapse 70, 139-146.

Fudala, P. J., Iwamoto, E. T., 1990. Conditioned aversion after delay place conditioning with amphetamine. Pharmacol. Biochem. Behav 35, 89-92.

Fujita, Y., Kunitachi, S., Iyo, M., Hashimoto, K., 2012. The antibiotic minocycline prevents methamphetamine-induced rewarding effects in mice. Pharmacol Biochem Behav 101, 303-306.

Fumagalli, F., Gainetdinov, R. R., Valenzano, K. J., Caron, M. G., 1998. Role of dopamine transporter in methamphetamine-induced neurotoxicity: evidence from mice lacking the transporter. J. Neurosci 18, 4861-4869.

Fumagalli, F., Gainetdinov, R. R., Wang, Y. M., Valenzano, K. J., Miller, G. W., Caron, M. G., 1999. Increased methamphetamine neurotoxicity in heterozygous vesicular monoamine transporter 2 knock-out mice. J. Neurosci 19, 2424-2431.

Gainetdinov, R. R., Bohn, L. M., Sotnikova, T. D., Cyr, M., Laakso, A., Macrae, A. D., Torres, G. E., Kim, K. M., Lefkowitz, R. J., Caron, M. G., Premont, R. T., 2003. Dopaminergic supersensitivity in G protein-coupled receptor kinase 6-deficient mice. Neuron 38, 291-303.

Galley, G., Beurier, A., Decoret, G., Goergler, A., Hutter, R., Mohr, S., Pahler, A., Schmid, P., Turck, D., Unger, R., Zbinden, K. G., Hoener, M. C., Norcross, R. D., 2016. Discovery and Characterization of 2-Aminooxazolines as Highly Potent, Selective, and Orally Active TAAR1 Agonists. ACS Med. Chem. Lett 7, 192-197.

Gannon, B. M., Williamson, A., Rice, K. C., Fantegrossi, W. E., 2018. Role of monoaminergic systems and ambient temperature in bath salts constituent 3,4-methylenedioxypyrovalerone (MDPV)-elicited hyperthermia and locomotor stimulation in mice. Neuropharmacology 134, 13-21.

Gannon, B. M., Williamson, A., Suzuki, M., Rice, K. C., Fantegrossi, W. E., 2016. Stereoselective Effects of Abused "Bath Salt" Constituent 3,4-Methylenedioxypyrovalerone in Mice: Drug Discrimination, Locomotor Activity, and Thermoregulation. J. Pharmacol. Exp. Ther 356, 615-623.

Gatch, M. B., Taylor, C. M., Forster, M. J., 2013. Locomotor stimulant and discriminative stimulus effects of 'bath salt' cathinones. Behav. Pharmacol 24, 437-447.

Geracitano, R., Federici, M., Prisco, S., Bernardi, G., Mercuri, N. B., 2004. Inhibitory effects of trace amines on rat midbrain dopaminergic neurons. Neuropharmacology 46, 807-814.

German, C. L., Hanson, G. R., Fleckenstein, A. E., 2012. Amphetamine and methamphetamine reduce striatal dopamine transporter function without concurrent dopamine transporter relocalization. J Neurochem 123, 288-297.

Giambalvo, C. T., 2004. Mechanisms underlying the effects of amphetamine on particulate PKC activity. Synapse 51, 128-139.

Giovanni, A., Liang, L. P., Hastings, T. G., Zigmond, M. J., 1995. Estimating hydroxyl radical content in rat brain using systemic and intraventricular salicylate: impact of methamphetamine. J Neurochem 64, 1819-1825.

Giros, B., Jaber, M., Jones, S. R., Wightman, R. M., Caron, M. G., 1996. Hyperlocomotion and indifference to cocaine and amphetamine in mice lacking the dopamine transporter. Nature 379, 606-612.

Glasner-Edwards, S., Mooney, L. J., 2014. Methamphetamine psychosis: epidemiology and management. CNS Drugs 28, 1115-1126.

Grace, C. E., Schaefer, T. L., Herring, N. R., Graham, D. L., Skelton, M. R., Gudelsky, G. A., Williams, M. T., Vorhees, C. V., 2010. Effect of a neurotoxic dose regimen of (+)-methamphetamine on behavior, plasma corticosterone, and brain monoamines in adult C57BL/6 mice. Neurotoxicol. Teratol 32, 346-355.

Granado, N., Ares-Santos, S., O'Shea, E., Vicario-Abejon, C., Colado, M. I., Moratalla, R., 2010. Selective vulnerability in striosomes and in the nigrostriatal dopaminergic pathway after methamphetamine administration : early loss of TH in striosomes after methamphetamine. Neurotox. Res 18, 48-58.

Granado, N., Ares-Santos, S., Oliva, I., O'Shea, E., Martin, E. D., Colado, M. I., Moratalla, R., 2011. Dopamine D2-receptor knockout mice are protected against dopaminergic neurotoxicity induced by methamphetamine or MDMA. Neurobiol. Dis 42, 391-403.

Granado, N., O'Shea, E., Bove, J., Vila, M., Colado, M. I., Moratalla, R., 2008. Persistent MDMA-induced dopaminergic neurotoxicity in the striatum and substantia nigra of mice. J Neurochem 107, 1102-1112.

Grandy, D. K., Miller, G. M., Li, J.-X., 2016. “TAARgeting Addiction”—The Alamo Bears Witness to Another Revolution: An Overview of the Plenary Symposium of the 2015 Behavior, Biology and Chemistry Conference. Drug and Alcohol Dependence 159, 9-16.

Green, A. R., Mechan, A. O., Elliott, J. M., O'Shea, E., Colado, M. I., 2003. The pharmacology and clinical pharmacology of 3,4-methylenedioxymethamphetamine (MDMA, "ecstasy"). Pharmacol Rev 55, 463-508.

Gregg, R. A., Rawls, S. M., 2014. Behavioral pharmacology of designer cathinones: a review of the preclinical literature. Life Sci 97, 27-30.

Gudelsky, G. A., Yamamoto, B. K., 2008. Actions of 3,4-methylenedioxymethamphetamine (MDMA) on cerebral dopaminergic, serotonergic and cholinergic neurons. Pharmacol Biochem Behav 90, 198-207.

Guilarte, T. R., Nihei, M. K., McGlothan, J. L., Howard, A. S., 2003. Methamphetamine-induced deficits of brain monoaminergic neuronal markers: distal axotomy or neuronal plasticity. Neuroscience 122, 499-513.

Guillot, T. S., Shepherd, K. R., Richardson, J. R., Wang, M. Z., Li, Y., Emson, P. C., Miller, G. W., 2008. Reduced vesicular storage of dopamine exacerbates methamphetamine-induced neurodegeneration and astrogliosis. J. Neurochem 106, 2205-2217.

Hadlock, G. C., Chu, P. W., Walters, E. T., Hanson, G. R., Fleckenstein, A. E., 2010. Methamphetamine-induced dopamine transporter complex formation and dopaminergic deficits: the role of D2 receptor activation. J. Pharmacol. Exp. Ther 335, 207-212.

Hanisch, U. K., 2002. Microglia as a source and target of cytokines. Glia 40, 140-155.

Hansen, J. P., Riddle, E. L., Sandoval, V., Brown, J. M., Gibb, J. W., Hanson, G. R., Fleckenstein, A. E., 2002. Methylenedioxymethamphetamine decreases plasmalemmal and vesicular dopamine transport: mechanisms and implications for neurotoxicity. J Pharmacol Exp Ther 300, 1093-1100.

Hanson, G. R., Sandoval, V., Riddle, E., Fleckenstein, A. E., 2004. Psychostimulants and vesicle trafficking: a novel mechanism and therapeutic implications. Ann N Y Acad Sci 1025, 146-150.

Harkness, J. H., Shi, X., Janowsky, A., Phillips, T. J., 2015. Trace Amine-Associated Receptor 1 Regulation of Methamphetamine Intake and Related Traits. Neuropsychopharmacology.

Harmeier, A., Obermueller, S., Meyer, C. A., Revel, F. G., Buchy, D., Chaboz, S., Dernick, G., Wettstein, J. G., Iglesias, A., Rolink, A., Bettler, B., Hoener, M. C., 2015. Trace amine-associated receptor 1 activation silences GSK3beta signaling of TAAR1 and D2R heteromers. Eur. Neuropsychopharmacol 25, 2049-2061.

Harvey, D. C., Lacan, G., Tanious, S. P., Melega, W. P., 2000. Recovery from methamphetamine induced long-term nigrostriatal dopaminergic deficits without substantia nigra cell loss. Brain Res 871, 259-270.

Hasler, F., Studerus, E., Lindner, K., Ludewig, S., Vollenweider, F. X., 2009. Investigation of serotonin-1A receptor function in the human psychopharmacology of MDMA. J Psychopharmacol 23, 923-935.

Hogan, K. A., Staal, R. G., Sonsalla, P. K., 2000. Analysis of VMAT2 binding after methamphetamine or MPTP treatment: disparity between homogenates and vesicle preparations. J. Neurochem 74, 2217-2220.

Homer, B. D., Solomon, T. M., Moeller, R. W., Mascia, A., DeRaleau, L., Halkitis, P. N., 2008. Methamphetamine abuse and impairment of social functioning: a review of the underlying neurophysiological causes and behavioral implications. Psychol Bull 134, 301-310.

Hoshi, R., Pratt, H., Mehta, S., Bond, A. J., Curran, H. V., 2006. An investigation into the sub-acute effects of ecstasy on aggressive interpretative bias and aggressive mood - are there gender differences? J Psychopharmacol 20, 291-301.

Ikemoto, S., 2002. Ventral striatal anatomy of locomotor activity induced by cocaine, D-amphetamine, dopamine and D1/D2 agonists. Neuroscience 113, 939-955.

Janowsky, A., Mah, C., Johnson, R. A., Cunningham, C. L., Phillips, T. J., Crabbe, J. C., Eshleman, A. J., Belknap, J. K., 2001a. Mapping genes that regulate density of dopamine transporters and correlated behaviors in recombinant inbred mice. J. Pharmacol. Exp. Ther 298, 634-643.

Janowsky, A., Neve, K., Eshleman, A. J., 2001b. Uptake and release of neurotransmitters. Curr. Protoc. Neurosci Chapter 7, Unit7.

Jayanthi, S., Ladenheim, B., Cadet, J. L., 1998. Methamphetamine-induced changes in antioxidant enzymes and lipid peroxidation in copper/zinc-superoxide dismutase transgenic mice. Ann N Y Acad Sci 844, 92-102.

Jentsch, J. D., Ashenhurst, J. R., Cervantes, M. C., Groman, S. M., James, A. S., Pennington, Z. T., 2014. Dissecting impulsivity and its relationships to drug addictions. Ann N Y Acad Sci, pp. 1-26.

Jing, L., Zhang, Y., Li, J. X., 2014. Effects of the trace amine associated receptor 1 agonist RO5263397 on abuse-related behavioral indices of methamphetamine in rats. Int. J. Neuropsychopharmacol 18.

John, J., Kukshal, P., Bhatia, T., Chowdari, K. V., Nimgaonkar, V. L., Deshpande, S. N., Thelma, B. K., 2017. Possible role of rare variants in Trace amine associated receptor 1 in schizophrenia. Schizophr. Res.

Johnson, E. A., O'Callaghan, J. P., Miller, D. B., 2004. Brain concentrations of d-MDMA are increased after stress. Psychopharmacology (Berl) 173, 278-286.

Johnson, E. A., Shvedova, A. A., Kisin, E., O'Callaghan, J. P., Kommineni, C., Miller, D. B., 2002. d-MDMA during vitamin E deficiency: effects on dopaminergic neurotoxicity and hepatotoxicity. Brain Res 933, 150-163.

Johnson, L. A., Guptaroy, B., Lund, D., Shamban, S., Gnegy, M. E., 2005. Regulation of amphetamine-stimulated dopamine efflux by protein kinase C beta. J. Biol. Chem 280, 10914-10919.

Kahlig, K. M., Binda, F., Khoshbouei, H., Blakely, R. D., McMahon, D. G., Javitch, J. A., Galli, A., 2005. Amphetamine induces dopamine efflux through a dopamine transporter channel. Proc. Natl. Acad. Sci. U. S. A 102, 3495-3500.

Kantor, L., Gnegy, M. E., 1998. Protein kinase C inhibitors block amphetamine-mediated dopamine release in rat striatal slices. J. Pharmacol. Exp. Ther 284, 592-598.

Karila, L., Billieux, J., Benyamina, A., Lancon, C., Cottencin, O., 2016. The effects and risks associated to mephedrone and methylone in humans: A review of the preliminary evidences. Brain Res Bull 126, 61-67.

Karila, L., Megarbane, B., Cottencin, O., Lejoyeux, M., 2015. Synthetic cathinones: a new public health problem. Curr Neuropharmacol 13, 12-20.

Karlsson, L., Andersson, M., Kronstrand, R., Kugelberg, F. C., 2014. Mephedrone, Methylone and 3,4-Methylenedioxypyrovalerone (MDPV) Induce Conditioned Place Preference in Mice. Basic Clin. Pharmacol. Toxicol.

Kelly, M. A., Low, M. J., Rubinstein, M., Phillips, T. J., 2008. Role of dopamine D1-like receptors in methamphetamine locomotor responses of D2 receptor knockout mice. Genes Brain Behav 7, 568-577.

Khoshbouei, H., Sen, N., Guptaroy, B., Johnson, L., Lund, D., Gnegy, M. E., Galli, A., Javitch, J. A., 2004. N-terminal phosphorylation of the dopamine transporter is required for amphetamine-induced efflux. PLoS. Biol 2, E78.

Kirkpatrick, M. G., de Wit, H., 2015. MDMA: a social drug in a social context. Psychopharmacology (Berl) 232, 1155-1163.

Kita, T., Miyazaki, I., Asanuma, M., Takeshima, M., Wagner, G. C., 2009. Dopamine-induced behavioral changes and oxidative stress in methamphetamine-induced neurotoxicity. Int. Rev. Neurobiol 88, 43-64.

Kita, T., Paku, S., Takahashi, M., Kubo, K., Wagner, G. C., Nakashima, T., 1998. Methamphetamine-induced neurotoxicity in BALB/c, DBA/2N and C57BL/6N mice. Neuropharmacology 37, 1177-1184.

Kitamura, O., Takeichi, T., Wang, E. L., Tokunaga, I., Ishigami, A., Kubo, S.-i., 2010. Microglial and astrocytic changes in the striatum of methamphetamine abusers. Legal Medicine 12, 57-62.

Kiyatkin, E. A., Sharma, H. S., 2009. Acute methamphetamine intoxication: brain hyperthermia, blood-brain barrier, brain edema, and morphological cell abnormalities. Int. Rev. Neurobiol 88, 65-100.

Kobeissy, F. H., Mitzelfelt, J. D., Fishman, I., Morgan, D., Gaskins, R., Zhang, Z., Gold, M. S., Wang, K. K., 2012. Methods in drug abuse models: comparison of different models of methamphetamine paradigms. Methods Mol Biol 829, 269-278.

Kohno, M., Loftis, J. M., Huckans, M., Dennis, L. E., McCready, H., Hoffman, W. F., 2018. The relationship between interleukin-6 and functional connectivity in methamphetamine users. Neuroscience Letters 677, 49-54.

Kokoshka, J. M., Metzger, R. R., Wilkins, D. G., Gibb, J. W., Hanson, G. R., Fleckenstein, A. E., 1998. Methamphetamine treatment rapidly inhibits serotonin, but not glutamate, transporters in rat brain. Brain Res 799, 78-83.

Kovács, T., Mikó, E., Vida, A., Sebő, É., Toth, J., Csonka, T., Boratkó, A., Ujlaki, G., Lente, G., Kovács, P., Tóth, D., Árkosy, P., Kiss, B., Méhes, G., Goedert, J. J., Bai, P., 2019. Cadaverine, a metabolite of the microbiome, reduces breast cancer aggressiveness through trace amino acid receptors. Scientific Reports 9, 1300.

Krasnova, I. N., Cadet, J. L., 2009. Methamphetamine toxicity and messengers of death. Brain Res. Rev 60, 379-407.

Kuhlmann, A. C., Guilarte, T. R., 1999. Regional and temporal expression of the peripheral benzodiazepine receptor in MPTP neurotoxicity. Toxicol. Sci 48, 107-116.

Kuhlmann, A. C., Guilarte, T. R., 2000. Cellular and subcellular localization of peripheral benzodiazepine receptors after trimethyltin neurotoxicity. J Neurochem 74, 1694-1704.

Kuhn, D. M., Angoa-Perez, M., Thomas, D. M., 2011. Nucleus accumbens invulnerability to methamphetamine neurotoxicity. ILAR. J 52, 352-365.

Ladenheim, B., Krasnova, I. N., Deng, X., Oyler, J. M., Polettini, A., Moran, T. H., Huestis, M. A., Cadet, J. L., 2000. Methamphetamine-induced neurotoxicity is attenuated in transgenic mice with a null mutation for interleukin-6. Mol. Pharmacol 58, 1247-1256.

Larsen, K. E., Fon, E. A., Hastings, T. G., Edwards, R. H., Sulzer, D., 2002. Methamphetamine-induced degeneration of dopaminergic neurons involves autophagy and upregulation of dopamine synthesis. J Neurosci 22, 8951-8960.

Lau, J. W., Senok, S., Stadlin, A., 2000. Methamphetamine-induced oxidative stress in cultured mouse astrocytes. Ann. N. Y. Acad. Sci 914, 146-156.

LaVoie, M. J., Card, J. P., Hastings, T. G., 2004. Microglial activation precedes dopamine terminal pathology in methamphetamine-induced neurotoxicity. Exp. Neurol 187, 47-57.

LaVoie, M. J., Hastings, T. G., 1999. Dopamine quinone formation and protein modification associated with the striatal neurotoxicity of methamphetamine: evidence against a role for extracellular dopamine. J. Neurosci 19, 1484-1491.

Lecomte, T., Paquin, K., Mueser, K. T., MacEwan, G. W., Goldner, E., Thornton, A. E., Brink, J., Lang, D., Kang, S., Barr, A. M., Honer, W. G., 2013. Relationships Among Depression, PTSD, Methamphetamine Abuse, and Psychosis. Journal of Dual Diagnosis 9, 115-122.

Leo, D., Mus, L., Espinoza, S., Hoener, M. C., Sotnikova, T. D., Gainetdinov, R. R., 2014. Taar1-mediated modulation of presynaptic dopaminergic neurotransmission: role of D2 dopamine autoreceptors. Neuropharmacology 81, 283-291.

Leo, D., Sukhanov, I., Zoratto, F., Illiano, P., Caffino, L., Sanna, F., Messa, G., Emanuele, M., Esposito, A., Dorofeikova, M., Budygin, E. A., Mus, L., Efimova, E. E., Niello, M., Espinoza, S., Sotnikova, T. D., Hoener, M. C., Laviola, G., Fumagalli, F., Adriani, W., Gainetdinov, R. R., 2018. PRONOUNCED HYPERACTIVITY, COGNITIVE DYSFUNCTIONS AND BDNF DYSREGULATION IN DOPAMINE TRANSPORTER KNOCKOUT RATS. J. Neurosci.

Leonardi, E. T., Azmitia, E. C., 1994. MDMA (ecstasy) inhibition of MAO type A and type B: comparisons with fenfluramine and fluoxetine (Prozac). Neuropsychopharmacology 10, 231-238.

Li, Y. C., Gao, W. J., 2011. GSK-3beta activity and hyperdopamine-dependent behaviors. Neurosci Biobehav Rev 35, 645-654.

Liang, N. Y., Rutledge, C. O., 1982. Comparison of the release of [3H]dopamine from isolated corpus striatum by amphetamine, fenfluramine and unlabelled dopamine. Biochem. Pharmacol 31, 983-992.

Liechti, M. E., 2014. Effects of MDMA on body temperature in humans. Temperature (Austin) 1, 192-200.

Lindemann, L., Ebeling, M., Kratochwil, N. A., Bunzow, J. R., Grandy, D. K., Hoener, M. C., 2005. Trace amine-associated receptors form structurally and functionally distinct subfamilies of novel G protein-coupled receptors. Genomics 85, 372-385.

Lindemann, L., Meyer, C. A., Jeanneau, K., Bradaia, A., Ozmen, L., Bluethmann, H., Bettler, B., Wettstein, J. G., Borroni, E., Moreau, J. L., Hoener, M. C., 2008. Trace amine-associated receptor 1 modulates dopaminergic activity. J. Pharmacol. Exp. Ther 324, 948-956.

Liu, J.-F., Li, J.-X., 2018a. TAAR1 in Addiction: Looking Beyond the Tip of the Iceberg. Frontiers in Pharmacology 9.

Liu, J. F., Li, J. X., 2018b. TAAR1 in Addiction: Looking Beyond the Tip of the Iceberg. Front Pharmacol 9, 279.

Liu, J. F., Seaman, R., Jr., Siemian, J. N., Bhimani, R., Johnson, B., Zhang, Y., Zhu, Q., Hoener, M. C., Park, J., Dietz, D. M., Li, J. X., 2018. Role of trace amine-associated receptor 1 in nicotine's behavioral and neurochemical effects. Neuropsychopharmacology.

Loftis, J. M., Janowsky, A., 2014. Neuroimmune basis of methamphetamine toxicity. Int. Rev. Neurobiol 118, 165-197.

Lohr, K. M., Stout, K. A., Dunn, A. R., Wang, M., Salahpour, A., Guillot, T. S., Miller, G. W., 2015. Increased Vesicular Monoamine Transporter 2 (VMAT2; Slc18a2) Protects against Methamphetamine Toxicity. ACS Chem. Neurosci 6, 790-799.

Lominac, K. D., McKenna, C. L., Schwartz, L. M., Ruiz, P. N., Wroten, M. G., Miller, B. W., Holloway, J. J., Travis, K. O., Rajasekar, G., Maliniak, D., Thompson, A. B., Urman, L. E., Phillips, T. J., Szumlinski, K. K., 2014. Mesocorticolimbic monoamine correlates of methamphetamine sensitization and motivation. Front Syst. Neurosci 8, 70.

Lominac, K. D., Quadir, S. G., Barrett, H. M., McKenna, C. L., Schwartz, L. M., Ruiz, P. N., Wroten, M. G., Campbell, R. R., Miller, B. W., Holloway, J. J., Travis, K. O., Rajasekar, G., Maliniak, D., Thompson, A. B., Urman, L. E., Kippin, T. E., Phillips, T. J., Szumlinski, K. K., 2016. Prefrontal glutamate correlates of methamphetamine sensitization and preference. Eur. J. Neurosci 43, 689-702.

Lopez-Arnau, R., Martinez-Clemente, J., Abad, S., Pubill, D., Camarasa, J., Escubedo, E., 2014. Repeated doses of methylone, a new drug of abuse, induce changes in serotonin and dopamine systems in the mouse. Psychopharmacology (Berl).

Lopez-Arnau, R., Martinez-Clemente, J., Pubill, D., Escubedo, E., Camarasa, J., 2012. Comparative neuropharmacology of three psychostimulant cathinone derivatives: butylone, mephedrone and methylone. Br. J Pharmacol 167, 407-420.

Madras, B. K., 2017. The Growing Problem of New Psychoactive Substances (NPS). Curr Top Behav Neurosci 32, 1-18.

Majd, S., Power, J. H., Grantham, H. J. M., 2015. Neuronal response in Alzheimer’s and Parkinson’s disease: the effect of toxic proteins on intracellular pathways. BMC Neuroscience 16, 69.

Mandela, P., Chandley, M., Xu, Y.-Y., Zhu, M.-Y., Ordway, G. A., 2010. Reserpine-induced reduction in norepinephrine transporter function requires catecholamine storage vesicles. Neurochemistry International 56, 760-767.

Mark, K. A., Soghomonian, J. J., Yamamoto, B. K., 2004. High-dose methamphetamine acutely activates the striatonigral pathway to increase striatal glutamate and mediate long-term dopamine toxicity. J Neurosci 24, 11449-11456.

Marusich, J. A., Antonazzo, K. R., Wiley, J. L., Blough, B. E., Partilla, J. S., Baumann, M. H., 2014. Pharmacology of novel synthetic stimulants structurally related to the "bath salts" constituent 3,4-methylenedioxypyrovalerone (MDPV). Neuropharmacology.

Matthews, A., Sutherland, R., Peacock, A., Van Buskirk, J., Whittaker, E., Burns, L., Bruno, R., 2017. I like the old stuff better than the new stuff? Subjective experiences of new psychoactive substances. Int J Drug Policy 40, 44-49.

McCann, U. D., Kuwabara, H., Kumar, A., Palermo, M., Abbey, R., Brasic, J., Ye, W., Alexander, M., Dannals, R. F., Wong, D. F., Ricaurte, G. A., 2008. Persistent cognitive and dopamine transporter deficits in abstinent methamphetamine users. Synapse 62, 91-100.

McCann, U. D., Mertl, M., Eligulashvili, V., Ricaurte, G. A., 1999. Cognitive performance in (+/-) 3,4-methylenedioxymethamphetamine (MDMA, "ecstasy") users: a controlled study. Psychopharmacology (Berl) 143, 417-425.

McConnell, S. E., O'Banion, M. K., Cory-Slechta, D. A., Olschowka, J. A., Opanashuk, L. A., 2015. Characterization of binge-dosed methamphetamine-induced neurotoxicity and neuroinflammation. Neurotoxicology 50, 131-141.

McDonnell-Dowling, K., Kelly, J. P., 2017. The Role of Oxidative Stress in Methamphetamine-induced Toxicity and Sources of Variation in the Design of Animal Studies. Curr Neuropharmacol 15, 300-314.

McFadden, L. M., Hadlock, G. C., Allen, S. C., Vieira-Brock, P. L., Stout, K. A., Ellis, J. D., Hoonakker, A. J., Andrenyak, D. M., Nielsen, S. M., Wilkins, D. G., Hanson, G. R., Fleckenstein, A. E., 2012. Methamphetamine Self-Administration Causes Persistent Striatal Dopaminergic Alterations and Mitigates the Deficits Caused by a Subsequent Methamphetamine Exposure. Journal of Pharmacology and Experimental Therapeutics 340, 295-303.

McGregor, C., Srisurapanont, M., Jittiwutikarn, J., Laobhripatr, S., Wongtan, T., White, J. M., 2005. The nature, time course and severity of methamphetamine withdrawal. Addiction 100, 1320-1329.

Metzger, R. R., Haughey, H. M., Wilkins, D. G., Gibb, J. W., Hanson, G. R., Fleckenstein, A. E., 2000. Methamphetamine-induced rapid decrease in dopamine transporter function: role of dopamine and hyperthermia. J. Pharmacol. Exp. Ther 295, 1077-1085.

Miller, D. B., O'Callaghan, J. P., 1994. Environment-, drug- and stress-induced alterations in body temperature affect the neurotoxicity of substituted amphetamines in the C57BL/6J mouse. J. Pharmacol. Exp. Ther 270, 752-760.

Miller, D. B., O'Callaghan, J. P., 1995. The role of temperature, stress, and other factors in the neurotoxicity of the substituted amphetamines 3,4-methylenedioxymethamphetamine and fenfluramine. Mol. Neurobiol 11, 177-192.

Miller, D. B., O'Callaghan, J. P., 2003. Elevated environmental temperature and methamphetamine neurotoxicity. Environ. Res 92, 48-53.

Miller, G. M., Verrico, C. D., Jassen, A., Konar, M., Yang, H., Panas, H., Bahn, M., Johnson, R., Madras, B. K., 2005. Primate trace amine receptor 1 modulation by the dopamine transporter. J. Pharmacol. Exp. Ther 313, 983-994.

Miner, N. B., Elmore, J. S., Baumann, M. H., Phillips, T. J., Janowsky, A., 2017a. Trace amine-associated receptor 1 regulation of methamphetamine-induced neurotoxicity. Neurotoxicology 63, 57-69.

Miner, N. B., O'Callaghan, J. P., Phillips, T. J., Janowsky, A., 2017b. The combined effects of 3,4-methylenedioxymethamphetamine (MDMA) and selected substituted methcathinones on measures of neurotoxicity. Neurotoxicol. Teratol.

Miyazaki, I., Asanuma, M., Diaz-Corrales, F. J., Fukuda, M., Kitaichi, K., Miyoshi, K., Ogawa, N., 2006. Methamphetamine-induced dopaminergic neurotoxicity is regulated by quinone-formation-related molecules. FASEB J 20, 571-573.

Mohamed, W. M., Ben, H. S., Cassel, J. C., de Vasconcelos, A. P., Jones, B. C., 2011. MDMA: interactions with other psychoactive drugs. Pharmacol Biochem Behav 99, 759-774.

Mooney, L. J., Glasner-Edwards, S., Marinelli-Casey, P., Hillhouse, M., Ang, A., Hunter, J., Haning, W., Colescott, P., Ling, W., Rawson, R., 2009. Health conditions in methamphetamine-dependent adults 3 years after treatment. J. Addict. Med 3, 155-163.

Moratalla, R., Khairnar, A., Simola, N., Granado, N., Garcia-Montes, J. R., Porceddu, P. F., Tizabi, Y., Costa, G., Morelli, M., 2017. Amphetamine-related drugs neurotoxicity in humans and in experimental animals: Main mechanisms. Prog Neurobiol 155, 149-170.

Moszczynska, A., Callan, S. P., 2017. Molecular, Behavioral, and Physiological Consequences of Methamphetamine Neurotoxicity: Implications for Treatment. J Pharmacol Exp Ther 362, 474-488.

Mounteney, J., Griffiths, P., Bo, A., Cunningham, A., Matias, J., Pirona, A., 2018. Nine reasons why ecstasy is not quite what it used to be. Int J Drug Policy 51, 36-41.

Mueller, M., Maldonado-Adrian, C., Yuan, J., McCann, U. D., Ricaurte, G. A., 2013. Studies of (+/-)-3,4-methylenedioxymethamphetamine (MDMA) metabolism and disposition in rats and mice: relationship to neuroprotection and neurotoxicity profile. J Pharmacol Exp Ther 344, 479-488.

Muhlhaus, J., Dinter, J., Jyrch, S., Teumer, A., Jacobi, S. F., Homuth, G., Kuhnen, P., Wiegand, S., Gruters, A., Volzke, H., Raile, K., Kleinau, G., Krude, H., Biebermann, H., 2017. Investigation of Naturally Occurring Single-Nucleotide Variants in Human TAAR1. Front Pharmacol 8, 807.

Nash, J. F., Yamamoto, B. K., 1992. Methamphetamine neurotoxicity and striatal glutamate release: comparison to 3,4-methylenedioxymethamphetamine. Brain Res 581, 237-243.

Nelson, D. A., Tolbert, M. D., Singh, S. J., Bost, K. L., 2007. Expression of neuronal trace amine-associated receptor (Taar) mRNAs in leukocytes. J. Neuroimmunol 192, 21-30.

NFLIS, 2010. National Forensic Laboratory Information System: 2010 Annual Report. U.S. Drug Enforcement Administration, Office of Diversion Control.

NFLIS, 2013. National Forensic Laboratory Information System: 2013 Annual Report. U.S. Drug Enforcement Administration, Office of Diversion Control.

NFLIS, 2018. National Forensic Laboratory Information System: 2016 Annual Report. U.S. Drug Enforcement Administration, Office of Diversion Control.

NINDS, 2018. Neurotoxicity information page.

NSDUH, 2017. Key substance use and mental health indicators in the United States: Results from the 2016 National Survey on Drug Use and Health. Substance Abuse and Mental Health Services Administration.

Nutt, D. J., Lingford-Hughes, A., Erritzoe, D., Stokes, P. R., 2015. The dopamine theory of addiction: 40 years of highs and lows. Nat Rev Neurosci 16, 305-312.

O'Callaghan, J. P., 2002. Measurement of glial fibrillary acidic protein. Curr Protoc. Toxicol Chapter 12, Unit12.

O'Callaghan, J. P., Kelly, K. A., VanGilder, R. L., Sofroniew, M. V., Miller, D. B., 2014. Early Activation of STAT3 Regulates Reactive Astrogliosis Induced by Diverse Forms of Neurotoxicity. PLoS. One 9, e102003.

O'Callaghan, J. P., Miller, D. B., 1994. Neurotoxicity profiles of substituted amphetamines in the C57BL/6J mouse. J Pharmacol Exp Ther 270, 741-751.

O'Callaghan, J. P., Sriram, K., 2005. Glial fibrillary acidic protein and related glial proteins as biomarkers of neurotoxicity. Expert. Opin Drug Saf 4, 433-442.

O'Callaghan, J. P., Sriram, K., Miller, D. B., 2008. Defining "neuroinflammation". Ann N Y Acad Sci 1139, 318-330.

O'Shea, E., Esteban, B., Camarero, J., Green, A. R., Colado, M. I., 2001. Effect of GBR 12909 and fluoxetine on the acute and long term changes induced by MDMA ('ecstasy') on the 5-HT and dopamine concentrations in mouse brain. Neuropharmacology 40, 65-74.

O'Callaghan, J. P., Miller, D. B., 2002. Neurotoxic Effects of Substituted Amphetamines in Rats and Mice. In: Massaro, E. J., (Ed), Handbook of Neurotoxicology: Volume II. Humana Press, Totowa, NJ, pp. 269-301.

Palamar, J. J., Salomone, A., Vincenti, M., Cleland, C. M., 2016. Detection of "bath salts" and other novel psychoactive substances in hair samples of ecstasy/MDMA/"Molly" users. Drug Alcohol Depend 161, 200-205.

Panas, H. N., Lynch, L. J., Vallender, E. J., Xie, Z., Chen, G. L., Lynn, S. K., Scanlan, T. S., Miller, G. M., 2010. Normal thermoregulatory responses to 3-iodothyronamine, trace amines and amphetamine-like psychostimulants in trace amine associated receptor 1 knockout mice. J. Neurosci. Res 88, 1962-1969.

Panas, M. W., Xie, Z., Panas, H. N., Hoener, M. C., Vallender, E. J., Miller, G. M., 2012. Trace amine associated receptor 1 signaling in activated lymphocytes. J. Neuroimmune. Pharmacol 7, 866-876.

Papadopoulos, V., Baraldi, M., Guilarte, T. R., Knudsen, T. B., Lacapere, J. J., Lindemann, P., Norenberg, M. D., Nutt, D., Weizman, A., Zhang, M. R., Gavish, M., 2006. Translocator protein (18kDa): new nomenclature for the peripheral-type benzodiazepine receptor based on its structure and molecular function. Trends Pharmacol. Sci 27, 402-409.

Paratz, E. D., Cunningham, N. J., MacIsaac, A. I., 2016. The Cardiac Complications of Methamphetamines. Heart Lung Circ 25, 325-332.

Partilla, J. S., Dempsey, A. G., Nagpal, A. S., Blough, B. E., Baumann, M. H., Rothman, R. B., 2006. Interaction of amphetamines and related compounds at the vesicular monoamine transporter. J. Pharmacol. Exp. Ther 319, 237-246.

Pei, Y., Asif-Malik, A., Canales, J. J., 2016. Trace Amines and the Trace Amine-Associated Receptor 1: Pharmacology, Neurochemistry, and Clinical Implications. Frontiers in Neuroscience 10.

Pei, Y., Asif-Malik, A., Hoener, M., Canales, J. J., 2017. A partial trace amine-associated receptor 1 agonist exhibits properties consistent with a methamphetamine substitution treatment. Addict. Biol 22, 1246-1256.

Pei, Y., Lee, J., Leo, D., Gainetdinov, R. R., Hoener, M. C., Canales, J. J., 2014. Activation of the trace amine-associated receptor 1 prevents relapse to cocaine seeking. Neuropsychopharmacology 39, 2299-2308.

Pei, Y., Mortas, P., Hoener, M. C., Canales, J. J., 2015. Selective activation of the trace amine-associated receptor 1 decreases cocaine's reinforcing efficacy and prevents cocaine-induced changes in brain reward thresholds. Prog. Neuropsychopharmacol. Biol. Psychiatry 63, 70-75.

Peraile, I., Granado, N., Torres, E., Gutierrez-Lopez, M. D., Moratalla, R., Colado, M. I., O'Shea, E., 2013. Cocaine potentiates MDMA-induced oxidative stress but not dopaminergic neurotoxicity in mice: implications for the pathogenesis of free radical-induced neurodegenerative disorders. Psychopharmacology (Berl) 230, 125-135.

Peraile, I., Torres, E., Mayado, A., Izco, M., Lopez-Jimenez, A., Lopez-Moreno, J. A., Colado, M. I., O'Shea, E., 2010. Dopamine transporter down-regulation following repeated cocaine: implications for 3,4-methylenedioxymethamphetamine-induced acute effects and long-term neurotoxicity in mice. Br J Pharmacol 159, 201-211.

Phillips, T. J., Shabani, S., 2015. An animal model of differential genetic risk for methamphetamine intake. Front Neurosci 9, 327.

Pifl, C., Drobny, H., Reither, H., Hornykiewicz, O., Singer, E. A., 1995. Mechanism of the dopamine-releasing actions of amphetamine and cocaine: plasmalemmal dopamine transporter versus vesicular monoamine transporter. Mol. Pharmacol 47, 368-373.

Pifl, C., Reither, H., Hornykiewicz, O., 2015. The profile of mephedrone on human monoamine transporters differs from 3,4-methylenedioxymethamphetamine primarily by lower potency at the vesicular monoamine transporter. Eur J Pharmacol 755, 119-126.

Potvin, S., Pelletier, J., Grot, S., Hebert, C., Barr, A. M., Lecomte, T., 2018. Cognitive deficits in individuals with methamphetamine use disorder: A meta-analysis. Addict Behav 80, 154-160.

Pristupa, Z. B., Wilson, J. M., Hoffman, B. J., Kish, S. J., Niznik, H. B., 1994. Pharmacological heterogeneity of the cloned and native human dopamine transporter: disassociation of [3H]WIN 35,428 and [3H]GBR 12,935 binding. Mol Pharmacol 45, 125-135.

Pu, C., Vorhees, C. V., 1993. Developmental dissociation of methamphetamine-induced depletion of dopaminergic terminals and astrocyte reaction in rat striatum. Brain Res. Dev. Brain Res 72, 325-328.

Pubill, D., Canudas, A. M., Pallas, M., Camins, A., Camarasa, J., Escubedo, E., 2003. Different glial response to methamphetamine- and methylenedioxymethamphetamine-induced neurotoxicity. Naunyn Schmiedebergs Arch Pharmacol 367, 490-499.

Puerta, E., Hervias, I., Aguirre, N., 2009. On the mechanisms underlying 3,4-methylenedioxymethamphetamine toxicity: the dilemma of the chicken and the egg. Neuropsychobiology 60, 119-129.

Raab, S., Wang, H., Uhles, S., Cole, N., Alvarez-Sanchez, R., Kunnecke, B., Ullmer, C., Matile, H., Bedoucha, M., Norcross, R. D., Ottaway-Parker, N., Perez-Tilve, D., Conde, K. K., Tschop, M. H., Hoener, M. C., Sewing, S., 2016. Incretin-like effects of small molecule trace amine-associated receptor 1 agonists. Mol. Metab 5, 47-56.

Raineri, M., Gonzalez, B., Rivero-Echeto, C., Muniz, J. A., Gutierrez, M. L., Ghanem, C. I., Cadet, J. L., Garcia-Rill, E., Urbano, F. J., Bisagno, V., 2015. Differential effects of environment-induced changes in body temperature on modafinil's actions against methamphetamine-induced striatal toxicity in mice. Neurotox. Res 27, 71-83.

Reed, C., Baba, H., Zhu, Z., Erk, J., Mootz, J. R., Varra, N. M., Williams, R. W., Phillips, T. J., 2018. A Spontaneous Mutation in Taar1 Impacts Methamphetamine-Related Traits Exclusively in DBA/2 Mice from a Single Vendor. Front Pharmacol 8, 993.

Ren, Q., Zhang, J. C., Ma, M., Fujita, Y., Wu, J., Hashimoto, K., 2014. 7,8-Dihydroxyflavone, a TrkB agonist, attenuates behavioral abnormalities and neurotoxicity in mice after administration of methamphetamine. Psychopharmacology (Berl) 231, 159-166.

Reneman, L., Lavalaye, J., Schmand, B., de Wolff, F. A., van den Brink, W., den Heeten, G. J., Booij, J., 2001. Cortical serotonin transporter density and verbal memory in individuals who stopped using 3,4-methylenedioxymethamphetamine (MDMA or "ecstasy"): preliminary findings. Arch Gen Psychiatry 58, 901-906.

Revel, F. G., Meyer, C. A., Bradaia, A., Jeanneau, K., Calcagno, E., Andre, C. B., Haenggi, M., Miss, M. T., Galley, G., Norcross, R. D., Invernizzi, R. W., Wettstein, J. G., Moreau, J. L., Hoener, M. C., 2012a. Brain-specific overexpression of trace amine-associated receptor 1 alters monoaminergic neurotransmission and decreases sensitivity to amphetamine. Neuropsychopharmacology 37, 2580-2592.

Revel, F. G., Moreau, J. L., Gainetdinov, R. R., Bradaia, A., Sotnikova, T. D., Mory, R., Durkin, S., Zbinden, K. G., Norcross, R., Meyer, C. A., Metzler, V., Chaboz, S., Ozmen, L., Trube, G., Pouzet, B., Bettler, B., Caron, M. G., Wettstein, J. G., Hoener, M. C., 2011. TAAR1 activation modulates monoaminergic neurotransmission, preventing hyperdopaminergic and hypoglutamatergic activity. Proc. Natl. Acad. Sci. U. S. A 108, 8485-8490.

Revel, F. G., Moreau, J. L., Gainetdinov, R. R., Ferragud, A., Velazquez-Sanchez, C., Sotnikova, T. D., Morairty, S. R., Harmeier, A., Groebke, Z. K., Norcross, R. D., Bradaia, A., Kilduff, T. S., Biemans, B., Pouzet, B., Caron, M. G., Canales, J. J., Wallace, T. L., Wettstein, J. G., Hoener, M. C., 2012b. Trace amine-associated receptor 1 partial agonism reveals novel paradigm for neuropsychiatric therapeutics. Biol. Psychiatry 72, 934-942.

Revel, F. G., Moreau, J. L., Pouzet, B., Mory, R., Bradaia, A., Buchy, D., Metzler, V., Chaboz, S., Groebke, Z. K., Galley, G., Norcross, R. D., Tuerck, D., Bruns, A., Morairty, S. R., Kilduff, T. S., Wallace, T. L., Risterucci, C., Wettstein, J. G., Hoener, M. C., 2013. A new perspective for schizophrenia: TAAR1 agonists reveal antipsychotic- and antidepressant-like activity, improve cognition and control body weight. Mol. Psychiatry 18, 543-556.

Ricaurte, G. A., Forno, L. S., Wilson, M. A., DeLanney, L. E., Irwin, I., Molliver, M. E., Langston, J. W., 1988. (+/-)3,4-Methylenedioxymethamphetamine selectively damages central serotonergic neurons in nonhuman primates. Jama 260, 51-55.

Riddle, E. L., Topham, M. K., Haycock, J. W., Hanson, G. R., Fleckenstein, A. E., 2002. Differential trafficking of the vesicular monoamine transporter-2 by methamphetamine and cocaine. Eur. J. Pharmacol 449, 71-74.

Rocher, C., Gardier, A. M., 2001. Effects of repeated systemic administration of d-Fenfluramine on serotonin and glutamate release in rat ventral hippocampus: comparison with methamphetamine using in vivo microdialysis. Naunyn Schmiedebergs Arch Pharmacol 363, 422-428.

Rothman, R. B., Baumann, M. H., 2003. Monoamine transporters and psychostimulant drugs. Eur. J. Pharmacol 479, 23-40.

Rothman, R. B., Baumann, M. H., Dersch, C. M., Romero, D. V., Rice, K. C., Carroll, F. I., Partilla, J. S., 2001. Amphetamine-type central nervous system stimulants release norepinephrine more potently than they release dopamine and serotonin. Synapse 39, 32-41.

Rudd, M. L., Nicolas, A. N., Brown, B. L., Fischer-Stenger, K., Stewart, J. K., 2005. Peritoneal macrophages express the serotonin transporter. Journal of Neuroimmunology 159, 113-118.

Rutigliano, G., Accorroni, A., Zucchi, R., 2017. The Case for TAAR1 as a Modulator of Central Nervous System Function. Front Pharmacol 8, 987.

Sanchez, V., Camarero, J., O'Shea, E., Green, A. R., Colado, M. I., 2003. Differential effect of dietary selenium on the long-term neurotoxicity induced by MDMA in mice and rats. Neuropharmacology 44, 449-461.

Sandoval, V., Hanson, G. R., Fleckenstein, A. E., 2000. Methamphetamine decreases mouse striatal dopamine transporter activity: roles of hyperthermia and dopamine. Eur J Pharmacol 409, 265-271.

Sandoval, V., Riddle, E. L., Hanson, G. R., Fleckenstein, A. E., 2003. Methylphenidate alters vesicular monoamine transport and prevents methamphetamine-induced dopaminergic deficits. J. Pharmacol. Exp. Ther 304, 1181-1187.

Sandoval, V., Riddle, E. L., Ugarte, Y. V., Hanson, G. R., Fleckenstein, A. E., 2001. Methamphetamine-induced rapid and reversible changes in dopamine transporter function: an in vitro model. J Neurosci 21, 1413-1419.

Saunders, C., Ferrer, J. V., Shi, L., Chen, J., Merrill, G., Lamb, M. E., Leeb-Lundberg, L. M., Carvelli, L., Javitch, J. A., Galli, A., 2000. Amphetamine-induced loss of human dopamine transporter activity: an internalization-dependent and cocaine-sensitive mechanism. Proc Natl Acad Sci U S A 97, 6850-6855.

Scherman, D., 1986. Dihydrotetrabenazine binding and monoamine uptake in mouse brain regions. J. Neurochem 47, 331-339.

Schifano, F., Di Furia, L., Forza, G., Minicuci, N., Bricolo, R., 1998. MDMA ('ecstasy') consumption in the context of polydrug abuse: a report on 150 patients. Drug Alcohol Depend 52, 85-90.

Schifano, F., Orsolini, L., Papanti, D., Corkery, J., 2017. NPS: Medical Consequences Associated with Their Intake. Curr Top Behav Neurosci 32, 351-380.

Schindler, C. W., Thorndike, E. B., Goldberg, S. R., Lehner, K. R., Cozzi, N. V., Brandt, S. D., Baumann, M. H., 2015. Reinforcing and neurochemical effects of the "bath salts" constituents 3,4-methylenedioxypyrovalerone (MDPV) and 3,4-methylenedioxy-N-methylcathinone (methylone) in male rats. Psychopharmacology (Berl).

Schmidt, C. J., Taylor, V. L., 1988. Direct central effects of acute methylenedioxymethamphetamine on serotonergic neurons. Eur J Pharmacol 156, 121-131.

Schwartz, M. D., Black, S. W., Fisher, S. P., Palmerston, J. B., Morairty, S. R., Hoener, M. C., Kilduff, T. S., 2017. Trace Amine-Associated Receptor 1 Regulates Wakefulness and EEG Spectral Composition. Neuropsychopharmacology 42, 1305-1314.

Seeman, P., Schwarz, J., Chen, J. F., Szechtman, H., Perreault, M., McKnight, G. S., Roder, J. C., Quirion, R., Boksa, P., Srivastava, L. K., Yanai, K., Weinshenker, D., Sumiyoshi, T., 2006. Psychosis pathways converge via D2high dopamine receptors. Synapse 60, 319-346.

Seeman, P., Weinshenker, D., Quirion, R., Srivastava, L. K., Bhardwaj, S. K., Grandy, D. K., Premont, R. T., Sotnikova, T. D., Boksa, P., El-Ghundi, M., O'dowd, B. F., George, S. R., Perreault, M. L., Mannisto, P. T., Robinson, S., Palmiter, R. D., Tallerico, T., 2005. Dopamine supersensitivity correlates with D2High states, implying many paths to psychosis. Proc. Natl. Acad. Sci. U. S. A 102, 3513-3518.

Seiden, L. S., Commins, D. L., Vosmer, G., Axt, K., Marek, G., 1988. Neurotoxicity in dopamine and 5-hydroxytryptamine terminal fields: a regional analysis in nigrostriatal and mesolimbic projections. Ann N Y Acad Sci 537, 161-172.

Sekine, Y., Ouchi, Y., Sugihara, G., Takei, N., Yoshikawa, E., Nakamura, K., Iwata, Y., Tsuchiya, K. J., Suda, S., Suzuki, K., Kawai, M., Takebayashi, K., Yamamoto, S., Matsuzaki, H., Ueki, T., Mori, N., Gold, M. S., Cadet, J. L., 2008. Methamphetamine Causes Microglial Activation in the Brains of Human Abusers. The Journal of Neuroscience 28, 5756-5761.

Shabani, S., Dobbs, L. K., Ford, M. M., Mark, G. P., Finn, D. A., Phillips, T. J., 2012a. A genetic animal model of differential sensitivity to methamphetamine reinforcement. Neuropharmacology 62, 2169-2177.

Shabani, S., Houlton, S. K., Hellmuth, L., Mojica, E., Mootz, J. R., Zhu, Z., Reed, C., Phillips, T. J., 2016. A Mouse Model for Binge-Level Methamphetamine Use. Front Neurosci 10, 493.

Shabani, S., McKinnon, C. S., Cunningham, C. L., Phillips, T. J., 2012b. Profound reduction in sensitivity to the aversive effects of methamphetamine in mice bred for high methamphetamine intake. Neuropharmacology 62, 1134-1141.

Shabani, S., McKinnon, C. S., Reed, C., Cunningham, C. L., Phillips, T. J., 2011. Sensitivity to rewarding or aversive effects of methamphetamine determines methamphetamine intake. Genes Brain Behav 10, 625-636.

Sharma, H. S., Kiyatkin, E. A., Patnaik, R., Lafuente, J. V., Muresanu, D. F., Sjoquist, P. O., Sharma, A., 2015. Exacerbation of Methamphetamine Neurotoxicity in Cold and Hot Environments: Neuroprotective Effects of an Antioxidant Compound H-290/51. Mol. Neurobiol 52, 1023-1033.

Shi, X., Walter, N. A., Harkness, J. H., Neve, K. A., Williams, R. W., Lu, L., Belknap, J. K., Eshleman, A. J., Phillips, T. J., Janowsky, A., 2016. Genetic Polymorphisms Affect Mouse and Human Trace Amine-Associated Receptor 1 Function. PLoS. One 11, e0152581.

Shin, E.-J., Bing, G., Chae, J. S., Kim, T. W., Bach, J.-H., Park, D. H., Yamada, K., Nabeshima, T., Kim, H.-C., 2009. Role of microsomal epoxide hydrolase in methamphetamine-induced drug dependence in mice. Journal of Neuroscience Research 87, 3679-3686.

Shuto, T., Seeman, P., Kuroiwa, M., Nishi, A., 2008. Repeated administration of a dopamine D1 receptor agonist reverses the increased proportions of striatal dopamine D1High and D2High receptors in methamphetamine-sensitized rats. Eur. J. Neurosci 27, 2551-2557.

Siemian, J. N., Zhang, Y., Li, J. X., 2017. Trace amine-associated receptor 1 agonists RO5263397 and RO5166017 attenuate quinpirole-induced yawning but not hypothermia in rats. Behav. Pharmacol.

Simmler, L. D., Buchy, D., Chaboz, S., Hoener, M. C., Liechti, M. E., 2016. In Vitro Characterization of Psychoactive Substances at Rat, Mouse, and Human Trace Amine-Associated Receptor 1. J. Pharmacol. Exp. Ther 357, 134-144.

Simmler, L. D., Buser, T. A., Donzelli, M., Schramm, Y., Dieu, L. H., Huwyler, J., Chaboz, S., Hoener, M. C., Liechti, M. E., 2013a. Pharmacological characterization of designer cathinones in vitro. Br. J Pharmacol 168, 458-470.

Simmler, L. D., Wandeler, R., Liechti, M. E., 2013b. Bupropion, methylphenidate, and 3,4-methylenedioxypyrovalerone antagonize methamphetamine-induced efflux of dopamine according to their potencies as dopamine uptake inhibitors: implications for the treatment of methamphetamine dependence. BMC Res Notes 6, 220.

Sokolov, B. P., Schindler, C. W., Cadet, J. L., 2004. Chronic methamphetamine increases fighting in mice. Pharmacol Biochem Behav 77, 319-326.

Sonsalla, P. K., Jochnowitz, N. D., Zeevalk, G. D., Oostveen, J. A., Hall, E. D., 1996. Treatment of mice with methamphetamine produces cell loss in the substantia nigra. Brain Res 738, 172-175.

Sotnikova, T. D., Budygin, E. A., Jones, S. R., Dykstra, L. A., Caron, M. G., Gainetdinov, R. R., 2004. Dopamine transporter-dependent and -independent actions of trace amine beta-phenylethylamine. J. Neurochem 91, 362-373.

Sprague, J. E., Everman, S. L., Nichols, D. E., 1998. An integrated hypothesis for the serotonergic axonal loss induced by 3,4-methylenedioxymethamphetamine. Neurotoxicology 19, 427-441.

Sriram, K., Benkovic, S. A., Hebert, M. A., Miller, D. B., O'Callaghan, J. P., 2004. Induction of gp130-related cytokines and activation of JAK2/STAT3 pathway in astrocytes precedes up-regulation of glial fibrillary acidic protein in the 1-methyl-4-phenyl-1,2,3,6-tetrahydropyridine model of neurodegeneration: key signaling pathway for astrogliosis in vivo? J. Biol. Chem 279, 19936-19947.

Sriram, K., Miller, D. B., O'Callaghan, J. P., 2006. Minocycline attenuates microglial activation but fails to mitigate striatal dopaminergic neurotoxicity: role of tumor necrosis factor-alpha. J. Neurochem 96, 706-718.

Staal, R. G., Hogan, K. A., Liang, C. L., German, D. C., Sonsalla, P. K., 2000. In vitro studies of striatal vesicles containing the vesicular monoamine transporter (VMAT2): rat versus mouse differences in sequestration of 1-methyl-4-phenylpyridinium. J Pharmacol Exp Ther 293, 329-335.

Stalder, H., Hoener, M. C., Norcross, R. D., 2011. Selective antagonists of mouse trace amine-associated receptor 1 (mTAAR1): discovery of EPPTB (RO5212773). Bioorg. Med. Chem. Lett 21, 1227-1231.

Stone, D. M., Johnson, M., Hanson, G. R., Gibb, J. W., 1988. Role of endogenous dopamine in the central serotonergic deficits induced by 3,4-methylenedioxymethamphetamine. J Pharmacol Exp Ther 247, 79-87.

Sukhanov, I., Caffino, L., Efimova, E. V., Espinoza, S., Sotnikova, T. D., Cervo, L., Fumagalli, F., Gainetdinov, R. R., 2016. Increased context-dependent conditioning to amphetamine in mice lacking TAAR1. Pharmacol. Res 103, 206-214.

Sulzer, D., Chen, T. K., Lau, Y. Y., Kristensen, H., Rayport, S., Ewing, A., 1995. Amphetamine redistributes dopamine from synaptic vesicles to the cytosol and promotes reverse transport. J. Neurosci 15, 4102-4108.

Sulzer, D., Rayport, S., 1990. Amphetamine and other psychostimulants reduce pH gradients in midbrain dopaminergic neurons and chromaffin granules: a mechanism of action. Neuron 5, 797-808.

Sulzer, D., Sonders, M. S., Poulsen, N. W., Galli, A., 2005. Mechanisms of neurotransmitter release by amphetamines: a review. Prog. Neurobiol 75, 406-433.

Sutherland, R., Bruno, R., Peacock, A., Lenton, S., Matthews, A., Salom, C., Dietze, P., Butler, K., Burns, L., Barratt, M. J., 2017. Motivations for new psychoactive substance use among regular psychostimulant users in Australia. Int J Drug Policy 43, 23-32.

Szumlinski, K. K., Lominac, K. D., Campbell, R. R., Cohen, M., Fultz, E. K., Brown, C. N., Miller, B. W., Quadir, S. G., Martin, D., Thompson, A. B., von, J. G., Klugmann, M., Phillips, T. J., Kippin, T. E., 2017. Methamphetamine Addiction Vulnerability: The Glutamate, the Bad, and the Ugly. Biol. Psychiatry 81, 959-970.

Szumska, J., Qatato, M., Rehders, M., Fuhrer, D., Biebermann, H., Grandy, D. K., Kohrle, J., Brix, K., 2015. Trace Amine-Associated Receptor 1 Localization at the Apical Plasma Membrane Domain of Fisher Rat Thyroid Epithelial Cells Is Confined to Cilia. Eur. Thyroid J 4, 30-41.

Teng, L., Crooks, P. A., Dwoskin, L. P., 1998. Lobeline displaces [3H]dihydrotetrabenazine binding and releases [3H]dopamine from rat striatal synaptic vesicles: comparison with d-amphetamine. J. Neurochem 71, 258-265.

Teng, L., Crooks, P. A., Sonsalla, P. K., Dwoskin, L. P., 1997. Lobeline and nicotine evoke [3H]overflow from rat striatal slices preloaded with [3H]dopamine: differential inhibition of synaptosomal and vesicular [3H]dopamine uptake. J. Pharmacol. Exp. Ther 280, 1432-1444.

Thomas, D. M., Angoa Perez, M., Francescutti-Verbeem, D. M., Shah, M. M., Kuhn, D. M., 2010. The role of endogenous serotonin in methamphetamine-induced neurotoxicity to dopamine nerve endings of the striatum. J Neurochem 115, 595-605.

Thomas, D. M., Dowgiert, J., Geddes, T. J., Francescutti-Verbeem, D., Liu, X., Kuhn, D. M., 2004a. Microglial activation is a pharmacologically specific marker for the neurotoxic amphetamines. Neurosci Lett 367, 349-354.

Thomas, D. M., Walker, P. D., Benjamins, J. A., Geddes, T. J., Kuhn, D. M., 2004b. Methamphetamine neurotoxicity in dopamine nerve endings of the striatum is associated with microglial activation. J Pharmacol Exp Ther 311, 1-7.

Tong, J., Fitzmaurice, P., Furukawa, Y., Schmunk, G. A., Wickham, D. J., Ang, L.-C., Sherwin, A., McCluskey, T., Boileau, I., Kish, S. J., 2014. Is brain gliosis a characteristic of chronic methamphetamine use in the human? Neurobiology of Disease 67, 107-118.

Torres, B., Ruoho, A. E., 2014. N-terminus regulation of VMAT2 mediates methamphetamine-stimulated efflux. Neuroscience 259, 194-202.

Truong, J. G., Newman, A. H., Hanson, G. R., Fleckenstein, A. E., 2004. Dopamine D2 receptor activation increases vesicular dopamine uptake and redistributes vesicular monoamine transporter-2 protein. Eur J Pharmacol 504, 27-32.

Truong, J. G., Rau, K. S., Hanson, G. R., Fleckenstein, A. E., 2003. Pramipexole increases vesicular dopamine uptake: implications for treatment of Parkinson's neurodegeneration. Eur J Pharmacol 474, 223-226.

Ugarte, Y. V., Rau, K. S., Riddle, E. L., Hanson, G. R., Fleckenstein, A. E., 2003. Methamphetamine rapidly decreases mouse vesicular dopamine uptake: role of hyperthermia and dopamine D2 receptors. Eur J Pharmacol 472, 165-171.

UNODC, 2017. United Nations Office on Drugs and Crime, World Drug Report 2017.

Urban, N. B., Girgis, R. R., Talbot, P. S., Kegeles, L. S., Xu, X., Frankle, W. G., Hart, C. L., Slifstein, M., Abi-Dargham, A., Laruelle, M., 2012. Sustained recreational use of ecstasy is associated with altered pre and postsynaptic markers of serotonin transmission in neocortical areas: a PET study with [(1)(1)C]DASB and [(1)(1)C]MDL 100907. Neuropsychopharmacology 37, 1465-1473.

Usiello, A., Baik, J. H., Rouge-Pont, F., Picetti, R., Dierich, A., LeMeur, M., Piazza, P. V., Borrelli, E., 2000. Distinct functions of the two isoforms of dopamine D2 receptors. Nature 408, 199-203.

Vaarmann, A., Gandhi, S., Abramov, A. Y., 2010. Dopamine induces Ca2+ signaling in astrocytes through reactive oxygen species generated by monoamine oxidase. J Biol Chem 285, 25018-25023.

Vallersnes, O. M., Dines, A. M., Wood, D. M., Yates, C., Heyerdahl, F., Hovda, K. E., Giraudon, I., Dargan, P. I., 2016. Psychosis associated with acute recreational drug toxicity: a European case series. BMC. Psychiatry 16, 293.

Vanderschuren, L. J., Kalivas, P. W., 2000. Alterations in dopaminergic and glutamatergic transmission in the induction and expression of behavioral sensitization: a critical review of preclinical studies. Psychopharmacology (Berl) 151, 99-120.

Vattai, A., Akyol, E., Kuhn, C., Hofmann, S., Heidegger, H., von Koch, F., Hermelink, K., Wuerstlein, R., Harbeck, N., Mayr, D., Spitzweg, C., Toth, B., Mahner, S., Jeschke, U., Ditsch, N., 2017. Increased trace amine-associated receptor 1 (TAAR1) expression is

associated with a positive survival rate in patients with breast cancer. J Cancer Res Clin Oncol 143, 1637-1647.

Vizeli, P., Liechti, M. E., 2017. Safety pharmacology of acute MDMA administration in healthy subjects. J Psychopharmacol 31, 576-588.

Vogels, N., Brunt, T. M., Rigter, S., van, D. P., Vervaeke, H., Niesink, R. J., 2009. Content of ecstasy in the Netherlands: 1993-2008. Addiction 104, 2057-2066.

Volkow, N. D., Chang, L., Wang, G. J., Fowler, J. S., Leonido-Yee, M., Franceschi, D., Sedler, M. J., Gatley, S. J., Hitzemann, R., Ding, Y. S., Logan, J., Wong, C., Miller, E. N., 2001. Association of dopamine transporter reduction with psychomotor impairment in methamphetamine abusers. Am. J. Psychiatry 158, 377-382.

Volkow, N. D., Koob, G. F., McLellan, A. T., 2016. Neurobiologic Advances from the Brain Disease Model of Addiction. N Engl J Med 374, 363-371.

Volkow, N. D., Morales, M., 2015. The Brain on Drugs: From Reward to Addiction. Cell 162, 712-725.

Volz, T. J., Farnsworth, S. J., King, J. L., Riddle, E. L., Hanson, G. R., Fleckenstein, A. E., 2007a. Methylphenidate Administration Alters Vesicular Monoamine Transporter-2 Function in Cytoplasmic and Membrane-Associated Vesicles. Journal of Pharmacology and Experimental Therapeutics 323, 738-745.

Volz, T. J., Fleckenstein, A. E., Hanson, G. R., 2007b. Methamphetamine-induced alterations in monoamine transport: implications for neurotoxicity, neuroprotection and treatment. Addiction 102, 44-48.

Wagner, G. C., Ricaurte, G. A., Seiden, L. S., Schuster, C. R., Miller, R. J., Westley, J., 1980. Long-lasting depletions of striatal dopamine and loss of dopamine uptake sites following repeated administration of methamphetamine. Brain Res 181, 151-160.

Wakabayashi, K. T., Ren, S. E., Kiyatkin, E. A., 2015. Methylenedioxypyrovalerone (MDPV) mimics cocaine in its physiological and behavioral effects but induces distinct changes in NAc glucose. Front Neurosci 9, 324.

Wan, F. J., Lin, H. C., Huang, K. L., Tseng, C. J., Wong, C. S., 2000. Systemic administration of d-amphetamine induces long-lasting oxidative stress in the rat striatum. Life Sci 66, Pl205-212.

Warner, M., Trinidad, J. P., Bastian, B. A., Minino, A. M., Hedegaard, H., 2016. Drugs Most Frequently Involved in Drug Overdose Deaths: United States, 2010-2014. Natl Vital Stat Rep 65, 1-15.

Wasik, A. M., Millan, M. J., Scanlan, T., Barnes, N. M., Gordon, J., 2012. Evidence for functional trace amine associated receptor-1 in normal and malignant B cells. Leuk. Res 36, 245-249.

Watterson, L. R., Hood, L., Sewalia, K., Tomek, S. E., Yahn, S., Johnson, C. T., Wegner, S., Blough, B. E., Marusich, J. A., Olive, M. F., 2012. The Reinforcing and Rewarding

Effects of Methylone, a Synthetic Cathinone Commonly Found in "Bath Salts". J Addict Res Ther Suppl 9.

Watterson, L. R., Kufahl, P. R., Nemirovsky, N. E., Sewalia, K., Grabenauer, M., Thomas, B. F., Marusich, J. A., Wegner, S., Olive, M. F., 2014. Potent rewarding and reinforcing effects of the synthetic cathinone 3,4-methylenedioxypyrovalerone (MDPV). Addict. Biol 19, 165-174.

Weinshenker, D., Ferrucci, M., Busceti, C. L., Biagioni, F., Lazzeri, G., Liles, L. C., Lenzi, P., Pasquali, L., Murri, L., Paparelli, A., Fornai, F., 2008. Genetic or pharmacological blockade of noradrenaline synthesis enhances the neurochemical, behavioral, and neurotoxic effects of methamphetamine. J Neurochem 105, 471-483.

Wheeler, J. M., Reed, C., Burkhart-Kasch, S., Li, N., Cunningham, C. L., Janowsky, A., Franken, F. H., Wiren, K. M., Hashimoto, J. G., Scibelli, A. C., Phillips, T. J., 2009. Genetically correlated effects of selective breeding for high and low methamphetamine consumption. Genes Brain Behav 8, 758-771.

Whitney, N. P., Eidem, T. M., Peng, H., Huang, Y., Zheng, J. C., 2009. Inflammation mediates varying effects in neurogenesis: relevance to the pathogenesis of brain injury and neurodegenerative disorders. J Neurochem 108, 1343-1359.

Wilson, J. M., Kalasinsky, K. S., Levey, A. I., Bergeron, C., Reiber, G., Anthony, R. M., Schmunk, G. A., Shannak, K., Haycock, J. W., Kish, S. J., 1996. Striatal dopamine nerve terminal markers in human, chronic methamphetamine users. Nat. Med 2, 699-703.

Wise, R. A., 2004. Dopamine, learning and motivation. Nat Rev Neurosci 5, 483-494.

Wolff, K., Tsapakis, E. M., Winstock, A. R., Hartley, D., Holt, D., Forsling, M. L., Aitchison, K. J., 2006. Vasopressin and oxytocin secretion in response to the consumption of ecstasy in a clubbing population. J Psychopharmacol 20, 400-410.

Wolinsky, T. D., Swanson, C. J., Smith, K. E., Zhong, H., Borowsky, B., Seeman, P., Branchek, T., Gerald, C. P., 2007. The Trace Amine 1 receptor knockout mouse: an animal model with relevance to schizophrenia. Genes Brain Behav 6, 628-639.

Xie, Z., Miller, G. M., 2007. Trace amine-associated receptor 1 is a modulator of the dopamine transporter. J. Pharmacol. Exp. Ther 321, 128-136.

Xie, Z., Miller, G. M., 2009a. A receptor mechanism for methamphetamine action in dopamine transporter regulation in brain. J. Pharmacol. Exp. Ther 330, 316-325.

Xie, Z., Miller, G. M., 2009b. Trace amine-associated receptor 1 as a monoaminergic modulator in brain. Biochem. Pharmacol 78, 1095-1104.

Xie, Z., Vallender, E. J., Yu, N., Kirstein, S. L., Yang, H., Bahn, M. E., Westmoreland, S. V., Miller, G. M., 2008a. Cloning, expression, and functional analysis of rhesus monkey trace amine-associated receptor 6: evidence for lack of monoaminergic association. J. Neurosci. Res 86, 3435-3446.

Xie, Z., Westmoreland, S. V., Bahn, M. E., Chen, G. L., Yang, H., Vallender, E. J., Yao, W. D., Madras, B. K., Miller, G. M., 2007. Rhesus monkey trace amine-associated receptor 1 signaling: enhancement by monoamine transporters and attenuation by the D2 autoreceptor in vitro. J. Pharmacol. Exp. Ther 321, 116-127.

Xie, Z., Westmoreland, S. V., Miller, G. M., 2008b. Modulation of monoamine transporters by common biogenic amines via trace amine-associated receptor 1 and monoamine autoreceptors in human embryonic kidney 293 cells and brain synaptosomes. J. Pharmacol. Exp. Ther 325, 629-640.

Xu, W., Zhu, J. P., Angulo, J. A., 2005. Induction of striatal pre- and postsynaptic damage by methamphetamine requires the dopamine receptors. Synapse 58, 110-121.

Yamamoto, B. K., Moszczynska, A., Gudelsky, G. A., 2010. Amphetamine toxicities: classical and emerging mechanisms. Ann N Y Acad Sci 1187, 101-121.

Yamamoto, B. K., Raudensky, J., 2008. The role of oxidative stress, metabolic compromise, and inflammation in neuronal injury produced by amphetamine-related drugs of abuse. J. Neuroimmune. Pharmacol 3, 203-217.

Yamamoto, B. K., Zhu, W., 1998. The effects of methamphetamine on the production of free radicals and oxidative stress. J Pharmacol Exp Ther 287, 107-114.

Yao, J., Erickson, J. D., Hersh, L. B., 2004. Protein kinase A affects trafficking of the vesicular monoamine transporters in PC12 cells. Traffic 5, 1006-1016.

Yingshan, P., Hall, F. S., Moriya, Y., Ito, M., Ohara, A., Kikura-Hanajiri, R., Goda, Y., Lesch, K. P., Murphy, D. L., Uhl, G. R., Sora, I., 2015. Methylone-induced hyperthermia and lethal toxicity: role of the dopamine and serotonin transporters. Behav. Pharmacol.

Yu, L., Liao, P. C., 2000. Sexual differences and estrous cycle in methamphetamine-induced dopamine and serotonin depletions in the striatum of mice. J. Neural Transm 107, 419-427.

Zaami, S., Giorgetti, R., Pichini, S., Pantano, F., Marinelli, E., Busardo, F. P., 2018. Synthetic cathinones related fatalities: an update. Eur Rev Med Pharmacol Sci 22, 268-274.

Zhang, L., Coffey, L. L., Reith, M. E., 1997. Regulation of the functional activity of the human dopamine transporter by protein kinase C. Biochem Pharmacol 53, 677-688.

Zhong, N., Jiang, H., Du, J., Zhao, Y., Sun, H., Xu, D., Li, C., Zhuang, W., Li, X., Hashimoto, K., Zhao, M., 2016. The cognitive impairments and psychological wellbeing of methamphetamine dependent patients compared with health controls. Progress in Neuro-Psychopharmacology and Biological Psychiatry 69, 31-37.

Zhu, J. P., Xu, W., Angulo, J. A., 2005. Disparity in the temporal appearance of methamphetamine-induced apoptosis and depletion of dopamine terminal markers in the striatum of mice. Brain Res 1049, 171-181.

Zhu, J. P., Xu, W., Angulo, N., Angulo, J. A., 2006. Methamphetamine-induced striatal apoptosis in the mouse brain: comparison of a binge to an acute bolus drug administration. Neurotoxicology 27, 131-136.